



RESEARCH & DEVELOPMENT

MEPDG Inputs for Warm-Mix Asphalts

Y. Richard Kim, Ph.D., P.E., F. ASCE

Jongsub Lee, Ph.D.

Yizhuang Wang

Dept. of Civil, Construction, & Environmental Engineering

North Carolina State University

NCDOT Project 2012-01

FHWA/NC/2012-01

November 2015

MEPDG Inputs for Warm Mix Asphalts

FINAL REPORT

Submitted to the North Carolina Department of Transportation
(Research Project No. HWY-2012-01)

Submitted by

Y. Richard Kim, Ph.D., P.E., F.ASCE
Campus Box 7908
Department of Civil, Construction & Environmental Engineering
North Carolina State University
Raleigh, NC 27695-7908
Tel: 919-515-7758, Fax: 919-515-7908
E-mail: kim@ncsu.edu

Jongsub Lee, Ph.D.
Former Graduate Research Assistant

Yizhuang Wang
Graduate Research Assistant

**Department of Civil, Construction, & Environmental Engineering
North Carolina State University
Raleigh, NC**

November 2015

Technical Report Documentation Page

1. Report No. FHWA/NC/2012-01	2. Government Accession No.	3. Recipient's Catalog No.	
4. Title and Subtitle MEPDG Inputs for Warm Mix Asphalts		5. Report Date August 2015	
		6. Performing Organization Code	
7. Author(s) Y. Richard Kim, Jongsub Lee, and Yizhuang Wang		8. Performing Organization Report No.	
9. Performing Organization Name and Address Campus Box 7908, Dept. of Civil, Construction, & Environmental Engrg. NCSU, Raleigh, NC 27695-7908		10. Work Unit No. (TRAIS)	
		11. Contract or Grant No.	
12. Sponsoring Agency Name and Address NC Department of Transportation Research and Analysis Group 1 South Wilmington Street Raleigh, NC 27601		13. Type of Report and Period Covered Final Report August 2011 – November 2014	
		14. Sponsoring Agency Code 2012-01	
15. Supplementary Notes			
<p>16. Abstract</p> <p>This report presents the findings from a laboratory experimental program that is designed to develop local calibration factors for warm mix asphalts using the AASHTOWare Pavement ME program. Double Barrel® foamed technology and Evotherm additive were selected for this study because they are the two WMA technologies that are used most commonly in North Carolina. These WMA technologies are applied to four different asphalt mixtures commonly used in North Carolina. Dynamic modulus, fatigue cracking performance, and rutting performance of control (i.e., hot-mix asphalt) and WMA mixtures are determined using axial compression dynamic modulus test (AASHTO PP61), direct tension cyclic test (AASHTO TP107), and triaxial repeated load permanent deformation (TRLPD) test (AASHTO TP79), respectively. Different propensities of WMA mixtures for aging and moisture damage are determined by conducting these laboratory tests on the control and WMA mixtures aged to different levels and with and without moisture conditioning.</p> <p>The main findings from the laboratory experimental program are: (1) the HMA mixtures showed higher stiffness values, more rutting resistance, and more fatigue resistance than the two WMA mixtures; (2) the aging effect on the rutting resistance of foamed WMA mixture was greater than the effect on WMA Evotherm and the HMA mixtures; (3) in terms of the fatigue cracking properties, foamed WMA mixture was more sensitive to aging than the HMA mixtures; and (4) the S-VECD analysis results suggest that the moisture susceptibility of the WMA Evotherm mixture is the lowest among all the mixtures.</p> <p>The results from the aging and moisture damage tests were applied to the Pavement ME program to compare the fatigue cracking and rutting performance of the HMA and WMA pavements at the structural level. It was concluded that the local calibration factors developed for the HMA mixtures could be used to analyze WMA pavement performance using the Pavement ME program and that no modification was necessary in terms of the input parameters. With regard to moisture damage, this study found that the moisture susceptibility of the WMA Evotherm mixtures was not statistically different from that of the corresponding HMA mixtures. Therefore, no correction was deemed necessary for the Evotherm mixtures in terms of moisture damage. However, the fatigue cracking performance of the foamed WMA mixtures was significantly affected by moisture conditioning, thereby necessitating modification of the local calibration factors (determined originally for the HMA mixtures). Statistical analysis and theoretical calculations based on moisture diffusion theories were conducted to reflect the different performance levels observed in the WMA Foam mixtures in the presence of moisture in the Pavement ME analysis. Based on the analysis, a 1.088 reduction factor must be incorporated for the fatigue life prediction of foamed WMA mixtures due to the relatively high moisture susceptibility of this WMA technology.</p> <p>It must be noted that different aging effects on fatigue performance of HMA and WMA mixtures cannot be accurately reflected in the local calibration factors because of the rigid way of GAS model being implemented in the Pavement ME program. Also the Pavement ME program does not account for the effect of moisture damage explicitly through a model; therefore, incorporation of different moisture susceptibility between HMA and WMA mixtures in the local calibration factors is only approximate at best. A more mechanistic pavement design methodology that expresses the effects of aging and moisture damage through performance models is warranted in order to fully capture the difference between HMA and WMA mixtures.</p>			
17. Key Words: MEPDG, Pavement ME, WMA, Aging, Moisture, Fatigue, Rutting		18. Distribution Statement	
19. Security Classif. (of this report)	20. Security Classif. (of this page)	21. No. of Pages 284	22. Price

DISCLAIMER

The contents of this report reflect the views of the authors and are not necessarily the views of North Carolina State University. The authors are responsible for the facts and the accuracy of the data presented herein. The contents do not necessarily reflect the official views or policies of the North Carolina Department of Transportation at the time of publication. This report does not constitute a standard, specification, or regulation.

ACKNOWLEDGEMENTS

This research was sponsored by the North Carolina Department of Transportation. The Steering and Implementation Committee was comprised of Clark Morrison, Ph.D., P.E. (Chair), Mustan Kadibhai, P.E. (PM), Richard Burley, Jack E. Cowsert, P.E., Dennis W. Jernigan, P.E., Vladmir Mitchev, P.E., James Phillips, P.E., Nilesh Surti, P.E., Todd W. Whittington, P.E., Mrinmay Biswas, Ph.D., P.E. (Friend), Judith Corley-Lay, Ph.D., P.E. (Friend), Joseph Geigle, P.E., (Friend), and Christopher Peoples, P.E. (Friend). These advisors have given invaluable direction and support to the research team throughout the project.

EXECUTIVE SUMMARY

Warm mix asphalt (WMA) has become a popular material that has been used over the past decade to help protect the environment and reduce energy consumption. Although the volumetric properties are similar between hot mix asphalt (HMA) and WMA mixtures, the performance of these mixtures may be different because of the lower mixing and compaction temperatures and effects of the various WMA technologies on the material properties. Specifically, this study evaluates the effects of aging and moisture damage on WMA performance in terms of fatigue cracking and rutting. The findings from this investigation are extended to pavement performance analysis using the AASHTOWare Pavement ME program (formerly called the MEPDG). This extension is important because state highway agencies have developed local calibration factors for the Pavement ME program using material properties and pavement performance data for HMA mixtures, not WMA mixtures. Therefore, the validity of local calibration factors that are based on HMA mixtures needs to be evaluated for WMA mixtures. Double Barrel® foamed technology and Evotherm additive were selected for this study because they are the two WMA technologies that are used most commonly in North Carolina.

First, the properties of WMA test mixtures were evaluated and compared with corresponding HMA mixtures in the laboratory. The HMA mixtures used for the comparison had the same volumetric properties (including asphalt content, aggregate gradation, air void content, etc.) as the WMA mixtures; only the fabrication procedures were different. The comparison results revealed that, in terms of the dynamic modulus, the HMA mixtures showed higher stiffness values than the two WMA mixtures, i.e., Evotherm and foamed, and the two WMA mixtures exhibited similar dynamic modulus values to each other. In terms of rutting, the HMA mixtures showed more rutting resistance (i.e., lower permanent deformation levels) than the two WMA mixtures. At high temperatures, the foamed WMA mixtures exhibited high levels of permanent deformation. In terms of fatigue properties, the HMA mixtures showed more fatigue resistance than both WMA mixtures.

For the aging study, the specimens were conditioned using three aging levels. The short-term aging (STA) was performed by oven conditioning loose mixture at 135°C for four hours before compaction. Long-term aging level I (LTA1) and long-term aging level III (LTA3) involved the oven aging of compacted, cored, and cut specimens at 85°C for two and eight days, respectively. Triaxial repeated load permanent deformation (TRLPD) tests and the direct tension test specified in AASHTO TP 107 were performed in order to investigate the rutting and fatigue properties, respectively, of the HMA and WMA mixtures. In addition, binder was extracted and recovered from each mixture to evaluate the effects of aging on the binder scale. The test results indicate that, in terms of the dynamic modulus values of the mixtures, the HMA mixtures always showed higher values than the two types of WMA mixtures, and the two WMA mixtures showed similar stiffness values to each other for the three aging levels. The dynamic modulus values of the WMA mixtures increased with an increase in aging level, and the aging effect on the dynamic modulus values was significant. However, for the HMA mixtures, the differences between the two aging levels, STA and LTA1, were not significant. In terms of rutting resistance, the TRLPD test results indicate that the permanent deformation values of the HMA mixtures were always the

lowest for each aging level at each temperature, which means that the HMA mixtures were more resistant to rutting than the WMA mixtures. According to the test results, the aging effect on the rutting resistance of WMA Foam was greater than the effect on WMA Evotherm and the HMA mixtures. In terms of the fatigue cracking properties, the HMA mixtures showed more ductility than the WMA mixtures. It also was observed that WMA Foam was more sensitive to aging than the HMA mixtures.

For the moisture damage study, the AASHTO T 283 moisture conditioning procedure was applied to the WMA and HMA mixtures, and direct tension cyclic fatigue tests were conducted using specimens with and without moisture conditioning. The simplified viscoelastic continuum damage (S-VECD) model was applied to the direct tension cyclic test data to estimate the moisture susceptibility of the WMA mixtures. The test results indicate that, based on the dynamic modulus test results, the HMA mixtures showed higher dynamic modulus values with moisture conditioning and without moisture conditioning than the two WMA mixtures. The dynamic modulus values of the foamed WMA mixture suggest that the foamed WMA mixture is more sensitive to moisture conditioning than the WMA Evotherm and HMA mixtures. Also, in terms of the fatigue properties due to moisture damage, the S-VECD analysis results suggest that the moisture susceptibility of the WMA Evotherm mixture is the lowest among all the mixtures.

The results from the aging and moisture damage tests were applied to the Pavement ME program to compare the fatigue cracking and rutting performance of the HMA and WMA pavements at the structural level. Input recommendations were developed based on this comparison. Because aging occurs mainly within the top few inches of a pavement, and because bottom-up fatigue cracking is related only to the properties of the bottom asphalt concrete layer in the Pavement ME prediction model, it was not necessary to make adjustments to the fatigue cracking predictions due to the aging effect. Also, according to previous studies, the effect of moisture damage on rutting is minor; therefore, a study of the effects of moisture on rutting performance was not necessary. In order to account for the effect of aging on the mixture performance, the Global Aging System (GAS) model was implemented in the Pavement ME software. Further investigation of the GAS model found that a temperature range of 25°C to 135°C was needed to apply this model effectively; otherwise, the model would not be valid. The aging effect study of the WMA mixtures in the rutting distress prediction of the Pavement ME determined that, although the WMA mixtures exhibited less resistance to permanent deformation according to the TRLPD test results, the effects of aging on the permanent-to-resilient strain ratio model used in the Pavement ME program were insignificant according to the statistical analyses. Therefore, it was concluded that the local calibration factors developed for the HMA mixtures could be used to analyze WMA pavement performance using the Pavement ME program and that no modification was necessary in terms of the input parameters. With regard to moisture damage, this study found that the moisture susceptibility of the WMA Evotherm mixtures was not statistically different from that of the corresponding HMA mixtures. Therefore, no correction was deemed necessary for the Evotherm mixtures in terms of moisture damage. However, the fatigue cracking performance of the foamed WMA mixtures was significantly affected by moisture conditioning, thereby necessitating modification of the local calibration factors (determined originally for the HMA mixtures). Statistical analysis and theoretical calculations based on moisture diffusion theories were conducted to reflect the different performance levels

observed in the WMA Foam mixtures in the presence of moisture in the Pavement ME analysis. Based on the analysis, a 1.088 reduction factor must be incorporated for the fatigue life prediction of WMA Foam mixtures due to the relatively high moisture susceptibility of this WMA technology. This factor can be merged into the local calibrations for foamed WMA mixtures.

It must be noted that different aging effects on fatigue performance of HMA and WMA mixtures cannot be accurately reflected in the local calibration factors because of the rigid way of GAS model being implemented in the Pavement ME program. Also the Pavement ME program does not account for the effect of moisture damage explicitly through a model; therefore, incorporation of different moisture susceptibility between HMA and WMA mixtures in the local calibration factors is only approximate at best. A more mechanistic pavement design methodology that expresses the effects of aging and moisture damage through performance models is warranted in order to fully capture the difference between HMA and WMA mixtures.

TABLE OF CONTENTS

LIST OF TABLES XII

LIST OF FIGURES XV

CHAPTER 1 INTRODUCTION	1
1.1 Introduction and Research Needs	1
1.2 Research Objectives and Approach	2
1.3 Literature Review	3
1.3.1 WMA Technologies	3
1.3.2 The Pavement ME Program	5
CHAPTER 2 COMPARISON OF LABORATORY EVALUATION PROPERTIES BETWEEN WMA MIXTURES AND HMA MIXTURES	8
2.1 Dynamic Modulus Evaluation	8
2.2 Rutting Performance Evaluation	9
2.3 Fatigue Properties Evaluation	10
2.4 Summary	10
CHAPTER 3 AGING EFFECTS ON WMA MIXTURES	12
3.1 Introduction	12
3.2 Laboratory Preparation and Material Conditioning	12
3.2.1 RS9.5C Mixture Verification	13
3.2.2 RS9.5B Mixture Verification	14
3.2.3 WMA Specimen Fabrication Procedure	15
3.2.4 Aging Protocol	17
3.2.5 Test Methods	18
3.3 Dynamic Modulus	19
3.3.1 Theory and Background	19
3.3.2 Results and Discussion	21
3.4 Permanent Deformation	27
3.4.1 Theory and Background	27
3.4.2 Test Preparation and Set-up	29

3.4.3	Results and Discussion	30
3.5	Fatigue Cracking.....	32
3.5.1	Theory and Background	32
3.5.2	Test Preparation and Set-up.....	34
3.5.3	Results and Discussion	34
3.6	Summary	35
CHAPTER 4	MOISTURE EFFECT ON WMA MIXTURES	37
4.1	Introduction and Laboratory Preparation.....	37
4.2	Test Results and Discussion	37
4.2.1	Linear Viscoelastic Material Properties	37
4.2.2	Damage Characterization of Viscoelastic Material.....	38
4.3	Summary	39
CHAPTER 5	DEVELOPMENT OF THE WMA MIXTURES' INCORPORATION INTO THE AASHTOWARE PAVEMENT ME PROGRAM.....	41
5.1	Introduction.....	41
5.1.1	Overview	41
5.1.2	The Pavement ME Program	42
5.2	Study for Aging in Pavement ME and Global Aging System (GAS) Model	46
5.2.1	Introduction to GAS model and Points to Claim.....	46
5.2.2	Utilization of GAS Model for WMA Mixtures in Pavement ME	51
5.3	Study of Permanent Deformation Predictions in Pavement ME	55
5.3.1	Aging Effect on Permanent Deformation Predictions for WMA Mixtures in Pavement ME	56
5.3.2	Permanent Deformation Coefficients in Pavement ME	124
5.4	Fatigue Life Prediction Study for WMA Mixtures in Pavement ME.....	127
5.4.1	Introduction	127
5.4.2	Fatigue Cracking Coefficients in Pavement ME.....	128
5.4.3	Moisture Effect on Fatigue Life Predictions and Development of Modification for WMA Mixtures in Pavement ME.....	131
5.5	Summary	146

CHAPTER 6	SUMMARY AND CONCLUSIONS	148
6.1	Comparison between WMA and HMA Mixtures.....	148
6.2	Evaluation of Aging and Moisture Effects on Mixture Properties	148
6.3	Input Recommendations for the Incorporation of WMA Mixtures into the Pavement ME Program.....	149
REFERENCES	150
APPENDIX A	TABLES AND FIGURES ABOUT AGING EFFECT ON PERMANENT STRAIN	156
APPENDIX B	TABLES AND FIGURES ABOUT AGING EFFECT ON STRAIN RATIO OF PERMANENT STRAIN TO RESILIENT STRAIN	196
APPENDIX C	THE USE OF CYCLIC DIRECT TENSION TESTS AND DIGITAL IMAGING ANALYSIS TO EVALUATE MOISTURE SUSCEPTIBILITY OF WARM MIX ASPHALT CONCRETE	239
APPENDIX D	PERFORMANCE-BASED MOISTURE SUSCEPTIBILITY EVALUATION OF WARM MIX ASPHALT CONCRETE THROUGH LABORATORY TESTS AND DIGITAL IMAGING ANALYSES	257
APPENDIX E	DEVELOPMENT OF MOISTURE CONDITIONING PROCEDURE FOR MOISTURE-INDUCED STRESS TESTER	276

LIST OF TABLES

Table 3.1 Comparison between JMF before and after Mix Design Verification for RS9.5C	13
Table 3.2 Comparison between JMF before and after Mix Design Verification for RS9.5B	15
Table 3.3 Material Properties, Test Methods, and Specifications	19
Table 3.4 Dynamic Modulus Results for WMA and HMA Mixtures at Different Aging Levels	22
Table 5.1 Pavement ME Inputs Required for Asphalt Binder and Asphalt Concrete	43
Table 5.2 Comparison between GAS Model-Predicted and Measured Long-term Aging Dynamic Modulus Values: (a) Comparison with Data Points All within Temperature Range and (b) Comparison with Some Data Points out of Temperature Range	50
Table 5.3 Predicted Values from GAS Model	52
Table 5.4 GAS Model Predictions of Equivalent Number of Years for Aging for Measured Long-term Aging	53
Table 5.5 T-test results of permanent strain of WMA Evotherm for different aging levels: (a) at 20°C, (b) at 40°C, and (c) at 54°C.	58
Table 5.6 T-test results of permanent strain of WMA Foam for different aging levels: (a) at 20°C, (b) at 40°C, and (c) at 54°C.	61
Table 5.7 T-test results of permanent strain of HMA mixtures for different aging levels: (a) at 20°C, (b) at 40°C, and (c) at 54°C.	64
Table 5.8 Statistical Results of EICM Pavement Temperatures (Raleigh, NC)	67
Table 5.9 T-test results of permanent strain for short-term aging of conditioned mixtures among different test temperatures: (a) WMA Evotherm, (b) WMA Foam, and (c) HMA.	68
Table 5.10 T-test results of permanent strain of long-term aging Level 1 conditioned mixtures at different test temperatures: (a) WMA Evotherm, (b) WMA Foam, and (c) HMA.	71
Table 5.11 T-test results of permanent strain among different mixtures at 20°C: (a) short-term aging conditioning (b) long-term aging condition Level 1, and (c) long-term aging condition Level 3.	79
Table 5.12 T-test results of permanent strain among different mixtures at 40°C: (a) short-term aging conditioning (b) long-term aging condition Level 1, and (c) long-term aging condition Level 3.	82

Table 5.13 T-test results of permanent strain among different mixtures at 54°C: (a) short-term aging conditioning (b) long-term aging condition Level 1, and (c) long-term aging condition Level 3.	85
Table 5.14 T-test results of strain ratios of WMA Evotherm at different aging levels: (a) at 20°C, (b) at 40°C, and (c) at 54°C.	89
Table 5.15 T-test results of permanent strain of WMA Foam among different aging levels: (a) at 20°C, (b) at 40°C, and (c) at 54°C.	92
Table 5.16 T-test results of strain of HMA mixtures among different aging levels: (a) at 20°C, (b) at 40°C, and (c) at 54°C.	95
Table 5.17 T-test results of permanent strain of short-term aging conditioned mixtures at different test temperatures: (a) WMA Evotherm, (b) WMA Foam, and (c) HMA.	101
Table 5.18 T-test results of strain ratios of long-term aging Level 1 conditioned mixtures at different test temperatures: (a) WMA Evotherm, (b) WMA Foam, and (c) HMA.	104
Table 5.19 T-test results of strain ratios of long-term aging Level 3 conditioned mixtures at different test temperatures: (a) WMA Evotherm, (b) WMA Foam, and (c) HMA.	107
Table 5.20 T-test results of strain ratios among different mixtures at 20°C: (a) short-term aging conditioning, (b) long-term aging condition Level 1, and (c) long-term aging condition Level 3.	113
Table 5.21 T-test results of strain ratios among different mixtures at 40°C: (a) short-term aging conditioning, (b) long-term aging condition Level 1, and (c) long-term aging condition Level 3.	116
Table 5.22 T-test results of strain ratios among different mixtures at 54°C: (a) short-term aging conditioning, (b) long-term aging condition Level 1, and (c) long-term aging condition Level 3.	119
Table 5.23 Rutting Coefficients for North Carolina Mixtures.....	127
Table 5.24 Fatigue Coefficients for North Carolina Mixtures (based on psi)	129
Table 5.25 Fatigue Coefficients for North Carolina Mixtures with Moisture Damage (based on psi).....	134
Table 5.26 Pavement ME Analysis Results for WMA Evotherm Mixtures.....	135
Table 5.27 Pavement ME analysis results for WMA Foam mixtures	137

Table 5.28 Pavement ME Output for WMA Foam under Equivalent Moisture Condition.....	144
Table 5.29 Final Recommended Local Calibration Factors for Alligator Cracking Prediction Models for WMA Mixtures	146

LIST OF FIGURES

Figure 2.1 Dynamic modulus tests results of WMA and HMA mixtures: (a) comparison in semi-log scale, (b) comparison in log-log scale, (c) phase angle, and (d) dynamic shear modulus results of binders extracted and recovered from specimens.....	9
Figure 2.2 TRLPD test results at different test temperatures: (a) - (c): comparisons in arithmetic scale, and (d) - (e): comparisons in log-log scale.	10
Figure 2.3 Damage characteristic curves of Evotherm, Foam, and HMA mixtures from direct tension tests.	10
Figure 3.1 Comparison between gradation curves before and after verification for RS9.5C.....	14
Figure 3.2 Asphalt binder modification procedure for mixes with Evotherm 3G chemical additive.....	16
Figure 3.3 Asphalt binder modification procedure for mixes using PTI foaming machine.	17
Figure 3.4 Example of establishing dynamic modulus curve using time-temperature superposition.	21
Figure 3.5 Dynamic modulus test results of HMA mixtures at different aging levels: (a) mastercurves in semi-log scale, (b) mastercurves in log-log scale, (c) phase angles in semi-log scale, and (d) dynamic shear modulus mastercurves from binder tests in log-log scale.....	23
Figure 3.6 Dynamic modulus test results of WMA Evotherm mixtures at different aging levels: (a) mastercurves in semi-log scale, (b) mastercurves in log-log scale, (c) phase angles in semi-log scale, and (d) dynamic shear modulus mastercurves from binder tests in log-log scale.....	24
Figure 3.7 Dynamic modulus test results of WMA Foam mixtures at different aging levels: (a) mastercurves in semi-log scale, (b) mastercurves in log-log scale, (c) phase angles in semi-log scale, and (d) dynamic shear modulus mastercurves from binder tests in log-log scale.....	25
Figure 3.8 Comparison of dynamic modulus mastercurves between WMA and control mixture within the same aging levels in log-log scale: (a), (c), and (e): short-term aged mixtures, and (b), (d), and (f): binder extracted from short-term aged specimens.	26

Figure 3.9 Typical TRLPD test permanent strain vs. number of cycles graph in arithmetic scale.	28
Figure 3.10 Typical TRLPD test recorded strain vs. number of cycles during primary stage.	29
Figure 3.11 TRLPD test set-up with AMPT.	30
Figure 3.12 Comparisons of permanent strain at different aging levels for HMA and WMA mixtures (grouped to show the effects of mixture type on the rutting performance).	31
Figure 3.13 Comparisons of permanent strain at different aging levels for HMA and WMA mixtures (grouped to show the effects of aging on the rutting performance).....	32
Figure 3.14 Direct tension fatigue test set-up.	34
Figure 3.15 Damage characteristic curves of Evotherm, foamed, and HMA mixtures from direct tension tests: (a), (b), (c): comparisons between aging levels, and (d), (e), (f): comparisons between different materials.....	35
Figure 4.1 (a) Dynamic modulus in semi-log scale, (b) dynamic modulus in log-log scale, (c) phase angle in semi-log scale, and (d) shift factor in semi-log scale for each mixture with and without moisture conditioning.	38
Figure 4.2 Damage characteristic curves of Evotherm, foamed, and HMA mixtures with and without moisture conditioning. (M in the legend indicates moisture-conditioned.).....	39
Figure 5.1 Overview of Pavement ME design procedure.....	45
Figure 5.2 Changes in viscosity of Evotherm binder with aging time and depth of pavement at different temperatures.	49
Figure 5.3 Comparison between GAS model-predicted and measured long-term aging dynamic modulus values: (a) data points all within temperature range and (b) some data points out of temperature range.	50
Figure 5.4 Comparison of the mastercurves of laboratory-measured data and GAS model prediction results.....	51
Figure 5.5 Aging rates of different mixtures obtained from laboratory measurements and GAS model predictions using different binders: (a), (b): GAS model-predicted using extracted and recovered binder, (c), (d): GAS model-predicted using NC PG64-22 binder, (e), (f): GAS model-predicted using NC PG70-22 binder, and (g), (h): GAS model-predicted using NC 76-22 binder.....	55

Figure 5.6 Comparison of permanent strain with different aging levels in arithmetic scales.	56
Figure 5.7 Comparison of permanent strain with different aging levels in log-log scale.....	57
Figure 5.8 Comparison of permanent strain for different test temperatures in arithmetic scale. .	74
Figure 5.9 Comparison of permanent strain among different test temperatures in log-log scale.	74
Figure 5.10 Comparison of permanent deformation for short-term aging replicates tested at different temperatures in arithmetic scale and log-log scale.	75
Figure 5.11 Comparison of permanent deformation for long-term aging Level 1 conditioned replicates tested at different temperatures in arithmetic scale and log-log scale.....	75
Figure 5.12 Comparison of permanent deformation for long-term aging Level 3 conditioned replicates tested at different temperatures in arithmetic scale and log-log scale.....	76
Figure 5.13 Comparison of permanent strain among different mixtures in arithmetic scale.	76
Figure 5.14 Comparison of permanent strain among different mixtures in log-log scale.	77
Figure 5.15 Comparison of permanent deformation among replicates of different mixtures at 20°C.	77
Figure 5.16 Comparison of permanent deformation among replicates of different mixtures at 40°C.	78
Figure 5.17 Comparison of permanent deformation among replicates of different mixtures at 54°C.	78
Figure 5.18 Comparison of strain ratios with different aging levels in arithmetic scale.....	98
Figure 5.19 Comparison of strain ratios with different aging levels in log-log scale.....	98
Figure 5.20 Comparison of strain ratios among replicates with different aging levels for WMA Evotherm.....	99
Figure 5.21 Comparison of strain ratios among replicates with different aging levels for WMA Foam.	99
Figure 5.22 Comparison of strain ratios among replicates with different aging levels for HMA.	100
Figure 5.23 Comparison of strain ratios for different temperatures in arithmetic scale.....	110
Figure 5.24 Comparison of strain ratio among different test temperatures in log-log scale.	110
Figure 5.25 Comparison of strain ratios among short-term aging replicates tested at different temperatures in arithmetic scale and log-log scale.	111

Figure 5.26 Comparison of strain ratios among long-term aging Level 1 conditioned replicates tested at different temperatures in arithmetic scale and log-log scale.	111
Figure 5.27 Comparison of strain ratios among long-term aging conditioned replicates tested at different temperatures in arithmetic scale and log-log scale.	112
Figure 5.28 Comparison of strain ratios among different mixtures in arithmetic scale.	122
Figure 5.29 Comparison of strain ratios among different mixtures in log-log scale.	122
Figure 5.30 Comparison of strain ratios among replicates of different mixtures at 20°C.	123
Figure 5.31 Comparison of strain ratios among replicates of different mixtures at 40°C.	123
Figure 5.32 Comparison of strain ratios among replicates of different mixtures at 54°C.	123
Figure 5.33 Schematic diagram showing the regression procedure for rutting using material-specific coefficients (Jadoun 2012).	126
Figure 5.34 Schematic flow chart showing the comparison of moisture susceptibility for WMA and HMA mixtures in Pavement ME.	133
Figure 5.35 Schematic of the diffusion curve.	142

CHAPTER 1 INTRODUCTION

1.1 Introduction and Research Needs

As a relatively new pavement technology, warm mix asphalt (WMA) has become a commonly used material in the United States. According to a survey from the National Center for Asphalt Technology (NCAT), WMA usage has been notably increasing; for example, between 20% and 30% of all plant mixes produced in 2011 were WMA. By comparison, the National Asphalt Pavement Association (NAPA) reported that, in 2010 and 2009, only 13.2% and 5.4% of plant mixes, respectively, were WMA (NCAT 2012). By 2012, 26 states had either fully implemented WMA or had a WMA implementation plan underway.

One of the primary advantages of WMA technologies is that they allow the plant mix asphalt to be produced at lower temperatures than hot mix asphalt (HMA) while maintaining the workability of HMA. Typically, WMA mixtures are fabricated at temperatures that are 20°C to 30°C lower than similar HMA mixture fabrication temperatures. The benefits of WMA technologies can generally be summarized as economical, operational, and environmental, and include advantages such as reduced fuel consumption, late season (cool weather) paving, good workability and compaction, reduced plant emissions of greenhouse gases, and improved working conditions for plant and paving crews (Anderson 2008). These benefits have encouraged the widespread application of WMA technologies, although the long-term performance of WMA pavements has not been fully understood and evaluated.

In general, there are four categories of WMA technologies: organic additives (i.e., wax additives), chemical additives (i.e., surfactants), water-bearing additives, and water-based processes (i.e., non-additive processes that are based on foaming). At present, some of the commercial WMA additives combine several of these categories of technologies. The NCAT found that water-injection foaming is the most commonly used WMA technology in the United States. Specifically, Double Barrel Green,[®] which uses a mixing chamber where water is injected through a nozzle, is one of the most commonly used WMA foam technologies in the United States. Evotherm 3G[®] is a chemical additive WMA technology. These two WMA technologies are the most commonly used WMA technologies in North Carolina; therefore, this study is focused on the properties of both Double Barrel Green[®] and Evotherm 3G[®] WMA mixtures.

Regardless of the benefits that WMA technologies can provide, the long-term performance of WMA mixtures needs to be investigated and understood. Furthermore, the AASHTOWare Pavement ME program (formerly known as the MEPDG), which is the primary pavement design and analysis program used by state highway agencies, consists of models and calibration factors that are based on the properties of HMA mixtures, not WMA mixtures. Thus, the reliability of the performance predictions obtained from the Pavement ME program for pavements made with WMA mixtures requires research. Specifically, the lower paving temperatures that are used for WMA pavements, compared to HMA paving temperatures, may affect the aging and moisture susceptibility of WMA mixtures. Therefore, the effects of different aging and moisture damage

characteristics on fatigue cracking and rutting performance need to be evaluated. In addition, the effects of the WMA performance characteristics on the Pavement ME pavement design and analysis need to be investigated.

1.2 Research Objectives and Approach

The primary research objective is to develop recommendations for Pavement ME software input parameters and local calibration factors for the WMA mixtures that are commonly used in North Carolina. Because the North Carolina Department of Transportation (NCDOT) does not have WMA pavement performance data that cover a sufficient number of years of service to run the necessary calibrations, the local calibration factors for the HMA mixtures developed in the NCDOT HWY-2007-07 project, *Local Calibration of the MEPDG for Flexible Pavement Design*, as well as climate and traffic data, were used for this study. In order to achieve the objective, the properties of the WMA and HMA mixtures were measured via laboratory performance testing. Among the various WMA technologies available in today's WMA market, two WMA technologies that are currently used in North Carolina, i.e., Evotherm 3G[®] and Double Barrel Green[®] foaming technology, are the focus of this study. In the laboratory, the WMA Foam mixtures were produced using a PTI Foamer machine. As the control mix, HMA mixtures that had the same component materials and volumetrics as the WMA mixtures also were evaluated for comparison.

Because of their low production temperatures, WMA mixtures should experience less short-term aging during construction than HMA mixtures. Therefore, the effect of aging on WMA mixtures is a significant performance factor. In this study, three aging conditions were investigated: short-term aging (STA), long-term aging level I (LTA1), and long-term aging level III (LTA3). Short-term oven conditioning is included in the mix design to simulate the absorption and aging of the binder that occurs during construction. It is appropriate to oven-condition WMA mixes for two hours at the compaction temperature. The same short-term conditioning procedure is used for the design of HMA mixtures, except that the conditioning time is four hours for HMA. For long-term oven aging, two days and eight days are the conditioning times for LTA1 and LTA3 at 85°C, respectively, to simulate two to five years and 15 to 20 years in the field, respectively, depending on the location of the field and the structure of the pavement. After age conditioning, fatigue tests were conducted according to AASHTO TP-107, and the fatigue performance of the mixtures was predicted using the Simplified Viscoelastic Continuum Damage (S-VECD) model. Also, rutting was measured by carrying out triaxial repeated load permanent deformation (TRLPD) tests. Furthermore, binders were extracted and recovered from undamaged specimens so that the changes in binder properties that resulted from aging could be evaluated.

Aging is described in the Pavement ME program using the Global Aging System (GAS) model, but the effects of moisture conditioning on performance are not taken into account explicitly. The effect of moisture susceptibility on the WMA mixtures is important because the low production temperature may lead to residual water on the surface of the aggregate. The moisture

conditioning procedure in AASHTO T 283 was used in this study. Similar to the aging study, fatigue properties also were tested using the TP-107 approach.

The Pavement ME program was used in this study to conduct a series of pavement performance analyses using the laboratory test results. Recommendations were developed for ways to incorporate the effects of the WMA technologies on pavement performance into the Pavement ME analysis; these recommendations are provided in this report.

1.3 Literature Review

A comprehensive literature review was conducted to help accomplish the research objectives. The literature review is divided into two topics: WMA technologies and Pavement ME program analysis.

1.3.1 WMA Technologies

Even though WMA technologies are relative new, several studies about not only their performance, but also their workability and other application issues, have been conducted in recent years. These studies have sought ways to better understand the multiple benefits of WMA as well as any pitfalls. The findings from these studies are summarized in the following text.

Moisture susceptibility has always been a concern regarding the adoption of WMA mixtures into pavement design, because the relatively low production temperatures could result in insufficiently dried aggregate. The moisture treatments typically used to investigate moisture susceptibility can be divided into three categories: using aggregate with moisture, conditioning after specimen fabrication, and using both methods together. The NCHRP Report 691 (Bonaquist 2011), *Mix Design Practices for Warm Mix Asphalt*, which resulted from the NCHRP 9-43 project, noted that, even though WMA and HMA may be designed with the same aggregate and binder, the moisture susceptibility of WMA and HMA is different when subjected to AASHTO T 283 conditioning, which is considered ‘severe’ conditioning. Anti-stripping additives have been found to improve the moisture resistance of WMA mixtures.

Other studies have shown that the WMA Foam mixture subjected to AASHTO T 283 conditioning is more susceptible to moisture-induced damage than HMA mixtures, based on indirect tensile (IDT) strength and TSR test results (Ali et al. 2012). In terms of other types of WMA technology, however, one study (Gandhi et al. 2010) showed that mixtures containing WMA additives (Aspha-min[®] and Sasobit[®]) had slightly higher TSR values than HMA mixtures, whereas the IDT strength values did not differ significantly. Another study that used foamed WMA mixtures found no significant additional reduction in moisture damage resistance. In general, studies (Sargand et al. 2012, Rushing et al. 2013) have shown that, in the laboratory, the moisture susceptibility of WMA mixtures subjected to AASHTO T 283 conditioning is more significant than that of the counterpart HMA mix, whereas no significant difference was found in

field performance surveys. Also, these studies indicate that IDT strength and TSR values are the most common indices used to evaluate moisture susceptibility.

The other moisture treatment for WMA mixtures found in the literature involves using aggregate that has not been dried completely. Some studies have concluded that moist aggregate particles can increase the moisture susceptibility of foamed WMA mixtures and that raising the compaction temperature can improve moisture resistance (Ali et al. 2013, Xiao et al. 2013). With regard to non-foaming WMA mixtures, studies have shown that the presence of WMA additives has a negative effect on moisture resistance, but that moisture resistance can be improved to some degree by adding hydrated lime (Punith et al. 2011, Khodaii et al. 2012, Hesami et al. 2013). Also, Caro et al. (2012) studied fine aggregate matrix (FAM) with regard to moisture susceptibility. They based their study on a viscoelastic-fracture model and obtained parameters from Dynamic Mechanical Analyzer tests. Their results indicate that moisture leads to more damage in WMA mixtures than in HMA mixtures and that the effect of the change in the values of the parameters for the model is significant.

Based on the afore-mentioned studies, moisture susceptibility could be a clear disadvantage of WMA technologies. However, although the detrimental effect of moisture on WMA materials has been illustrated by these studies, the actual pavement distress, i.e., fatigue cracking, which moisture could possibly cause, has not yet been realized for WMA mixtures; that is, the effect of moisture was reflected indirectly in these previous studies. Therefore, further studies should be conducted that account for damage and other performance-related factors.

Rutting resistance is also considered a critical factor for WMA materials, because the lower production temperatures may cause less short-term aging and less stiffness, based not only on NCHRP Report 691, but based also on other articles. A high potential for rutting damage has been observed in laboratory tests involving foaming, chemical additive, and other types of WMA technologies (Bennert et al. 2011, Ali et al. 2013, Rushing et al. 2013). However, different results were obtained from other studies. For example, Prowell et al. (2007) and Leng et al. (2014) found that the behavior of WMA mixtures is similar to that of HMA mixtures in terms of rutting, both in the laboratory and in the field. Other studies have pointed out that the flow number test, which is the traditional method used to evaluate the rutting resistance of a material, may lead to different results and produce different rankings of materials as the conditions (e.g., temperature) of the test change (Porras et al. 2012). In addition, one article noted that, in terms of rutting performance, wax WMA mixtures differed from other types of WMA technology, because the wax helped to stiffen the mixture and, thus, improved its rutting resistance. In summary, because different studies have drawn different conclusions, and the results have varied as the tested mixtures and test methods were changed, tests that focus on local mixtures need to be carried out in order to gain a better understanding of local mixtures and mechanisms of rutting performance.

Furthermore, the effects of specimen reheating are also important to the investigation of WMA mixtures. The NCHRP Report 691 indicates that, because mixtures are further aged when they are reheated to the compaction temperature, extra stiffness is gained by this additional aging. The

dynamic modulus values are 60% to 150% higher after reheating than their initial values, whereas in reality mixtures are compacted immediately after production, without reheating or gaining the subsequent aging that is caused by reheating. Laboratory test results show that WMA mixtures with Aspha-min[®] are more sensitive to the effects of reheating than the HMA control, Evotherm[®], and Sasobit[®] mixtures.

In addition, the effects of curing and storage time should be studied, especially for foamed WMA mixtures, because the presence of foam decreases the binder viscosity in order to improve the workability of the mixture at relatively low temperatures. Note that curing time is the time the specimen exists in the compacted state before testing begins, and storage time is the time the material exists in a loose state prior to compaction. The process of foam dissipation after fabrication and construction may affect the properties of the mixture, which is related to curing time. In 2012, it was observed using a high-resolution synchrotron-based X-ray microtomography system, that moisture dissipates in high performance grade (PG) binders faster than in low PG binders, and that the size distribution of moisture bubbles varies in different binders (Kutay and Ozturk 2012). Another study of foamed WMA mixtures recommended that production testing for volumetric properties should be carried out within four hours after manufacturing foamed WMA at the plant (Kasozi et al. 2012). Another study also pointed out that the effect of curing time on the performance of WMA mixtures varies with changes in the material properties and type of additive (Leng et al. 2014). Based on the literature, the effects of storage and curing time on foamed WMA mixtures are more significant than on HMA mixtures, and the magnitude of these effects on foamed WMA mixtures depends on the type and properties of the mixtures.

WMA mixtures are considered to be an ideal material to mix with reclaimed asphalt pavement (RAP), because the relatively high stiffness value of aged RAP material can alleviate the effect of low short-term aging rates that are due to the low production temperatures of the WMA. The NCHRP Report 691 notes that the process of mixing virgin binder with RAP binder is time-dependent and that during storage, the mixing process actually continues. Two hours of short-term aging is recommended in NCHRP Report 691, and this study applies the same recommendation.

To sum up, WMA mixtures are relatively new and popular materials that have been used increasingly in recent years for pavement design. Although no significant change in the design method between WMA mixtures and HMA mixtures is needed in order to meet volumetric properties specifications, the behavior of WMA mixtures is different from that of HMA mixtures in terms of moisture susceptibility, rutting resistance, curing and storage time, etc., based on several studies found in the literature. Therefore, as previously noted, further study is needed to evaluate the properties of WMA mixtures using local materials.

1.3.2 The Pavement ME Program

The Pavement ME program is a product of NCHRP Project 1-37A, *Development of the 2002 Guide for Design of New and Rehabilitated Pavement Structures*. This program provides design

analysis for a wide variety of materials based on currently available mechanical model and field performance data. The Pavement ME program has been the primary pavement design and analysis program used by state highway agencies. Therefore, for this study, it was necessary to conduct a series of studies about factors that affect the application of this program, i.e., local calibration, sensitivity analysis, and properties of the mechanical and empirical prediction models embedded in the program. To this end, a literature review of the projects and studies that are similar to or have contributed to this research is discussed in this section.

The Pavement ME program is used to predict pavement performance and provide suggestions about pavement materials and structures. Thus, the reliability of the predictions is worthy of close attention. Azari et al. (2008) found that, although their flow number test results and Accelerated Loading Facility (ALF) test results showed close agreement regarding rutting performance, the predictions obtained from the Pavement ME program using Level 3 analysis showed only fair agreement, and the predictions using Level 1 analysis, which relies on local calibration, over-predicted rutting. The NCHRP 1-37A dynamic modulus model that uses MEPDG Level 3 binder inputs produced the most accurate predictions and least biased modulus estimates for the 27 mixtures used in Idaho (El-Badawy et al. 2012). However, Flintsch et al. (2007) recommended using Level 1 inputs to account for the stiffness of the mixtures in the Pavement ME program and, for regions where thermal cracking is not severe, such as Virginia, they recommended Level 2 and Level 3 inputs for tensile creep and strength evaluation. Bayat and Knight (2010) proved that, based on laboratory test results, the stiffness parameter in the Pavement ME program is proportional to asphalt longitudinal strain measured in the field. Biligiri and Way (2014) found that the NCHRP 1-40D dynamic modulus model also yields good correlation with measured data, which means that using Level 1 inputs in the Pavement ME program is reasonable in most cases. In terms of distress predictions derived from the Pavement ME program, other than resilient moduli or dynamic moduli, additional factors such as air void content should be taken into account for rutting predictions (Archilla and Diaz 2011). However, the permanent deformation prediction model and fatigue prediction model is more empirical than mechanistic, and the accuracy of the model is related closely to the calibration and regression results obtained from laboratory tests (Erik 2011). Therefore, based on the reviewed literature, the accuracy and reliability of the test results vary among different states and materials when Level 1 inputs are compared to Level 2 and Level 3 inputs. The distress predictions have been compared and evaluated for HMA, but predictions for WMA materials, especially in North Carolina, have not been studied.

Studies also have been carried out with the objective to develop local calibrations and utilize new materials, which is similar to the objective of this study. In 2009, tests using asphalt rubber (AR) mixes, a new type of material used in Arizona which, like WMA materials, had not been included in the Pavement ME program, were carried out to investigate material properties, i.e., rutting and fatigue cracking, and to compare the results with field data. Inputs to the Pavement ME software eventually were provided for this new material (Rodezno and Kaloush 2009). In 2008, it was found that, in order to calibrate the fatigue cracking distress, not only the calibration factors β_{f1} , β_{f2} , and β_{f3} should be calibrated, but also the C_1 and C_2 in the transfer function (Muthadi and Kim 2008). Local calibration has been conducted successfully in many states and

even in other countries (Hall et al. 2011, Aragão et al. 2010, Caliendo 2012, Tarefder and Rodriguez-Ruiz 2013). The calibration methods used in the aforementioned studies were applied in the previous local calibration work for NC by the NCSU research team and in this project.

CHAPTER 2 COMPARISON OF LABORATORY EVALUATION PROPERTIES BETWEEN WMA MIXTURES AND HMA MIXTURES

The performance of WMA mixtures has always been a serious concern ever since the WMA technologies were first developed. In this chapter, the laboratory tests results of WMA mixtures and HMA mixtures without any long-term conditioning (i.e., aging or moisture damage conditioning) are presented, and the properties of the mixtures are compared. Three different tests were conducted in order to evaluate the material properties of the mixtures: dynamic modulus tests to measure the fundamental linear viscoelastic material properties, TRLPD tests to examine rutting resistance, and direct tension cyclic tests, the results of which were analyzed using the S-VECD model, to investigate the fatigue properties of the materials. This Chapter 2 presents the test results and summarizes the conclusions, and Chapter 3 provides details, i.e., mixture information and test protocols.

2.1 Dynamic Modulus Evaluation

The dynamic modulus describes the linear viscoelastic properties of a mixture. Three types of mixtures were tested in this study and, of these three, two WMA technologies were applied: a chemical additive type of WMA technology, i.e., Evotherm, and a foaming type of WMA technology, i.e., Double Barrel Green. Representing the third type of mixture, HMA mixtures served as the control mixtures. For this study, the next chapter (Chapter 3) provides details regarding the mixture information and test methods.

Figure 2.1 presents the dynamic modulus test results for the WMA Evotherm, WMA Foam, and HMA mixtures. The dynamic modulus values of the HMA mixtures are shown to be always greater than those of both WMA mixtures, and the dynamic modulus values of the two WMA mixtures are similar to each other. Also, Figure 2.1 (c) indicates that the phase angle values of the HMA mixture differ significantly from those of the WMA mixtures. This finding suggests that the HMA mixture is more elastic than both types of WMA mixtures. In addition, binders were extracted and recovered from the WMA and HMA specimens. The dynamic shear modulus values of the binders were measured using the Dynamic Shear Rheometer (DSR). Figure 2.1 (d) presents the DSR test results. According to the plots, the modulus values of the HMA binder are greater than those of the WMA mixtures, and the modulus values of the WMA binders are similar to each other, which is similar to the trend observed in the mixture tests.

Because the design properties, i.e., gradations, volumetric properties, and also the materials used in the mixtures, are exactly the same, except for the application of the WMA technologies, it can be concluded that the differences in the dynamic modulus values of the three mixtures are due to the differences in the properties of the binders, which are owing to the effect of the low production temperatures and the type of WMA technology.

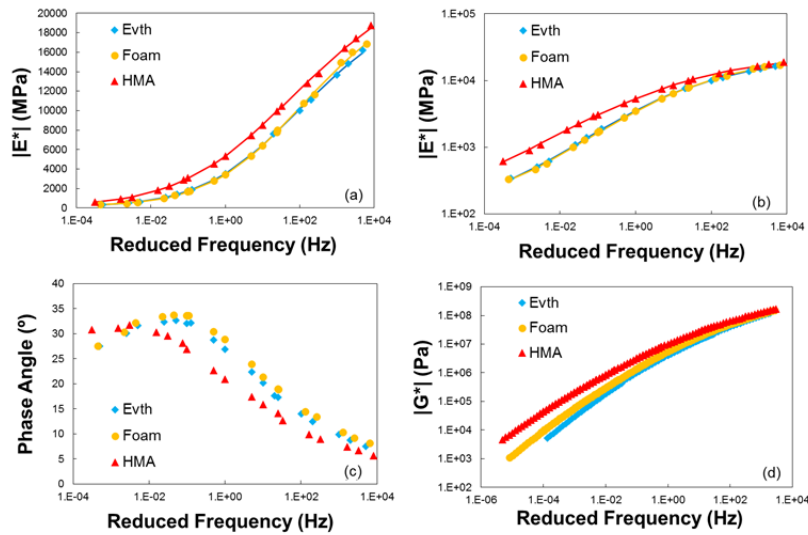


Figure 2.1 Dynamic modulus tests results of WMA and HMA mixtures: (a) comparison in semi-log scale, (b) comparison in log-log scale, (c) phase angle, and (d) dynamic shear modulus results of binders extracted and recovered from specimens.

2.2 Rutting Performance Evaluation

TRLPD tests were conducted to investigate the rutting resistance of the three mixtures. Figure 2.2 presents the tests results for the three mixtures at three different test temperatures. Figure 2.2 indicates that the HMA mixture exhibited less permanent deformation than the WMA mixtures at all three temperatures, and that at the higher temperatures, i.e., 40°C and 54°C, the WMA Foam mixture experienced higher permanent deformation levels than the WMA Evotherm mixture, which means that the rutting resistance of WMA Foam is less than that of WMA Evotherm. When the stiffness of the mixtures was tested, the modulus values of the WMA Foam and WMA Evotherm mixtures were found to be similar, as shown in Figure 2.1; therefore, the differences between the rutting depths of these two WMA mixtures suggest that their rutting behavior is not necessarily related to their stiffness.

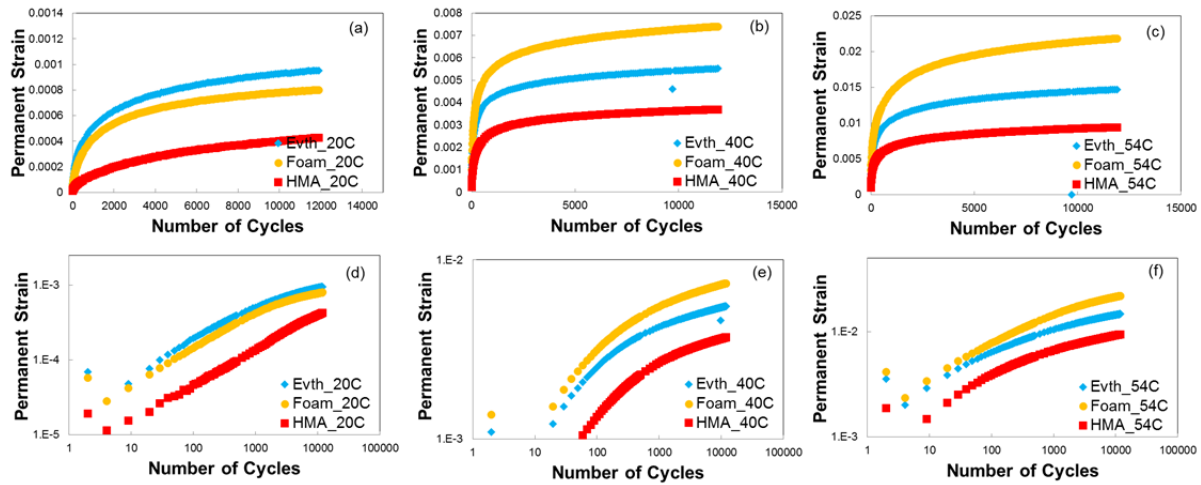


Figure 2.2 TRLPD test results at different test temperatures: (a) - (c): comparisons in arithmetic scale, and (d) - (e): comparisons in log-log scale.

2.3 Fatigue Properties Evaluation

Direct tension cyclic tests were conducted and the results were analyzed using the S-VECD model in order to examine the fatigue properties of the study mixtures. The pseudo stiffness (C) versus damage (S) curve represents the fundamental fatigue property of a mixture and is independent of the loading mode. According to Figure 2.3, the HMA mixture has the highest C vs. S curve and, in this case, the WMA Evotherm mixture has the lowest and shortest C vs. S curve.

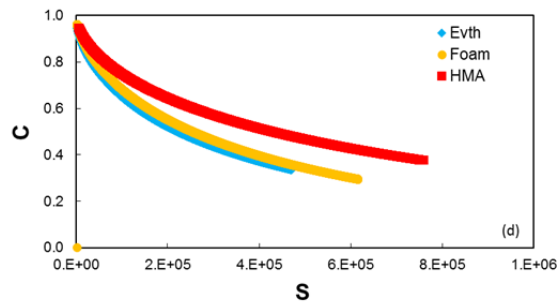


Figure 2.3 Damage characteristic curves of Evotherm, Foam, and HMA mixtures from direct tension tests.

2.4 Summary

Based on the test results and discussion, conclusions regarding the laboratory evaluation of the WMA and HMA mixtures can be summarized as follows:

- In terms of the dynamic modulus, the HMA mixture showed higher stiffness values than the two WMA mixtures, i.e., Evotherm and Foam. The two WMA mixtures exhibited similar modulus values to each other.
- In terms of rutting, the HMA mixture showed more rutting resistance (i.e., lower permanent deformation levels) than the two WMA mixtures. At high temperatures, the WMA Foam mixture exhibited high levels of permanent deformation.
- In terms of the fatigue properties, the HMA mixture showed more fatigue resistance than the WMA mixtures.

CHAPTER 3 AGING EFFECTS ON WMA MIXTURES

3.1 Introduction

Aging is an important factor of pavement performance. Aging is generally defined as changes in the physical properties of asphalt binders and mixtures over time. Due to the low production temperatures of WMA, the main difference between WMA and HMA mixtures in terms of aging is seen in the short-term aging stage when mixing and construction are in process. During this stage, the high temperatures and large surface areas of the heated aggregate cause rapid volatilization and oxidation, which are the two major irreversible chemical changes associated with aging. However, owing to the low mixing and compaction temperatures used for WMA mixtures, less volatilization and oxidation occur in the short-term aging stage, resulting in less overall aging of WMA mixtures compared to HMA mixtures.

Based on the literature and previous tests (conducted prior to this study), frequency sweep test results indicate that, in general, the binder dynamic shear modulus ($|G^*|$) value increases as an effect of aging, which is favorable for rutting resistance, but undesirable for fatigue performance. Meanwhile, the phase angle (δ) decreases, which is beneficial for both fatigue and rutting resistance. Because the aging process and the mechanisms associated with aging are complex, and because the aging process of WMA mixtures is different from that of HMA mixtures, it is necessary to study the aging properties of WMA mixtures in order to make good predictions for pavement performance and to develop reliable pavement designs.

The GAS model is embedded in the current Pavement ME Design program to predict the long-term performance of pavements. However, the GAS model was established based on data obtained from HMA mixtures, not WMA mixtures. For relatively new technologies such as WMA, the GAS model and the Pavement ME program need to be evaluated to determine whether they are able to make good and reliable predictions.

3.2 Laboratory Preparation and Material Conditioning

Superpave mixtures with four different gradations were tested in this study. These mixtures are referred to as RS9.5C, RS9.5B, RI19C, and RB25B. Note that the nomenclature used by the NCDOT can be explained in this way, using the RS9.5B mix as an example: 'R' means that RAP materials are contained in the mixture; 'S' means that this mixture generally is used in the surface layer; '9.5' indicates the nominal maximum aggregate size (NMAS) of the mixture; and 'B' means that it is designed for lower traffic volumes than 'C' mixtures, i.e., 0.3 to 3 million equivalent single-axle loads (ESALs). These mixtures are common Superpave mixtures used by the NCDOT.

The first two mixtures, RS9.5C and RS9.5B, typically are used as surface layer materials, and the other two, RI19C and RB25B, typically are used as an intermediate layer and bottom layer,

respectively. Because aging occurs mainly within the top few inches of a pavement, a typical surface layer material, i.e., the RS9.5C mixture in this case, was conditioned and tested for the aging study. For the moisture susceptibility tests, a surface layer mixture and a bottom layer mixture, RS9.5C and RB25B, respectively, were conditioned and tested. In this context, only the laboratory test results of the RS9.5C mixture are shown, because the trends of the other mixtures are similar to those of the RS9.5C mixture.

3.2.1 RS9.5C Mixture Verification

Because the surface layer in a pavement ages the most, the RS9.5C mixture, was adopted for the aging study. This mixture has a 9.5 mm NMAS and contains about 20% RAP materials. The specimens were fabricated based on the job mix formula (JMF) obtained from the plant; however, the stockpile blending process required some adjustments in order to match the designed gradation curves. The gradation was redesigned based on the sieve analysis results and the JMF, and some slight changes were made in order to match the volumetric properties. Table 3.1 and Figure 3.1 present the changes before and after verification.

Table 3.1 Comparison between JMF before and after Mix Design Verification for RS9.5C

JMF ID: 08-100-171; Contractor: Rea Garner – AS 165; Binder: NuStar Wilmington AT 31 – PG 70-22			
Material	Aggregate Source	Original JMF Blend (%)	After Verification JMF Blend (%)
Coarse #78M	Martin Marietta Garner	32.0	26.0
Screenings	Martin Marietta Garner	12.0	15.9
Manufactured sand	Martin Marietta Garner	37.0	37.6
RAP	Asphalt plant stockpile	19.0	19.0
Bag-house fines	Asphalt plant	-	1.5
Mixture Properties			
Parameter		Original JMF Blend (%)	After Verification JMF Blend (%)
N_{mi}/N_{des}		7/75	7/75
Total binder		5.4%	6.1%
Binder from RAP		1.0%	1.0%
Virgin binder		4.4%	5.1%
New binder grade		PG 70-22	PG 70-22
Mix temperature		157°C	157°C
Maximum specific gravity (G_{mm})		2.433	2.419
Bulk specific gravity (G_{mb})		2.336	2.322
Designed air void		4.0	4.0
Voids in mineral aggregate (VMA)		16.1	17.1
Voids filled with asphalt (VFA)		74.0	76.0

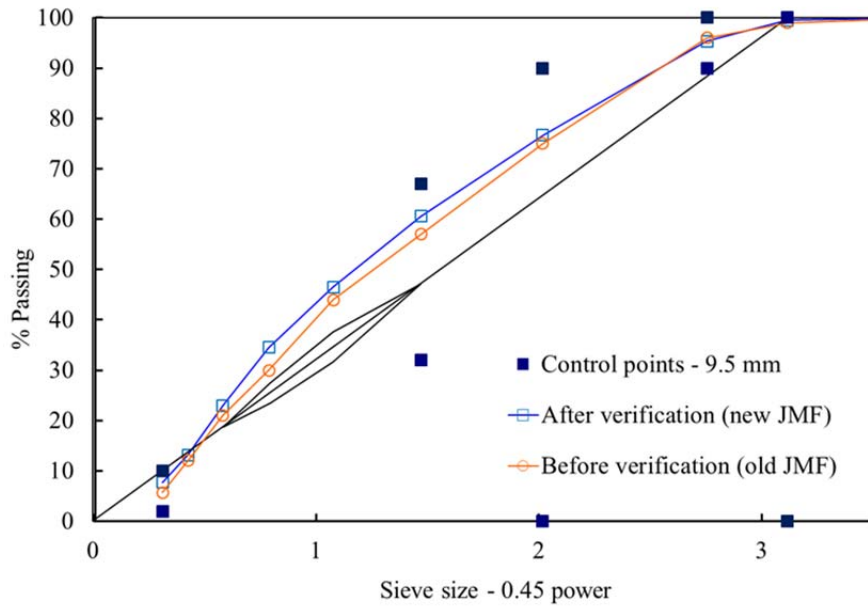


Figure 3.1 Comparison between gradation curves before and after verification for RS9.5C.

3.2.2 RS9.5B Mixture Verification

The RS9.5B mixture is one of the most frequently used surface pavement materials in North Carolina. Although it was not used in the aging study, its properties were tested for the rest of the study. Some verification and modifications were necessary to ensure that the mixture complied with the JMF. The results of the verification are presented in Table 3.2.

Table 3.2 Comparison between JMF before and after Mix Design Verification for RS9.5B

JMF ID: 08-100-171; Contractor: Rea Garner – AS 165; Asphalt binder: NuStar Wilmington AT 32 - PG 64-22			
Material	Aggregate Source	Original JMF Blend (%)	After Verification JMF Blend (%)
Coarse #78M	Martin Marietta Garner	32.0	26.0
Screenings	Martin Marietta Garner	12.0	15.9
Manufactured sand	Martin Marietta Garner	37.0	37.6
RAP	Asphalt plan stockpile	19.0	19.0
Bag house fines	Asphalt plant	-	1.5
Mixture Properties			
Parameter	Original JMF Blend (%)	After Verification JMF Blend (%)	
N_{ini}/N_{des}	7/75	7/75	
Total binder	5.4%	6.1%	
Binder from RAP	1.0%	1.0%	
Virgin binder	4.4%	5.1%	
New binder grade	PG 64-22	PG 64-22	
Mix temperature	149°C	149°C	
Maximum specific gravity (G_{mm})	2.433	2.442	
Bulk specific gravity (G_{mb})	2.336	2.345	
Designed air void	4.0	4.0	
Voids in the mineral aggregate (VMA)	16.1	15.4	
Voids filled with asphalt (VFA)	74.0	74.3	

3.2.3 WMA Specimen Fabrication Procedure

The RS9.5C WMA mixtures were fabricated using the same aggregate materials and gradations as were used for the RS9.5C HMA mixture, which is composed of 19% RAP, granite aggregate, and 6.7% (5.2% from virgin binder and 1.5% from RAP) PG 70-22 binder. For the WMA Evotherm mix, Evotherm 3G was added to the asphalt binder at 130°C at the level of 0.5% by weight of total asphalt. No anti-stripping agent was used for the Evotherm mixture. Figure 3.2 presents the asphalt binder modification and mixing procedures for the Evotherm mixture.

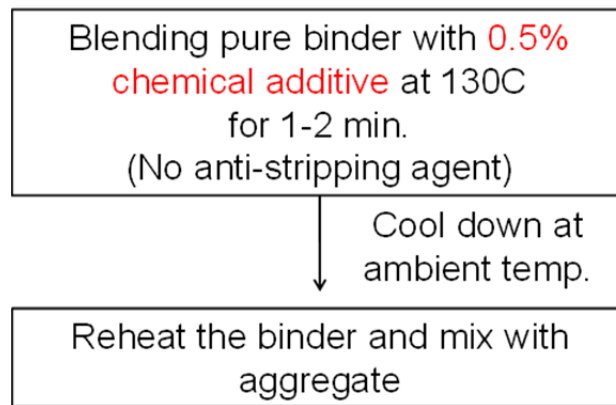


Figure 3.2 Asphalt binder modification procedure for mixes with Evotherm 3G chemical additive.

The temperatures of the aggregate, RAP, and binder at the time of mixing were 135°C, 110°C, and 157°C, respectively. Short-term oven aging was applied to all the mixtures at 117°C for two hours. A Servopac Superpave gyratory compactor was used to compact the test specimens at 117°C. For the fatigue performance and moisture susceptibility evaluations, specimens with dimensions of 100 mm x 150 mm and 100 mm x 130 mm were cored and cut from gyratory specimens that were 150 mm x 178 mm; the two specimen geometries were used for the dynamic modulus and cyclic direct tension tests, respectively.

For the WMA Foam mix, the fabrication procedure (including mix design parameters, mixing and compacting temperatures, and specimen geometry) was the same as for WMA Evotherm, except that instead of adding chemical additive to the binder to lower the fabrication temperature, the binder was foamed using a PTI foaming machine with 2% water injected into the binder. The binder used in the RS9.5C WMA Foam mix was the same as that used in the RS9.5C HMA mix, which contained 0.7% anti-stripping agent. After mixing and compaction, all the WMA Foam specimens were stored for 12 days for curing. Figure 3.3 presents the procedure for WMA Foam specimen fabrication.

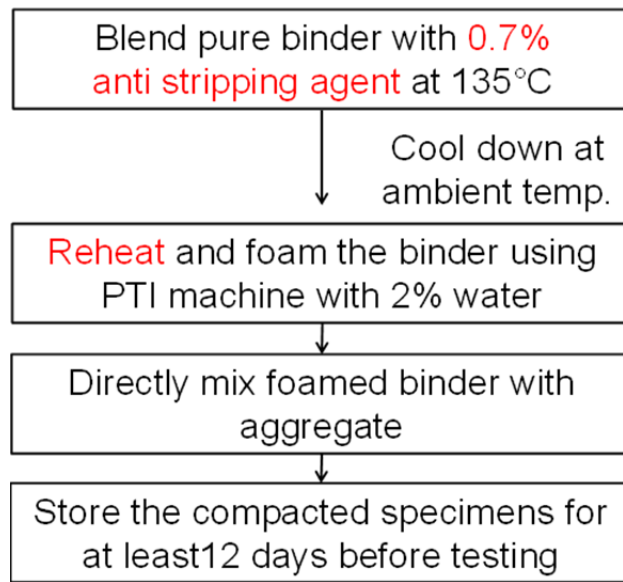


Figure 3.3 Asphalt binder modification procedure for mixes using PTI foaming machine.

3.2.4 Aging Protocol

The NCHRP 9-23 project found that the Strategic Highway Research Program (SHRP) protocol was not sufficient to simulate field-aging behavior in the laboratory because of its inability to account for variables such as field-aging conditions and mix properties. Nevertheless, the SHRP method has some advantages to be considered for this study: 1) it is simple to implement; 2) it provides a general relationship between laboratory- and field-aging behavior; and 3) it has been used successfully in previous studies conducted at North Carolina State University (NCSU). Therefore, three levels of asphalt mixture aging based on the SHRP protocol were conducted in this study, as follows.

Short-term aging (STA)

For HMA: Loose, uncompacted mixture was conditioned at 135°C for four hours and then compacted. Then, specimens were cored and cut for testing.

For WMA: Loose, uncompacted mixture was conditioned at the construction compaction temperature for two hours and then compacted. Then, specimens were cored and cut for testing.

Long-term aging, Level 1 (LTA1)

The aging procedure for LTA1 is the same as for STA, except the specimens were conditioned at 85°C for two days after coring and cutting prior to testing. This process simulates the mixture's condition two to five years after construction, depending on the environment and pavement properties.

Long-term aging, Level 3 (LTA3)

The aging procedure for LTA3 is the same as for STA, except the specimens were conditioned at 85°C for eight days after coring and cutting prior to testing. This process simulates the mixture's condition 10 to 15 years after construction, depending on the environment and pavement properties.

These three aging processes for asphalt mixtures follow AASHTO R30 specifications and also the findings of the NCHRP 9-43 project for WMA short-term conditioning, with the exception that two different long-term aging times are used. To minimize slump in the specimens during long-term oven aging, the method suggested by the NCHRP 9-23 project was adopted whereby specimens are wrapped in wire mesh, and the mesh is held in place by three steel clamps.

Binders were extracted from the specimens used in the dynamic modulus tests for each aging level. The binders were extracted from the whole specimen, which means that they represent the average degree of aging of a whole specimen.

3.2.5 Test Methods

Because linear viscoelastic properties are among the most important mechanical properties of asphalt mixtures, dynamic modulus tests were performed according to AASHTO PP 61/2009 to capture the basic viscoelastic mechanisms of the study mixtures. Three specimens were tested for each mixture type at six frequencies, 25 Hz, 10 Hz, 5 Hz, 1 Hz, 0.5 Hz, and 0.1 Hz, and at three temperatures, 4°C, 20°C, and 40°C, respectively. It should be emphasized that the load strain should be controlled within the limit of 50 $\mu\epsilon$ to 75 $\mu\epsilon$; thus, tests were conducted in linear viscoelastic range wherein there is no difference whether a compression load or tensile load is applied.

In terms of the performance tests conducted in this study, fatigue tests were performed according to the TP-107 procedure. Four specimens were tested, with two replicates at two different strain levels to characterize the fatigue behavior of the asphalt mixtures under each condition. The target temperature for these tests was 19°C to avoid the effect of viscoplasticity. Also, TRLPD tests for rutting were performed according to AASHTO TP-79. Two specimens were tested at each temperature: 20°C, 40°C, and 54°C. The deviator stress level was 70 psi, and the confining pressure was 10 psi for all the test temperatures. The test protocols are summarized in Table 3.3. The binders were extracted and recovered from the tested dynamic modulus specimens at different aging levels. Frequency sweep tests were conducted using the DSR, and the results were compared with the mixture test results.

Table 3.3 Material Properties, Test Methods, and Specifications

Material property	Test method	Specification
Dynamic modulus	Axial compression cyclic test	AASHTO PP-61
Fatigue cracking performance	Direct tension cyclic test	AASHTO TP-107
Rutting performance	TRLPD (flow number) test	AASHTO TP-79

3.3 Dynamic Modulus

3.3.1 Theory and Background

Dynamic modulus tests were conducted to investigate any changes in the mixtures' linear viscoelasticity that are caused by aging. The theory behind these tests is explained simply in the following text.

For non-aging linear viscoelastic material, the stress-strain relationship can be expressed by convolution integrals, as shown in Equation (4.1) and Equation (4.2).

$$\sigma = \int_0^t E(t-\tau) \frac{d\varepsilon}{d\tau} d\tau \quad (4.1)$$

$$\varepsilon = \int_0^t D(t-\tau) \frac{d\sigma}{d\tau} d\tau \quad (4.2)$$

where

$E(t)$ = relaxation modulus;

$D(t)$ = creep compliance; and

τ = integration variable.

In addition to the relaxation modulus and creep compliance, under different load modes the complex modulus (E^*) can also capture the linear viscoelastic properties of asphalt materials. The complex modulus can be expanded into two items, the storage modulus E' and the loss modulus E'' , as presented in Equation (4.3).

$$E^* = E' + iE'' \quad (4.3)$$

Another important property for viscoelastic materials involves the time-temperature superposition principle. The stiffness of viscoelastic materials is related to both loading time and temperature. By horizontally shifting the modulus at different temperatures to a certain reference temperature and obtaining a series of new reduced frequency f_R , one mastercurve can be drawn. The reduced frequency can be calculated using Equation (4.4). Note that the shift factor a_T at the reference temperature should be equal to zero.

$$f_R = f \times a_T \quad (4.4)$$

where

f = frequency in Hz; and

a_T = shift factor .

$$\log a_T = \alpha_1 T^2 + \alpha_2 T + \alpha_3 \quad (4.5)$$

where

$\alpha_1, \alpha_2,$ and α_3 = coefficients; and

T = temperature.

The mastercurve obtained by shifting can be regressed and expressed as a sigmoidal function, as shown in Equation (4.6). The modulus value at a certain temperature for a full range of frequency then can be captured. An example is given in Figure 3.4 which describes the procedure to establish a dynamic modulus mastercurve using one set of test data at the reference temperature of 20°C. Using the mastercurve, the modulus of the mixture at the reference temperature can be obtained for a full range of frequency, even far beyond the frequency range that a test machine can apply in reality.

$$\log |E^*| = a + \frac{b}{1 + \frac{1}{e^{d+g \cdot \log f_R}}} \quad (4.6)$$

where

a, b, c and d = coefficients; and

f_R = reduced frequency.

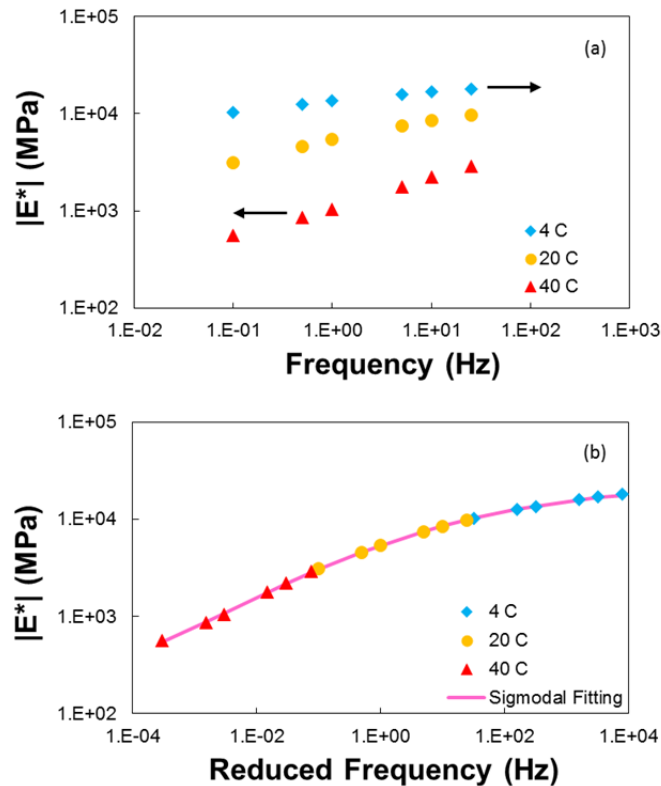


Figure 3.4 Example of establishing dynamic modulus curve using time-temperature superposition.

3.3.2 Results and Discussion

All the dynamic modulus tests were conducted in load control mode and were in accordance with the AASHTO PP61/2009 test protocol using the Asphalt Mixture Performance Tester (AMPT). The load levels were determined by a trial and error process so that the resulting strain amplitudes were controlled between $50 \mu\epsilon$ and $75 \mu\epsilon$ in order to keep the testing within the linear viscoelastic range. In this study, three mixtures were used: HMA as the control mixture, WMA Evotherm, and WMA Foam. For each mixture, specimens were tested at three aging levels: STA, LTA1, and LTA3. The test data were shifted into dynamic modulus mastercurves using a second-order polynomial for the time-temperature shift factors. Table 3.4 presents the dynamic modulus data for the three mixtures at the three aging levels. Figure 3.5 to Figure 3.8 present comparisons of the results. The dynamic shear modulus data from the extracted and recovered binders also are included.

Table 3.4 Dynamic Modulus Results for WMA and HMA Mixtures at Different Aging Levels

Temperature (C°)	Frequency (Hz)	E* (MPa)								
		WMA Evotherm			WMA Foam			HMA Control		
		STA	LTA1	LTA3	STA	LTA1	LTA3	STA	LTA1	LTA3
4	25	16198.31	17311.73	18001.14	16835.19	17374.98	18342.48	18742.55	18464.61	18815.62
	10	14828.95	16002.29	16871.4	15993.31	16373.04	17239.87	17436.3	17323.27	18244.56
	5	13648.96	14853.06	15891.25	14909.33	15363.79	16212.86	16400.49	16325.97	17406.72
	1	11129.59	12359.69	13501.84	11635.67	12606.97	13766.72	13815.38	13739.88	14782.5
	0.5	9986.629	11215.8	12566.36	10746.76	11703.47	12772.35	12815.23	12740.75	14110.62
	0.1	7618.619	8859.707	10321.58	7963.498	9189.783	10356.67	10498.01	10414.9	11654.99
25	25	7906.713	8942.117	9763.337	7789.01	8929.78	9914.437	9924.351	10372.07	11298.22
	10	6419.907	7379.451	8479.083	6370.523	7513.287	8542.338	8516.406	8823.987	9873.453
	5	5385.548	6306.27	7435.617	5314.726	6505.189	7479.389	7428.023	7758.835	8825.726
	1	3534.604	4337.183	5392.083	3435.392	4454.19	5383.058	5333.012	5624.056	6739.612
	0.5	2862.916	3581.744	4580.921	2761.441	3727.318	4537.686	4528.258	4789.907	5888.656
	0.1	1742.76	2319.871	3117.299	1663.123	2400.842	3101.614	3082.104	3222.274	4269.394
40	25	1895.461	2335.545	2905.697	1730.109	2183.195	2960.686	2885.612	2871.365	3893.354
	10	1387.879	1745.323	2226.537	1282.827	1628.663	2266.701	2267.923	2348.57	3078.577
	5	1079.001	1371.927	1782	987.3392	1258.958	1825.802	1825.972	1870.404	2557.976
	1	615.4713	781.6086	1043.994	566.6641	755.0385	1045.474	1096.62	1086.934	1571.452
	0.5	503.2407	641.3589	857.1177	465.4906	622.6982	856.6259	902.7202	891.0011	1312.852
	0.1	339.0467	432.8267	560.2467	330.4867	460.2067	542.6932	620.155	568.3444	838.9042

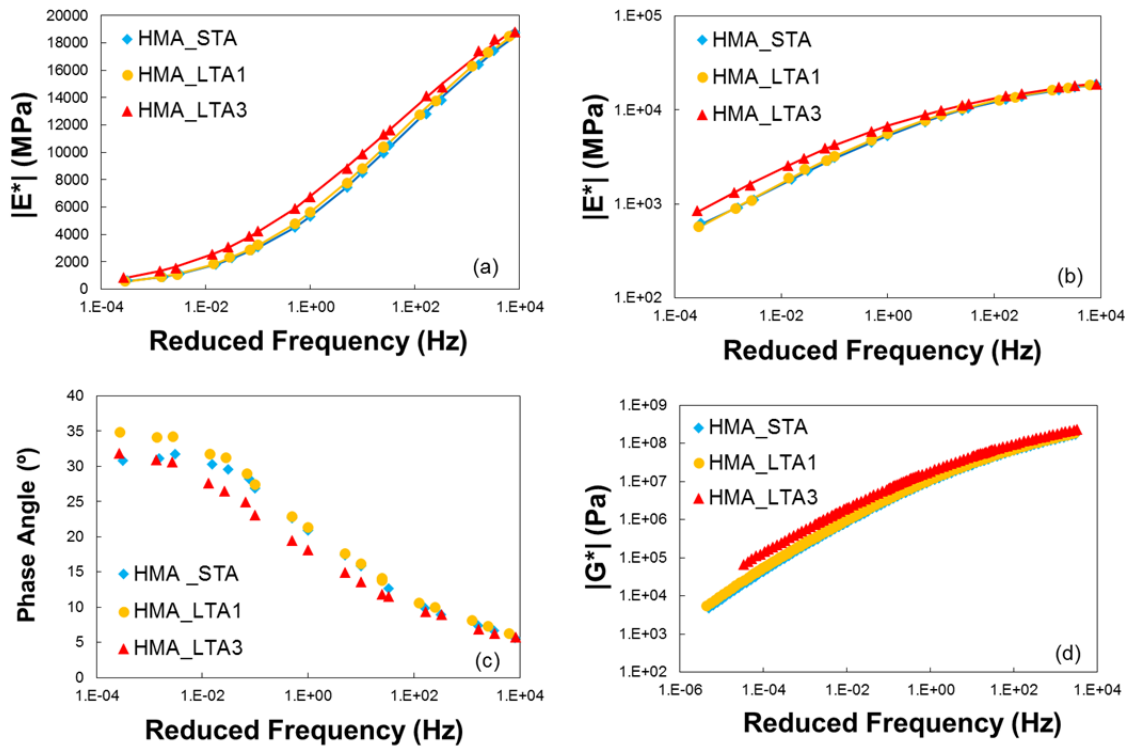


Figure 3.5 Dynamic modulus test results of HMA mixtures at different aging levels: (a) mastercurves in semi-log scale, (b) mastercurves in log-log scale, (c) phase angles in semi-log scale, and (d) dynamic shear modulus mastercurves from binder tests in log-log scale.

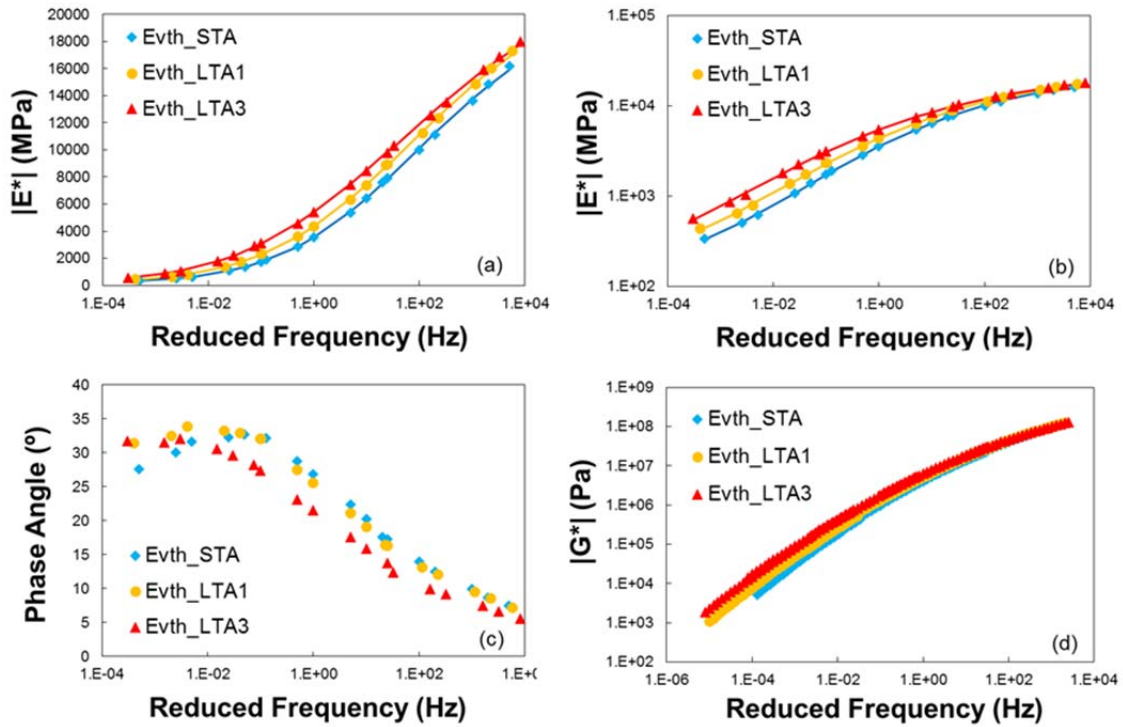


Figure 3.6 Dynamic modulus test results of WMA Evotherm mixtures at different aging levels: (a) mastercurves in semi-log scale, (b) mastercurves in log-log scale, (c) phase angles in semi-log scale, and (d) dynamic shear modulus mastercurves from binder tests in log-log scale.

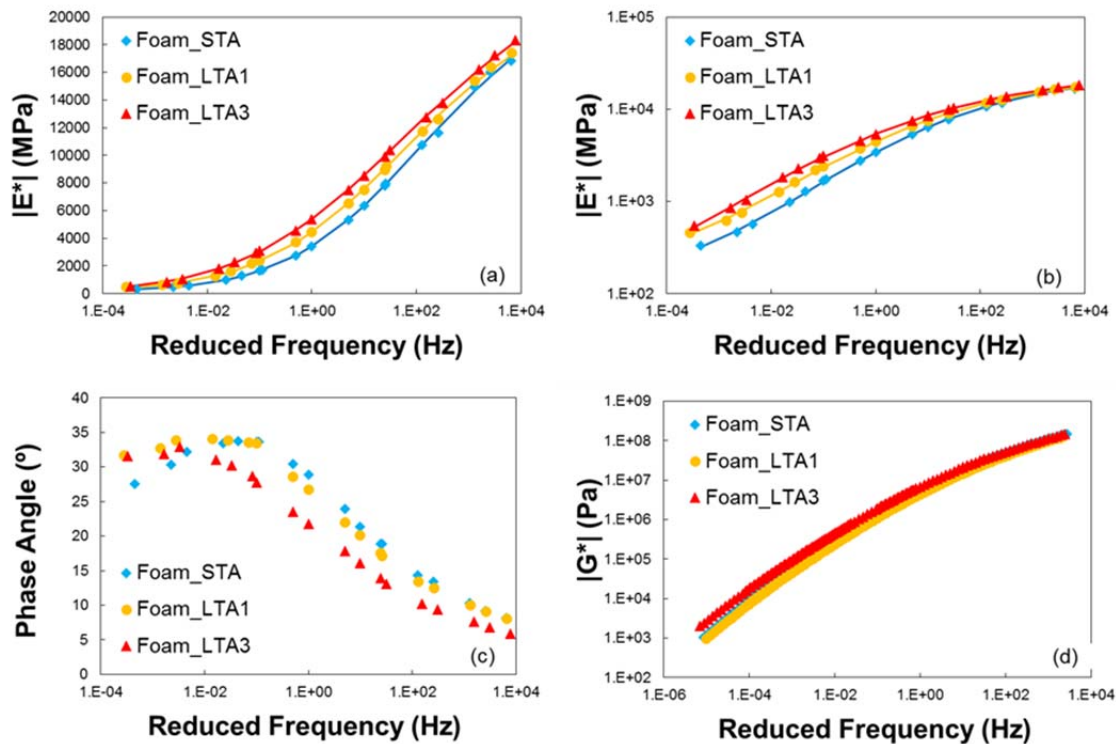


Figure 3.7 Dynamic modulus test results of WMA Foam mixtures at different aging levels: (a) mastercurves in semi-log scale, (b) mastercurves in log-log scale, (c) phase angles in semi-log scale, and (d) dynamic shear modulus mastercurves from binder tests in log-log scale.

Figure 3.5 to Figure 3.7 describe the changes in the dynamic modulus value of each mixture as aging increases. These figures indicate that for all three mixtures, the dynamic modulus values increase as the age of the mixtures increases. The same trend can be found in the binder data. Because the specimens for all the aging levels were fabricated together, and critical parameters, such as air void content, do not differ significantly before age conditioning, it can be concluded that the change in stiffness values stems from the changes in binder properties. In terms of phase angle, the phase angles of each mixture for LTA3 are always the lowest when compared with the phase angles of the mixtures at other aging levels at the same reduced frequency. This finding indicates that, as the mixture ages, the viscosity component of the mixture decreases and the elasticity component increases, which can lead to changes in the performance of the mixture. Compared to the HMA control mixture, the differences in the dynamic modulus values of the WMA mixtures between LTA1 and STA are significant. This finding indicates that, for both WMA Evotherm and WMA Foam, the stiffness values increase quickly and thus the mixtures age quickly in the first period of their service life.

Figure 3.8 presents comparisons among the WMA mixtures and the control HMA mixture. At each aging level, it can be observed that the dynamic modulus value of the HMA mixture is higher than that of the WMA mixtures, and the dynamic modulus values of the two WMA mixtures, WMA Evotherm and WMA Foam, are similar to each other. The same trend was found

for the binders extracted from the mixtures. Also, it can be observed that the differences between the HMA and WMA mixtures at STA are greater than the differences at LTA1 and LTA3, which indicates that the WMA mixtures have a faster aging rate than the HMA mix.

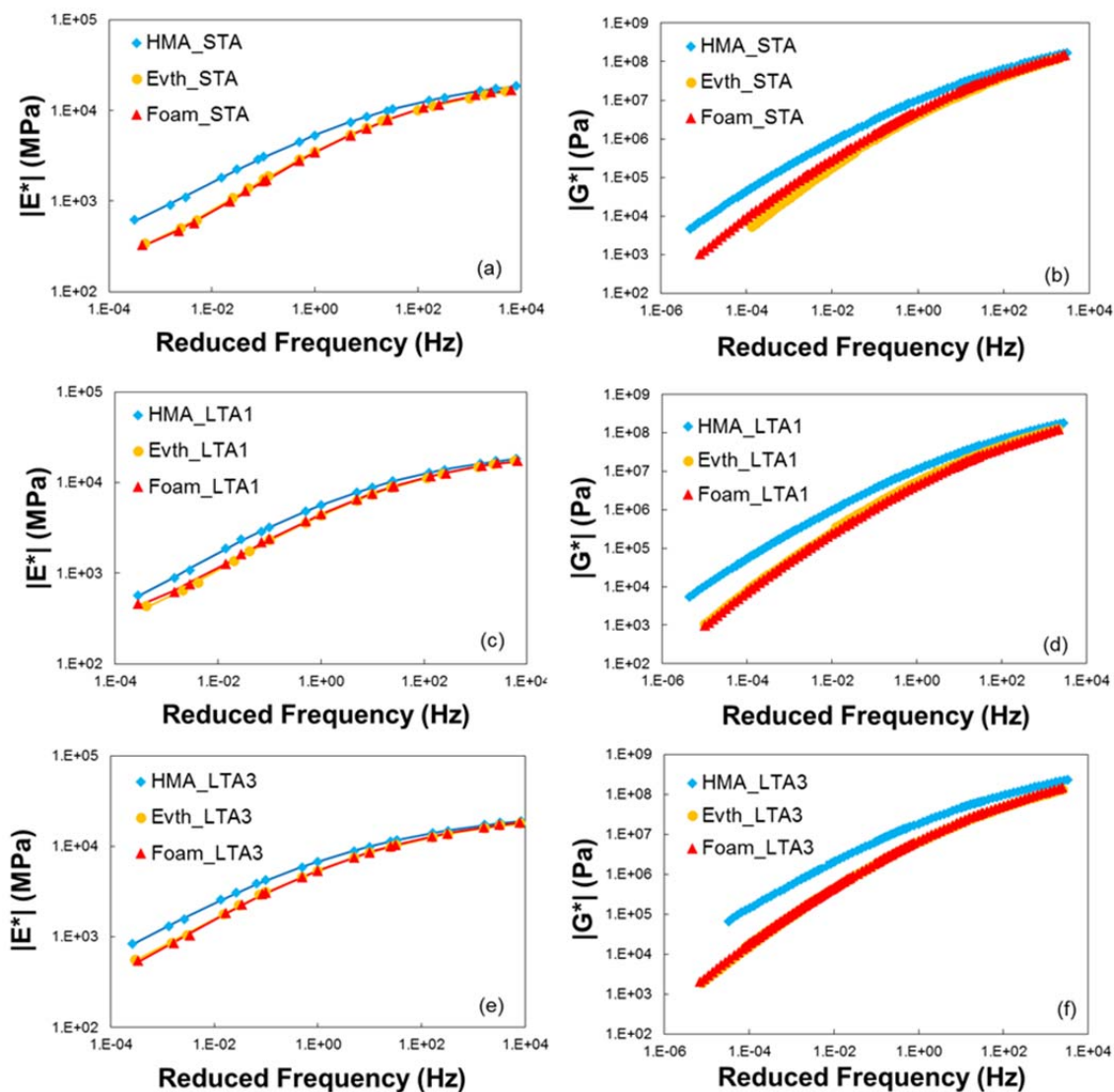


Figure 3.8 Comparison of dynamic modulus mastercurves between WMA and control mixture within the same aging levels in log-log scale: (a), (c), and (e): short-term aged mixtures, and (b), (d), and (f): binder extracted from short-term aged specimens.

3.4 Permanent Deformation

3.4.1 Theory and Background

Permanent deformation (also called rutting), which normally occurs underneath the wheelpath, is a pavement distress that can cause a vehicle to hydroplane when the ruts fill with water. There are two basic types of rutting: mix rutting and subgrade rutting. Mix rutting is when the pavement surface exhibits wheelpath depressions as a result of compaction/mix design problems while the subgrade does not rut. This study focuses on mix rutting because only flexible pavement materials are studied. Two mechanisms cause rutting: densification and shear flow. Although densification occurs mainly at the start of the pavement life, shear flow is the main cause of rutting and occurs throughout the pavement life.

An incremental model is embedded in the Pavement ME program to predict rut depth. The total rut depth is the summation of each layer, including unbound and bound layers. Equation (4.7) is applied for the calculation of total rut depth.

$$RD = \sum_{i=1}^n \epsilon_{p,i} h_i \quad (4.7)$$

where

- RD = rut depth (total),
- i = number of sublayers,
- n = total number of sublayers,
- $\epsilon_{p,i}$ = plastic strain in sublayer I, and
- h_i = thickness of sublayer i.

The model presented as Equation (4.8) is used in the Pavement ME program to predict permanent deformation in the asphalt concrete layer.

$$\frac{\epsilon_p}{\epsilon_r} = K_z * \beta_{r1} * 10^{k_{r1}} T^{\beta_{r2} * k_{r2}} N^{\beta_{r3} * k_{r3}} \quad (4.8)$$

where

- ϵ_p = plastic strain,
- ϵ_r = resilient strain,
- T = temperature of layer at mid-depth (°F),
- N = number of load repetitions,
- $\beta_{r1}, \beta_{r2}, \beta_{r3}$ = local calibration coefficients,
- k_1, k_2, k_3 = national coefficients, $k_1 = -3.35312, k_2 = 1.5606, k_3 = 0.4791$,
- K_z = depth function = $(C_1 + C_2 \times D) \times (0.328196)^D$,

$$\begin{aligned}
C_1 &= -0.1039 \times h_{ac}^2 + 2.4868 \times h_{ac} - 17.342 \\
C_2 &= 0.0172 \times h_{ac}^2 - 1.7331 \times h_{ac} + 27.428, \text{ and} \\
h_{ac} &= \text{total thickness of asphalt layer(s)}.
\end{aligned}$$

So, because the resilient strain can be calculated based on the stiffness of the pavement, the permanent deformation in asphalt concrete layers can be predicted using the given parameters k_{r1}, k_{r2} , and k_{r3} and local calibration factors β_{r1}, β_{r2} , and β_{r3} .

In this study, TRLPD tests were conducted following the AASHTO TP 79 protocol. The tests were performed using a cyclic load that consisted of a 0.1-second haversine pulse load and 0.9-second rest time. The total number of cycles was 12,000, and no failure was detected in all the tests conducted for this study with the number of load cycles. For each mixture, the tests were carried out at three temperatures, 20°C, 40°C, and 54°C, respectively, and with 10 psi confining pressure and 70 psi deviatoric stress. TRLPD tests typically are divided into three stages, primary, secondary, and tertiary, as shown in Figure 3.9. The permanent strain and resilient strain within one cycle are defined as shown in Figure 3.10, and the parameters in Equation (4.8) can be regressed using the data from the secondary stage of the TRLPD test using a numerical optimization method. The fitting procedure is explained in CHAPTER 5. For each mixture, two replicates were tested and the variability was examined.

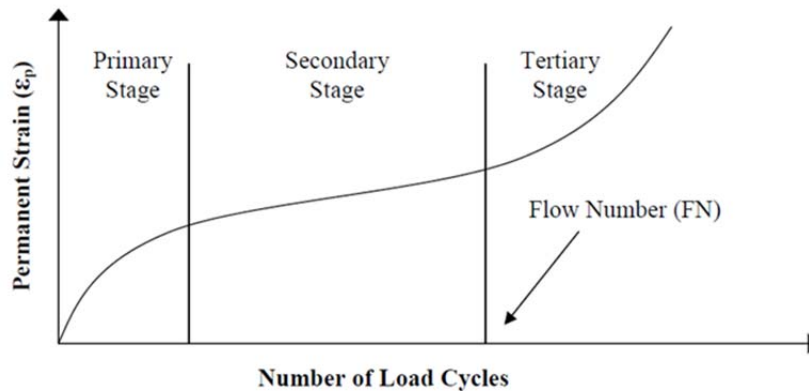


Figure 3.9 Typical TRLPD test permanent strain vs. number of cycles graph in arithmetic scale.

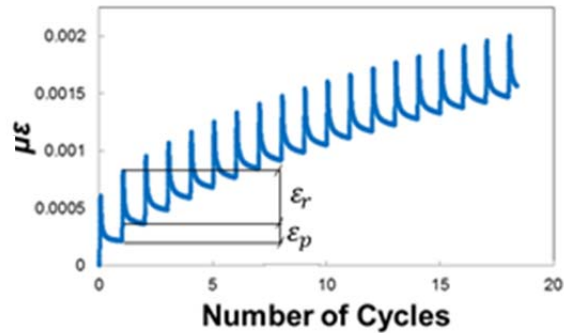


Figure 3.10 Typical TRLPD test recorded strain vs. number of cycles during primary stage.

3.4.2 Test Preparation and Set-up

The TRLPD tests in this study were conducted in accordance with AASHTO TP 79 specifications. Prior to testing, the specimens were prepared and the devices were set up in strict accordance with the test protocol, as follows.

The specimens were cut and cored from specimens 150 mm in diameter by 178 mm in height to make specimens that were 100 mm in diameter and 150 mm in height. Targets then were glued at a gauge length of 100 mm. Latex membrane was stretched around the specimens and caulked where the targets were punched through the membrane. Next, four loose-core linear variable differential transformers (LVDTs) were attached at room temperature. Specimens were conditioned in an external chamber for three hours at the target temperature before being moved to the AMPT. Confining pressure was applied immediately to 10 psi, and no more than four bubbles per second came out of the external hose into the bottle of water. After completing these steps, and after one-hour temperature conditioning in the AMPT chamber, the tests could be run. The data were collected using a LabView program. Also, before beginning the formal tests, a short fingerprint test was run in order to evaluate specimen-to-specimen viability.

Figure 3.11 shows a photograph of the test set-up with the AMPT. After 12,000 cycles, the testing stopped automatically, and the test data were analyzed using a MATLAB program developed at NCSU.



Figure 3.11 TRLPD test set-up with AMPT.

3.4.3 Results and Discussion

Figure 3.12 presents the permanent strain levels obtained from the TRLPD tests for the HMA, WMA Foam, and WMA Evotherm mixtures. The figure shows that the HMA mixture exhibited the least permanent deformation at all three aging levels and at all three test temperatures. At LTA1 and LTA3, the permanent deformation level of the Evotherm WMA mix is shown as the highest of all the mixes at the end of the testing, i.e., at 12,000 cycles.

Figure 3.13 presents the changes in permanent strain levels for the HMA, WMA Evotherm, and WMA Foam mixtures as the aging level changes. It can be observed that aging did not have a significant effect on the permanent strain of the HMA mix and that the foamed material is the most susceptible to aging of all the mixtures tested. Compared to the HMA control and WMA Evotherm mixtures, the dispersion of the water and bubbles appears to have affected the aging properties of the WMA Foam mix to some extent. It is worth mentioning that, in some cases, the results for the WMA Evotherm and WMA Foam mixtures at 20°C differ from those at 40°C and 54°C. This difference is due to the fact that within 12,000 cycles at 20°C, the material is still in the viscoelastic range rather than in the viscoplastic range, so the material will respond differently than it does at higher temperatures.

In addition, it can be observed that the permanent strain levels of the foamed WMA mix decreased significantly from STA to LTA1, whereas the difference in permanent strain of the

WMA Evotherm mix between STA and LTA1 is not as much as that observed for WMA Foam. This finding explains the reason that the permanent deformation level of the Evotherm mixture is higher than that of the foamed mixture at LTA1 at 54°C.

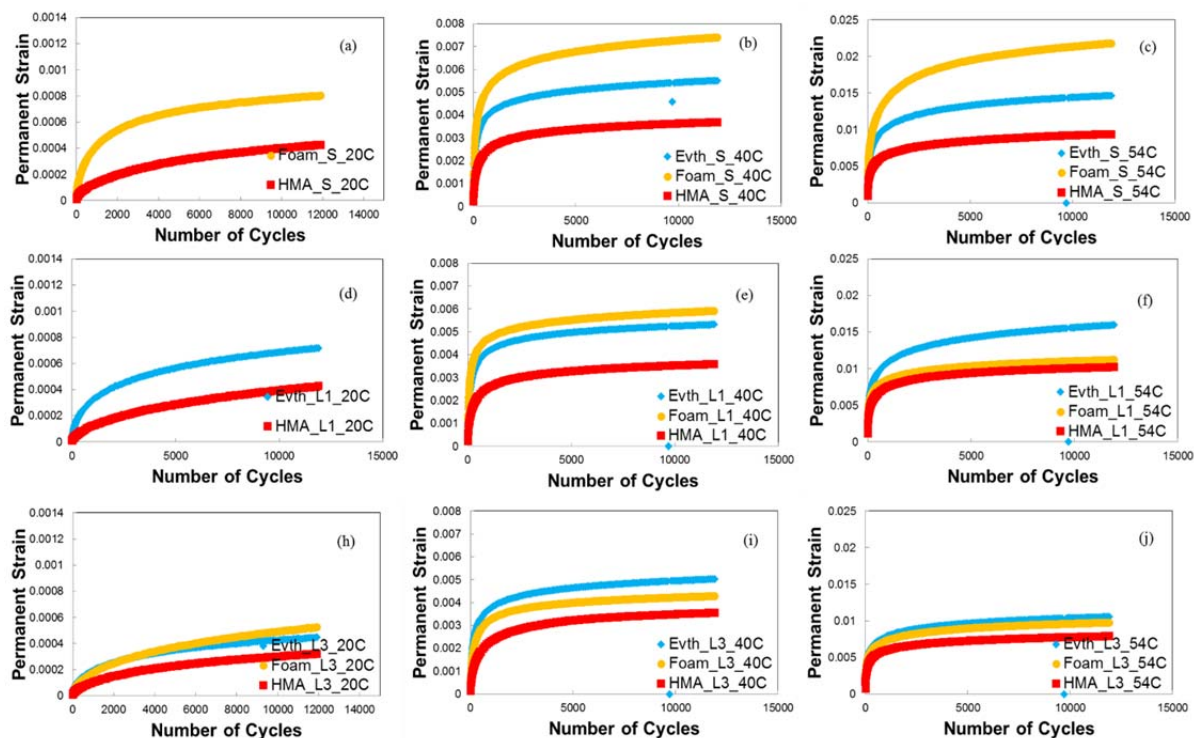


Figure 3.12 Comparisons of permanent strain at different aging levels for HMA and WMA mixtures (grouped to show the effects of mixture type on the rutting performance).

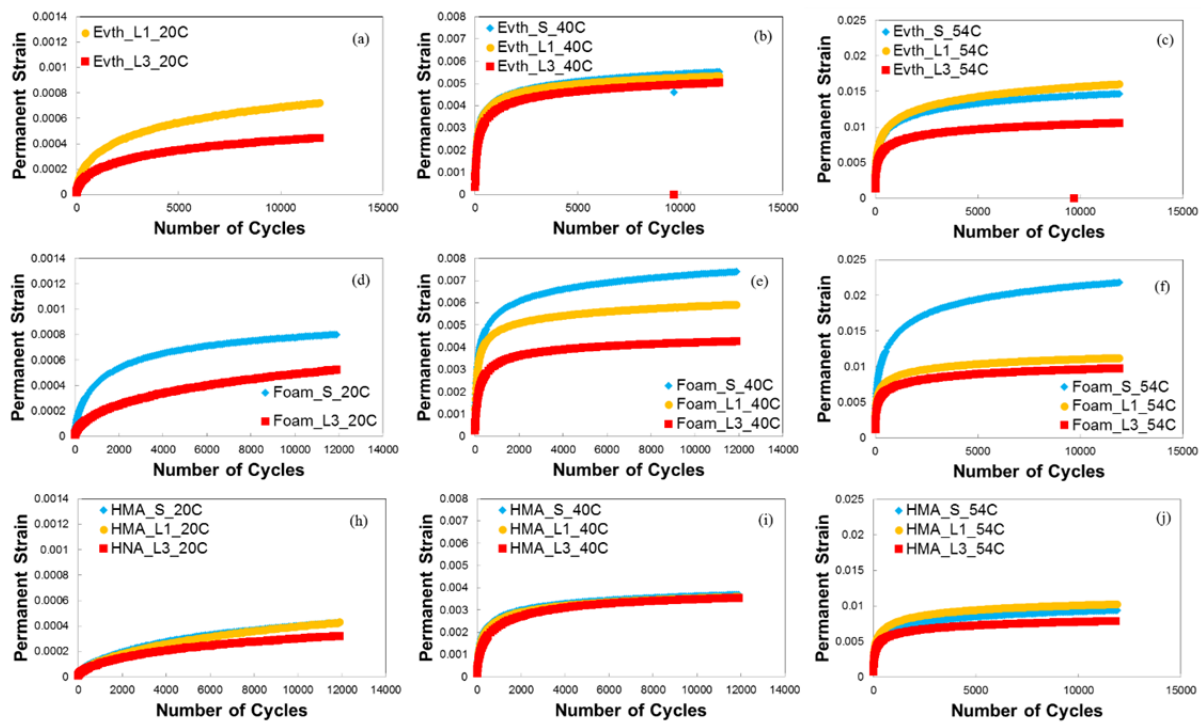


Figure 3.13 Comparisons of permanent strain at different aging levels for HMA and WMA mixtures (grouped to show the effects of aging on the rutting performance).

3.5 Fatigue Cracking

Fatigue cracking is a type of distress that should not be ignored. It can occur only a couple of years after opening a roadway to traffic due to traffic loading and environmental changes. Fatigue cracking typically is divided into two categories: bottom-up cracking (also called alligator cracking) and top-down cracking (or longitudinal cracking). In this study, alligator cracking is studied primarily because the top-down cracking model in Pavement ME has not been finalized. Alligator cracking usually is caused by tensile strain at the bottom of the asphalt bound layers. The S-VECD model, developed at NCSU, was adopted for this evaluation in this study.

3.5.1 Theory and Background

The theories behind the S-VECD model are described in the following text.

The viscoelastic continuum damage (VECD) theory focuses only on the net effect of the change in a material's microstructure on its macroscale properties by ignoring the details of microcracking. The work potential theory was developed by Schapery for elastic materials with growing damage. In this theory, damage is defined as an internal state variable. For viscoelastic materials, by transforming the physical variables into the Laplace domain, the viscoelastic problem can be modeled within the same formula as the elastic materials. The transforming

procedure, which is called the elastic-viscoelastic correspondence principle, is illustrated in the follow equations:

$$\varepsilon^R = \frac{1}{E_R} \int_0^t E(t-\tau) \frac{d\varepsilon}{d\tau} d\tau \quad (4.9)$$

where

- ε^R = pseudo strain,
- ε = physical strain,
- E_R = the reference modulus, typically considered as 1, and
- $E(t)$ = the relaxation modulus.

After the transformation, the constitutive relationship of the viscoelastic material can simply be described in Equation (4.10), similarly to the elastic materials.

$$\sigma = E_R \varepsilon^R \quad (4.10)$$

Schapery's theory can be applied to viscoelastic materials via the correspondence principle. The VECD theory consists of the following basic equations.

Pseudo strain energy density function:

$$W^R = f(\varepsilon^R, S) \quad (4.11)$$

Stress-pseudo strain relationship:

$$\sigma = \frac{\partial W^R}{\partial \varepsilon^R} \quad (4.12)$$

Damage evolution law:

$$\frac{\partial S}{\partial t} = \left(-\frac{\partial W^R}{\partial S} \right)^\alpha \quad (4.13)$$

where

- W^R = the pseudo strain energy density
- S = the damage parameter (internal state variable), and
- α = the damage evolution rate.

For the uniaxial mode of loading, the pseudo strain energy density function can be written as

$$W^R = \frac{1}{2} C(S) (\varepsilon^R)^2 \quad (4.14)$$

where C = pseudo stiffness.

The pseudo stiffness C is only a function of damage S . In this way, the C versus S curve can be drawn and is considered to represent the fundamental damage characteristics of a material.

3.5.2 Test Preparation and Set-up

The direct tension fatigue tests were conducted according to the S-VECD protocol developed at NCSU, which later was developed into AASHTO TP 107 specifications. Specimens with dimensions of 75 mm × 150 mm were cored and cut from gyratory-compacted specimens that were 150 mm × 178 mm. The specimens were glued to metal plates at both ends before being inserted into the MTS chamber. Four LVDTs were attached to the specimen at a gauge length of 75 mm. The tests were conducted in control actuator displacement mode at 19°C. Similar to the process for the dynamic modulus and TRLPD tests, a short fingerprint test was carried out prior to the formal tests.



Figure 3.14 Direct tension fatigue test set-up.

3.5.3 Results and Discussion

Figure 3.15 presents the damage characteristic curves determined from the cyclic direct tension tests at different aging levels; these curves describe the deterioration of the material integrity (pseudo stiffness) as damage (S) grows. Similar to the aging effect on the dynamic modulus, although no significant differences were found between the WMA Foam and WMA Evotherm mixtures at the same aging level, the HMA control mixture has higher C versus S curves. As shown in the comparisons among the different aging levels, for the WMA mixtures, the pseudo stiffness values increase slightly as the aging levels increase, but for the HMA mixture, the increase is insignificant. In order to predict the fatigue life accurately, the linear viscoelastic property, the material integrity with damage accumulation, and the failure criterion should be considered together.

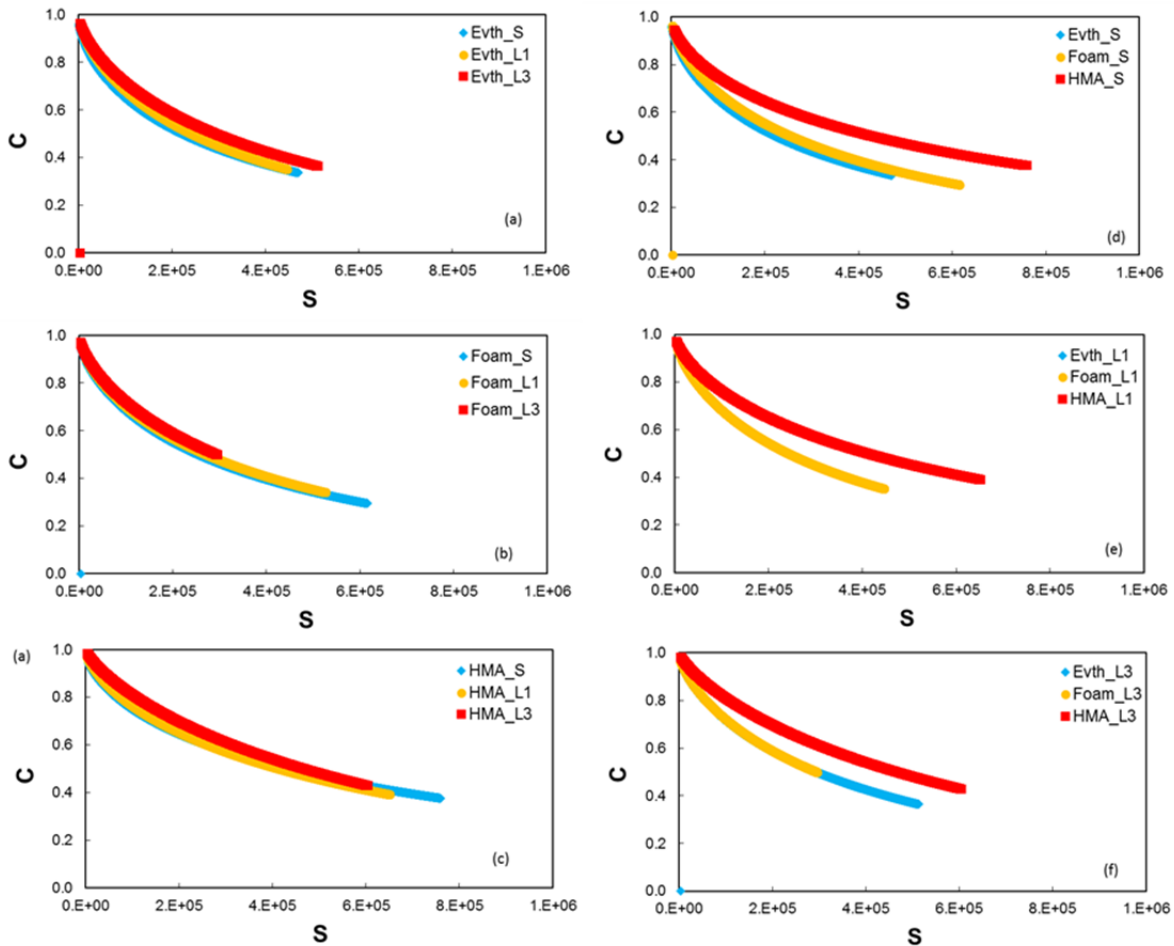


Figure 3.15 Damage characteristic curves of Evotherm, foamed, and HMA mixtures from direct tension tests: (a), (b), (c): comparisons between aging levels, and (d), (e), (f): comparisons between different materials.

3.6 Summary

Chapter 3 presents the evaluation of the dynamic modulus and rutting and fatigue properties of the HMA and WMA mixtures in terms of different aging levels. The conclusions, based on the laboratory evaluation and comparisons, are summarized as follows:

- In terms of the dynamic modulus values of the mixtures, the HMA mixture always showed higher values than the two types of WMA mixtures, and the two WMA mixtures showed similar stiffness values to each other for the three aging levels. The dynamic modulus values of the WMA mixtures increased with an increase in aging level, and the aging effect on the dynamic modulus values was significant. However, for the HMA mixture, the differences between the two aging levels, STA and LTA1, were not significant.

- In terms of rutting resistance, the TRLPD test results indicate that the permanent deformation values of the HMA mixture were always the lowest for each aging level at each temperature, which means that the HMA mixture was more resistant to rutting than the WMA mixtures. According to the test results, the aging effect on the rutting resistance of WMA Foam was greater than the effect on WMA Evotherm and the HMA mixture.
- In terms of the fatigue cracking properties, the WMA Foam mixtures were more sensitive to aging than the HMA mixture.

CHAPTER 4 MOISTURE EFFECT ON WMA MIXTURES

4.1 Introduction and Laboratory Preparation

The objective of this section of the study is to evaluate the moisture susceptibility of the WMA mixtures based on laboratory test results. The fundamental properties of the WMA and HMA mixtures with and without moisture damage, such as their linear viscoelastic properties and fatigue performance, are presented in this chapter, and they are used also in the analysis presented in the latter part of this study.

Dynamic modulus and controlled crosshead cyclic direct tension tests were performed to evaluate the linear viscoelastic properties and fatigue life of the RS9.5C WMA Evotherm, WMA Foam, and HMA control mixtures. Based on the linear viscoelastic and damage characteristic properties of the three mixes, strain-controlled direct tension fatigue test simulations were conducted to derive the tensile strain-based fatigue model coefficients (k_1 , k_2 , and k_3) that are used in the Pavement ME program for fatigue performance predictions. The regression process and theoretical background are explained in detail in CHAPTER 5.

The volumetric properties and fabrication procedures for the RS9.5C WMA and HMA mixtures are exactly the same as those explained in Chapter 3. The moisture conditioning procedure found in AASHTO T283 was applied to the cored and cut specimens. After applying vacuum pressure of 13~67 kPa to the specimens submerged in a vacuum container at 25°C in order to match saturation levels of 65%~80%, the saturated specimens were placed in a water bath at 60°C for 24 hours. After completely conditioning the specimens for moisture damage, the hot specimens were transferred to a water bath at room temperature to cool. The wet specimens were dried using an electric fan at room temperature and then core-dried to minimize thermal stress. The completely dried moisture-conditioned specimens thus could be used for testing to avoid the effects of changing saturation levels.

For the fatigue performance and moisture susceptibility evaluation, specimens with geometries of 100 mm x 150 mm and 100 mm x 130 mm were cored and cut from 150-mm x 178-mm gyratory specimens and were used for the dynamic modulus tests and cyclic direct tension tests, respectively.

4.2 Test Results and Discussion

4.2.1 Linear Viscoelastic Material Properties

Dynamic modulus testing was performed in load-controlled mode in axial compression following the protocol given in AASHTO PP 61. Figure 4.1 describes the linear viscoelastic material properties for the WMA Evotherm, WMA Foam, and HMA mixtures with and without moisture conditioning.

The test results show that the reduction in dynamic modulus values that is due to moisture conditioning is minor for WMA Evotherm in comparison to the WMA Foam and HMA mixtures. Within the linear viscoelastic range, the moisture susceptibility of the WMA Evotherm mixture is low, whereas that of the foamed mixture is higher than the others.

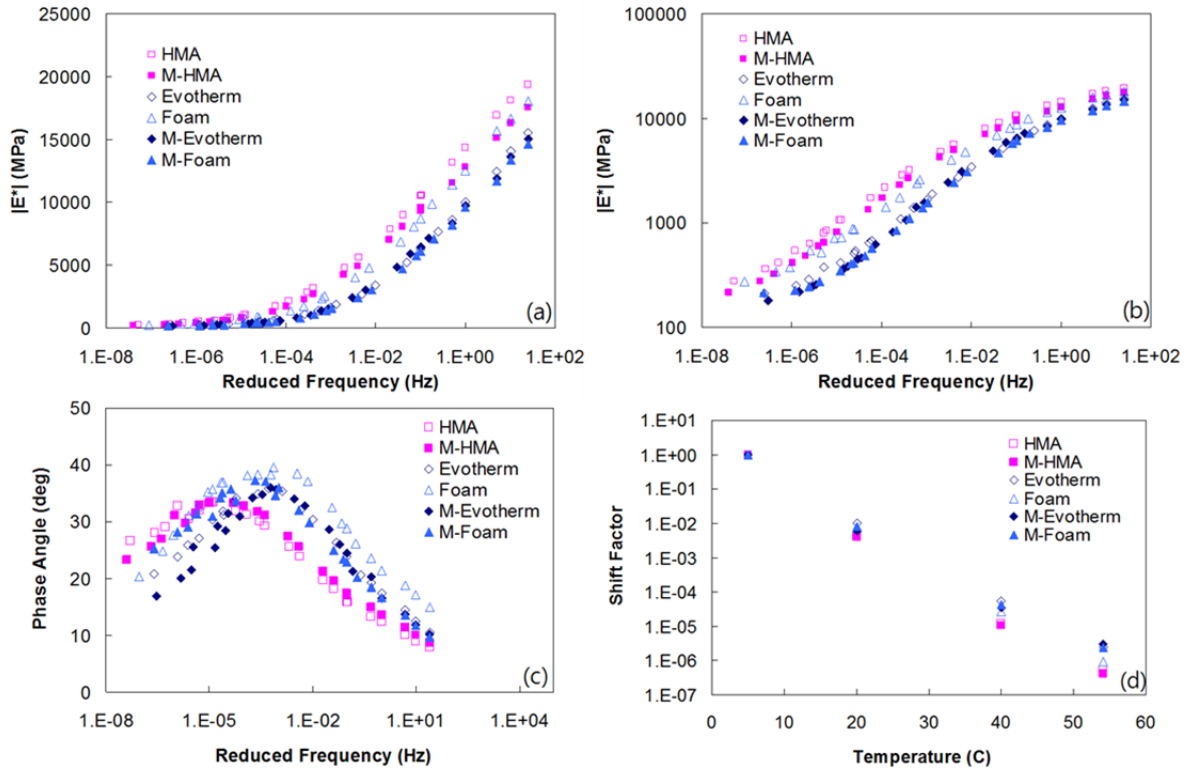


Figure 4.1 (a) Dynamic modulus in semi-log scale, (b) dynamic modulus in log-log scale, (c) phase angle in semi-log scale, and (d) shift factor in semi-log scale for each mixture with and without moisture conditioning.

4.2.2 Damage Characterization of Viscoelastic Material

The direct tension tests and S-VECD analysis were performed using the mixtures with and without moisture damage. Figure 4.2 shows that that the moisture susceptibility of the Evotherm mixture is less than that of the other two mixtures.

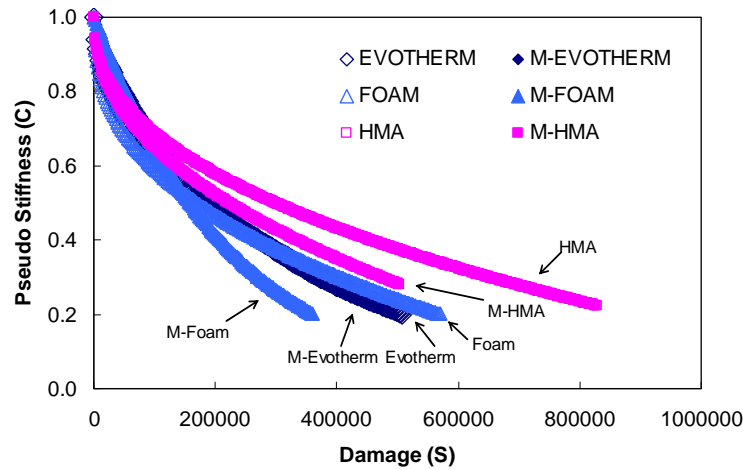


Figure 4.2 Damage characteristic curves of Evotherm, foamed, and HMA mixtures with and without moisture conditioning. (M in the legend indicates moisture-conditioned.)

Figure 4.2 indicates that, although the HMA mixture has the highest C versus S curves, the change in the WMA Foam is the greatest between the moisture-conditioned and nonmoisture-conditioned specimens. WMA Evotherm seems to have the least moisture susceptibility of the three mixtures.

In addition, in APPENDIX C and APPENDIX D, digital image analysis was applied to evaluate the moisture susceptibility of the WMA mixtures. It was found that the fatigue life predicted by the S-VECD models has a strong correlation with the percentage of stripping determined from specimen surfaces that were fractured during the cyclic direct tension testing of the HMA and WMA mixtures with various asphalt contents. Also, fatigue life ratios obtained from the S-VECD model combined with layered viscoelastic analysis were determined to be the most sensitive indicators for moisture susceptibility. In APPENDIX E, a new moisture conditioning method using the Moisture-Induced Stress Tester (MIST) was developed. By implementing the universal conditions with MIST, it can cause the same damage characteristics and stripping as those of the AASHTO T 283 procedure for mechanical test specimens.

4.3 Summary

Based on the laboratory test results for the specimens with and without moisture conditioning, the conclusions with regard to the moisture susceptibility of the mixtures are summarized as follows:

- Based on the dynamic modulus test results, the HMA mixture showed higher dynamic modulus values with moisture conditioning and without moisture conditioning than the two WMA mixtures. The dynamic modulus values of the WMA Foam mixture suggest that WMA Foam was more sensitive to aging than the WMA Evotherm and HMA mixtures.

- In terms of the fatigue properties due to moisture damage, the S-VECD analysis results suggest that the moisture susceptibility of the WMA Evotherm mixtures is the least among all the mixtures.

CHAPTER 5 DEVELOPMENT OF THE WMA MIXTURES’ INCORPORATION INTO THE AASHTOWARE PAVEMENT ME PROGRAM

5.1 Introduction

5.1.1 Overview

The objective of this chapter is to develop recommendations to incorporate WMA mixtures into the AASHTOWare Pavement ME program. The following NCDOT projects established the local asphalt materials and traffic databases and developed the local calibration factors:

- HWY 2003-09: *Typical Dynamic Moduli for North Carolina Asphalt Concrete Mixes*
- HWY-2007-07: *Local Calibration of the MEPDG for Flexible Pavement Design*
- HWY-2008-11: *Development of Traffic Data Input Resources for the Mechanistic Empirical-Pavement Design Process*

Because the use of WMA mixtures has become increasingly widespread, and because the properties of WMA mixtures and HMA mixtures differ, this study was undertaken to determine the input parameters of WMA mixtures for the Pavement ME program. The studies (presented in previous chapters) of the aging and moisture effects on the performance of WMA mixtures were carried out mostly at the material level. The comparisons and conclusions presented in this chapter, by contrast, were made based on the structural analysis and utilizations inherent of the Pavement ME program.

Also, it has been noted that aging occurs mainly in the top few inches of the pavement. Bottom-up cracking, however, initiates from the bottom of the pavement. Thus, the effects of aging on the bottom-up fatigue cracking predictions in the Pavement ME program are not included in this study. Also, according to previous studies, the effects of moisture on rutting are not significant; therefore, the effects of moisture on the rut depth predictions in the Pavement ME likewise are not part of this project.

This chapter presents a study of the prediction models in the Pavement ME program that may be applicable for WMA mixtures. In terms of aging, GAS model predictions are compared against the measured results and discussed with regard to the WMA mixtures. Also, rutting and fatigue prediction models are evaluated for the possible incorporation of WMA mixtures. Because the moisture effects on asphalt materials are not evaluated explicitly by models in the Pavement ME program and are taken into account via local calibration factors, the effects of moisture on the WMA mixtures are discussed in this chapter to ensure that the performance predictions obtained from the Pavement ME program for WMA mixtures are close to those obtained in practice. Finally, Pavement ME program input recommendations that account for the behavior of WMA materials are given at the end of the chapter.

5.1.2 The Pavement ME Program

5.1.2.1 Hierarchical Materials Data Input Levels

Three types of input are recommended for adoption in the Pavement ME program, based on requirements of the project in design and the data that users can obtain for the materials.

- Level 1 input reflects the designers' high degree of knowledge of the materials in the pavement design. Level 1 input parameters are measured either directly from the site or near the site under study, or determined through laboratory testing.
- Level 2 input reflects a medium level of knowledge of the materials in the pavement design. Level 2 input parameters are determined based on state-wide averages or estimated based on known parameters through statistical correlations and relationships.
- Level 3 input reflects the least amount of knowledge about the materials in the pavement design. Level 3 input parameters are estimated based on regional values or national values, i.e., the Pavement ME default values.

Table 5.1 presents the required data for the different input levels for asphalt binders and asphalt mixtures in the Pavement ME program. For this study, only Level 1 input was used.

Table 5.1 Pavement ME Inputs Required for Asphalt Binder and Asphalt Concrete

Material	Input Level	Data Required	Allowable Range	
HMA Mixture	Level 1	Dynamic modulus, psi. Min. 3 temperatures and 3 frequencies; max. 8 temperatures and 6 frequencies	NA	NA
	Levels 2 and 3	Cumulative percentage retained on 3/4" sieve	0	100
		Cumulative percentage retained on 3/8" sieve	0	100
		Cumulative percentage retained on #4 sieve	0	100
		Percentage passing #200 sieve	0	100
	Levels 1, 2, and 3	Reference temperature (°F)	50	104
		As-built effective binder content by volume (%)	2	20
		As-built air voids (%)	0	20
		As-built total unit weight (pcf)	100	200
		Poisson's ratio	0.2	0.45
Thermal conductivity of asphalt (BTU/hr-ft-°F)		0.5	1	
	Heat capacity of asphalt (BTU/lb-ft)	0.1	0.5	
Asphalt Binder	Levels 1 and 2	Option 1: Shear modulus, Pa Phase angle for RTFO binder Angular frequency of 10 radians/sec Min. 3 temperatures	NA	NA
		Option 2: Temperature (°F) at softening point = 13000 P Absolute viscosity (P) at 140°F Kinematic viscosity (CS) at 275°F Specific gravity at 77°F, penetration/ optional Brookfield viscosity/ optional	NA	NA
	Level 3	Superpave binder grade <i>or</i> viscosity grade <i>or</i> penetration grade	NA	NA

5.1.2.2 Overview of the Pavement ME Procedure

In order to use the Pavement ME program to obtain reliable design results, it is necessary to understand the program's step-by-step design procedure. Figure 5.1 presents a flow chart showing the overall procedure for using the Pavement ME program. The first step requires users to input traffic, materials, and climatic data for the project. In the second step, users need to assume a certain pavement trial design structure based on a combination of engineering knowledge, experience, and pre-Pavement ME program design procedures. The third step involves executing the Pavement ME program to predict pavement performance parameters at the end of a desired design life. The predicted performance parameters are then compared to criteria set by the agency for various performance measures. If the predicted performance parameters pass the pre-set criteria, the trial design structure becomes a candidate design structure. If any of the predicted performance parameters fail the performance criteria, users should modify the first trial design structure and repeat the steps until a structure that satisfies all criteria is found.

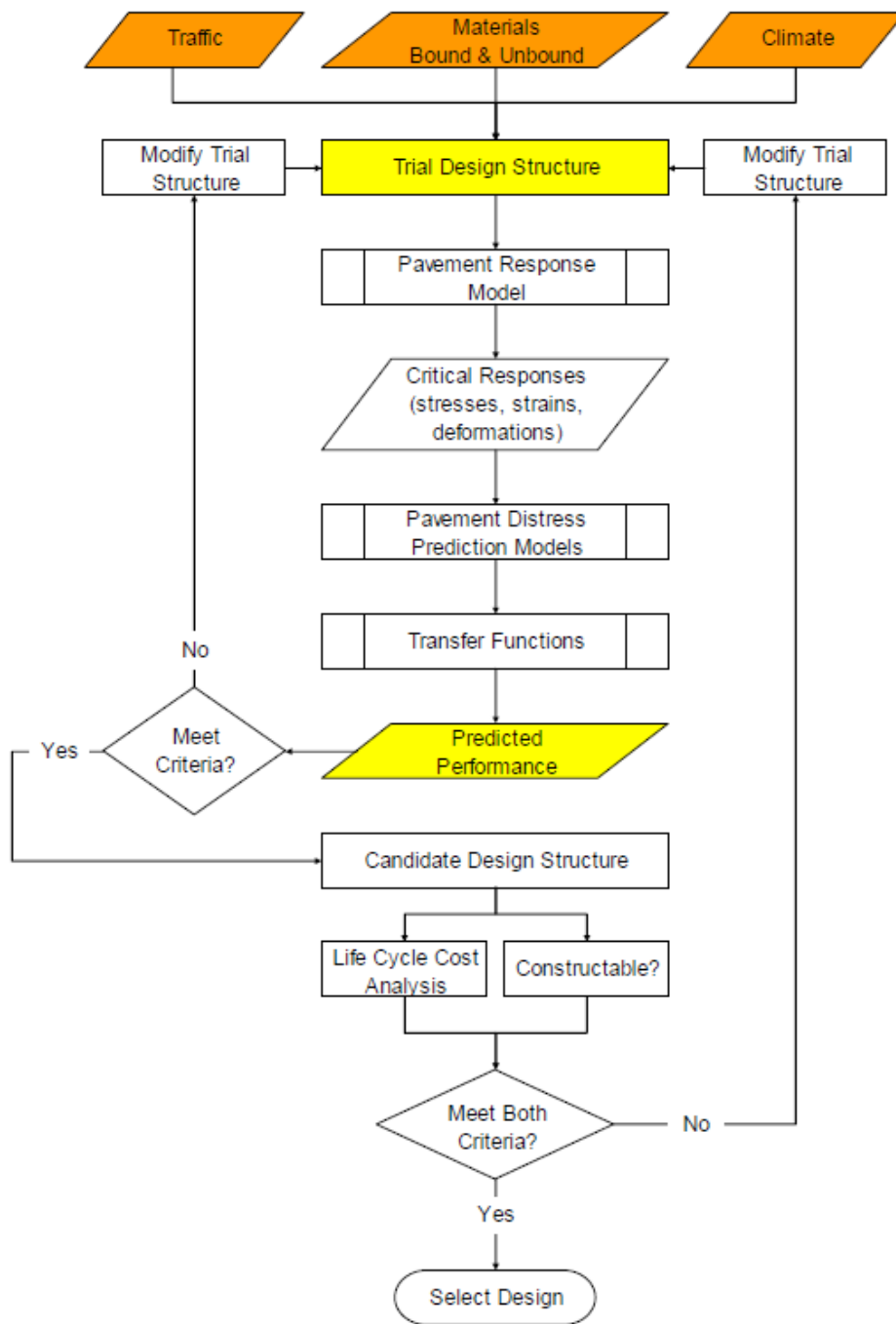


Figure 5.1 Overview of Pavement ME design procedure.

5.2 Study for Aging in Pavement ME and Global Aging System (GAS) Model

5.2.1 Introduction to GAS model and Points to Claim

The GAS model was first presented by Mirza and Witczak in 1995 to predict the dynamic modulus of an asphalt mixture after aging at a certain depth of the pavement. The model is based on the regression of a large number of data points. The GAS model has been incorporated into the Pavement ME program and has been used in numerous research studies. In order to reflect the different aging propensities of different WMA mixtures in the Pavement ME program, it is necessary to examine the GAS model and the results it provides. The GAS model uses a sigmoidal function to describe the dynamic modulus curve, and the shift factor is calculated based on the viscosity of the binder. By predicting the viscosity of the binder at one specific time and one specific depth of the pavement, the dynamic modulus of the particular mixture in the pavement can be predicted. The following paragraphs describe the procedures required to implement the GAS model.

The viscosity levels of short-term aged binder must either be measured or calculated. Although the Pavement ME program requires the binder viscosity input to be at the time of the mix/lay-down or after rolling thin-film oven (RTFO) conditioning, the model in this project uses binder that has been extracted and recovered from short-term aging specimens after those specimens have undergone dynamic modulus testing. There are two reasons that it is necessary to use such binders. First, the focus of this study is WMA mixtures, and it has been pointed out that there are some differences between WMA mixtures and HMA mixtures in terms of aging, which means RTFO conditioning may not represent the short-term aging process of WMA binders. Second, WMA binders sometimes contain additives, as is the case with Evotherm 3G; hence, conditioning only virgin binder is not sufficient. Furthermore, these short-term aging mixtures contain RAP binder, and therefore, the extracted and recovered binder reflects the status of the actual binder in the specimens after short-term aging conditioning. By converting the binder stiffness data at each temperature into viscosity data using Equation (6.1), and using linear regression to fit the parameters, A and VTS in Equation (6.2), the relationship between binder viscosity and temperature can be established.

$$\eta = \frac{G^*}{10} \left(\frac{1}{\sin \delta} \right)^{4.8628} \quad (6.1)$$

$$\log \log \eta = A + VTS \log T_R \quad (6.2)$$

where

G^* = binder complex shear modulus, Pa,

δ = binder phase angle, degree,

η = viscosity, Pa·s, with a maximum value of 2.7×10^{10} Poise,

T_R = temperature in Rankine at which the viscosity was estimated, and

A, VTS = regression parameters.

After obtaining the parameters using Equation (6.2), the viscosity can be calculated at any temperature. The laboratory dynamic modulus data then can be shifted into a smooth mastercurve using Equation (6.3).

$$\log(E^*) = \delta + \frac{\alpha}{1 + e^{\beta + \gamma(\log(t) - c[\log(\eta) - \log(\eta_{t_r})])}} \quad (6.3)$$

$$t_r = \frac{t}{a(T)} \quad (6.4)$$

$$\log[a(T)] = \log(t) - c[\log(\eta) - \log(\eta_{t_r})] \quad (6.5)$$

where

- E^* = dynamic modulus, psi,
- t = time of loading (pulse time), s,
- η = viscosity at temperature of measurement, CPoise,
- η_{t_r} = viscosity at reference temperature, CPoise,
- $\alpha, \beta, \delta, \gamma, c$ = mixture-specific fitting parameters,
- t_r = reduced loading time, s, and
- $a(T)$ = shift factor.

The parameters, $\alpha, \beta, \delta, \gamma$, and c , which define the time-temperature dependency of the dynamic modulus over the design life, are obtained by numerical optimization. The dynamic modulus mastercurves of the short-term aging specimens can be plotted using Equations (6.3) through (6.5).

Equations (6.6) and (6.7) can be used to predict the viscosity of the binders for the long-term aging predictions.

$$\log \log(\eta_{aged}) = \frac{\log \log(\eta_{t=0}) + At}{1 + Bt} \quad (6.6)$$

$$\eta_{t,z} = \frac{\eta_t(4 + E) - E(\eta_{t=0})(1 - 4z)}{4(1 + Ez)} \quad (6.7)$$

where

$$A = 0.004166 + 1.41213(C) + (C) \log(Maat) + (D) \log \log(\eta_{t=0}),$$

$$B = 0.197725 + 0.068384 \log(C),$$

$$C = 10^{274.4996 - 193.831 \log(T_R) + 33.9366 \log(T_R)^2},$$

$$D = -14.5521 + 10.476622 \log(T_R) - 1.88161 \log(T_R)^2,$$

$$\eta_{aged} = \text{aged viscosity, cP},$$

$$\eta_{t=0} = \text{viscosity at mix/lay-down, cP},$$

$$T_R = \text{temperature in Rankine},$$

t = time in months,
 $\eta_{t,z}$ = aged viscosity at time t , and depth z , cP,
 η_t = aged surface viscosity, cP,
 $E = 23.83e^{(-0.0308Maat)}$, and
 $Maat$ = mean annual air temperature, °F.

Once the binder viscosity is predicted, the dynamic modulus value of an aged mixture at any temperature and any depth can be predicted. Equation (6.3) is still used and is re-presented here as Equation (6.8).

$$\log(E^*) = \delta + \frac{\alpha}{1 + e^{\beta + \gamma(\log(t) - c[\log(\eta_{t,z}) - \log(\eta_r)])}} \quad (6.8)$$

where

$\eta_{t,z}$ = aged viscosity at time t and depth z , CPoise, and
 η_r = viscosity at reference temperature at STA, CPoise.

Note that in Equation (6.8), α , β , δ , γ , and c are the same values as used in Equation (6.3), and no numerical optimization is needed.

It is extremely important to present the correct way to utilize the GAS model here, because it has been used improperly in many studies. The correct temperature range that is needed to apply the GAS model for the prediction of dynamic modulus values and the viscosity of aged binders is from 25°C to 135°C. For example, Equation (6.6) (the so-called ‘surface aging model’) was derived from a total of 1,382 data points from 16 test roads and 149 test sections at 25°C, 60°C, and 135°C. However, the prediction results for the binder and mixtures at temperatures below 25°C are unreasonable and unexpected.

Figure 5.2 presents the changes in the predicted Evotherm binder stiffness values as the aging time and depth of the pavement increase. Figure 5.2 shows that, within the temperature range, the viscosity of the binder at shallow depths increased as the aging time increased, and the effect of depth on aging is significant. However, the viscosity values of the binder at temperatures below 25°C increased extremely fast, and the binder viscosity limit was reached in an unreasonably short time; so, the effect of depth at those temperatures is no longer significant.

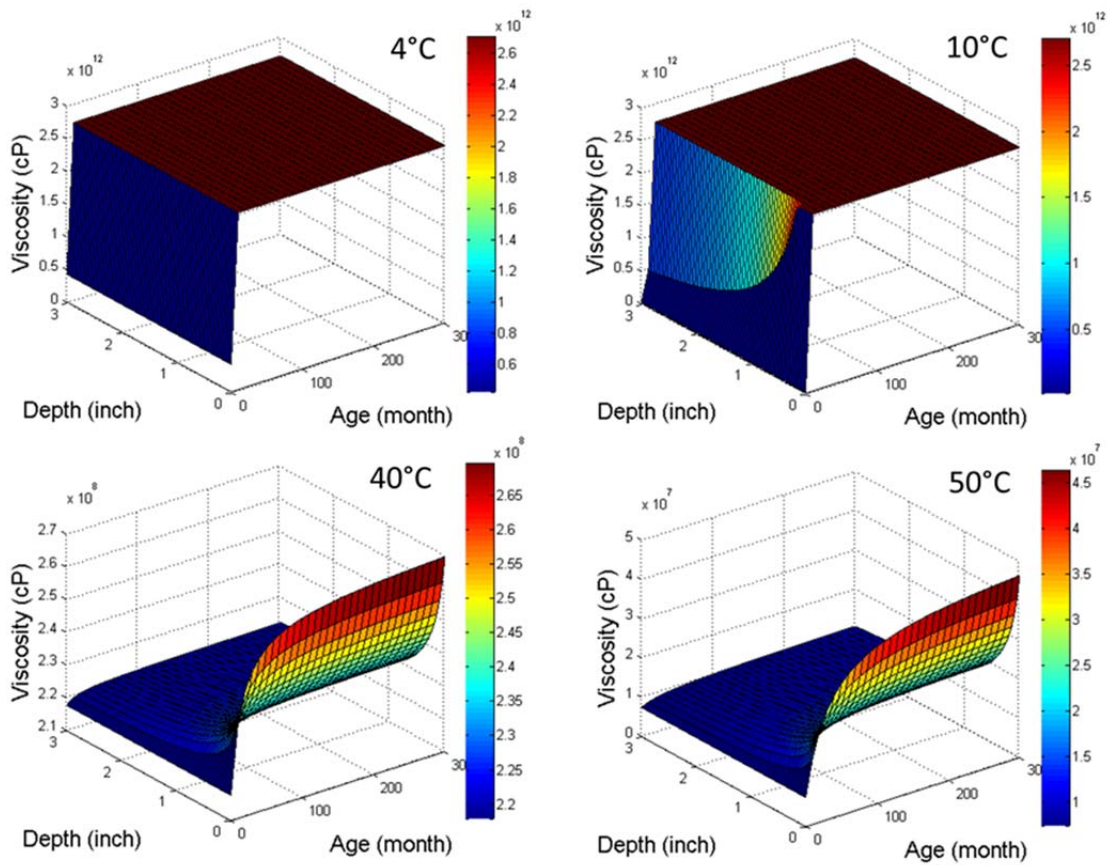


Figure 5.2 Changes in viscosity of Evotherm binder with aging time and depth of pavement at different temperatures.

Figure 5.3 presents a comparison between the RS9.5C WMA Evotherm dynamic modulus values at 0.25-inch depth after eight years of aging that were predicted using the GAS model and the measured long-term aging dynamic modulus values (LTA3, subjected to AASHTO R30). Figure 5.3 (a) and Figure 5.3 (b) present the predicted dynamic modulus values within the temperature range and outside the temperature range, respectively. Table 5.2 shows the values of the data points plotted in Figure 5.3.

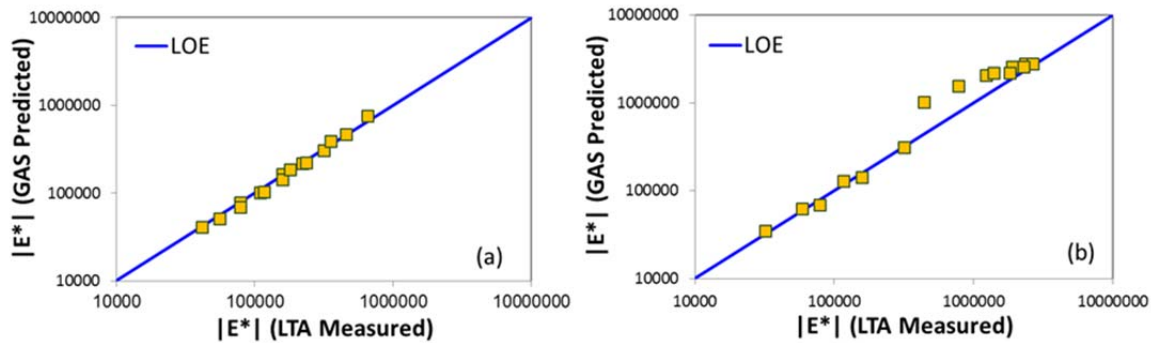


Figure 5.3 Comparison between GAS model-predicted and measured long-term aging dynamic modulus values: (a) data points all within temperature range and (b) some data points out of temperature range.

Table 5.2 Comparison between GAS Model-Predicted and Measured Long-term Aging Dynamic Modulus Values: (a) Comparison with Data Points All within Temperature Range and (b) Comparison with Some Data Points out of Temperature Range

Temp. (°C)	Pulse Time (s)	R30 (psi)	STA (psi)	GAS (psi)
50	0.1	158085	99480	165056
50	1	78489	50455	78268
50	10	41239	29552	41376
45	0.1	221598	137625	219567
45	1	109486	66657	102245
45	10	55582	36535	51496
40	0.1	316717	197956	309194
40	1	158414	92858	143639
40	10	78646	47654	69058
35	0.1	455980	292904	468046
35	1	235589	136181	223691
35	10	116492	66040	104095
25	0.1	912540	650859	1286786
25	1	533417	326905	782691
25	10	281323	152396	408936

(a)

Temp. (°C)	Pulse Time (s)	R30 (psi)	STA (psi)	GAS (psi)
55	0.1	116014	75130	129085
55	1	58548	40148	62854
55	10	31941	25012	34828
40	0.1	316799	197954	309194
40	1	158537	92854	143639
40	10	78655	47656	69058
20	0.1	1234507	938028	2055847
20	1	783532	512969	1547060
20	10	442877	248095	1014289
5	0.1	2359980	2065319	2815093
5	1	1902140	1547356	2552809
5	10	1401389	1009890	2175534
0	0.1	2690167	2408587	2815093
0	1	2302107	1965419	25528089
0	10	2360852	1435119	2175534

(b)

Based on Figure 5.3 and Table 5.2, when the data points were calculated within the temperature range, the GAS model could provide results from the R30 mix tests very well. However, the data points for temperatures below 25°C did not lead to good predictions. Therefore, in order to make reliable predictions using the GAS model, the model must be implemented within the appropriate temperature range, as it was presented first in 1995.

Another point to be made is that it is appropriate to use the predicted dynamic modulus, but the mastercurve should not be used. That is, the Pavement ME does not really use the mastercurve. Instead, the predicted dynamic modulus values should be used and compared at different temperatures and frequencies directly. However, because data at low temperatures must be used in order to plot an entire mastercurve, and based on the temperature limit of the GAS model, the prediction results at low temperatures are not available. Hence, any comparison using mastercurves cannot be accurate.

Figure 5.4 presents the mastercurves of the predicted dynamic modulus values of WMA Evotherm at eight years and a depth of 0.25 inch. According to Figure 5.3 (a), at eight years and 0.25-inch depth, although the predicted data points derived using the GAS model collapse with the lab-measured data at the right temperature, because the mastercurve contains data points out of the temperature range, a big difference is observed between the mastercurves. Thus, it is inappropriate to calculate the equivalent time of the GAS model to laboratory-conditioned samples or field cores by checking the collapse of the dynamic modulus mastercurves obtained from measurements and mastercurves predicted from the GAS model, as has been reported in some articles.

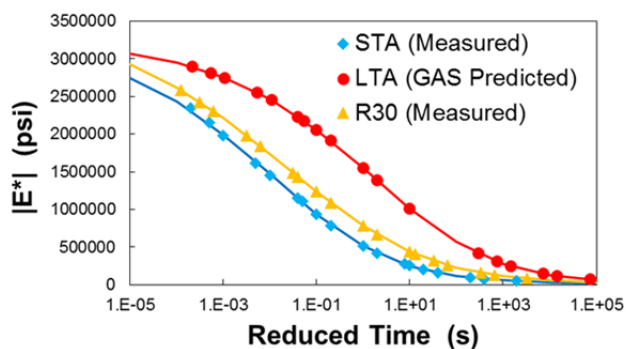


Figure 5.4 Comparison of the mastercurves of laboratory-measured data and GAS model prediction results.

5.2.2 Utilization of GAS Model for WMA Mixtures in Pavement ME

Table 5.3 presents the results obtained using the GAS model to predict RS9.5C WMA Evotherm dynamic modulus values at nine years and 0.25 inch below the surface of the pavement. Different predicted values can be obtained by changing the aging time, and then the residual, which is the absolute value of the difference between the dynamic modulus values of the GAS model predictions and the laboratory measurements in logarithmic scale, can be calculated. The minimum sum of error can be found by changing the aging time while controlling the depth of the pavement. In this way, the equivalent number of years of the GAS model predictions for long-term oven aging conditioning can be obtained for a single depth measurement.

Table 5.3 Predicted Values from GAS Model

Temp.	Pulse Time	R30	STA	GAS	Residual
°C	s	psi	psi	psi	$ \log(R30)-\log(GAS) $
50	0.1	158085	99480	166572	0.0227
50	1	78485	50455	78925	0.0024
50	10	41239	29552	41654	0.0043
45	0.1	221598	137625	221253	0.0007
45	1	109486	66657	103001	0.0265
45	10	55582	36535	51814	0.0305
40	0.1	316717	197956	311274	0.0075
40	1	158417	92858	144631	0.0395
40	10	78646	47654	69482	0.0538
35	0.1	455980	292904	471114	0.0142
35	1	235589	136181	225325	0.0193
35	10	116497	66040	104828	0.0458
30	0.1	651957	438528	767570	0.0709
30	1	355164	208379	399205	0.0508
30	10	179063	97480	187918	0.0210
Total Error					0.4100

Table 5.4 presents the equivalent time of the GAS model for the laboratory conditioning method for different mixtures at different depths. For the HMA mix, the equivalent time is 26 years at the surface, which is reasonable because eight days of conditioning in the oven is supposed to simulate field aging for around 20 years. At deeper pavement depths, the GAS model has difficulty predicting values as high as those of the LTA3 mix, which indicates that the GAS model was designed based on the theory that aging occurs only at the pavement surface. However, for the WMA mixtures, the equivalent times for the GAS model and the R30 mix are much shorter than for the HMA mix. The WMA Evotherm and WMA Foam times also differ. Note that the binders used here were extracted and recovered from short-term aged specimens, rather than RTFO-conditioned virgin binder.

Table 5.4 GAS Model Predictions of Equivalent Number of Years for Aging for Measured Long-term Aging

	Depth (inch)	Equivalent Time (year)	
		LTA3	LTA1
HMA	0	26	0
	0.25	infinity	0
	0.5	infinity	0
Evotherm	0	1.8	0.4
	0.25	9	1
	0.5	infinity	1.8
Foam	0	14	0.8
	0.25	infinity	3
	0.5	infinity	10

In order to investigate the efficiency of the GAS model in the Pavement ME program for WMA mixtures, the aging process of the WMA mixtures and HMA control mixture was studied. Assume that for LTA3, eight days of laboratory oven conditioning represents 15 years of aging in the field, regardless of the variability of environmental factors; also, simply assume that LTA1 represents five years of aging in the field. The rate of aging or *aging rate* (AR) is one way to evaluate aging. The AR is the ratio of the modulus at a certain time to the modulus at a short-term aging time. The ARs of the WMA mixtures and HMA mixture were plotted over time. For the GAS model predictions, different types of binder were used, i.e., extracted and recovered binder from STA samples and three types of North Carolina default binder. Figure 5.5 presents the increase in AR obtained from both laboratory measurements and GAS model predictions. Note that *ARL* in the plots means aging rate in logarithmic scale, which can be calculated as Equation (6.9).

$$ARL = \frac{\left| \log \left(\left| E_{aged}^* \right| \right) \right|}{\left| \log \left(\left| E_{STA}^* \right| \right) \right|} \quad (6.9)$$

Figure 5.5 illustrates that by using extracted and recovered binder data in the GAS model, not only are the mixtures different, but the predicted results derived from the GAS model are different. The slight differences between WMA Foam and WMA Evotherm in terms of aging can be observed, and the lower AR of the HMA mixture can be represented. The differences between results derived from the laboratory conditioning and the GAS model cannot be ignored, and it should also be noted that the number of years reflected at the x-axis of the plots is based only on

an engineering assumption. However, in practice, technicians tend to use existing North Carolina binder data rather than extracted and recovered tested binder data.

Figure 5.5 (c) to (h) present plots of the GAS model predictions and the North Carolina binder data. The figures indicate that once the same binder data are employed for the three mixtures, the differences among the ARs of the three mixtures predicted by the GAS model are minor. Among the binders adopted, PG64-22, PG70-22, and PG76-22, it can be observed that PG70-22, the virgin binder used in the three mixtures, has better aging behavior. For the case of the HMA mixture with PG70-22 binder, the prediction results are the closest to the laboratory measurements. For the WMA mixtures, the AR trend can generally be maintained by using PG70-22 binder. Therefore, although no binders were extracted and recovered from the WMA STA samples, employing North Carolina PG70-22 binder can be an alternative way.

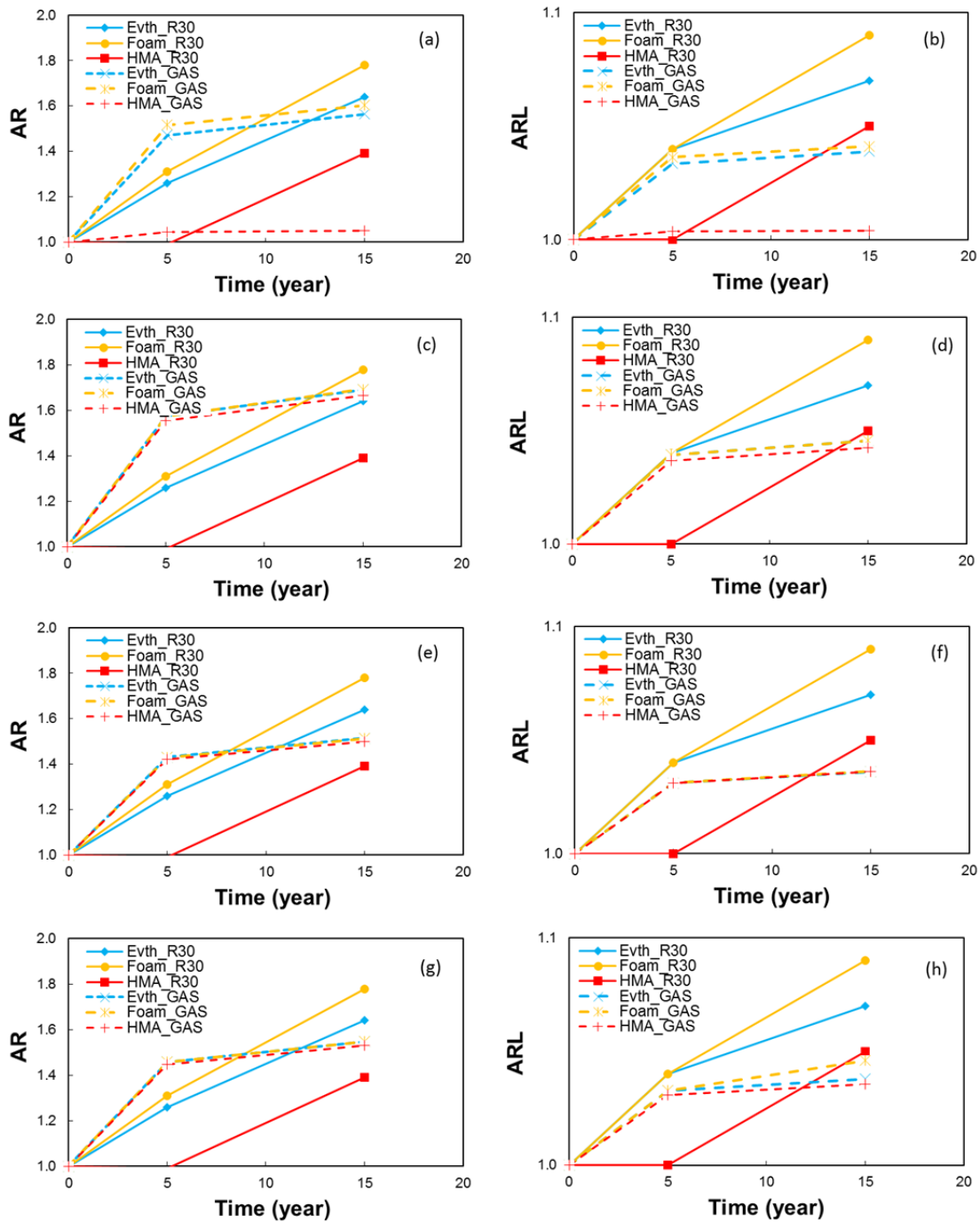


Figure 5.5 Aging rates of different mixtures obtained from laboratory measurements and GAS model predictions using different binders: (a), (b): GAS model-predicted using extracted and recovered binder, (c), (d): GAS model-predicted using NC PG64-22 binder, (e), (f): GAS model-predicted using NC PG70-22 binder, and (g), (h): GAS model-predicted using NC 76-22 binder.

5.3 Study of Permanent Deformation Predictions in Pavement ME

5.3.1 Aging Effect on Permanent Deformation Predictions for WMA Mixtures in Pavement ME

5.3.1.1 Aging Effect on Permanent Strain in Pavement ME

As shown in previous chapters, the aging behavior of WMA mixtures is different from that of HMA conventional mixtures; therefore, the properties that are related directly or indirectly to aging may also differ. Although aging may cause an increase in the stiffness of a mixture and rutting depth is affected by the stiffness of that mixture, it is still necessary to study the aging effect on permanent deformation and on the prediction model in the Pavement ME program.

Given the large numbers of figures and tables that would be applicable to this section, most of the figures and tables are contained in APPENDIX A and APPENDIX B. APPENDIX A presents analysis mainly about permanent strain, and APPENDIX B presents analysis mainly about the permanent strain and resilient strain ratios that play an important role in the rutting model in the current Pavement ME program.

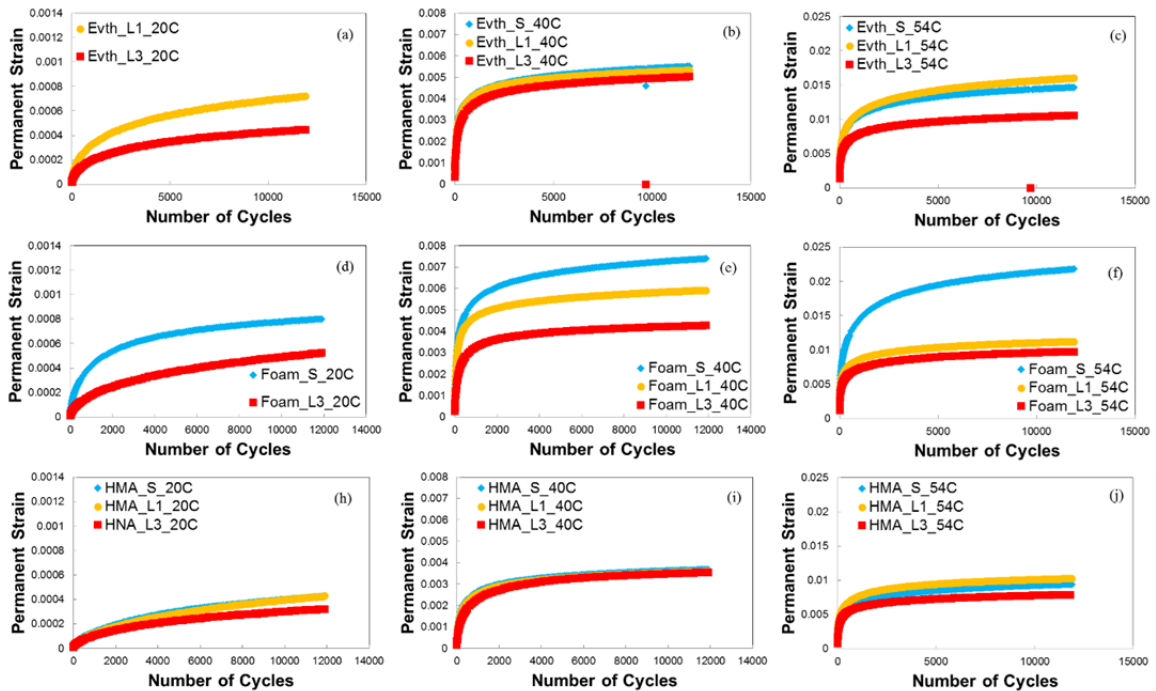


Figure 5.6 Comparison of permanent strain with different aging levels in arithmetic scales.

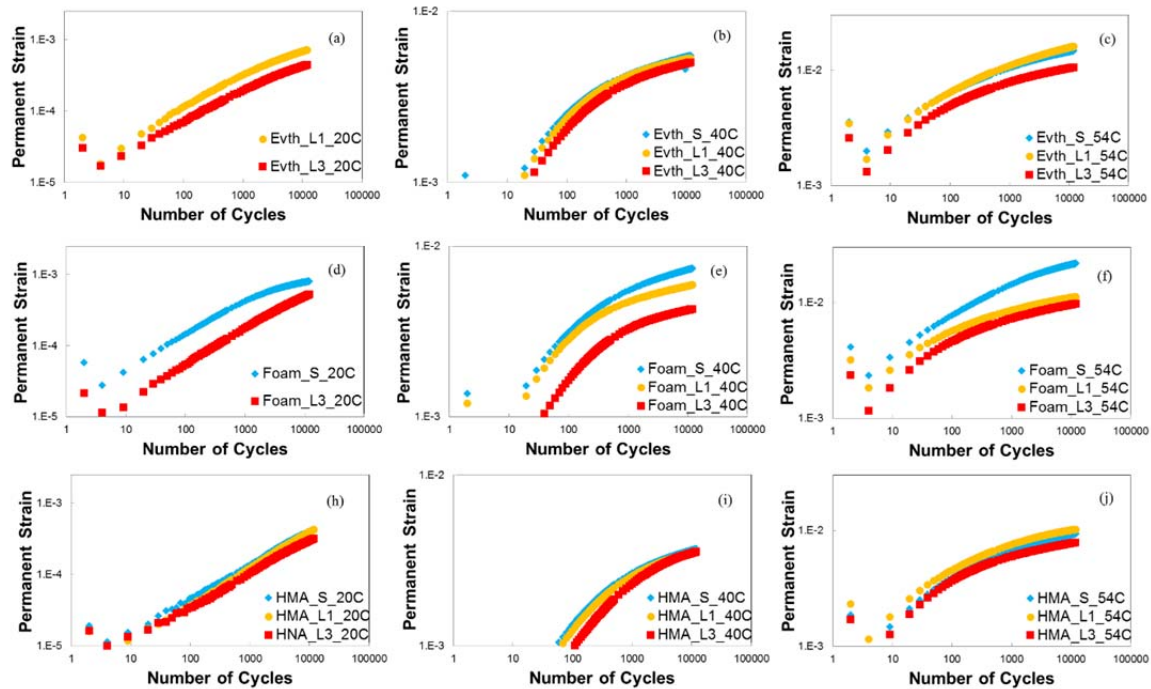


Figure 5.7 Comparison of permanent strain with different aging levels in log-log scale.

Figure 5.6 and Figure 5.7 present the aging effects on rutting for the different test mixtures. According to these figures, the differences in permanent strain levels among the different aging levels are not significant for the HMA mix, and the WMA Evotherm mixture has the second smallest difference among all the mixtures. Statistical analysis was performed to evaluate the differences quantitatively. All the experimental tests were conducted with two replicates for each experiment, and the results of the two replicate tests were averaged if the variability was acceptable. Note that some of the replicate data were removed based on reasonable engineering judgment. One-tail t-tests with two-sample equal variance were conducted for the different treatment levels.

Table 5.5, Table 5.6, and Table 5.7 present the p-values for the t-tests. Generally, the critical p-value is 0.05; that is, if the p-value was smaller than 0.05, then the two samples were considered to be statistically significantly different. Otherwise, the two samples were not considered to be statistically significantly different. Table 5.5 to Table 5.7 show that, in most of the cases, and taking into consideration engineering judgment based on the figure data, the permanent strain levels of the WMA Evotherm mix and the HMA control mix were not significantly different for the different aging levels, except at 54°C and after long-term aging Level 3 conditioning, which represent extreme pavement conditions.

Table 5.5 T-test results of permanent strain of WMA Evotherm for different aging levels: (a) at 20°C, (b) at 40°C, and (c) at 54°C.

(a)

Permanent Strain @ 5,000 cycles_Evth_20°C					
arithmetic scale			log-log scale		
ST	L1	L3	ST	L1	L3
	0.000565	0.000279			-3.55458
		0.000421			-3.37622
P-values					
ST vs. L1	L1 vs. L3	L3 vs. ST	ST vs. L1	L1 vs. L3	L3 vs. ST
Permanent Strain @ 8,500 cycles_Evth_20°C					
arithmetic scale			log-log scale		
ST	L1	L3	ST	L1	L3
	0.000659	0.000327			-3.485
		0.000487			-3.31262
P-values					
ST vs. L1	L1 vs. L3	L3 vs. ST	ST vs. L1	L1 vs. L3	L3 vs. ST
Permanent Strain 3@ 12,000 cycles_Evth_20°C					
arithmetic scale			log-log scale		
ST	L1	L3	ST	L1	L3
	0.000719	0.000364		-3.14308	-3.43856
		0.000529			-3.27673
P-values					
ST vs. L1	L1 vs. L3	L3 vs. ST	ST vs. L1	L1 vs. L3	L3 vs. ST

(b)

Permanent Strain @ 5,000 cycles_Evth_ 40°C					
arithmetic scale			log-log scale		
ST	L1	L3	ST	L1	L3
0.005859	0.004725	0.004921	-2.23215	-2.32556	-2.30798
0.004313	0.005224	0.004373	-2.36522	-2.28202	-2.35924
P-values					
ST vs. L1	L1 vs. L3	L3 vs. ST	ST vs. L1	L1 vs. L3	L3 vs. ST
0.451673	0.234636	0.322873	0.474277	0.234352	0.33637
Permanent Strain @ 8,500 cycles_Evth_ 40°C					
arithmetic scale			log-log scale		
ST	L1	L3	ST	L1	L3
0.006158	0.004939	0.005152	-2.21055	-2.30632	-2.28806
0.004538	0.005447	0.004618	-2.34317	-2.26383	-2.33559
P-values					
ST vs. L1	L1 vs. L3	L3 vs. ST	ST vs. L1	L1 vs. L3	L3 vs. ST
0.436149	0.245117	0.320744	0.458421	0.244863	0.334406
Permanent Strain @ 12,000 cycles_Evth_ 40°C					
arithmetic scale			log-log scale		
ST	L1	L3	ST	L1	L3
0.006346	0.005066	0.005296	-2.1975	-2.29535	-2.27605
0.004683	0.005583	0.00477	-2.32943	-2.25315	-2.32151
P-values					
ST vs. L1	L1 vs. L3	L3 vs. ST	ST vs. L1	L1 vs. L3	L3 vs. ST
0.423551	0.256143	0.31801	0.445268	0.255943	0.331522

(c)

Permanent Strain @ 5,000 cycles_ Evth_54°C					
arithmetic scale			log-log scale		
ST	L1	L3	ST	L1	L3
0.014214	0.013652	0.009605	-1.84728	-1.86481	-2.01748
0.013315	0.014835	0.009755	-1.87567	-1.82872	-2.01076
P-values					
ST vs. L1	L1 vs. L3	L3 vs. ST	ST vs. L1	L1 vs. L3	L3 vs. ST
0.292715	0.008323	0.006116	0.293729	0.005908	0.004503
Permanent Strain @ 8,500 cycles_ Evth_54°C					
arithmetic scale			log-log scale		
ST	L1	L3	ST	L1	L3
0.01506	0.014671	0.010127	-1.82217	-1.83353	-1.99454
0.01417	0.015965	0.010334	-1.84863	-1.79682	-1.98574
P-values					
ST vs. L1	L1 vs. L3	L3 vs. ST	ST vs. L1	L1 vs. L3	L3 vs. ST
0.232496	0.008094	0.005343	0.232848	0.00572	0.00401
Permanent Strain @ 12,000 cycles_ Evth_54°C					
arithmetic scale			log-log scale		
ST	L1	L3	ST	L1	L3
0.015559	0.015307	0.010439	-1.80802	-1.81511	-1.98134
0.01468	0.01667	0.010686	-1.83328	-1.77807	-1.9712
P-values					
ST vs. L1	L1 vs. L3	L3 vs. ST	ST vs. L1	L1 vs. L3	L3 vs. ST
0.198026	0.007951	0.004947	0.197741	0.005615	0.003783

Table 5.6 T-test results of permanent strain of WMA Foam for different aging levels: (a) at 20°C, (b) at 40°C, and (c) at 54°C.

(a)

Permanent Strain @ 5,000 cycles_Foam_ 20°C					
arithmetic scale			log-log scale		
ST	L1	L3	ST	L1	L3
0.000642		0.000386	-3.1928		-3.41392
0.000729		0.000357	-3.13699		-3.44793
P-values					
ST vs. L1	L1 vs. L3	L3 vs. ST	ST vs. L1	L1 vs. L3	L3 vs. ST
		0.010507			0.007378
Permanent Strain @ 8,500 cycles_Foam_ 20°C					
arithmetic scale			log-log scale		
ST	L1	L3	ST	L1	L3
0.000701		0.000479	-3.15449		-3.3195
0.000815		0.000444	-3.08859		-3.35298
P-values					
ST vs. L1	L1 vs. L3	L3 vs. ST	ST vs. L1	L1 vs. L3	L3 vs. ST
		0.019331			0.014186
Permanent Strain @ 12,000 cycles_Foam_ 20°C					
arithmetic scale			log-log scale		
ST	L1	L3	ST	L1	L3
0.00074		0.000543	-3.13106		-3.26481
0.000863		0.000503	-3.06396		-3.2985
P-values					
ST vs. L1	L1 vs. L3	L3 vs. ST	ST vs. L1	L1 vs. L3	L3 vs. ST
		0.025282			0.01957

(b)

Permanent Strain @ 5,000 cycles_ Foam_ 40°C					
arithmetic scale			log-log scale		
ST	L1	L3	ST	L1	L3
0.006777	0.005043	0.003947	-2.16899	-2.29734	-2.40375
	0.005728	0.004389		-2.24198	-2.35762
P-values					
ST vs. L1	L1 vs. L3	L3 vs. ST	ST vs. L1	L1 vs. L3	L3 vs. ST
	0.048165			0.045576	
Permanent Strain@ 8,500 cycles_ Foam_ 40°C					
arithmetic scale			log-log scale		
ST	L1	L3	ST	L1	L3
0.007157	0.005277	0.004126	-2.14526	-2.2776	-2.38444
	0.005954	0.004543		-2.22517	-2.34261
P-values					
ST vs. L1	L1 vs. L3	L3 vs. ST	ST vs. L1	L1 vs. L3	L3 vs. ST
	0.042187			0.03949	
Permanent Strain @ 12,000 cycles_ Foam_ 40°C					
arithmetic scale			log-log scale		
ST	L1	L3	ST	L1	L3
0.007397	0.005452	0.004237	-2.13095	-2.26344	-2.37289
	0.00608	0.004636		-2.21607	-2.33385
P-values					
ST vs. L1	L1 vs. L3	L3 vs. ST	ST vs. L1	L1 vs. L3	L3 vs. ST
	0.035082			0.032923	

(c)

Permanent Strain @ 5,000 cycles_ Foam_54°C					
arithmetic scale			log-log scale		
ST	L1	L3	ST	L1	L3
0.019476	0.009797	0.008843	-1.71051	-2.0089	-2.05341
0.019902	0.009954	0.008607	-1.70111	-2.00199	-2.06516
P-values					
ST vs. L1	L1 vs. L3	L3 vs. ST	ST vs. L1	L1 vs. L3	L3 vs. ST
0.000267	0.007415	0.000246	0.000189	0.007821	0.000226
Permanent Strain @ 8,500 cycles_ Foam_54°C					
arithmetic scale			log-log scale		
ST	L1	L3	ST	L1	L3
0.020922	0.010369	0.009316	-1.67939	-1.98426	-2.03079
0.022294	0.010453	0.008921	-1.65181	-1.98075	-2.04958
P-values					
ST vs. L1	L1 vs. L3	L3 vs. ST	ST vs. L1	L1 vs. L3	L3 vs. ST
0.001873	0.011741	0.001625	0.000959	0.013189	0.000989
Permanent Strain @ 12,000 cycles_ Foam_54°C					
arithmetic scale			log-log scale		
ST	L1	L3	ST	L1	L3
0.0218	0.010712	0.009592	-1.66154	-1.97012	-2.01809
0.023853	0.010752	0.009202	-1.62245	-1.9685	-2.0361
P-values					
ST vs. L1	L1 vs. L3	L3 vs. ST	ST vs. L1	L1 vs. L3	L3 vs. ST
0.003565	0.010422	0.003	0.001776	0.011806	0.001554

Table 5.7 T-test results of permanent strain of HMA mixtures for different aging levels: (a) at 20°C, (b) at 40°C, and (c) at 54°C.

(a)

Permanent Strain @ 5,000 cycles_ HMA_20°C					
arithmetic scale			log-log scale		
ST	L1	L3	ST	L1	L3
0.000262	0.000234	0.000226	-3.58188	-3.63153	-3.64576
0.00035	0.000342	0.00023	-3.45551	-3.46623	-3.63774
P-values					
ST vs. L1	L1 vs. L3	L3 vs. ST	ST vs. L1	L1 vs. L3	L3 vs. ST
0.408402	0.193116	0.110207	0.399522	0.189174	0.095699
Permanent Strain @ 8,500 cycles_ HMA_20°C					
arithmetic scale			log-log scale		
ST	L1	L3	ST	L1	L3
0.000328	0.000294	0.000277	-3.4838	-3.53146	-3.55708
0.000425	0.000437	0.000289	-3.37119	-3.35984	-3.53957
P-values					
ST vs. L1	L1 vs. L3	L3 vs. ST	ST vs. L1	L1 vs. L3	L3 vs. ST
0.453374	0.184105	0.097525	0.437943	0.178023	0.084015
Permanent Strain @ 12,000 cycles_ HMA_20°C					
arithmetic scale			log-log scale		
ST	L1	L3	ST	L1	L3
0.000371	0.000341	0.000313	-3.43015	-3.46702	-3.50476
0.000481	0.000515	0.00033	-3.31766	-3.28846	-3.48208
P-values					
ST vs. L1	L1 vs. L3	L3 vs. ST	ST vs. L1	L1 vs. L3	L3 vs. ST
0.494439	0.172632	0.099425	0.487144	0.163697	0.086329

(b)

Permanent Strain @ 5,000 cycles_ HMA_40°C					
arithmetic scale			log-log scale		
ST	L1	L3	ST	L1	L3
0.003005	0.00285	0.002665	-2.52213	-2.54509	-2.57429
0.003754	0.003716	0.003441	-2.42552	-2.42992	-2.46338
P-values					
ST vs. L1	L1 vs. L3	L3 vs. ST	ST vs. L1	L1 vs. L3	L3 vs. ST
0.440949	0.364974	0.302998	0.436204	0.366461	0.301424
Permanent Strain @ 8,500 cycles_ HMA_40°C					
arithmetic scale			log-log scale		
ST	L1	L3	ST	L1	L3
0.003206	0.00302	0.002829	-2.4941	-2.51994	-2.54837
0.003942	0.003929	0.00364	-2.4043	-2.4057	-2.43886
P-values					
ST vs. L1	L1 vs. L3	L3 vs. ST	ST vs. L1	L1 vs. L3	L3 vs. ST
0.44061	0.365753	0.299537	0.434287	0.367333	0.297272
Permanent Strain @ 12,000 cycles_ HMA_40°C					
arithmetic scale			log-log scale		
ST	L1	L3	ST	L1	L3
0.003325	0.00312	0.002926	-2.47825	-2.50583	-2.53379
0.004058	0.004053	0.00375	-2.39167	-2.39218	-2.42593
P-values					
ST vs. L1	L1 vs. L3	L3 vs. ST	ST vs. L1	L1 vs. L3	L3 vs. ST
0.438139	0.364059	0.293718	0.431159	0.365853	0.291386

(c)

Permanent Strain @ 5,000 cycles_ HMA_54°C					
arithmetic scale			log-log scale		
ST	L1	L3	ST	L1	L3
0.008291	0.009425	0.007045	-2.08141	-2.02573	-2.15211
0.008385		0.007499	-2.07649	#NUM!	-2.12498
P-values					
ST vs. L1	L1 vs. L3	L3 vs. ST	ST vs. L1	L1 vs. L3	L3 vs. ST
		0.022128			0.024792
Permanent Strain @ 8,500 cycles_ HMA_54°C					
arithmetic scale			log-log scale		
ST	L1	L3	ST	L1	L3
0.008981	0.009935	0.007442	-2.04666	-2.00282	-2.12832
0.008937		0.00788	-2.0488	#NUM!	-2.10348
P-values					
ST vs. L1	L1 vs. L3	L3 vs. ST	ST vs. L1	L1 vs. L3	L3 vs. ST
		0.013788			0.015933
Permanent Strain @ 12,000 cycles_ HMA_54°C					
arithmetic scale			log-log scale		
ST	L1	L3	ST	L1	L3
0.009408	0.010227	0.0077	-2.02652	-1.99024	-2.11349
0.009237		0.008103	-2.03448	#NUM!	-2.09136
P-values					
ST vs. L1	L1 vs. L3	L3 vs. ST	ST vs. L1	L1 vs. L3	L3 vs. ST
		0.011445			0.012856

Table 5.8 provides representative pavement temperatures in North Carolina. The table shows that high pavement temperatures (over 50°C) occur only 2.36% of the time, even at the surface of the pavement. Therefore, it is appropriate to conclude that the effects of aging on the permanent deformation of the WMA Evotherm and HMA mixtures in North Carolina pavements are minor. In terms of the WMA Foam mixture, however, based on the statistical test results and the figures, the aging effects cannot be ignored for each test temperature and between each of the two aging levels.

In terms of other factors that can affect permanent deformation, Table 5.9, Table 5.10, and Figure 5.8 to Figure 5.12 show that pavement temperature contributes significantly to rut depth. Figure 5.13 to Figure 5.17 and Table 5.11 to Table 5.13 indicate that mixture type is the primary factor that dominates permanent deformation. The HMA mixture shows lower permanent strain levels than the WMA mixtures at any given time, whereas at low aging levels, the WMA Foam mix shows an increase in deformation. As the service time increased, the rut depth of the WMA Evotherm mix became the most significant of all the mixtures.

Table 5.8 Statistical Results of EICM Pavement Temperatures (Raleigh, NC)

Frequency	Depth of Pavement (inch)										
Temperature (°C)	0	2.54	5.08	7.62	10.16	12.7	15.24	17.78	20.32	22.86	25.4
0-10	384	296	236	152	90	41	10	6	0	0	0
10-20	1597	1610	1612	1604	1597	1583	1560	1497	1445	1400	1343
20-30	2686	2710	2769	2871	2934	3000	3037	3079	3126	3189	3272
30-40	2596	2711	2775	2904	3028	3147	3273	3394	3506	3586	3607
40-50	1183	1174	1155	1073	981	869	760	664	563	465	417
50-60	193	139	93	36	10	0	0	0	0	0	0
60-70	1	0	0	0	0	0	0	0	0	0	0
70-80	0	0	0	0	0	0	0	0	0	0	0
Over 50°C Overall Proportion (%)	2.23	1.61	1.08	0.42	0.12	0.00	0.00	0.00	0.00	0.00	0.00

Table 5.9 T-test results of permanent strain for short-term aging of conditioned mixtures among different test temperatures: (a) WMA Evotherm, (b) WMA Foam, and (c) HMA.

(a)

Permanent Strain @ 5,000 cycles_ Evth_STA					
arithmetic scale			log-log scale		
20°C	40°C	54°C	20°C	40°C	54°C
	0.005859	0.014214		-2.23215	-1.84728
	0.004313	0.013315		-2.36522	-1.87567
P-values					
20 vs. 40	40 vs. 54	54 vs. 20	20 vs. 40	40 vs. 54	54 vs. 20
	0.005229			0.011685	
Permanent Strain @ 8,500 cycles_ Evth_STA					
arithmetic scale			log-log scale		
20°C	40°C	54°C	20°C	40°C	54°C
	0.006158	0.01506		-2.21055	-1.82217
	0.004538	0.01417		-2.34317	-1.84863
P-values					
20 vs. 40	40 vs. 54	54 vs. 20	20 vs. 40	40 vs. 54	54 vs. 20
	0.004902			0.011333	
Permanent Strain @ 12,000 cycles_ Evth_STA					
arithmetic scale			log-log scale		
20°C	40°C	54°C	20°C	40°C	54°C
	0.006346	0.015559		-2.1975	-1.80802
	0.004683	0.01468		-2.32943	-1.83328
P-values					
20 vs. 40	40 vs. 54	54 vs. 20	20 vs. 40	40 vs. 54	54 vs. 20
	0.004726			0.011121	

(b)

Permanent Strain @ 5,000 cycles_ Foam_STA					
arithmetic scale			log-log scale		
20°C	40°C	54°C	20°C	40°C	54°C
0.000642	0.006777	0.019476	-3.1928	-2.16899	-1.71051
0.000729		0.019902	-3.13699		-1.70111
P-values					
20 vs. 40	40 vs. 54	54 vs. 20	20 vs. 40	40 vs. 54	54 vs. 20
		6.54E-05			0.000188
Permanent Strain @ 8,500 cycles_ Foam_STA					
arithmetic scale			log-log scale		
20°C	40°C	54°C	20°C	40°C	54°C
0.000701	0.007157	0.020922	-3.15449	-2.14526	-1.67939
0.000815		0.022294	-3.08859	#NUM!	-1.65181
P-values					
20 vs. 40	40 vs. 54	54 vs. 20	20 vs. 40	40 vs. 54	54 vs. 20
		0.000544			0.000301
Permanent Strain @ 12,000 cycles_ Foam_STA					
arithmetic scale			log-log scale		
20°C	40°C	54°C	20°C	40°C	54°C
0.00074	0.007397	0.0218	-3.13106	-2.13095	-1.66154
0.000863		0.023853	-3.06396	#NUM!	-1.62245
P-values					
20 vs. 40	40 vs. 54	54 vs. 20	20 vs. 40	40 vs. 54	54 vs. 20
		0.001087			0.000355

(c)

Permanent Strain @ 5,000 cycles_ HMA_STA					
arithmetic scale			log-log scale		
20°C	40°C	54°C	20°C	40°C	54°C
0.000262	0.003005	0.008291	-3.58188	-2.52213	-2.08141
0.00035	0.003754	0.008385	-3.45551	-2.42552	-2.07649
P-values					
20 vs. 40	40 vs. 54	54 vs. 20	20 vs. 40	40 vs. 54	54 vs. 20
0.007356	0.00287	3.24E-05	0.002872	0.007337	0.000962
Permanent Strain @ 8,500 cycles_ HMA_STA					
arithmetic scale			log-log scale		
20°C	40°C	54°C	20°C	40°C	54°C
0.000328	0.003206	0.008981	-3.4838	-2.4941	-2.04666
0.000425	0.003942	0.008937	-3.37119	-2.4043	-2.0488
P-values					
20 vs. 40	40 vs. 54	54 vs. 20	20 vs. 40	40 vs. 54	54 vs. 20
0.006612	0.002328	1.93E-05	0.002687	0.006142	0.000831
Permanent Strain @ 12,000 cycles_ HMA_STA					
arithmetic scale			log-log scale		
20°C	40°C	54°C	20°C	40°C	54°C
0.000371	0.003325	0.009408	-3.43015	-2.47825	-2.02652
0.000481	0.004058	0.009237	-3.31766	-2.39167	-2.03448
P-values					
20 vs. 40	40 vs. 54	54 vs. 20	20 vs. 40	40 vs. 54	54 vs. 20
0.006328	0.002222	6.51E-05	0.002833	0.005679	0.000879

Table 5.10 T-test results of permanent strain of long-term aging Level 1 conditioned mixtures at different test temperatures: (a) WMA Evotherm, (b) WMA Foam, and (c) HMA.

(a)

Permanent Strain @ 5,000 cycles_ Evth_LTA1					
arithmetic scale			log-log scale		
20°C	40°C	54°C	20°C	40°C	54°C
0.000565	0.004725	0.013652	-3.24794	-2.32556	-1.86481
	0.005224	0.014835		-2.28202	-1.82872
P-values					
20 vs. 40	40 vs. 54	54 vs. 20	20 vs. 40	40 vs. 54	54 vs. 20
	0.00238			0.001903	
Permanent Strain @ 8,500 cycles_ Evth_LTA1					
arithmetic scale			log-log scale		
20°C	40°C	54°C	20°C	40°C	54°C
0.000659	0.004939	0.014671	-3.18109	-2.30632	-1.83353
	0.005447	0.015965		-2.26383	-1.79682
P-values					
20 vs. 40	40 vs. 54	54 vs. 20	20 vs. 40	40 vs. 54	54 vs. 20
	0.00234			0.001775	
Permanent Strain @ 12,000 cycles_ Evth_LTA1					
arithmetic scale			log-log scale		
20°C	40°C	54°C	20°C	40°C	54°C
0.000719	0.005066	0.015307	-3.14308	-2.29535	-1.81511
	0.005583	0.01667	#NUM!	-2.25315	-1.77807
P-values					
20 vs. 40	40 vs. 54	54 vs. 20	20 vs. 40	40 vs. 54	54 vs. 20
	0.002319			0.001718	

(b)

Permanent Strain @ 5,000 cycles_ Foam_LTA1					
arithmetic scale			log-log scale		
20°C	40°C	54°C	20°C	40°C	54°C
	0.005043	0.009797		-2.29734	-2.0089
	0.005728	0.009954		-2.24198	-2.00199
P-values					
20 vs. 40	40 vs. 54	54 vs. 20	20 vs. 40	40 vs. 54	54 vs. 20
	0.003039			0.005483	
Permanent Strain @ 8,500 cycles_ Foam_LTA1					
arithmetic sscale			log-log scale		
20°C	40°C	54°C	20°C	40°C	54°C
	0.005277	0.010369		-2.2776	-1.98426
	0.005954	0.010453		-2.22517	-1.98075
P-values					
20 vs. 40	40 vs. 54	54 vs. 20	20 vs. 40	40 vs. 54	54 vs. 20
	0.002512			0.004707	
Permanent Strain @ 12,000 cycles_ Foam_LTA1					
arithmetic sscale			log-log scale		
20°C	40°C	54°C	20°C	40°C	54°C
	0.005452	0.010712		-2.26344	-1.97012
	0.00608	0.010752		-2.21607	-1.9685
P-values					
20 vs. 40	40 vs. 54	54 vs. 20	20 vs. 40	40 vs. 54	54 vs. 20
	0.001997			0.003795	

(c)

Permanent Strain @ 5,000 cycles_ HMA_LTA1					
arithmetic scale			log-log scale		
20°C	40°C	54°C	20°C	40°C	54°C
0.000234	0.00285	0.009425	-3.63153	-2.54509	-2.02573
0.000342	0.003716		-3.46623	-2.42992	#NUM!
P-values					
20 vs. 40	40 vs. 54	54 vs. 20	20 vs. 40	40 vs. 54	54 vs. 20
0.010275			0.004444		
Permanent Strain @ 8,500 cycles_ HMA_LTA1					
arithmetic scale			log-log scale		
20°C	40°C	54°C	20°C	40°C	54°C
0.000294	0.00302	0.009935	-3.53146	-2.51994	-2.00282
0.000437	0.003929		-3.35984	-2.4057	#NUM!
P-values					
20 vs. 40	40 vs. 54	54 vs. 20	20 vs. 40	40 vs. 54	54 vs. 20
0.010594			0.005411		
Permanent Strain @ 12,000 cycles_ HMA_LTA1					
arithmetic scale			log-log scale		
20°C	40°C	54°C	20°C	40°C	54°C
0.000341	0.00312	0.010227	-3.46702	-2.50583	-1.99024
0.000515	0.004053		-3.28846	-2.39218	#NUM!
P-values					
20 vs. 40	40 vs. 54	54 vs. 20	20 vs. 40	40 vs. 54	54 vs. 20
0.010921			0.006368		

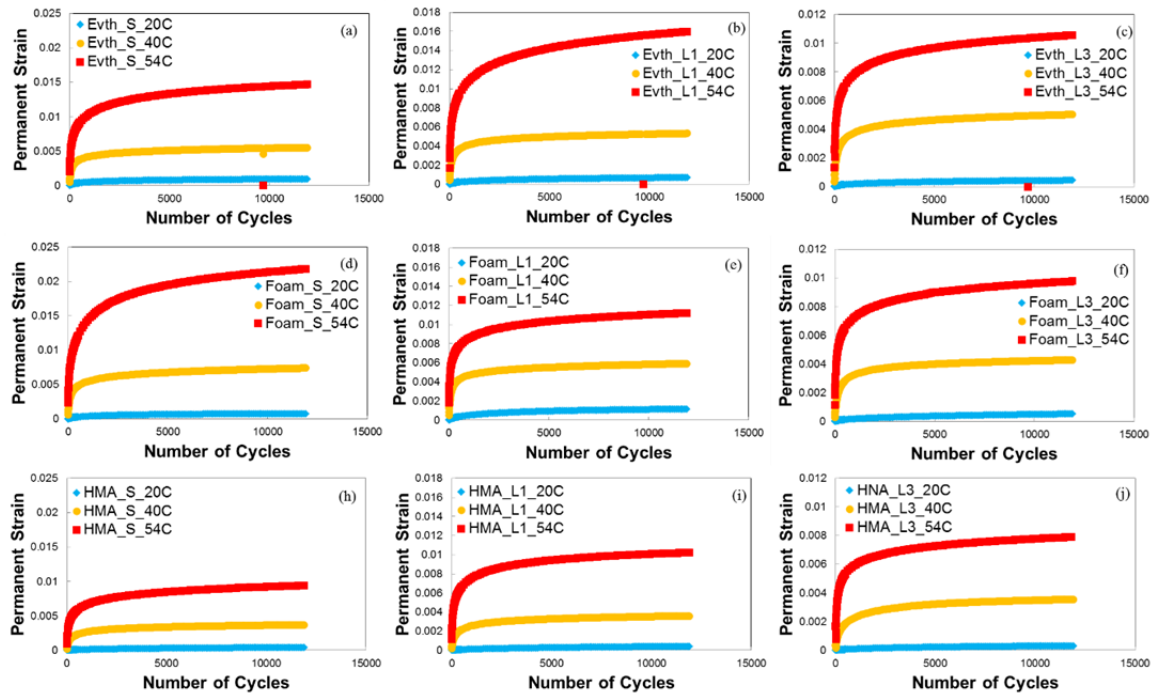


Figure 5.8 Comparison of permanent strain for different test temperatures in arithmetic scale.

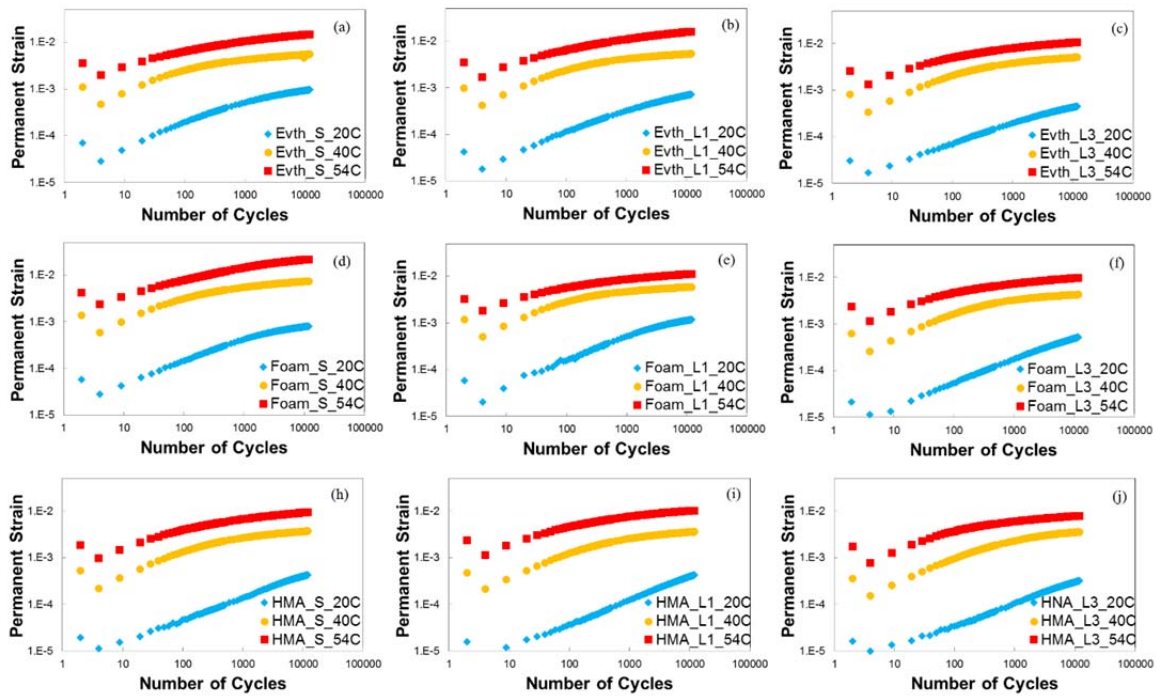


Figure 5.9 Comparison of permanent strain among different test temperatures in log-log scale.

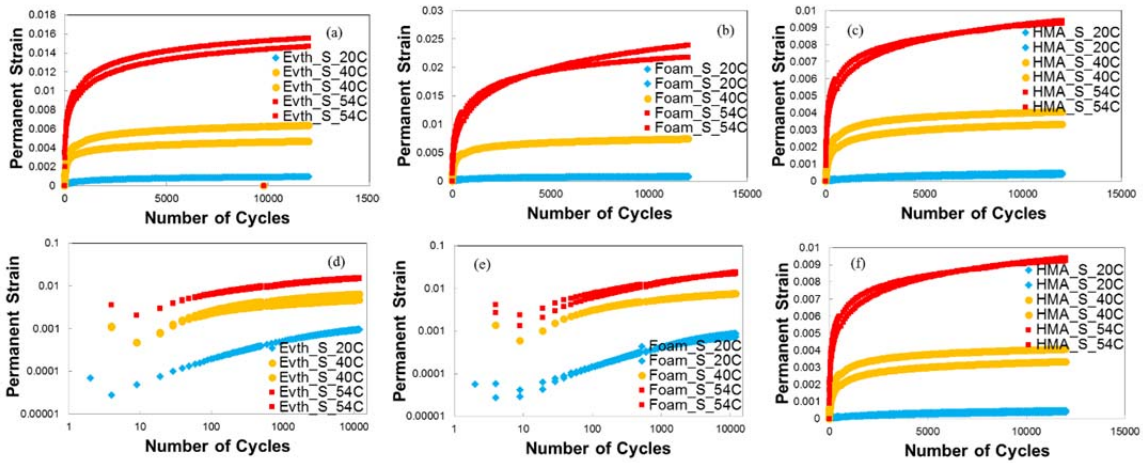


Figure 5.10 Comparison of permanent deformation for short-term aging replicates tested at different temperatures in arithmetic scale and log-log scale.

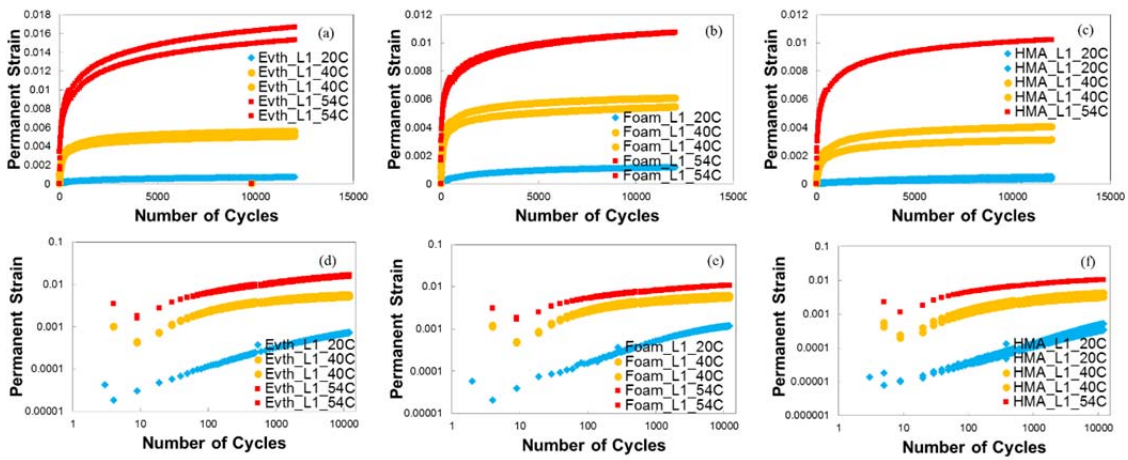


Figure 5.11 Comparison of permanent deformation for long-term aging Level 1 conditioned replicates tested at different temperatures in arithmetic scale and log-log scale.

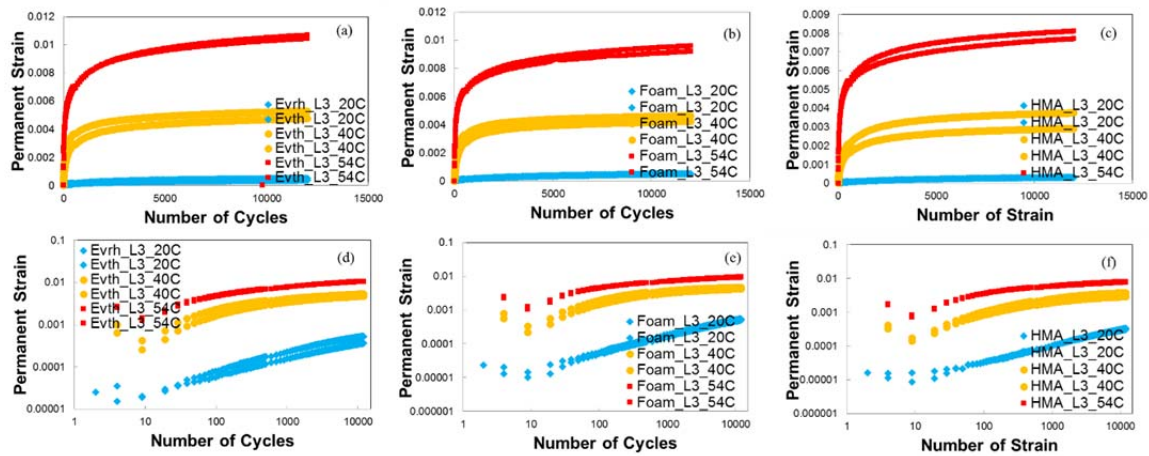


Figure 5.12 Comparison of permanent deformation for long-term aging Level 3 conditioned replicates tested at different temperatures in arithmetic scale and log-log scale.

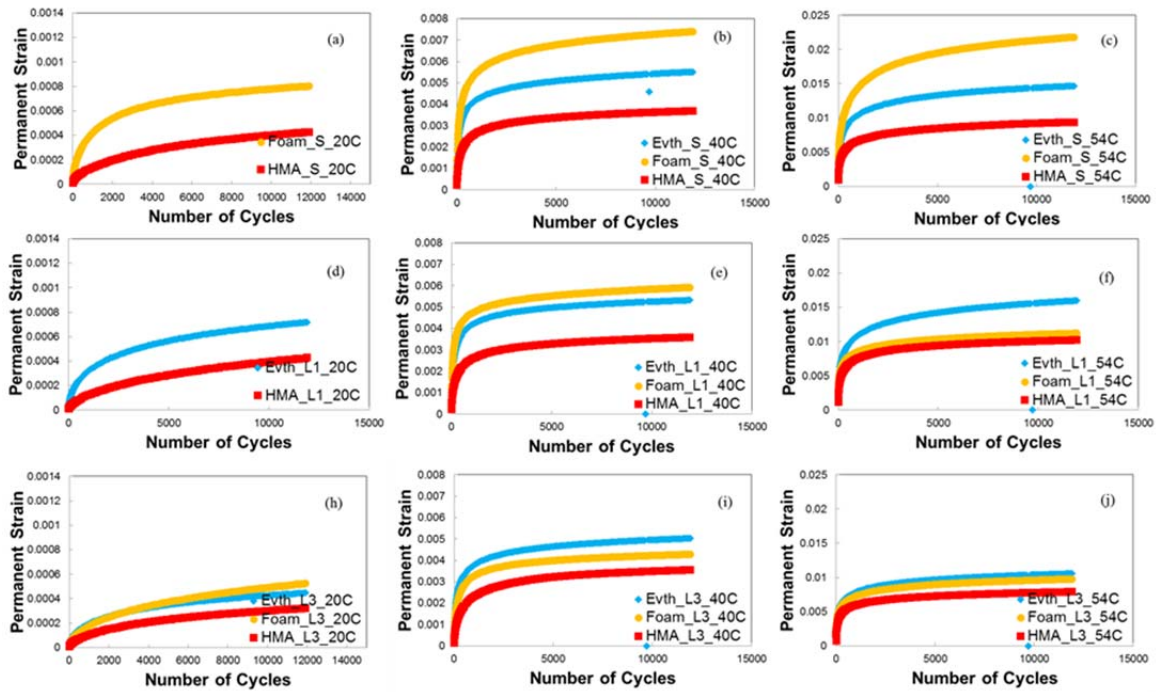


Figure 5.13 Comparison of permanent strain among different mixtures in arithmetic scale.

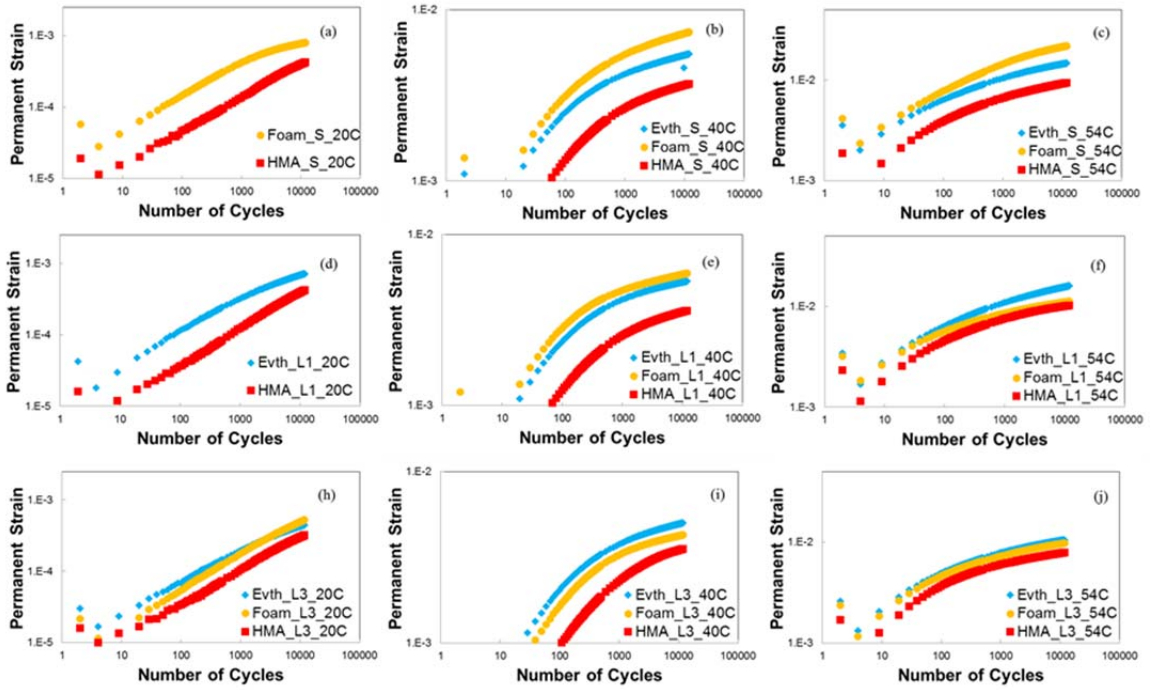


Figure 5.14 Comparison of permanent strain among different mixtures in log-log scale.

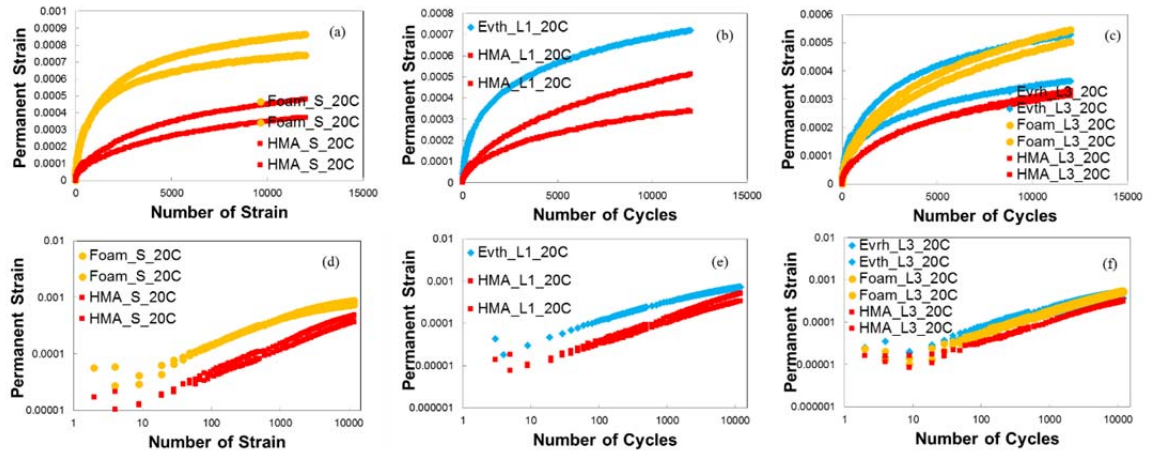


Figure 5.15 Comparison of permanent deformation among replicates of different mixtures at 20°C.

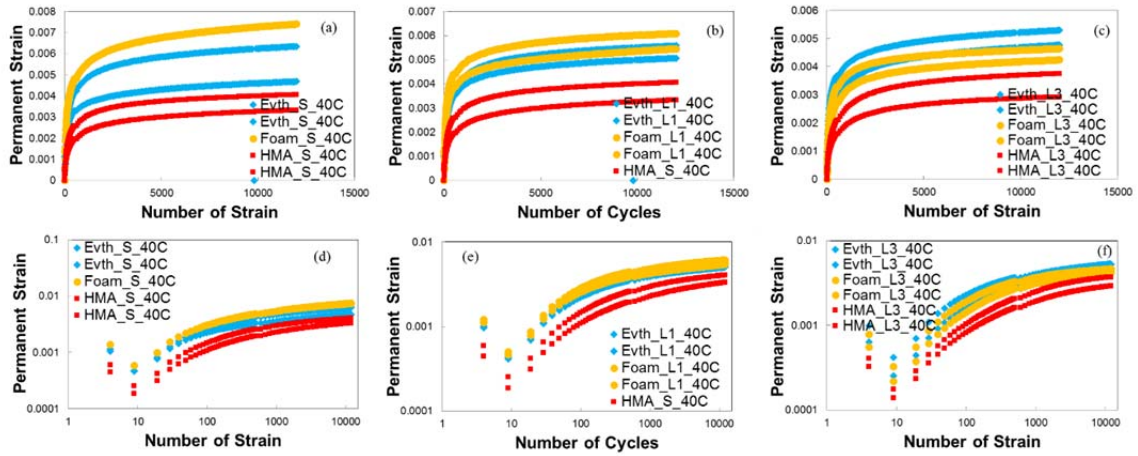


Figure 5.16 Comparison of permanent deformation among replicates of different mixtures at 40°C.

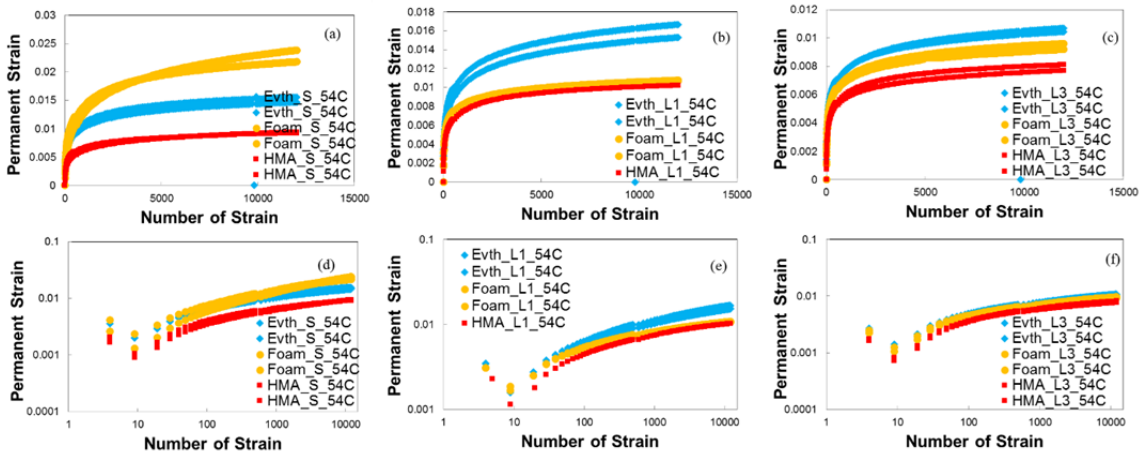


Figure 5.17 Comparison of permanent deformation among replicates of different mixtures at 54°C.

Table 5.11 T-test results of permanent strain among different mixtures at 20°C: (a) short-term aging conditioning (b) long-term aging condition Level 1, and (c) long-term aging condition Level 3.

(a)

Permanent Strain @ 5,000 cycles_ STA_20°C					
arithmetic scale			log-log scale		
Evth	Foam	HMA	Evth	Foam	HMA
	0.000642	0.000262		-3.1928	-3.58188
	0.000729	0.00035		-3.13699	-3.45551
P-values					
Evth vs. Foam	Foam vs. HMA	HMA vs. Evth	Evth vs. Foam	Foam vs. HMA	HMA vs. Evth
	0.012991			0.018033	
Permanent Strain @ 8,500 cycles_ STA_20°C					
arithmetic scale			log-log scale		
Evth	Foam	HMA	Evth	Foam	HMA
	0.000701	0.000328		-3.15449	-3.4838
	0.000815	0.000425		-3.08859	-3.37119
P-values					
Evth vs. Foam	Foam vs. HMA	HMA vs. Evth	Evth vs. Foam	Foam vs. HMA	HMA vs. Evth
	0.018387			0.021289	
Permanent Strain @ 12,000 cycles_ STA_20°C					
arithmetic scale			log-log scale		
Evth	Foam	HMA	Evth	Foam	HMA
	0.00074	0.000371		-3.13106	-3.43015
	0.000863	0.000481		-3.06396	-3.31766
P-values					
Evth vs. Foam	Foam vs. HMA	HMA vs. Evth	Evth vs. Foam	Foam vs. HMA	HMA vs. Evth
	0.022654			0.02591	

(b)

Permanent Strain @ 5,000 cycles_ LTA1_20°C					
arithmetic scale			log-log scale		
Evth	Foam	HMA	Evth	Foam	HMA
0.000565		0.000234	-3.24794		-3.63153
		0.000342			-3.46623
P-values					
Evth vs. Foam	Foam vs. HMA	HMA vs. Evth	Evth vs. Foam	Foam vs. HMA	HMA vs. Evth
Permanent Strain @ 8,500 cycles_ LTA1_20°C					
arithmetic scale			log-log scale		
Evth	Foam	HMA	Evth	Foam	HMA
0.000659		0.000294	-3.18109		-3.53146
		0.000437			-3.35984
P-values					
Evth vs. Foam	Foam vs. HMA	HMA vs. Evth	Evth vs. Foam	Foam vs. HMA	HMA vs. Evth
Permanent Strain @ 12,000 cycles_ LTA1_20°C					
arithmetic scale			log-log scale		
Evth	Foam	HMA	Evth	Foam	HMA
0.000719		0.000341	-3.14308		-3.46702
		0.000515			-3.28846
P-values					
Evth vs. Foam	Foam vs. HMA	HMA vs. Evth	Evth vs. Foam	Foam vs. HMA	HMA vs. Evth

(c)

Permanent Strain @ 5,000 cycles_ LTA3_ 20°C					
arithmetic scale			log-log scale		
Evth	Foam	HMA	Evth	Foam	HMA
0.000279	0.000386	0.000226	-3.55458	-3.41392	-3.64576
0.000421	0.000357	0.00023	-3.37622	-3.44793	-3.63774
P-values					
Evth vs. Foam	Foam vs. HMA	HMA vs. Evth	Evth vs. Foam	Foam vs. HMA	HMA vs. Evth
0.397854	0.005192	0.114216	0.37032	0.003398	0.093443
Permanent Strain @ 8,500 cycles_ LTA3_ 20°C					
arithmetic scale			log-log scale		
Evth	Foam	HMA	Evth	Foam	HMA
0.000327	0.000479	0.000277	-3.485	-3.3195	-3.55708
0.000487	0.000444	0.000289	-3.31262	-3.35298	-3.53957
P-values					
Evth vs. Foam	Foam vs. HMA	HMA vs. Evth	Evth vs. Foam	Foam vs. HMA	HMA vs. Evth
0.287274	0.005385	0.130396	0.274991	0.00392	0.11326
Permanent Strain @ 12,000 cycles_ LTA3_ 20°C					
arithmetic scale			log-log scale		
Evth	Foam	HMA	Evth	Foam	HMA
0.000364	0.000543	0.000313	-3.43856	-3.26481	-3.50476
0.000529	0.000503	0.00033	-3.27673	-3.2985	-3.48208
P-values					
Evth vs. Foam	Foam vs. HMA	HMA vs. Evth	Evth vs. Foam	Foam vs. HMA	HMA vs. Evth
0.230449	0.005799	0.134345	0.22746	0.004536	0.119232

Table 5.12 T-test results of permanent strain among different mixtures at 40°C: (a) short-term aging conditioning (b) long-term aging condition Level 1, and (c) long-term aging condition Level 3.

(a)

Permanent Strain @ 5,000 cycles_ STA_40°C					
arithmetic scale			log-log scale		
Evth	Foam	HMA	Evth	Foam	HMA
0.005859	0.006777	0.003005	-2.23215	-2.16899	-2.52213
0.004313		0.003754	-2.36522		-2.42552
P-values					
Evth vs. Foam	Foam vs. HMA	HMA vs. Evth	Evth vs. Foam	Foam vs. HMA	HMA vs. Evth
		0.092667			0.08345
Permanent Strain @ 8,500 cycles_ STA_40°C					
arithmetic scale			log-log scale		
Evth	Foam	HMA	Evth	Foam	HMA
0.006158	0.007157	0.003206	-2.21055	-2.14526	-2.4941
0.004538		0.003942	-2.34317		-2.4043
P-values					
Evth vs. Foam	Foam vs. HMA	HMA vs. Evth	Evth vs. Foam	Foam vs. HMA	HMA vs. Evth
		0.092191			0.082145
Permanent Strain @ 12,000 cycles_ STA_40°C					
arithmetic scale			log-log scale		
Evth	Foam	HMA	Evth	Foam	HMA
0.006346	0.007397	0.003325	-2.1975	-2.13095	-2.47825
0.004683		0.004058	-2.32943		-2.39167
P-values					
Evth vs. Foam	Foam vs. HMA	HMA vs. Evth	Evth vs. Foam	Foam vs. HMA	HMA vs. Evth
		0.091292			0.080906

(b)

Permanent Strain @ 5,000 cycles_ LTA1_40°C					
arithmetic scale			log-log scale		
Evth	Foam	HMA	Evth	Foam	HMA
0.004725	0.005043	0.00285	-2.32556	-2.29734	-2.54509
0.005224	0.005728	0.003716	-2.28202	-2.24198	-2.42992
P-values					
Evth vs. Foam	Foam vs. HMA	HMA vs. Evth	Evth vs. Foam	Foam vs. HMA	HMA vs. Evth
0.217295	0.031288	0.038611	0.217376	0.038154	0.048169
Permanent Strain @ 8,500 cycles_ LTA1_40°C					
arithmetic scale			log-log scale		
Evth	Foam	HMA	Evth	Foam	HMA
0.004939	0.005277	0.00302	-2.30632	-2.2776	-2.51994
0.005447	0.005954	0.003929	-2.26383	-2.22517	-2.4057
P-values					
Evth vs. Foam	Foam vs. HMA	HMA vs. Evth	Evth vs. Foam	Foam vs. HMA	HMA vs. Evth
0.211669	0.03173	0.040385	0.211629	0.03907	0.050099
Permanent Strain @ 12,000 cycles_ LTA1_40°C					
arithmetic scale			log-log scale		
Evth	Foam	HMA	Evth	Foam	HMA
0.005066	0.005452	0.00312	-2.29535	-2.26344	-2.50583
0.005583	0.00608	0.004053	-2.25315	-2.21607	-2.39218
P-values					
Evth vs. Foam	Foam vs. HMA	HMA vs. Evth	Evth vs. Foam	Foam vs. HMA	HMA vs. Evth
0.195406	0.030314	0.041365	0.195192	0.038367	0.051102

(c)

Permanent Strain @ 5,000 cycles_ LTA3_ 40°C					
arithmetic scale			log-log scale		
Evth	Foam	HMA	Evth	Foam	HMA
0.004921	0.003947	0.002665	-2.30798	-2.40375	-2.57429
0.004373	0.004389	0.003441	-2.35924	-2.35762	-2.46338
P-values					
Evth vs. Foam	Foam vs. HMA	HMA vs. Evth	Evth vs. Foam	Foam vs. HMA	HMA vs. Evth
0.153424	0.06487	0.039201	0.152706	0.074068	0.046868
Permanent Strain @ 8,500 cycles_ LTA3_ 40°C					
arithmetic scale			log-log scale		
Evth	Foam	HMA	Evth	Foam	HMA
0.005152	0.004126	0.002829	-2.28806	-2.38444	-2.54837
0.004618	0.004543	0.00364	-2.33559	-2.34261	-2.43886
P-values					
Evth vs. Foam	Foam vs. HMA	HMA vs. Evth	Evth vs. Foam	Foam vs. HMA	HMA vs. Evth
0.123114	0.068677	0.038402	0.122024	0.07833	0.046509
Permanent Strain @ 12,000 cycles_ LTA3_ 40°C					
arithmetic scale			log-log scale		
Evth	Foam	HMA	Evth	Foam	HMA
0.005296	0.004237	0.002926	-2.27605	-2.37289	-2.53379
0.00477	0.004636	0.00375	-2.32151	-2.33385	-2.42593
P-values					
Evth vs. Foam	Foam vs. HMA	HMA vs. Evth	Evth vs. Foam	Foam vs. HMA	HMA vs. Evth
0.10636	0.069267	0.03708	0.105017	0.079104	0.045249

Table 5.13 T-test results of permanent strain among different mixtures at 54°C: (a) short-term aging conditioning (b) long-term aging condition Level 1, and (c) long-term aging condition Level 3.

(a)

Permanent Strain @ 5,000 cycles_ STA_54°C					
arithmetic scale			log-log scale		
Evth	Foam	HMA	Evth	Foam	HMA
0.014214	0.019476	0.008291	-1.84728	-1.71051	-2.08141
0.013315	0.019902	0.008385	-1.87567	-1.70111	-2.07649
P-values					
Evth vs. Foam	Foam vs. HMA	HMA vs. Evth	Evth vs. Foam	Foam vs. HMA	HMA vs. Evth
0.00349	0.000184	0.003436	0.004549	0.000101	0.002179
Permanent Strain @ 8,500 cycles_ STA_54°C					
arithmetic scale			log-log scale		
Evth	Foam	HMA	Evth	Foam	HMA
0.01506	0.020922	0.008981	-1.82217	-1.67939	-2.04666
0.01417	0.022294	0.008937	-1.84863	-1.65181	-2.0488
P-values					
Evth vs. Foam	Foam vs. HMA	HMA vs. Evth	Evth vs. Foam	Foam vs. HMA	HMA vs. Evth
0.006698	0.001465	0.003075	0.006215	0.000654	0.001942
Permanent Strain @ 12,000 cycles_ STA_54°C					
arithmetic scale			log-log scale		
Evth	Foam	HMA	Evth	Foam	HMA
0.015559	0.0218	0.009408	-1.80802	-1.66154	-2.02652
0.01468	0.023853	0.009237	-1.83328	-1.62245	-2.03448
P-values					
Evth vs. Foam	Foam vs. HMA	HMA vs. Evth	Evth vs. Foam	Foam vs. HMA	HMA vs. Evth
0.010179	0.002884	0.002959	0.008275	0.001313	0.00198

(b)

Permanent Strain @ 5,000 cycles_ LTA1_54°C					
arithmetic scale			log-log scale		
Evth	Foam	HMA	Evth	Foam	HMA
0.013652	0.009797	0.009425	-1.86481	-2.0089	-2.02573
0.014835	0.009954		-1.82872	-2.00199	#NUM!
P-values					
Evth vs. Foam	Foam vs. HMA	HMA vs. Evth	Evth vs. Foam	Foam vs. HMA	HMA vs. Evth
0.009078			0.006571		
Permanent Strain @ 8,500 cycles_ LTA1_54°C					
arithmetic scale			log-log scale		
Evth	Foam	HMA	Evth	Foam	HMA
0.014671	0.010369	0.009935	-1.83353	-1.98426	-2.00282
0.015965	0.010453		-1.79682	-1.98075	#NUM!
P-values					
Evth vs. Foam	Foam vs. HMA	HMA vs. Evth	Evth vs. Foam	Foam vs. HMA	HMA vs. Evth
0.008509			0.005964		
Permanent Strain @ 12,000 cycles_ LTA1_54°C					
arithmetic scale			log-log scale		
Evth	Foam	HMA	Evth	Foam	HMA
0.015307	0.010712	0.010227	-1.81511	-1.97012	-1.99024
0.01667	0.010752		-1.77807	-1.9685	#NUM!
P-values					
Evth vs. Foam	Foam vs. HMA	HMA vs. Evth	Evth vs. Foam	Foam vs. HMA	HMA vs. Evth
0.008206			0.005663		

(c)

Permanent Strain @ 5,000 cycles_ LTA3_54°C					
arithmetic scale			log-log scale		
Evth	Foam	HMA	Evth	Foam	HMA
0.009605	0.008843	0.007045	-2.01748	-2.05341	-2.15211
0.009755	0.008607	0.007499	-2.01076	-2.06516	-2.12498
P-values					
Evth vs. Foam	Foam vs. HMA	HMA vs. Evth	Evth vs. Foam	Foam vs. HMA	HMA vs. Evth
0.010363	0.014835	0.004859	0.010859	0.016539	0.006193
Permanent Strain @ 8,500 cycles_ LTA3_54°C					
arithmetic scale			log-log scale		
Evth	Foam	HMA	Evth	Foam	HMA
0.010127	0.009316	0.007442	-1.99454	-2.03079	-2.12832
0.010334	0.008921	0.00788	-1.98574	-2.04958	-2.10348
P-values					
Evth vs. Foam	Foam vs. HMA	HMA vs. Evth	Evth vs. Foam	Foam vs. HMA	HMA vs. Evth
0.018944	0.01928	0.00439	0.020193	0.019906	0.005402
Permanent Strain @ 12,000 cycles_ LTA3_54°C					
arithmetic scale			log-log scale		
Evth	Foam	HMA	Evth	Foam	HMA
0.010439	0.009592	0.0077	-1.98134	-2.01809	-2.11349
0.010686	0.009202	0.008103	-1.9712	-2.0361	-2.09136
P-values					
Evth vs. Foam	Foam vs. HMA	HMA vs. Evth	Evth vs. Foam	Foam vs. HMA	HMA vs. Evth
0.018498	0.016667	0.00389	0.01947	0.017022	0.004591

5.3.1.2 Aging Effect on Strain Ratio of Permanent Strain to Resilient Strain in Pavement ME

The strain ratio of the permanent strain to the resilient strain is an important concept in the Pavement ME program. The rut depth is calculated based on Equation (6.10):

$$\frac{\varepsilon_p}{\varepsilon_r} = K_1 T^{K_2} N^{K_3} \quad (6.10)$$

where

ε_p = permanent strain,

ε_r = resilient strain,

T = temperature, °F,

N = number of cycles, and

K_1, K_2, K_3 = constants.

For the WMA Evotherm and HMA mixtures, as shown in, Table 5.14, and Figure 5.18 to Figure 5.22, the aging level does not affect the strain ratio significantly, which indicates that, in terms of rutting, the accuracy of the aging prediction model that is embedded in the Pavement ME program is not a concern when those two mixtures are used. As for the WMA Foam mix, even though Table 5.15 shows that oftentimes the differences in the strain ratios among the aging levels are not statistically significant, the strain ratios at 54°C, however, especially the slope of the strain ratio shown in Figure 5.21 that plays an important role in Equation (6.10), are different as the aging levels change. Nevertheless, as mentioned before, 54°C can be considered to be an extreme condition for pavements in North Carolina, and thus, the aging effect on permanent deformation for the WMA Foam mix can be ignored. Therefore, it can be concluded that the aging effect on the strain ratios for the WMA and HMA mixtures is not significant, and the aging effect on the permanent strain that was observed for the WMA Foam mix can be taken into account by the resilient strain, which changes as the stiffness increases with aging.

The effect of temperature on the strain ratio is noted as K_2 in the model; however, as shown in Table 5.17 to Table 5.19 and also in Figure 5.23 to Figure 5.27, the differences between the strain ratios at 40°C and at 54°C for all three mixtures are not significantly different. Moreover, one of the explanations of the phenomenon that the strain ratio at 20°C increases differently from the strain ratios at 40°C and 54°C is that when the test temperature is as low as 20°C, the mixture still remains in the viscoelastic domain rather than the viscoplastic domain. The implication is that, if the loading history could be longer than 12,000 cycles, which does not allow full development of viscoplasticity, even at 20°C the strain ratio would eventually reach the same level as it does at 40°C and 54°C. Therefore, the formula of the model should be reconsidered based on this finding; however, such work is beyond the scope of this project.

With regard to the effect of mixture type on the strain ratio, based on Table 5.20 to Table 5.22 and Figure 5.28 to Figure 5.32, the differences between the different mixtures are minor, especially at the low temperature in log-log scale, which also indicates that the differences in permanent strain levels among the mixtures are reflected eventually by the differences in resilient strain.

To sum up, the aging effects on the permanent strain of the WMA Evotherm and HMA mixtures are not significant when the statistical results and climate of North Carolina are taken into account. However, aging does affect permanent strain for the WMA Foam mixture. With respect to the strain ratios of permanent strain to resilient strain, which are important to the Pavement ME program, the aging effect is minor for all the WMA mixes and the HMA control mix.

Table 5.14 T-test results of strain ratios of WMA Evotherm at different aging levels: (a) at 20°C, (b) at 40°C, and (c) at 54°C.

(a)

Strain Ratio @ 5,000 cycles_ Evth_ 20°C					
arithmetic scale			log-log scale		
ST	L1	L3	ST	L1	L3
	7.141502	5.152874			0.71205
		9.623962			0.983354
P-values					
ST vs. L1	L1 vs. L3	L3 vs. ST	ST vs. L1	L1 vs. L3	L3 vs. ST
Strain Ratio @ 8,500 cycles_ Evth_ 20°C					
arithmetic scale			log-log scale		
ST	L1	L3	ST	L1	L3
	8.155994	5.932188			0.773215
		11.46401			1.059337
P-values					
ST vs. L1	L1 vs. L3	L3 vs. ST	ST vs. L1	L1 vs. L3	L3 vs. ST
Strain Ratio @ 12,000 cycles_ Evth_ 20°C					
arithmetic scale			log-log scale		
ST	L1	L3	ST	L1	L3
	8.979274	6.553235			0.816456
		12.36862			1.092321
P-values					
ST vs. L1	L1 vs. L3	L3 vs. ST	ST vs. L1	L1 vs. L3	L3 vs. ST

(b)

Strain Ratio @ 5,000 cycles_Evth_ 40°C					
arithmetic scale			log-log scale		
ST	L1	L3	ST	L1	L3
10.89405	12.59632	12.26551	1.037189	1.100244	1.088686
9.922292	13.39525	14.03911	0.996612	1.126951	1.14734
P-values					
ST vs. L1	L1 vs. L3	L3 vs. ST	ST vs. L1	L1 vs. L3	L3 vs. ST
0.02716	0.443467	0.056595	0.028844	0.451782	0.052567
Strain Ratio @ 8,500 cycles_Evth_ 40°C					
arithmetic scale			log-log scale		
ST	L1	L3	ST	L1	L3
11.29919	12.72356	13.02858	1.053047	1.104609	1.114897
10.07441	13.81084	14.08564	1.00322	1.14022	1.148776
P-values					
ST vs. L1	L1 vs. L3	L3 vs. ST	ST vs. L1	L1 vs. L3	L3 vs. ST
0.043834	0.369501	0.035532	0.045641	0.369172	0.037512
Strain Ratio @ 12,000 cycles_Evth_ 40°C					
arithmetic scale			log-log scale		
ST	L1	L3	ST	L1	L3
11.58211	13.02858	12.6895	1.063788	1.114897	1.103444
10.27509	14.08564	14.69109	1.011786	1.148776	1.167054
P-values					
ST vs. L1	L1 vs. L3	L3 vs. ST	ST vs. L1	L1 vs. L3	L3 vs. ST
0.044416	0.458539	0.073542	0.046902	0.466595	0.070514

(c)

Strain Ratio @ 5,000 cycles_ Evth_54°C					
arithmetic scale			log-log scale		
ST	L1	L3	ST	L1	L3
11.46044	12.59632	11.31418	1.059201	1.100244	1.053623
11.4558	13.39525	12.4257	1.059025	1.126951	1.094321
P-values					
ST vs. L1	L1 vs. L3	L3 vs. ST	ST vs. L1	L1 vs. L3	L3 vs. ST
0.030673	0.120857	0.267943	0.027575	0.122527	0.270612
Strain Ratio @ 8,500 cycles_ Evth_54°C					
arithmetic scale			log-log scale		
ST	L1	L3	ST	L1	L3
12.3397	13.43433	11.74404	1.091305	1.128216	1.069818
11.99485	14.59956	12.91518	1.078995	1.16434	1.1111
P-values					
ST vs. L1	L1 vs. L3	L3 vs. ST	ST vs. L1	L1 vs. L3	L3 vs. ST
0.046542	0.088907	0.407599	0.042589	0.089404	0.414149
Strain Ratio @ 12,000 cycles_ Evth_54°C					
arithmetic scale			log-log scale		
ST	L1	L3	ST	L1	L3
14.17402	13.79157	11.99134	1.151493	1.139614	1.078868
12.2867	15.04503	13.1922	1.089435	1.177393	1.120317
P-values					
ST vs. L1	L1 vs. L3	L3 vs. ST	ST vs. L1	L1 vs. L3	L3 vs. ST
0.202186	0.085001	0.31282	0.202462	0.085224	0.316099

Table 5.15 T-test results of permanent strain of WMA Foam among different aging levels: (a) at 20°C, (b) at 40°C, and (c) at 54°C.

(a)

Strain Ratio @ 5,000 cycles_Foam_ 20°C					
arithmetic scale			log-log scale		
ST	L1	L3	ST	L1	L3
7.504659		6.941492	0.875331		0.841453
8.849322		5.985289	0.94691		0.777085
P-values					
ST vs. L1	L1 vs. L3	L3 vs. ST	ST vs. L1	L1 vs. L3	L3 vs. ST
		0.086701			0.084291
Strain Ratio @ 8,500 cycles_Foam_ 20°C					
arithmetic scale			log-log scale		
ST	L1	L3	ST	L1	L3
8.252886		8.696009	0.916606		0.93932
10.01729		7.313989	1.00075		0.864154
P-values					
ST vs. L1	L1 vs. L3	L3 vs. ST	ST vs. L1	L1 vs. L3	L3 vs. ST
		0.209705			0.209536
Strain Ratio @ 12,000 cycles_Foam_ 20°C					
arithmetic scale			log-log scale		
ST	L1	L3	ST	L1	L3
8.879583		9.868516	0.948393		0.994252
10.55557		8.284869	1.023482		0.918286
P-values					
ST vs. L1	L1 vs. L3	L3 vs. ST	ST vs. L1	L1 vs. L3	L3 vs. ST
		0.317089			0.317193

(b)

Strain Ratio @ 5,000 cycles_ Foam_ 40°C					
arithmetic scale			log-log scale		
ST	L1	L3	ST	L1	L3
12.73183	13.44824	14.6257	1.104891	1.128666	1.165117
	15.42935	15.68564		1.188348	1.195502
P-values					
ST vs. L1	L1 vs. L3	L3 vs. ST	ST vs. L1	L1 vs. L3	L3 vs. ST
	0.294356			0.290897	
Strain Ratio @ 8,500 cycles_ Foam_ 40°C					
arithmetic scale			log-log scale		
ST	L1	L3	ST	L1	L3
13.2394	13.66436	15.11122	1.121868	1.135589	1.1793
	15.59484	15.94732		1.192981	1.202688
P-values					
ST vs. L1	L1 vs. L3	L3 vs. ST	ST vs. L1	L1 vs. L3	L3 vs. ST
	0.241248			0.239784	
Strain Ratio @ 12,000 cycles_ Foam_ 40°C					
arithmetic scale			log-log scale		
ST	L1	L3	ST	L1	L3
13.60369	13.58569	15.35089	1.133657	1.133082	1.186134
	15.87612	16.27989		1.200744	1.211651
P-values					
ST vs. L1	L1 vs. L3	L3 vs. ST	ST vs. L1	L1 vs. L3	L3 vs. ST
	0.236372			0.234877	

(c)

Strain Ratio @ 5,000 cycles_ Foam_54°C					
arithmetic scale			log-log scale		
ST	L1	L3	ST	L1	L3
14.25064	11.30305	11.75784	1.153834	1.053196	1.070328
16.95711	10.94626	13.74333	1.229352	1.039266	1.138092
P-values					
ST vs. L1	L1 vs. L3	L3 vs. ST	ST vs. L1	L1 vs. L3	L3 vs. ST
0.040824	0.124142	0.11561	0.031612	0.11785	0.113564
Strain Ratio @ 8,500 cycles_ Foam_54°C					
arithmetic scale			log-log scale		
ST	L1	L3	ST	L1	L3
14.96906	11.7026	12.07905	1.175195	1.068282	1.082033
18.50324	11.23492	12.02638	1.267248	1.05057	1.080135
P-values					
ST vs. L1	L1 vs. L3	L3 vs. ST	ST vs. L1	L1 vs. L3	L3 vs. ST
0.048988	0.065592	0.058882	0.037323	0.067787	0.046547
Strain Ratio @ 12,000 cycles_ Foam_54°C					
arithmetic scale			log-log scale		
ST	L1	L3	ST	L1	L3
15.33064	11.88811	12.46742	1.18556	1.075113	1.095777
19.50535	11.37183	12.24402	1.290154	1.05583	1.087924
P-values					
ST vs. L1	L1 vs. L3	L3 vs. ST	ST vs. L1	L1 vs. L3	L3 vs. ST
0.055286	0.061539	0.068229	0.041713	0.063394	0.054216

Table 5.16 T-test results of strain of HMA mixtures among different aging levels: (a) at 20°C, (b) at 40°C, and (c) at 54°C.

(a)

Strain Ratio @ 5,000 cycles_ HMA_20°C					
arithmetic scale			log-log scale		
ST	L1	L3	ST	L1	L3
4.031286	4.440774	4.221761	0.605444	0.647459	0.625494
5.296495	5.728652	4.143566	0.723989	0.758052	0.617374
P-values					
ST vs. L1	L1 vs. L3	L3 vs. ST	ST vs. L1	L1 vs. L3	L3 vs. ST
0.343463	0.148458	0.263491	0.342532	0.140066	0.271026
Strain Ratio @ 8,500 cycles_ HMA_20°C					
arithmetic scale			log-log scale		
ST	L1	L3	ST	L1	L3
5.094207	5.646302	5.224059	0.707077	0.751764	0.718008
6.488092	7.271562	5.277425	0.812117	0.861628	0.722422
P-values					
ST vs. L1	L1 vs. L3	L3 vs. ST	ST vs. L1	L1 vs. L3	L3 vs. ST
0.29822	0.13781	0.259752	0.299315	0.128172	0.26594
Strain Ratio @ 12,000 cycles_ HMA_20°C					
arithmetic scale			log-log scale		
ST	L1	L3	ST	L1	L3
5.768832	6.628273	5.922251	0.761088	0.8214	0.772487
7.302311	8.5912	6.04776	0.86346	0.934054	0.781595
P-values					
ST vs. L1	L1 vs. L3	L3 vs. ST	ST vs. L1	L1 vs. L3	L3 vs. ST
0.239665	0.120165	0.274235	0.240213	0.108371	0.281876

(b)

Strain Ratio @ 5,000 cycles_ HMA_40°C					
arithmetic scale			log-log scale		
ST	L1	L3	ST	L1	L3
10.86398	12.38435	13.55399	1.035989	1.092873	1.132067
12.43678	16.61517	16.50677	1.094708	1.220505	1.217662
P-values					
ST vs. L1	L1 vs. L3	L3 vs. ST	ST vs. L1	L1 vs. L3	L3 vs. ST
0.167013	0.428034	0.090364	0.16158	0.417515	0.084653
Strain Ratio @ 8,500 cycles_ HMA_40°C					
arithmetic scale			log-log scale		
ST	L1	L3	ST	L1	L3
11.32464	12.68839	13.95263	1.054024	1.103406	1.144656
12.74515	17.64943	17.35552	1.105345	1.246731	1.239438
P-values					
ST vs. L1	L1 vs. L3	L3 vs. ST	ST vs. L1	L1 vs. L3	L3 vs. ST
0.174225	0.443342	0.09432	0.168405	0.430804	0.086209
Strain Ratio @ 12,000 cycles_ HMA_40°C					
arithmetic scale			log-log scale		
ST	L1	L3	ST	L1	L3
11.57699	12.82351	14.33945	1.063596	1.108007	1.156533
13.11984	18.21532	17.59216	1.117929	1.260437	1.245319
P-values					
ST vs. L1	L1 vs. L3	L3 vs. ST	ST vs. L1	L1 vs. L3	L3 vs. ST
0.187742	0.450123	0.0911	0.18371	0.433635	0.084256

(c)

Strain Ratio @ 5,000 cycles_ HMA_54°C					
arithmetic scale			log-log scale		
ST	L1	L3	ST	L1	L3
11.40035	12.18612	14.99973	1.056918	1.085866	1.176083
10.06244		11.99022	1.002703		1.078827
P-values					
ST vs. L1	L1 vs. L3	L3 vs. ST	ST vs. L1	L1 vs. L3	L3 vs. ST
		0.117656			0.110771
Strain Ratio @ 8,500 cycles_ HMA_54°C					
arithmetic scale			log-log scale		
ST	L1	L3	ST	L1	L3
12.0952	12.69333	15.31799	1.082613	1.103575	1.185202
10.465		12.32842	1.019739		1.090908
P-values					
ST vs. L1	L1 vs. L3	L3 vs. ST	ST vs. L1	L1 vs. L3	L3 vs. ST
		0.13692			0.132479
Strain Ratio @ 12,000 cycles_ HMA_54°C					
arithmetic scale			log-log scale		
ST	L1	L3	ST	L1	L3
12.53475	12.88881	15.49023	1.098116	1.110213	1.190058
10.68156		12.60436	1.028635		1.100521
P-values					
ST vs. L1	L1 vs. L3	L3 vs. ST	ST vs. L1	L1 vs. L3	L3 vs. ST
		0.14543			0.142595

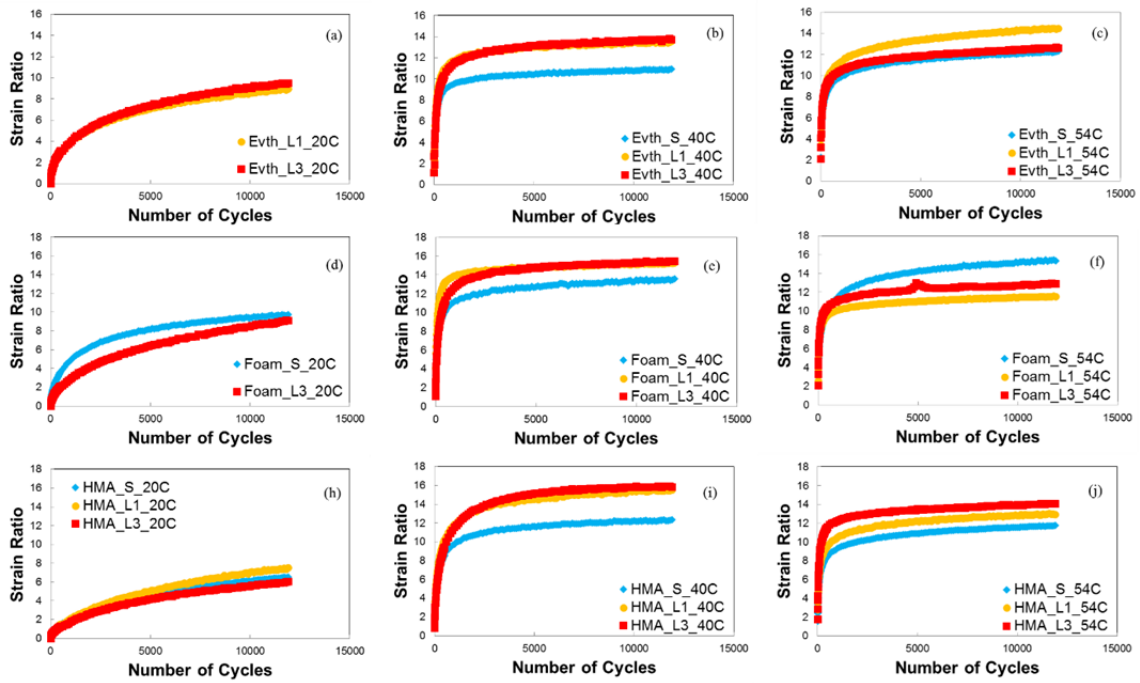


Figure 5.18 Comparison of strain ratios with different aging levels in arithmetic scale.

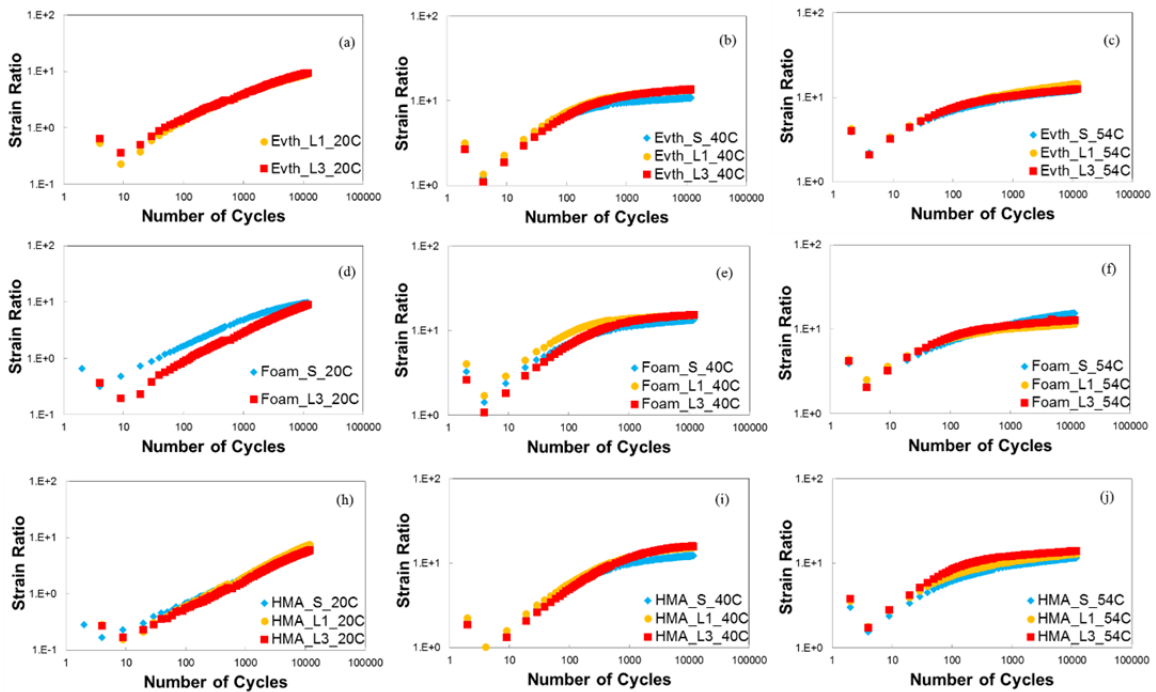


Figure 5.19 Comparison of strain ratios with different aging levels in log-log scale.

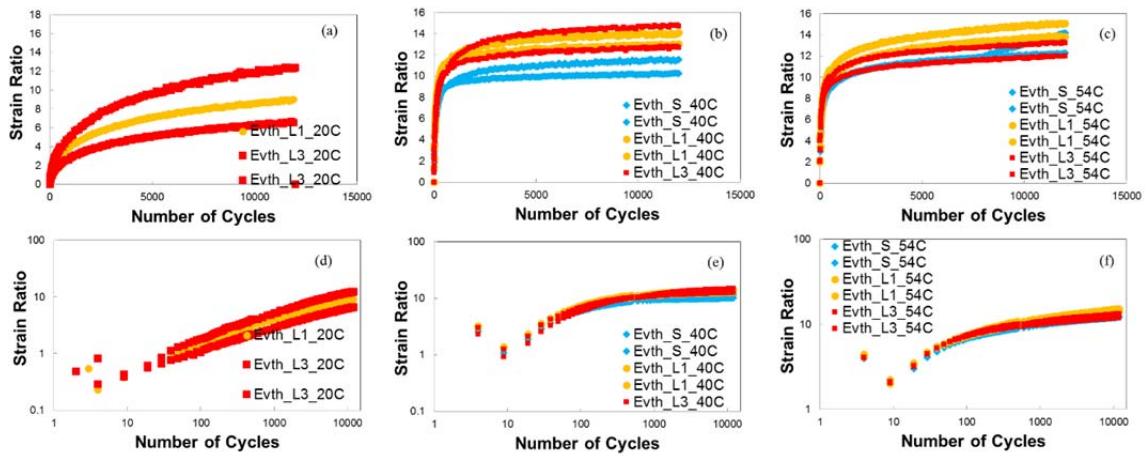


Figure 5.20 Comparison of strain ratios among replicates with different aging levels for WMA Evotherm.

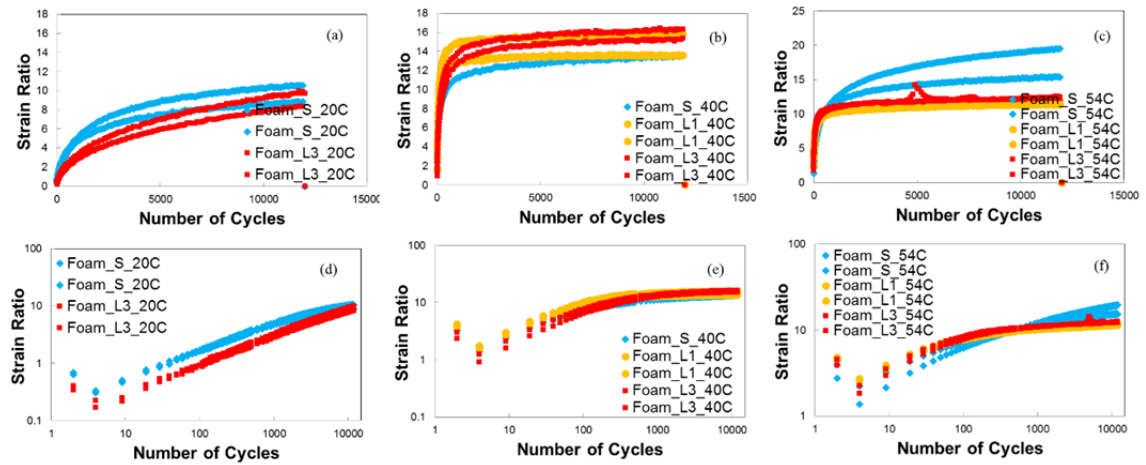


Figure 5.21 Comparison of strain ratios among replicates with different aging levels for WMA Foam.

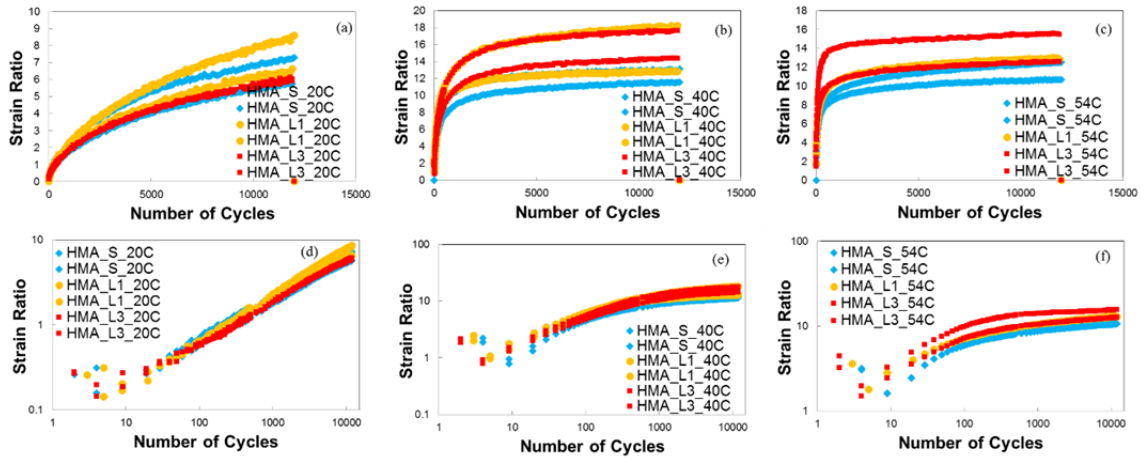


Figure 5.22 Comparison of strain ratios among replicates with different aging levels for HMA.

Table 5.17 T-test results of permanent strain of short-term aging conditioned mixtures at different test temperatures: (a) WMA Evotherm, (b) WMA Foam, and (c) HMA.

(a)

Strain Ratio @ 5,000 cycles_ Evth_STA					
arithmetic scale			log-log scale		
20°C	40°C	54°C	20°C	40°C	54°C
	10.89405	11.46044		1.037189	1.059201
	9.922292	11.4558		0.996612	1.059025
P-values					
20 vs. 40	40 vs. 54	54 vs. 20	20 vs. 40	40 vs. 54	54 vs. 20
	0.081631			0.086482	#NUM!
Strain Ratio @ 8,500 cycles_ Evth_STA					
arithmetic scale			log-log scale		
20°C	40°C	54°C	20°C	40°C	54°C
	11.29919	12.3397		1.053047	1.091305
	10.07441	11.99485		1.00322	1.078995
P-values					
20 vs. 40	40 vs. 54	54 vs. 20	20 vs. 40	40 vs. 54	54 vs. 20
	0.072717			0.078201	
Strain Ratio @ 12,000 cycles_ Evth_STA					
arithmetic scale			log-log scale		
20°C	40°C	54°C	20°C	40°C	54°C
	11.58211	14.17402		1.063788	1.151493
	10.27509	12.2867		1.011786	1.089435
P-values					
20 vs. 40	40 vs. 54	54 vs. 20	20 vs. 40	40 vs. 54	54 vs. 20
	0.091394			0.088934	

(b)

Strain Ratio @ 5,000 cycles_ Foam_STA					
arithmetic scale			log-log scale		
20°C	40°C	54°C	20°C	40°C	54°C
7.504659	12.73183	14.25064	0.875331	1.104891	1.153834
8.849322		16.95711	0.94691	#NUM!	1.229352
P-values					
20 vs. 40	40 vs. 54	54 vs. 20	20 vs. 40	40 vs. 54	54 vs. 20
		0.019495			0.016364
Strain Ratio @ 8,500 cycles_ Foam_STA					
arithmetic scale			log-log scale		
20°C	40°C	54°C	20°C	40°C	54°C
8.252886	13.2394	14.96906	0.916606	1.121868	1.175195
10.01729		18.50324	1.00075	#NUM!	1.267248
P-values					
20 vs. 40	40 vs. 54	54 vs. 20	20 vs. 40	40 vs. 54	54 vs. 20
		0.030684			0.026024
Strain Ratio @ 12,000 cycles_ Foam_STA					
arithmetic scale			log-log scale		
20°C	40°C	54°C	20°C	40°C	54°C
8.879583	13.60369	15.33064	0.948393	1.133657	1.18556
10.55557		19.50535	1.023482	#NUM!	1.290154
P-values					
20 vs. 40	40 vs. 54	54 vs. 20	20 vs. 40	40 vs. 54	54 vs. 20
		0.037877			0.029767

(c)

Strain Ratio @ 5,000 cycles_ HMA_STA					
arithmetic scale			log-log scale		
20°C	40°C	54°C	20°C	40°C	54°C
4.031286	10.86398	11.40035	0.605444	1.035989	1.056918
5.296495	12.43678	10.06244	0.723989	1.094708	1.002703
P-values					
20 vs. 40	40 vs. 54	54 vs. 20	20 vs. 40	40 vs. 54	54 vs. 20
0.010119	0.233662	0.01113	0.013096	0.233829	0.015211
Strain Ratio @ 8,500 cycles_ HMA_STA					
arithmetic scale			log-log scale		
20°C	40°C	54°C	20°C	40°C	54°C
5.094207	11.32464	12.0952	0.707077	1.054024	1.082613
6.488092	12.74515	10.465	0.812117	1.105345	1.019739
P-values					
20 vs. 40	40 vs. 54	54 vs. 20	20 vs. 40	40 vs. 54	54 vs. 20
0.012236	0.278667	0.018059	0.015884	0.277554	0.020677
Strain Ratio @ 12,000 cycles_ HMA_STA					
arithmetic scale			log-log scale		
20°C	40°C	54°C	20°C	40°C	54°C
5.768832	11.57699	12.53475	0.761088	1.063596	1.098116
7.302311	13.11984	10.68156	0.86346	1.117929	1.028635
P-values					
20 vs. 40	40 vs. 54	54 vs. 20	20 vs. 40	40 vs. 54	54 vs. 20
0.016637	0.300883	0.02594	0.020338	0.29897	0.027837

Table 5.18 T-test results of strain ratios of long-term aging Level 1 conditioned mixtures at different test temperatures: (a) WMA Evotherm, (b) WMA Foam, and (c) HMA.

(a)

Strain Ratio @ 5,000 cycles_ Evth_LTA1					
arithmetic scale			log-log scale		
20°C	40°C	54°C	20°C	40°C	54°C
7.141502	12.59632	12.59632	0.85379	1.100244	1.100244
	13.39525	13.39525		1.126951	1.126951
P-values					
20 vs. 40	40 vs. 54	54 vs. 20	20 vs. 40	40 vs. 54	54 vs. 20
	0.5			0.5	
Strain Ratio @ 8,500 cycles_ Evth_LTA1					
arithmetic scale			log-log scale		
20°C	40°C	54°C	20°C	40°C	54°C
8.155994	12.72356	13.43433	0.911477	1.104609	1.128216
	13.81084	14.59956	#NUM!	1.14022	1.16434
P-values					
20 vs. 40	40 vs. 54	54 vs. 20	20 vs. 40	40 vs. 54	54 vs. 20
	0.223044			0.223042	
Strain Ratio @ 12,000 cycles_ Evth_LTA1					
arithmetic scale			log-log scale		
20°C	40°C	54°C	20°C	40°C	54°C
8.979274	13.02858	13.79157	0.953241	1.114897	1.139614
	14.08564	15.04503	#NUM!	1.148776	1.177393
P-values					
20 vs. 40	40 vs. 54	54 vs. 20	20 vs. 40	40 vs. 54	54 vs. 20
	0.201859			0.201758	

(b)

Strain Ratio @ 5,000 cycles_ Foam_LTA1					
arithmetic scale			log-log scale		
20°C	40°C	54°C	20°C	40°C	54°C
	13.44824	11.30305		1.128666	1.053196
	15.42935	10.94626		1.188348	1.039266
P-values					
20 vs. 40	40 vs. 54	54 vs. 20	20 vs. 40	40 vs. 54	54 vs. 20
	0.04058			0.03354	
Strain Ratio @ 8,500 cycles_ Foam_LTA1					
arithmetic scale			log-log scale		
20°C	40°C	54°C	20°C	40°C	54°C
	13.66436	11.7026		1.135589	1.068282
	15.59484	11.23492		1.192981	1.05057
P-values					
20 vs. 40	40 vs. 54	54 vs. 20	20 vs. 40	40 vs. 54	54 vs. 20
	0.043079			0.036569	
Strain Ratio @ 12,000 cycles_ Foam_LTA1					
arithmetic scale			log-log scale		
20°C	40°C	54°C	20°C	40°C	54°C
	13.58569	11.88811		1.133082	1.075113
	15.87612	11.37183		1.200744	1.05583
P-values					
20 vs. 40	40 vs. 54	54 vs. 20	20 vs. 40	40 vs. 54	54 vs. 20
	0.059201			0.051081	

(c)

Strain Ratio @ 5,000 cycles_ HMA_LTA1					
arithmetic scale			log-log scale		
20°C	40°C	54°C	20°C	40°C	54°C
4.440774	12.38435	12.18612	0.647459	1.092873	1.085866
5.728652	16.61517		0.758052	1.220505	#NUM!
P-values					
20 vs. 40	40 vs. 54	54 vs. 20	20 vs. 40	40 vs. 54	54 vs. 20
0.02549			0.016452		
Strain Ratio @ 8,500 cycles_ HMA_LTA1					
arithmetic scale			log-log scale		
20°C	40°C	54°C	20°C	40°C	54°C
5.646302	12.68839	12.69333	0.751764	1.103406	1.103575
7.271562	17.64943		0.861628	1.246731	#NUM!
P-values					
20 vs. 40	40 vs. 54	54 vs. 20	20 vs. 40	40 vs. 54	54 vs. 20
0.039639			0.027579		
Strain Ratio @ 12,000 cycles_ HMA_LTA1					
arithmetic scale			log-log scale		
20°C	40°C	54°C	20°C	40°C	54°C
6.628273	12.82351	12.88881	0.8214	1.108007	1.110213
8.5912	18.21532		0.934054	1.260437	#NUM!
P-values					
20 vs. 40	40 vs. 54	54 vs. 20	20 vs. 40	40 vs. 54	54 vs. 20
0.055117			0.041885		

Table 5.19 T-test results of strain ratios of long-term aging Level 3 conditioned mixtures at different test temperatures: (a) WMA Evotherm, (b) WMA Foam, and (c) HMA.

(a)

Strain Ratio @ 5,000 cycles_ Evth_LTA3					
arithmetic scale			log-log scale		
20°C	40°C	54°C	20°C	40°C	54°C
5.152874	12.26551	11.31418	0.71205	1.088686	1.053623
9.623962	14.03911	12.4257	0.983354	1.14734	1.094321
P-values					
20 vs. 40	40 vs. 54	54 vs. 20	20 vs. 40	40 vs. 54	54 vs. 20
0.069382	0.172585	0.095567	0.095407	0.171297	0.120406
Strain Ratio @ 8,500 cycles_ Evth_LTA3					
arithmetic scale			log-log scale		
20°C	40°C	54°C	20°C	40°C	54°C
5.932188	13.02858	11.74404	0.773215	1.114897	1.069818
11.46401	14.08564	12.91518	1.059337	1.148776	1.1111
P-values					
20 vs. 40	40 vs. 54	54 vs. 20	20 vs. 40	40 vs. 54	54 vs. 20
0.113287	0.129977	0.163831	0.136617	0.130683	0.17571
'Strain Ratio @ 12,000 cycles_ Evth_LTA3					
arithmetic scale			log-log scale		
20°C	40°C	54°C	20°C	40°C	54°C
6.553235	12.6895	11.99134	0.816456	1.103444	1.078868
12.36862	14.69109	13.1922	1.092321	1.167054	1.120317
P-values					
20 vs. 40	40 vs. 54	54 vs. 20	20 vs. 40	40 vs. 54	54 vs. 20
0.151405	0.222968	0.201119	0.164807	0.223368	0.203589

(b)

Strain Ratio @ 5,000 cycles_ Foam_LTA3					
arithmetic scale			log-log scale		
20°C	40°C	54°C	20°C	40°C	54°C
6.941492	14.6257	11.75784	0.841453	1.165117	1.070328
5.985289	15.68564	13.74333	0.777085	1.195502	1.138092
P-values					
20 vs. 40	40 vs. 54	54 vs. 20	20 vs. 40	40 vs. 54	54 vs. 20
0.003338	0.083025	0.014684	0.004538	0.088472	0.012098
Strain Ratio @ 8,500 cycles_ Foam_LTA3					
arithmetic scale			log-log scale		
20°C	40°C	54°C	20°C	40°C	54°C
8.696009	15.11122	12.07905	0.93932	1.1793	1.082033
7.313989	15.94732	12.02638	0.864154	1.202688	1.080135
P-values					
20 vs. 40	40 vs. 54	54 vs. 20	20 vs. 40	40 vs. 54	54 vs. 20
0.005663	0.007104	0.013984	0.009009	0.005602	0.020621
Strain Ratio @ 12,000 cycles_ Foam_LTA3					
arithmetic scale			log-log scale		
20°C	40°C	54°C	20°C	40°C	54°C
9.868516	15.35089	12.46742	0.994252	1.186134	1.095777
8.284869	16.27989	12.24402	0.918286	1.211651	1.087924
P-values					
20 vs. 40	40 vs. 54	54 vs. 20	20 vs. 40	40 vs. 54	54 vs. 20
0.009029	0.00927	0.027322	0.013103	0.0076	0.03549

(c)

Strain Ratio @ 5,000 cycles_ HMA_LTA3					
arithmetic scale			log-log scale		
20°C	40°C	54°C	20°C	40°C	54°C
4.221761	13.55399	14.99973	0.625494	1.132067	1.176083
4.143566	16.50677	11.99022	0.617374	1.217662	1.078827
P-values					
20 vs. 40	40 vs. 54	54 vs. 20	20 vs. 40	40 vs. 54	54 vs. 20
0.009018	0.27107	0.012573	0.00299	0.270196	0.004586
Strain Ratio @ 8,500 cycles_ HMA_LTA3					
arithmetic scale			log-log scale		
20°C	40°C	54°C	20°C	40°C	54°C
5.224059	13.95263	15.31799	0.718008	1.144656	1.185202
5.277425	17.35552	12.32842	0.722422	1.239438	1.090908
P-values					
20 vs. 40	40 vs. 54	54 vs. 20	20 vs. 40	40 vs. 54	54 vs. 20
0.012863	0.251865	0.014547	0.00498	0.252033	0.00626
Strain Ratio @ 12,000 cycles_ HMA_LTA3					
arithmetic scale			log-log scale		
20°C	40°C	54°C	20°C	40°C	54°C
5.922251	14.33945	15.49023	0.772487	1.156533	1.190058
6.04776	17.59216	12.60436	0.781595	1.245319	1.100521
P-values					
20 vs. 40	40 vs. 54	54 vs. 20	20 vs. 40	40 vs. 54	54 vs. 20
0.012788	0.23532	0.015313	0.005451	0.235309	0.007303

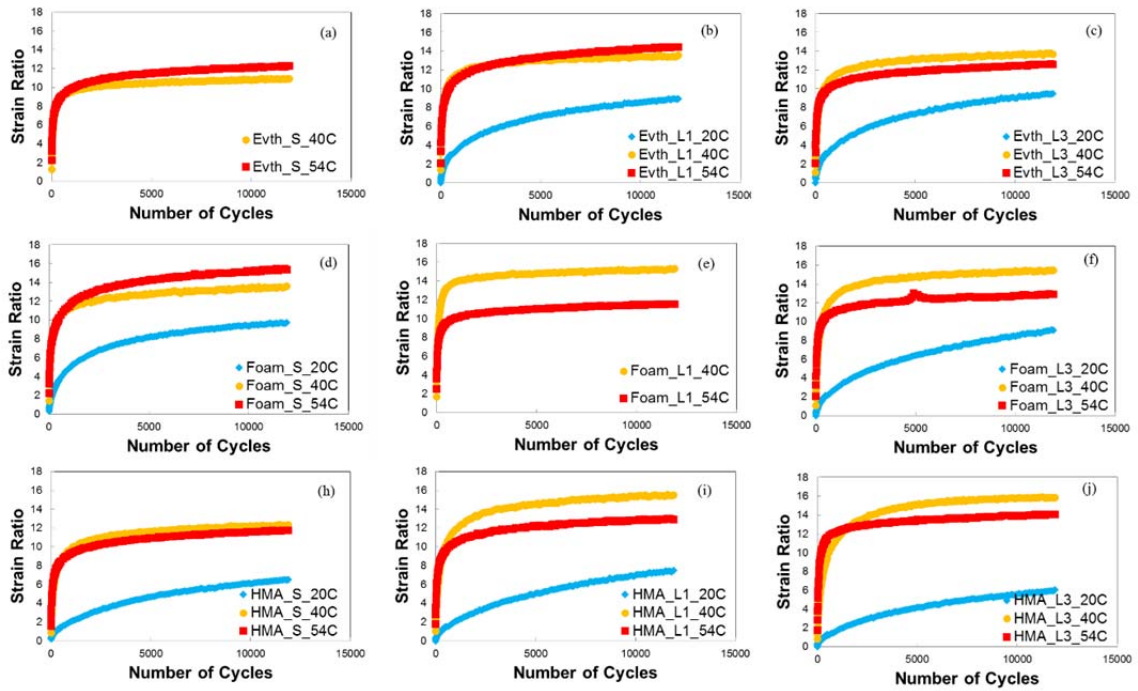


Figure 5.23 Comparison of strain ratios for different temperatures in arithmetic scale.

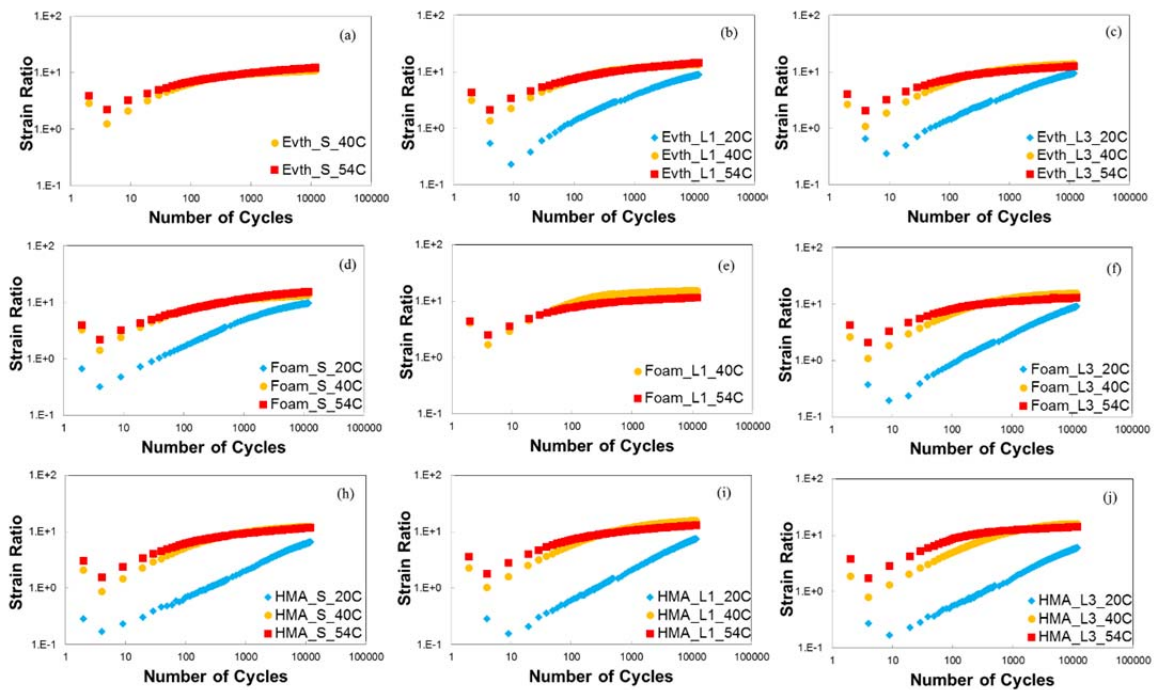


Figure 5.24 Comparison of strain ratio among different test temperatures in log-log scale.

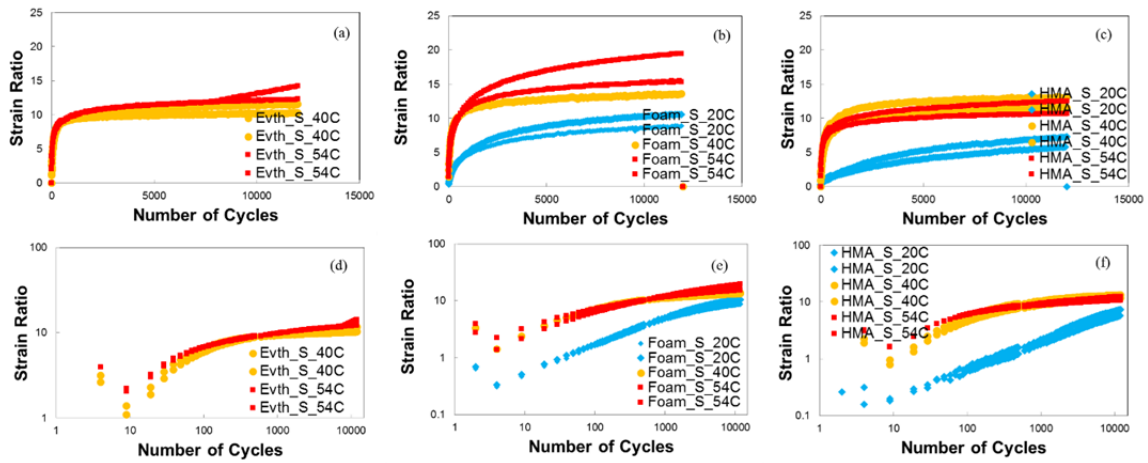


Figure 5.25 Comparison of strain ratios among short-term aging replicates tested at different temperatures in arithmetic scale and log-log scale.

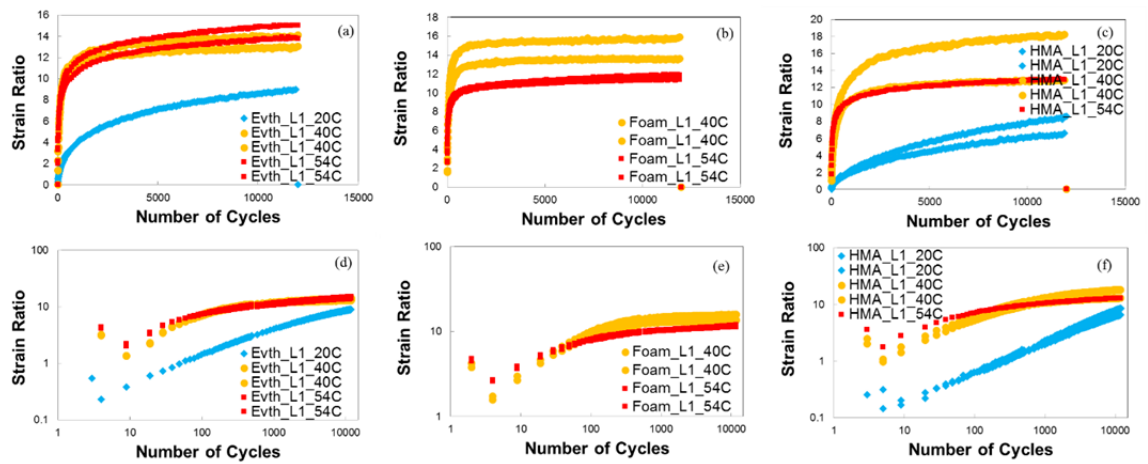


Figure 5.26 Comparison of strain ratios among long-term aging Level 1 conditioned replicates tested at different temperatures in arithmetic scale and log-log scale.

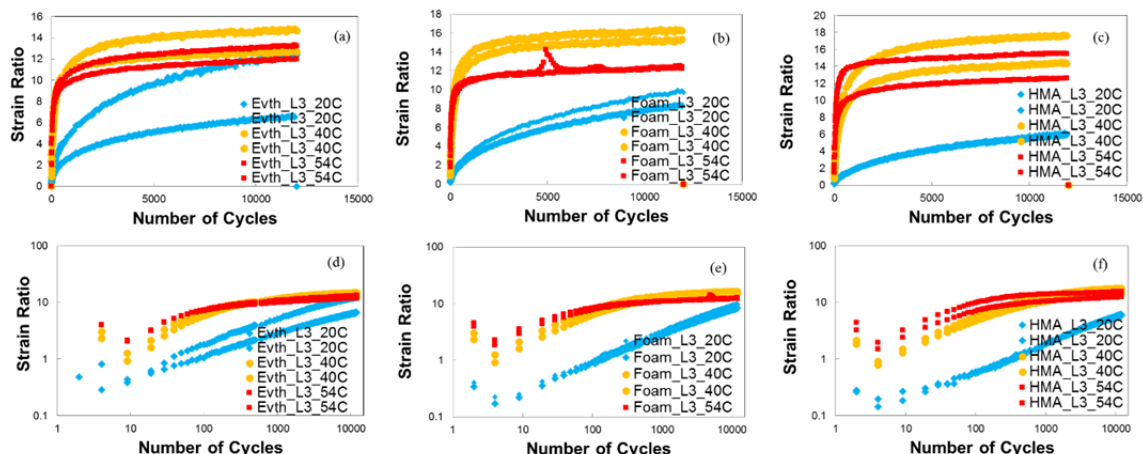


Figure 5.27 Comparison of strain ratios among long-term aging conditioned replicates tested at different temperatures in arithmetic scale and log-log scale.

Table 5.20 T-test results of strain ratios among different mixtures at 20°C: (a) short-term aging conditioning, (b) long-term aging condition Level 1, and (c) long-term aging condition Level 3.

(a)

Strain Ratio @ 5,000 cycles_ STA_ 20C					
arithmetic scale			log-log scale		
Evth	Foam	HMA	Evth	Foam	HMA
	7.504659	4.031286		0.875331	0.605444
	8.849322	5.296495		0.94691	0.723989
P-values					
Evth vs. Foam	Foam vs. HMA	HMA vs. Evth	Evth vs. Foam	Foam vs. HMA	HMA vs. Evth
	0.031317			0.035345	
Strain Ratio @ 8,500 cycles_ STA_ 20°C					
arithmetic scale			log-log scale		
Evth	Foam	HMA	Evth	Foam	HMA
	8.252886	5.094207		0.916606	0.707077
	10.01729	6.488092		1.00075	0.812117
P-values					
Evth vs. Foam	Foam vs. HMA	HMA vs. Evth	Evth vs. Foam	Foam vs. HMA	HMA vs. Evth
	0.048445			0.048893	
Strain Ratio @ 12,000 cycles_ STA_ 20°C					
arithmetic scale			log-log scale		
Evth	Foam	HMA	Evth	Foam	HMA
	8.879583	5.768832		0.948393	0.761088
	10.55557	7.302311		1.023482	0.86346
P-values					
Evth vs. Foam	Foam vs. HMA	HMA vs. Evth	Evth vs. Foam	Foam vs. HMA	HMA vs. Evth
	0.053649			0.055837	

(b)

Strain Ratio @ 5,000 cycles_ LTA1_20°C					
arithmetic scale			log-log scale		
Evth	Foam	HMA	Evth	Foam	HMA
7.141502		4.440774	0.85379		0.647459
		5.728652			0.758052
P-values					
Evth vs. Foam	Foam vs. HMA	HMA vs. Evth	Evth vs. Foam	Foam vs. HMA	HMA vs. Evth
Strain Ratio @ 8,500 cycles_ LTA1_20°C					
arithmetic scale			log-log scale		
Evth	Foam	HMA	Evth	Foam	HMA
8.155994		5.646302	0.911477		0.751764
		7.271562			0.861628
P-values					
Evth vs. Foam	Foam vs. HMA	HMA vs. Evth	Evth vs. Foam	Foam vs. HMA	HMA vs. Evth
Strain Ratio @ 12,000 cycles_ LTA1_20°C					
arithmetic scale			log-log scale		
Evth	Foam	HMA	Evth	Foam	HMA
8.979274		6.628273	0.953241		0.8214
		8.5912			0.934054
P-values					
Evth vs. Foam	Foam vs. HMA	HMA vs. Evth	Evth vs. Foam	Foam vs. HMA	HMA vs. Evth

(c)

Strain Ratio @ 5,000 cycles_ LTA3_20°C					
arithmetic scale			log-log scale		
Evth	Foam	HMA	Evth	Foam	HMA
5.152874	6.941492	4.221761	0.71205	0.841453	0.625494
9.623962	5.985289	4.143566	0.983354	0.777085	0.617374
P-values					
Evth vs. Foam	Foam vs. HMA	HMA vs. Evth	Evth vs. Foam	Foam vs. HMA	HMA vs. Evth
0.36246	0.020751	0.144027	0.404338	0.014277	0.118697
Strain Ratio @ 8,500 cycles_ LTA3_20°C					
arithmetic scale			log-log scale		
Evth	Foam	HMA	Evth	Foam	HMA
5.932188	8.696009	5.224059	0.773215	0.93932	0.718008
11.46401	7.313989	5.277425	1.059337	0.864154	0.722422
P-values					
Evth vs. Foam	Foam vs. HMA	HMA vs. Evth	Evth vs. Foam	Foam vs. HMA	HMA vs. Evth
0.415289	0.028821	0.169416	0.465333	0.020212	0.152065
Strain Ratio @ 12,000 cycles_ LTA3_20°C					
arithmetic scale			log-log scale		
Evth	Foam	HMA	Evth	Foam	HMA
6.553235	9.868516	5.922251	0.816456	0.994252	0.772487
12.36862	8.284869	6.04776	1.092321	0.918286	0.781595
P-values					
Evth vs. Foam	Foam vs. HMA	HMA vs. Evth	Evth vs. Foam	Foam vs. HMA	HMA vs. Evth
0.455104	0.030058	0.177265	0.495354	0.021332	0.163749

Table 5.21 T-test results of strain ratios among different mixtures at 40°C: (a) short-term aging conditioning, (b) long-term aging condition Level 1, and (c) long-term aging condition Level 3.

(a)

Strain Ratio @ 5,000 cycles_ STA_ 40°C					
arithmetic scale			log-log scale		
Evth	Foam	HMA	Evth	Foam	HMA
10.89405	12.73183	10.86398	1.037189	1.104891	1.035989
9.922292		12.43678	0.996612		1.094708
P-values					
Evth vs. Foam	Foam vs. HMA	HMA vs. Evth	Evth vs. Foam	Foam vs. HMA	HMA vs. Evth
		0.155584			0.153747
Strain Ratio @ 8,500 cycles_ STA_ 40°C					
arithmetic scale			log-log scale		
Evth	Foam	HMA	Evth	Foam	HMA
11.29919	13.2394	11.32464	1.053047	1.121868	1.054024
10.07441		12.74515	1.00322		1.105345
P-values					
Evth vs. Foam	Foam vs. HMA	HMA vs. Evth	Evth vs. Foam	Foam vs. HMA	HMA vs. Evth
		0.143572			0.143099
Strain Ratio @ 12,000 cycles_ STA_ 40°C					
arithmetic scale			log-log scale		
Evth	Foam	HMA	Evth	Foam	HMA
11.58211	13.60369	11.57699	1.063788	1.133657	1.063596
10.27509		13.11984	1.011786		1.117929
P-values					
Evth vs. Foam	Foam vs. HMA	HMA vs. Evth	Evth vs. Foam	Foam vs. HMA	HMA vs. Evth
		0.147688			0.147129

(b)

Strain Ratio @ 5,000 cycles_ LTA1_ 40°C					
arithmetic scale			log-log scale		
Evth	Foam	HMA	Evth	Foam	HMA
12.59632	13.44824	12.38435	1.100244	1.128666	1.092873
13.39525	15.42935	16.61517	1.126951	1.188348	1.220505
P-values					
Evth vs. Foam	Foam vs. HMA	HMA vs. Evth	Evth vs. Foam	Foam vs. HMA	HMA vs. Evth
0.154613	0.490774	0.278549	0.151623	0.49088	0.288302
Strain Ratio @ 8,500 cycles_ LTA1_ 40°C					
arithmetic scale			log-log scale		
Evth	Foam	HMA	Evth	Foam	HMA
12.72356	13.66436	12.68839	1.104609	1.135589	1.103406
13.81084	15.59484	17.64943	1.14022	1.192981	1.246731
P-values					
Evth vs. Foam	Foam vs. HMA	HMA vs. Evth	Evth vs. Foam	Foam vs. HMA	HMA vs. Evth
0.1719	0.429087	0.266012	0.170387	0.45085	0.274887
Strain Ratio @ 12,000 cycles_ LTA1_ 40°C					
arithmetic scale			log-log scale		
Evth	Foam	HMA	Evth	Foam	HMA
13.02858	13.58569	12.82351	1.114897	1.133082	1.108007
14.08564	15.87612	18.21532	1.148776	1.200744	1.260437
P-values					
Evth vs. Foam	Foam vs. HMA	HMA vs. Evth	Evth vs. Foam	Foam vs. HMA	HMA vs. Evth
0.225145	0.406501	0.274582	0.225879	0.427389	0.285678

(c)

Strain Ratio @ 5,000 cycles_ LTA3_ 40°C					
arithmetic scale			log-log scale		
Evth	Foam	HMA	Evth	Foam	HMA
12.26551	14.6257	13.55399	1.088686	1.165117	1.132067
14.03911	15.68564	16.50677	1.14734	1.195502	1.217662
P-values					
Evth vs. Foam	Foam vs. HMA	HMA vs. Evth	Evth vs. Foam	Foam vs. HMA	HMA vs. Evth
0.096019	0.471806	0.194685	0.09996	0.457763	0.193751
Strain Ratio @ 8,500 cycles_ LTA3_ 40°C					
arithmetic scale			log-log scale		
Evth	Foam	HMA	Evth	Foam	HMA
13.02858	15.11122	13.95263	1.114897	1.1793	1.144656
14.08564	15.94732	17.35552	1.148776	1.202688	1.239438
P-values					
Evth vs. Foam	Foam vs. HMA	HMA vs. Evth	Evth vs. Foam	Foam vs. HMA	HMA vs. Evth
0.049807	0.474847	0.180153	0.051375	0.492372	0.177072
Strain Ratio @ 12,000 cycles_ LTA3_ 40°C					
arithmetic scale			log-log scale		
Evth	Foam	HMA	Evth	Foam	HMA
12.6895	15.35089	14.33945	1.103444	1.186134	1.156533
14.69109	16.27989	17.59216	1.167054	1.211651	1.245319
P-values					
Evth vs. Foam	Foam vs. HMA	HMA vs. Evth	Evth vs. Foam	Foam vs. HMA	HMA vs. Evth
0.096974	0.468621	0.177822	0.102202	0.484444	0.176089

Table 5.22 T-test results of strain ratios among different mixtures at 54°C: (a) short-term aging conditioning, (b) long-term aging condition Level 1, and (c) long-term aging condition Level 3.

(a)

Strain Ratio @ 5,000 cycles_ STA_ 54°C					
arithmetic scale			log-log scale		
Evth	Foam	HMA	Evth	Foam	HMA
11.46044	14.25064	11.40035	1.059201	1.153834	1.056918
11.4558	16.95711	10.06244	1.059025	1.229352	1.002703
P-values					
Evth vs. Foam	Foam vs. HMA	HMA vs. Evth	Evth vs. Foam	Foam vs. HMA	HMA vs. Evth
0.046035	0.042029	0.19541	0.036255	0.036778	0.196361
Strain Ratio @ 8,500 cycles_ STA_ 54°C					
arithmetic scale			log-log scale		
Evth	Foam	HMA	Evth	Foam	HMA
12.3397	14.96906	12.0952	1.091305	1.175195	1.082613
11.99485	18.50324	10.465	1.078995	1.267248	1.019739
P-values					
Evth vs. Foam	Foam vs. HMA	HMA vs. Evth	Evth vs. Foam	Foam vs. HMA	HMA vs. Evth
0.061812	0.053577	0.199241	0.0497	0.046369	0.200018
Strain Ratio @ 12,000 cycles_ STA_ 54°C					
arithmetic scale			log-log scale		
Evth	Foam	HMA	Evth	Foam	HMA
12.53475	15.33064	11.57699	1.098116	1.18556	1.063596
10.68156	19.50535	13.11984	1.028635	1.290154	1.117929
P-values					
Evth vs. Foam	Foam vs. HMA	HMA vs. Evth	Evth vs. Foam	Foam vs. HMA	HMA vs. Evth
0.062987	0.075198	0.300883	0.05438	0.064974	0.29897

(b)

Strain Ratio @ 5,000 cycles_ LTA1_ 54°C					
arithmetic sscale			log-log scale		
Evth	Foam	HMA	Evth	Foam	HMA
12.59632	11.30305	12.18612	1.100244	1.053196	1.085866
13.39525	10.94626		1.126951	1.039266	#NUM!
P-values					
Evth vs. Foam	Foam vs. HMA	HMA vs. Evth	Evth vs. Foam	Foam vs. HMA	HMA vs. Evth
0.025279			0.023261		
Strain Ratio @ 8,500 cycles_ LTA1_ 54°C					
arithmetic sscale			log-log scale		
Evth	Foam	HMA	Evth	Foam	HMA
13.43433	11.7026	12.69333	1.128216	1.068282	1.103575
14.59956	11.23492		1.16434	1.05057	#NUM!
P-values					
Evth vs. Foam	Foam vs. HMA	HMA vs. Evth	Evth vs. Foam	Foam vs. HMA	HMA vs. Evth
0.027838			0.024841		
Strain Ratio @ 12,000 cycles_ LTA1_ 54°C					
arithmetic sscale			log-log scale		
Evth	Foam	HMA	Evth	Foam	HMA
13.79157	11.88811	12.88881	1.139614	1.075113	1.110213
15.04503	11.37183		1.177393	1.05583	#NUM!
P-values					
Evth vs. Foam	Foam vs. HMA	HMA vs. Evth	Evth vs. Foam	Foam vs. HMA	HMA vs. Evth
0.027161			0.024119		

(c)

Strain Ratio @ 5,000 cycles_ LTA3_54°C					
arithmetic scale			log-log scale		
Evth	Foam	HMA	Evth	Foam	HMA
11.31418	11.75784	14.99973	1.053623	1.070328	1.176083
12.4257	13.74333	11.99022	1.094321	1.138092	1.078827
P-values					
Evth vs. Foam	Foam vs. HMA	HMA vs. Evth	Evth vs. Foam	Foam vs. HMA	HMA vs. Evth
0.25994	0.359861	0.208831	0.262091	0.366377	0.208537
Strain Ratio @ 8,500 cycles_ LTA3_54°C					
arithmetic scale			log-log scale		
Evth	Foam	HMA	Evth	Foam	HMA
11.74404	12.07905	15.31799	1.069818	1.082033	1.185202
12.91518	12.02638	12.32842	1.1111	1.080135	1.090908
P-values					
Evth vs. Foam	Foam vs. HMA	HMA vs. Evth	Evth vs. Foam	Foam vs. HMA	HMA vs. Evth
0.341587	0.178988	0.225199	0.347255	0.175234	0.226356
Strain Ratio @ 12,000 cycles_ LTA3_54°C					
arithmetic scale			log-log scale		
Evth	Foam	HMA	Evth	Foam	HMA
11.99134	12.46742	15.49023	1.078868	1.095777	1.190058
13.1922	12.24402	12.60436	1.120317	1.087924	1.100521
P-values					
Evth vs. Foam	Foam vs. HMA	HMA vs. Evth	Evth vs. Foam	Foam vs. HMA	HMA vs. Evth
0.368184	0.181469	0.225004	0.374392	0.178218	0.22604

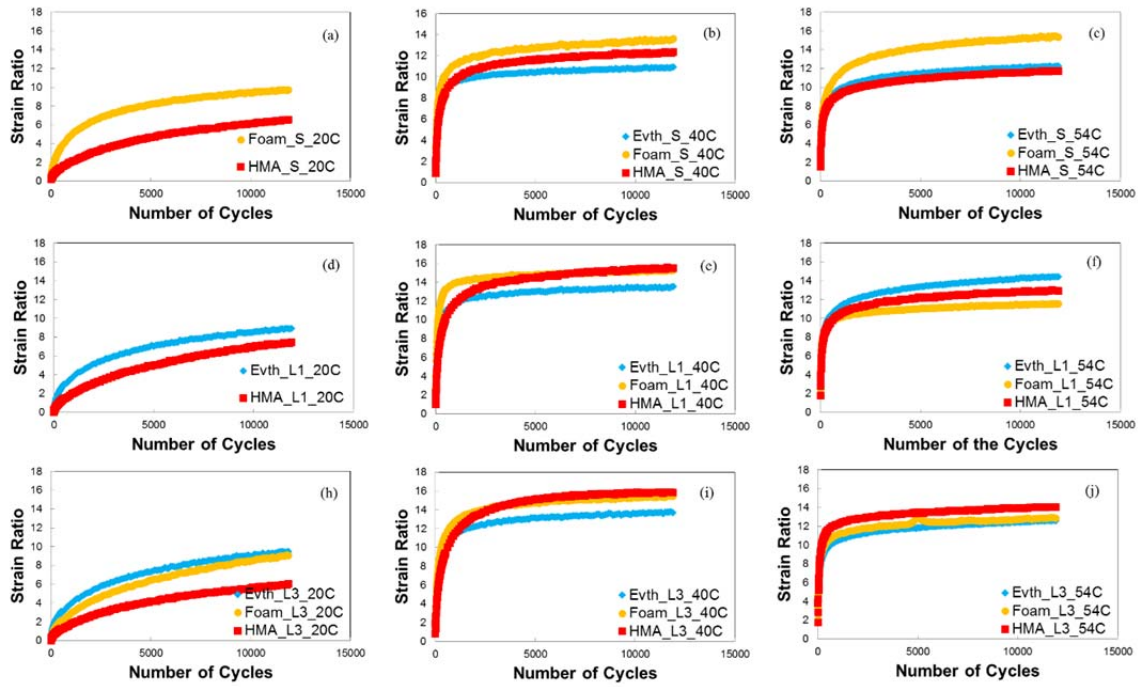


Figure 5.28 Comparison of strain ratios among different mixtures in arithmetic scale.

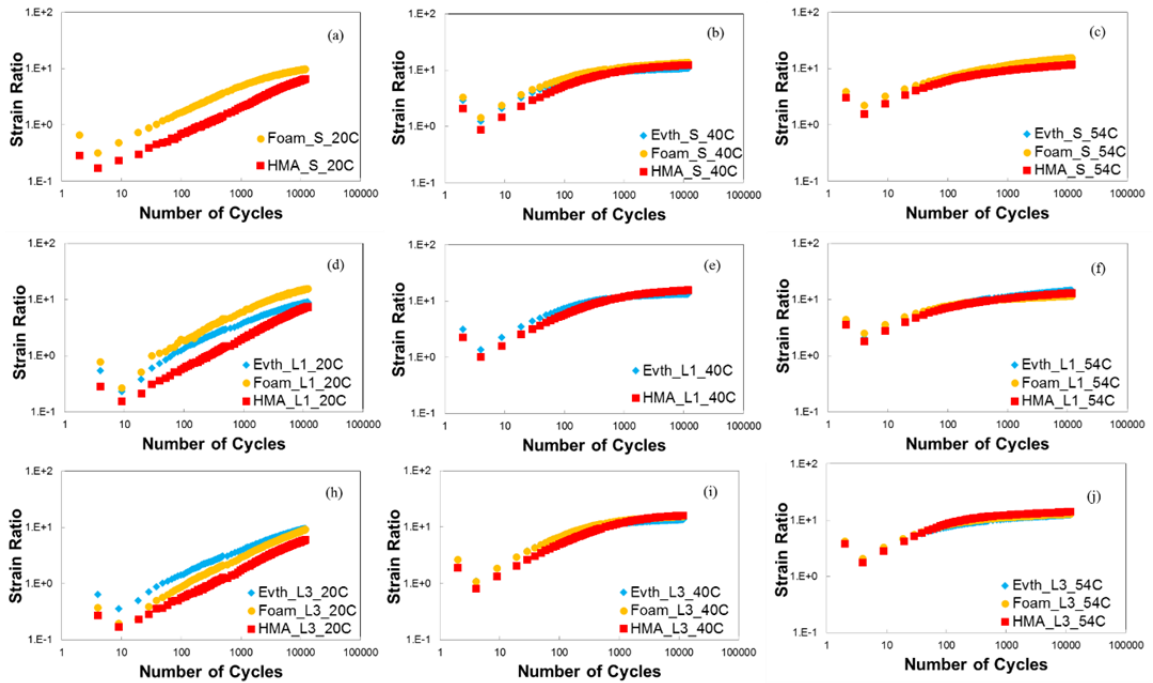


Figure 5.29 Comparison of strain ratios among different mixtures in log-log scale.

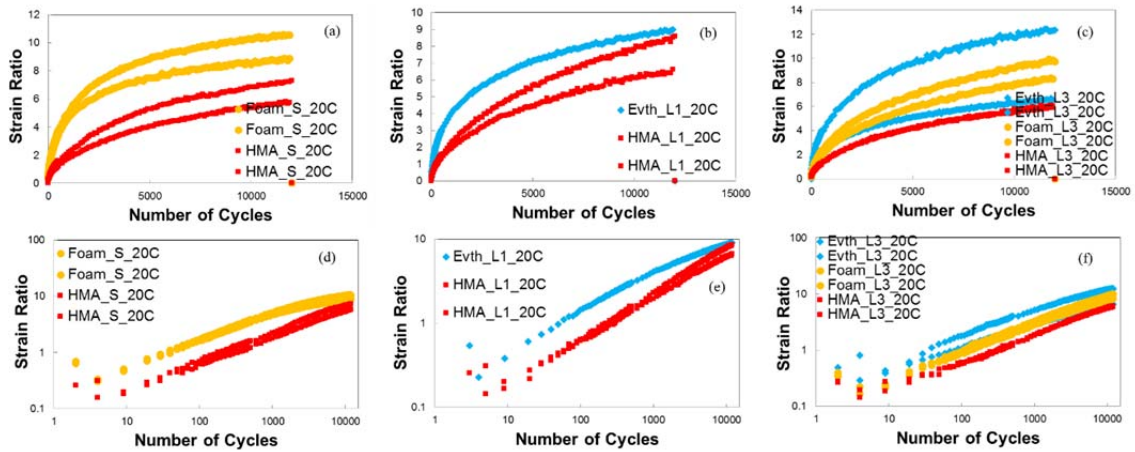


Figure 5.30 Comparison of strain ratios among replicates of different mixtures at 20°C.

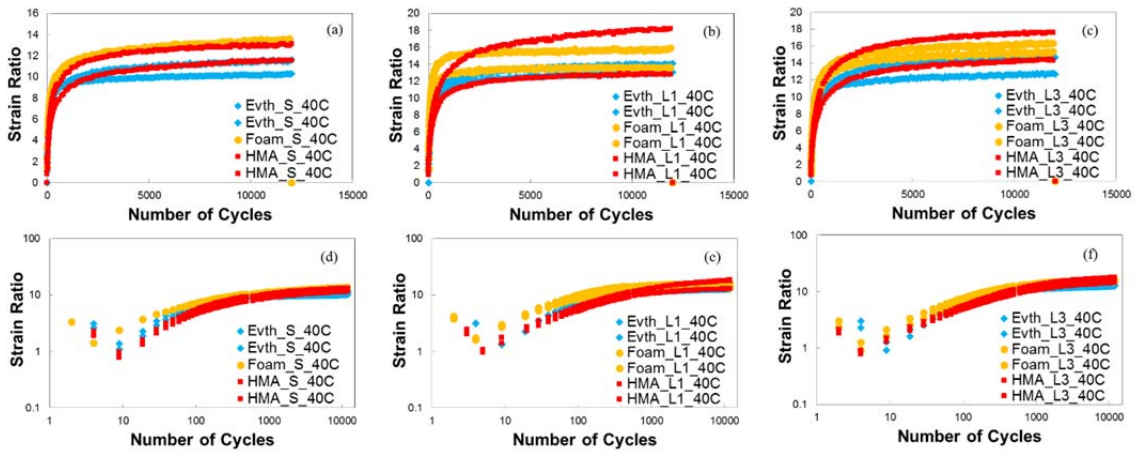


Figure 5.31 Comparison of strain ratios among replicates of different mixtures at 40°C.

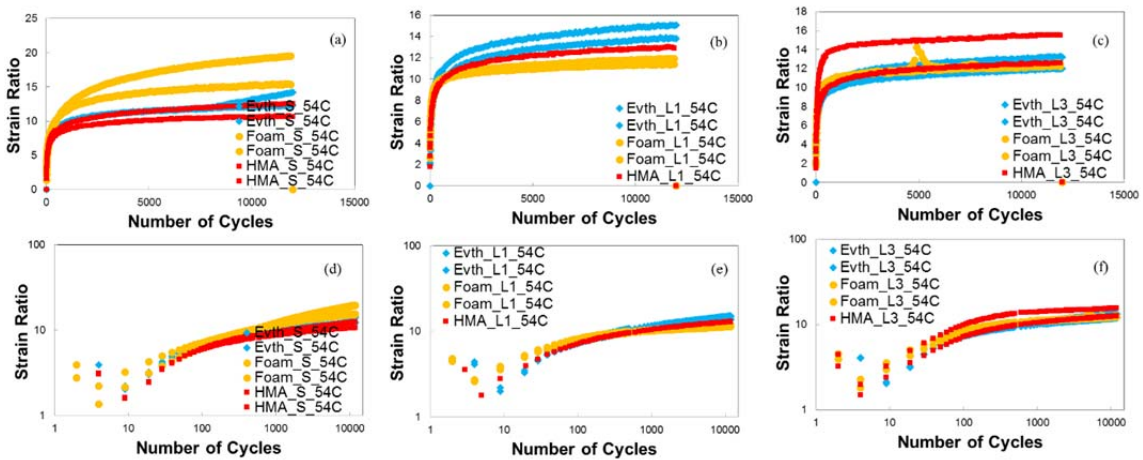


Figure 5.32 Comparison of strain ratios among replicates of different mixtures at 54°C.

5.3.2 Permanent Deformation Coefficients in Pavement ME

5.3.2.1 Permanent Deformation Coefficients Regression Procedure

One of the design steps in the Pavement ME program is to input the rutting material-specific coefficients, because these coefficients differentiate the materials and directly reflect the rutting resistance of the utilized material. Otherwise, the volumetric properties and linear viscoelastic properties of the materials alone are not sufficient to predict the permanent deformation of the pavement throughout the design life. Also, the material-specific coefficients should be obtained prior to state-wise local calibration. This study used the TRLPD test as the rutting test method, and the coefficients for the Pavement ME program were regressed based on the laboratory test results. The prediction theory is presented in Section 3.4.1, and the governing equation for the asphalt concrete layers are re-presented here as Equation (6.11).

$$\frac{\varepsilon_p}{\varepsilon_r} = K_z * \beta_{r1} * 10^{k_{r1}} T^{\beta_{r2} * k_{r2}} N^{\beta_{r3} * k_{r3}} \quad (6.11)$$

In Equation (5.11), K_z functions as a laboratory-to-field shift factor, and although $\beta_{r1}, \beta_{r2}, \beta_{r3}$ can be obtained by state-wise local calibration, k_{r1}, k_{r2}, k_{r3} are the material-specific coefficients. The test methods are presented in Section 3.4.1, and the regression procedure is summarized in the following text.

Note that, for the sake of the laboratory experimental study and because the coefficients should be obtained prior to the structural design and local calibration, the laboratory-to-field shift factor K_z and local calibration factors $\beta_{r1}, \beta_{r2}, \beta_{r3}$ should be used with value 1. Therefore, Equation (6.11) can be reintroduced as Equation (6.12):

$$\frac{\varepsilon_p}{\varepsilon_r} = K_1 T^{K_2} N^{K_3} \quad (6.12)$$

where $K_1 = \beta_{r1} * 10^{k_{r1}}$

$$K_2 = k_{r2} * \beta_{r2}$$

$$K_3 = k_{r3} * \beta_{r3}$$

Let $K_1 T^{K_2} = A$ to obtain:

$$\log\left(\frac{\varepsilon_p}{\varepsilon_r}\right) = \log(A) + K_3 \log(N) \quad (6.13)$$

and

$$\log(A) = \log(K_1) + K_2 \log(T) \quad (6.14)$$

The first step of regression is to obtain the K_3 value. For this study, in order to ensure that the regression was conducted in the secondary stage, as shown Figure 3.9 in which $\log \frac{\varepsilon_p}{\varepsilon_r}$ and $\log N$ have a linear relationship, data for the last 5,000 cycles of the total 12,000 loading cycles were adopted, because none of the tested North Carolina mixtures had a tertiary flow stage. The $\log \frac{\varepsilon_p}{\varepsilon_r}$ versus $\log N$ curves were plotted at each corresponding temperature, and three K_3 values representing each temperature, i.e., K_{3-20} , K_{3-40} , K_{3-54} , were obtained. The final K_3 is the average of K_{3-20} , K_{3-40} , and K_{3-54} . Using the single K_3 value rather than the three K_3 values for each temperature, the Microsoft Excel Solver numerical optimization routine was run three times for three sets of data at the three temperatures by changing the $\log A_{20}$, $\log A_{40}$, and $\log A_{54}$ to obtain the least sum square error of $\log \frac{\varepsilon_p}{\varepsilon_r}$, respectively, and the optimized $\log A_{20}$, $\log A_{40}$, and $\log A_{54}$ could be obtained. Using the three temperatures in Fahrenheit as well as $\log A_{20}$, $\log A_{40}$, and $\log A_{54}$, $\log K_1$ and K_2 in Equation (6.14) also could be obtained by fitting. In this way, the material-specific coefficients k_{r1} , k_{r2} , and k_{r3} could be calculated.

It is necessary to point out that, although the values of K_{3-40} and K_{3-54} are not significantly different, a large difference exists between K_{3-20} and the other two. This difference might be because the tests for K_{3-20} were conducted at a relatively low temperature, so 12,000 cycles were not sufficient to allow the mixtures to change from the viscoelastic domain to the viscoplastic domain. However, K_{3-20} was utilized anyway for two reasons: 1) the 20°C data are important because the time with the relatively low pavement temperatures consumes a large part of a day, and 2) the final fitting results were better with K_{3-20} than without K_{3-20} .

The regression procedure used in this study is consistent with previous work conducted at NCSU. Details and explanations can be found in Jadoun (2011); Figure 5.6 presents a schematic diagram from Jadoun (2011) that succinctly describes the whole procedure.

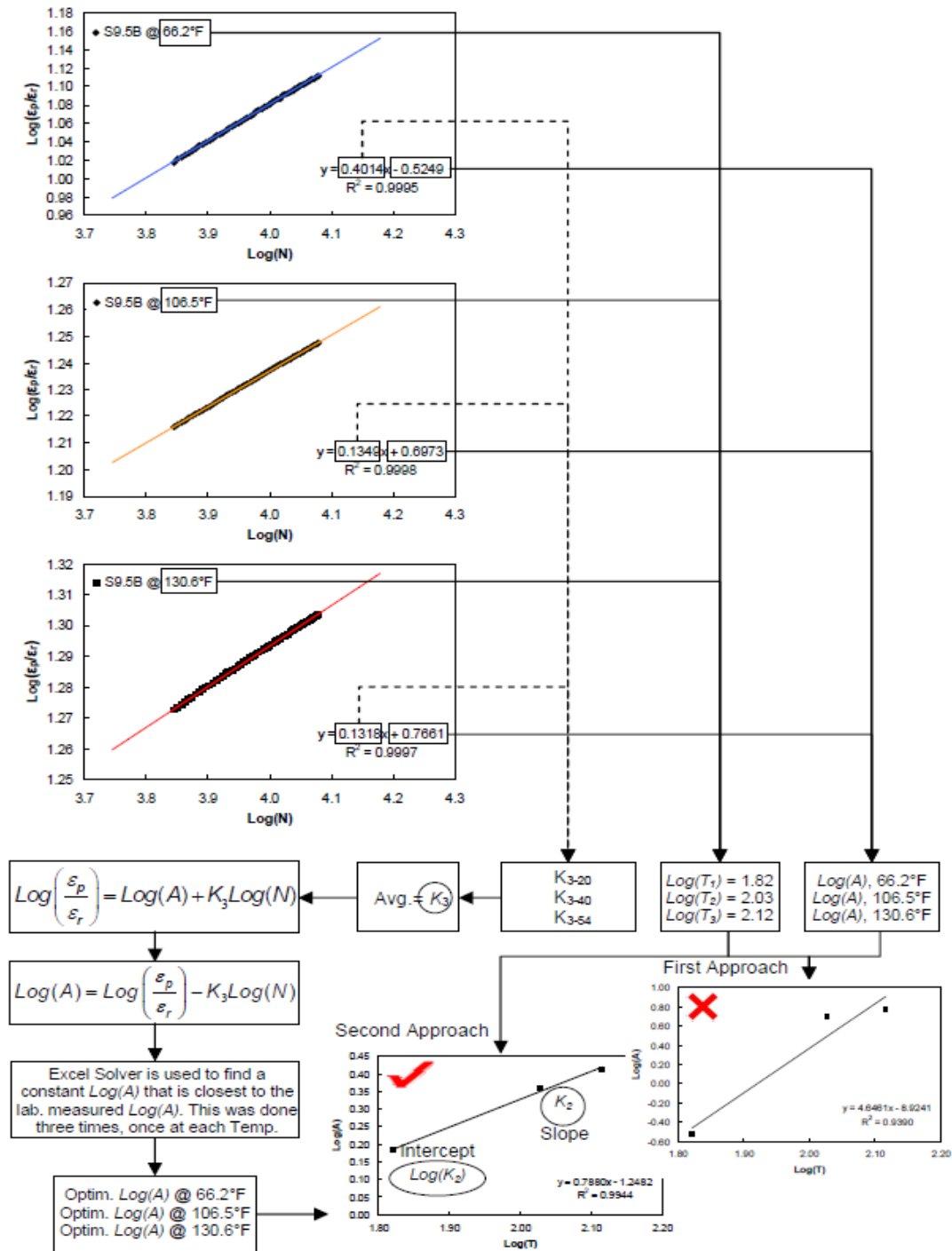


Figure 5.33 Schematic diagram showing the regression procedure for rutting using material-specific coefficients (Jadoun 2012).

5.3.2.2 Rutting Material-Specific Coefficients for North Carolina Mixtures

By applying the above approach, the rutting material-specific coefficients for North Carolina mixtures were obtained based on the TRLPD test results. Table 5.23 presents the coefficients for the mixtures, including WMA Evotherm and WMA Foam mixtures, for future use in North Carolina.

Table 5.23 Rutting Coefficients for North Carolina Mixtures

Mixture Type		k_{r1}	k_{r2}	k_{r3}
RS9.5C	WMA Evth	-0.24754	0.513981	0.061183
	WMA Foam	-0.8794	0.763128	0.114194
	HMA	-1.92069	1.11076	0.17308
RS9.5B	WMA Evth	0.313374	0.197491	0.102648
	WMA Foam	0.08046	0.329389	0.101918
	HMA	-0.50618	0.50202	0.116839
RI19C	WMA Evth	-1.04352	0.788562	0.128583
	WMA Foam	0.094325	0.258147	0.117736
	HMA	-2.63026	1.501635	0.151597

5.4 Fatigue Life Prediction Study for WMA Mixtures in Pavement ME

5.4.1 Introduction

In CHAPTER 3 and CHAPTER 4, the fatigue properties were evaluated in terms of materials using the S-VECD model, which is a fundamental mechanical model. However, the Pavement ME program uses an empirical model initially developed by Shell Oil and the Asphalt Institute (MS-1) for fatigue cracking predictions. The mechanisms of fatigue cracking are described briefly in the following text.

Three steps typically are taken to evaluate or predict alligator cracking in the field. First, Equation (6.15) is employed to calculate the fatigue life. After obtaining the dynamic modulus value of the bottom layer mixture and the critical tensile strain at the bottom boundary from the structural response analysis, the number of cycles that is required to fail the pavement under the specific traffic loading and environmental conditions can be obtained. Second, in order to calculate the amount of fatigue damage, Miner's law, as shown in Equation (6.16), is used to convert the predicted number of cycles to failure (N_f) to equivalent damage as a summation of the damage at different combinations of traffic loading and environmental conditions. Eventually, by using the alligator cracking transfer function shown in Equation (6.17), the predicted damage can be converted to alligator cracking as a percentage of lane area. In this way, alligator cracking can be predicted.

$$N_f = 0.00432 * C * \beta_{f1} * k_{f1} * \left(\frac{1}{\varepsilon_t}\right)^{\beta_{f2} * k_{f2}} \left(\frac{1}{|E^*|}\right)^{\beta_{f3} * k_{f3}} \quad (6.15)$$

where

$$C = 10^M ;$$

$$M = 4.84 \left(\frac{V_b}{V_a + V_b} - 0.69 \right) ;$$

$\beta_{f1}, \beta_{f2}, \beta_{f3}$ = local calibration factor; and

k_{f1}, k_{f2}, k_{f3} = material specific

$$Damage = \sum_{i=1}^T \frac{n_i}{N_{fi}} \quad (6.16)$$

$$Alligator\ Cracking = \left(\frac{6000}{1 + e^{(C_1 * C_1' + C_2 * C_2' * \log_{10}(\%Damage))}} \right) * \left(\frac{1}{60} \right) \quad (6.17)$$

where

$$C_1' = -2C_2' ; \text{ and}$$

$$C_2' = -2.40874 - 39.748 * (1 + h_{ac})^{-2.856} .$$

5.4.2 Fatigue Cracking Coefficients in Pavement ME

5.4.2.1 Fatigue Cracking Coefficients Regression Theory

In the process of predicting alligator cracking, it can be observed that the material-specific fatigue coefficients k_{f1}, k_{f2}, k_{f3} , are as important as the rutting coefficients. In this study, the fatigue properties were evaluated using direct tension tests and analyzed using the S-VECD model. It has been proven that the material-specific coefficients regressed from the direct tension tests can describe the performance of the material. The material-specific coefficients also can be regressed from bending beam fatigue test results, which originally were used in the Shell or MS-1 model. The theory that allows the material-specific fatigue coefficients to be regressed from the S-VECD model is presented in the following text.

The tests were conducted in direct tension controlled-crosshead (also called control displacement) mode. The number of cycles to failure used in the tests is the number of the cycle where the phase angle drops rapidly. The pseudo stiffness C at the failure point and the damage parameter S at the failure point were extracted from the S-VECD model analyzed data and denoted as C_f and S_f , respectively, and then used as failure criteria because they are independent of loading mode. Based on a series of derivations from Equations (6.18) to (6.25), the relationship between fatigue life and a given initial strain could be obtained using Equation (6.25). Note that pseudo strain ε^R is a function of initial strain. In this way, the material-specific coefficients could be fitted.

$$\frac{dS}{dt} = \left(-\frac{1}{2} \frac{dC}{dS} (\varepsilon^R)^2 \right)^\alpha = \left(-\frac{1}{2} \frac{dC}{dt} \frac{dt}{dS} (\varepsilon^R)^2 \right)^\alpha = \left(-\frac{1}{2} \frac{dC}{dt} (\varepsilon^R)^2 \right)^\alpha \frac{1}{f_{red}} \quad (6.18)$$

$$S \cong \sum_{i=1}^n \left(-\frac{(\varepsilon^R)^2}{2} (C_i - C_{i-1}) \right)^{\frac{\alpha}{1+\alpha}} (t_i - t_{i-1})^{\frac{1}{1+\alpha}} \quad (6.19)$$

$$C(S) = 1 - c_{11} S^{c_{12}} \quad (6.20)$$

$$\frac{dC}{dS} = -c_{11} c_{12} S^{c_{12}-1} \quad (6.21)$$

$$\frac{dS}{dN} = \frac{dS}{dt} \frac{dt}{dN} = \frac{dS}{dt} \frac{1}{f_{red}} = \left(-\frac{1}{2} (\varepsilon^R)^2 \frac{\partial C}{\partial S} \right)^\alpha \left(\frac{1}{f_{red}} \right) \quad (6.22)$$

$$\left(S^{(c_{12}-1)} \right)^{-\alpha} dS = \left(\frac{1}{2} (\varepsilon^R)^2 c_{11} c_{12} \right)^\alpha \left(\frac{1}{f_{red}} \right) dN \quad (6.23)$$

$$\int_{S_{ini}}^{S_{failure}} \left(S^{(c_{12}-1)} \right)^{-\alpha} dS = \int_1^{N_{failure}} \left(\frac{1}{2} (\varepsilon^R)^2 c_{11} c_{12} \right)^\alpha \left(\frac{1}{f_{red}} \right) dN \quad (6.24)$$

$$N_{failure} = \frac{(f_{red}) (2^\alpha) S_{failure}^{\alpha - \alpha c_{12} + 1}}{(\alpha - \alpha c_{12} + 1) (c_{11} c_{12})^\alpha (\varepsilon^R)^{2\alpha}} \quad (6.25)$$

5.4.2.2 Fatigue Material-Specific Coefficients for North Carolina Mixtures

Using this method, the material-specific fatigue coefficients were regressed and are presented in Table 5.24, which includes the WMA Foam and WMA Evotherm mixtures for future use.

Table 5.24 Fatigue Coefficients for North Carolina Mixtures (based on psi)

Mixture Type		k_{f1}	k_{f2}	k_{f3}
RS9.5C	WMA Evth	1008.255	7.74	4.4
	WMA Foam	0.485009	7.88	4.039
	HMA	87.54228	8.74	4.768
RI19C	WMA Evth	2.81E-13	7.5	1.916
	WMA Foam	1.89E-11	7.68	2.3
	HMA	8.65E-16	8.94	2.333
RB25B	WMA Evth	9.53E-20	6.64	0.264
	WMA Foam	1.82E-18	7.7	1.112
	HMA	1.99E-19	8.52	1.404

5.4.2.3 Application of Material-Specific Fatigue Coefficients in Pavement ME

The material-specific fatigue coefficients of the tested WMA and HMA North Carolina mixtures are presented in the previous section. Note that, among the mixture types, several k_{f1} coefficients have values as small as 1×10^{-10} . However, as far as the authors are aware, the Pavement ME program can take no more than eight digits after the decimal point when coded. Hence, if these values, as implemented in Equation (6.15), are input directly into the Pavement ME program, the predicted number of cycles to failure at each combination of traffic loading and environmental condition would be zero, which is not acceptable. For this reason, an adjustment method was developed to allow the Pavement ME program to read those coefficients that need more than eight digits without affecting the final results.

When a material has a small k_{f1} value, for example, $k_{f1} = 1.818E - 16$, then $k_{f1} = 1.818E - 06$ should be input. Then, the calculated number of cycles to failure (N_f) is multiplied by 10^{10} in Equation (6.15), and the calculated percentage of damage (*Damage*) in Equation (6.16) decreases by 10^{10} times. The new decreased percentage of damage is noted as *%Damage* in the following equations. In order to obtain the correct alligator cracking values, 10^{10} in the original equation is multiplied to *%Damage* in Equation (6.26). However, this modification cannot be made directly because the model is built into the Pavement ME program and the code cannot be changed by users. Nevertheless, this modification can be achieved by adjusting the input local calibration factors, C_1 and C_2 . It is noted that Equation (6.27) is equivalent to Equation (6.26). C_{1new} is defined in Equations (6.28) and (6.29) and is the C_1 value the user should input. Based on previous work at NCSU (Jadoun 2011), when local calibration factors are applied, the original C_1 and C_2 values are equal to 0.25, and then, the input values should be -1 for C_1 and 0.25 for C_2 . Likewise, if local calibrations are not included in the design process, the original C_1 and C_2 are equal to 1.0, and then, the input values for C_1 and C_2 should be -4 and 1, respectively. In addition, the asphalt concrete bottom cracking standard deviation also should be changed from Equation (6.32) to Equation (6.33) as well, because the formula can be changed directly, unlike the case for the built-in model.

$$Alligator\ Cracking = \frac{6000}{1 + e^{(C_1 * C_1' + C_2 * C_2' * \log_{10}(\%Damage * 10^{10}))}} * \frac{1}{60} \quad (6.26)$$

$$Alligator\ Cracking = \frac{6000}{1 + e^{(C_1 * C_1' + 10 * C_2 * C_2' + C_2 * C_2' * \log_{10}(\%Damage))}} * \frac{1}{60} \quad (6.27)$$

$$C_{1new} * C_1' = C_1 * C_1' + 10 * C_2 * C_2' \quad (6.28)$$

$$C_{1new} = \frac{C_1 * C_1' + 10 * C_2 * C_2'}{C_1'} = C_1 - 5 * C_2 \quad (6.29)$$

$$C_{1new} = C_1 - 5 * C_2 = 0.25 - 5 * 0.25 = -1 \quad (\text{for local calibration}) \quad (6.30)$$

$$C_{1new} = C_1 - 5 * C_2 = 1 - 5 * 1 = -4 \quad (\text{for default values}) \quad (6.31)$$

$$S = 1.13 + \frac{13}{1 + e^{(7.57 - 15.5 * \log_{10}(BOTTOM + 0.0001))}} \quad (6.32)$$

$$S = 1.13 + \frac{13}{1 + e^{(7.57 - 155 - 15.5 * \log_{10}(BOTTOM + 0.000000000000001))}} \quad (6.33)$$

Even after implementing this adjustment method, the k_{f1} values of some of the materials were still smaller than 10^{-8} , an increase of ten decades. Hence, more work needed to be done in order to implement the coefficients. In Equation (6.15), it can be seen that k_{f1} and β_{f1} are both items that are multiplied directly by other items. Therefore, users can continue to increase k_{f1} by several decades and decrease β_{f1} simultaneously using the same amount. For example, for the RB25B WMA Evotherm mix, by applying the above method and changing the C_1 value, the k_{f1} value can be changed from 9.53E-20 to 9.53E-10, and the user can then input 9.53E-5 instead of 9.53E-20. At the same time, the β_{f1} value should be input as 1E-05 (without local calibration), or any other calibrated value increased by five decades. In this way, the Pavement ME program can capture the small material-specific fatigue coefficients, i.e., the k_{f1} values.

In summary, the steps required to implement the material-specific fatigue coefficients with small k_{f1} values are as follows:

1. Input the C_1 and C_2 values. If local calibration factors are used, input -1 and 0.25 for C_1 and C_2 , respectively. If default values are used, input -4 and 1, respectively.
2. Change the k_{f1} value. Raise the k_{f1} value for ten decades. If the modified k_{f1} is larger than 10^{-8} , then input this value. If the modified k_{f1} is still smaller than 10^{-8} , then continue to raise the k_{f1} value for enough decades to ensure that the raised value is larger than 10^{-8} and, at the same time, decrease the β_{f1} value for the same number of decades. Input the modified k_{f1} and β_{f1} values.

5.4.3 Moisture Effect on Fatigue Life Predictions and Development of Modification for WMA Mixtures in Pavement ME

5.4.3.1 Introduction

Several factors can cause or accelerate alligator cracking, and moisture damage is an important one of them. When moisture starts to permeate and erode the pavement, it weakens the strength of the aggregate-asphalt bond (the so-called adhesion problem) as well as the connection strength inside the FAM and mastic (the so-called cohesion problem). Hence, fracture may propagate easily in the asphalt mixtures. It is noted that the Pavement ME program does not address the effects of moisture on pavement performance explicitly; rather, these effects are smeared into the calibration factors. Also, both national and local calibration factors were developed using performance data based on HMA pavements, not WMA pavements. Therefore, it is necessary to develop methodology that considers the effects of moisture on WMA pavements, which differ from the effects of moisture on HMA pavements.

5.4.3.2 Study Method

Local calibration factors for the Pavement ME program were developed in previous work, namely the NCDOT HWY-2007-07 project, *Local Calibration of the MEPDG for Flexible Pavement Design*. By running the Pavement ME program nearly one thousand times for nearly 30 pavement sections and a series of numerical optimizations using comparisons found in the survey database, it was postulated that local calibration factors can account for the moisture effect on fatigue cracking predictions for HMA pavements. However, the question remained as to whether the same local calibration factors could account for the effects of moisture on WMA mixtures.

In order to answer this question, the Pavement ME program was run using multiple pavement sections and was run several times using different materials. The materials used in each pavement section can be categorized as follows:

- nonmoisture-damaged HMA material without local calibration factors
- moisture-damaged HMA material without local calibration factors
- nonmoisture-damaged WMA material without local calibration factors
- moisture-damaged WMA material without local calibration factors

The ratio of the percentage of fatigue damage output from the Pavement ME program using the moisture-damaged HMA materials to the percentage of fatigue damage using the nonmoisture-damaged HMA materials was calculated, and is denoted as M_H . Using a corresponding process, M_W for WMA materials also was calculated. Then, the ratio of M_W to M_H was calculated in order to compare the moisture susceptibility of the WMA and HMA mixtures to the pavement performance predicted by the Pavement ME program. If M_W and M_H were similar to each other, then the effect of moisture on the WMA mixtures and on the HMA mixtures would not be significantly different. Figure 5.34 presents the comparison process briefly. Note that the percent damage from the Pavement ME program is adopted here, which, unlike the percentage of alligator cracking, does not have an upper limit.

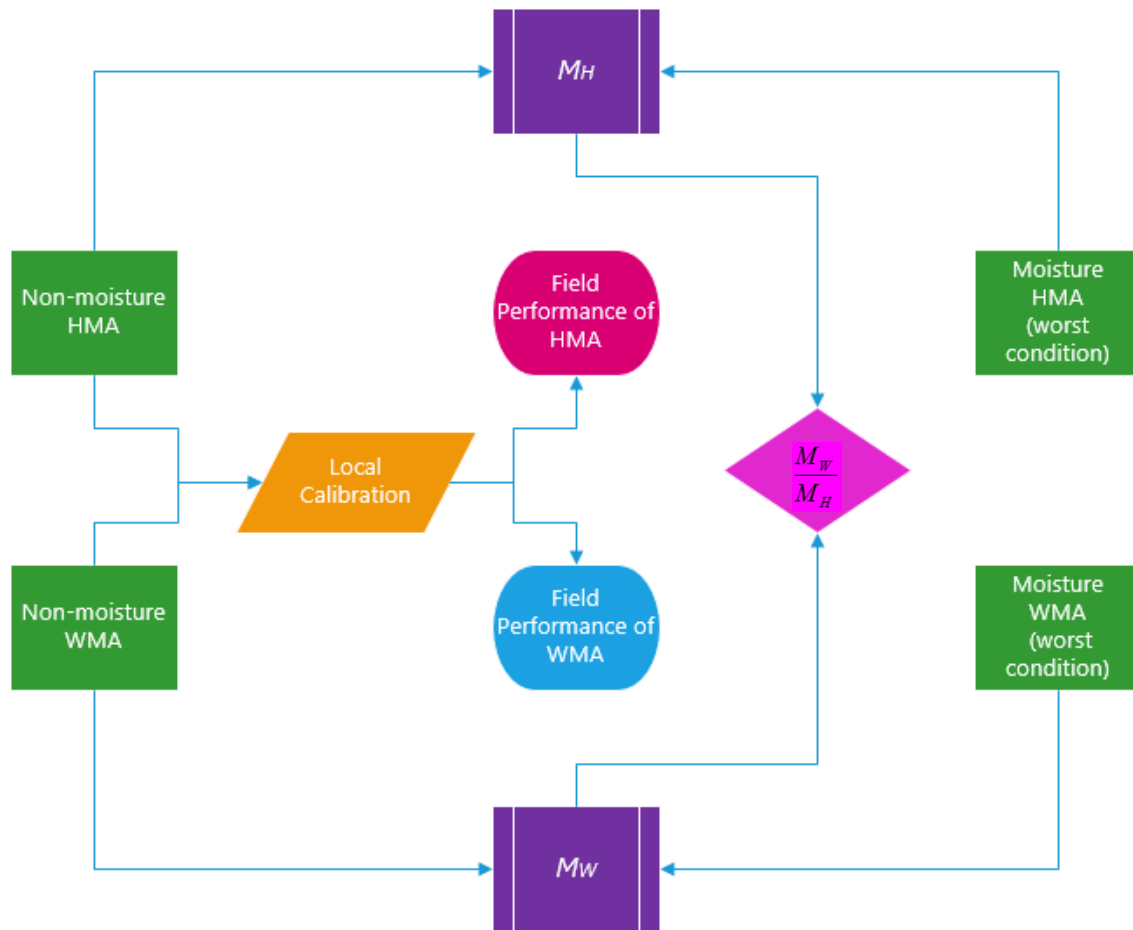


Figure 5.34 Schematic flow chart showing the comparison of moisture susceptibility for WMA and HMA mixtures in Pavement ME.

In this study, two types of mixtures, RS9.5C and RB25B, were moisture-conditioned in the laboratory and tested using dynamic modulus tests and direct tension fatigue tests. The material-specific fatigue coefficients were derived using the same method as described earlier and were input to the Pavement ME program along with the dynamic modulus data.

Table 5.25 presents the material-specific fatigue coefficients for the moisture-conditioned mixtures. Note that the pavement section information is from the NCDOT HWY-2007-07 project, and none of the sections were designed for WMA mixtures. The sections include thin and thick pavements and most of them had several layers. For this study, the traffic, climate, and structural data were not changed from the previous study for those sections; however, only the RS9.5C and RB25B mixtures with and without moisture damage were used. Thus, for those sections, the original designed mixtures were substituted with the RS9.5C and RB25B mixtures, depending on the similarity of those mixtures to the original mixtures. For example, the original RS12.5C and

S9.5B mixtures were substituted by the RS9.5C mixture, and the RI19C and B25B mixtures in the bottom and intermediate layers were substituted by the RB25B mixture. Therefore, all the sections that were input and run in the Pavement ME program for this study were virtual sections, because the aim of this study is to examine the effect of moisture susceptibility on various pavement structures that are as realistic as possible.

Also, when the moisture-damaged materials were used as inputs to the program, the condition was designated as the ‘worst’ condition, because moisture damage was applied throughout the entire pavement since the first day of the pavement service life, and AASHTO T283 moisture conditioning is a relatively harsh treatment. This designation of ‘worst’ condition was necessary because the damaging moisture effect on pavement performance as a function of time could not be included in the Pavement ME program. Thus, although the virtual phenomenon would not occur in the field, the model is nonetheless beneficial for research into moisture susceptibility in terms of pavement structural analysis.

Table 5.25 Fatigue Coefficients for North Carolina Mixtures with Moisture Damage (based on psi)

Mixture Type		k_{f1}	k_{f2}	k_{f3}
RS9.5C	WMA Evth	0.000827	7.5	3.36
	WMA Foam	0.000827	7.5	3.36
	HMA	0.020587	8.16	3.922
RB25B	WMA Evth	2.98E-15	7.6	1.451
	WMA Foam	9.66E-11	7.88	2.317
	HMA	4.85E-18	9.24	2.196

5.4.3.3 Moisture Susceptibility in Pavement ME Analysis Results and Discussion

Using the method introduced in the previous section, several random sections were selected to be evaluated using the Pavement ME software. The analysis results are presented in Table 5.26 and Table 5.27 for the WMA Evotherm and WMA Foam mixtures, respectively.

With regard to the WMA Evotherm mixture, based on Table 5.26, $\frac{M_W}{M_H}$ in the last column has an average of about 0.3 and the variability is small, which means that the effect of the worst moisture conditioning on the performance of pavements with WMA Evotherm is only about 30% of that of HMA mixtures. Therefore, it can be concluded that using WMA Evotherm in the Pavement ME program for fatigue cracking predictions in terms of moisture damage evolution leads to conservative outcomes, and no further modification to the software program is needed to address the effect of moisture on fatigue performance predictions.

Table 5.26 Pavement ME Analysis Results for WMA Evotherm Mixtures

Section ID	Total AC Thickness (in.)	Mixture	Condition	%Damage	M_W and M_H	$\frac{M_W}{M_H}$
371817	4.6	HMA	non-moisture	66.1	6.701967	0.297358
			moisture	443		
		Evth	non-moisture	562	1.992883	
			moisture	1120		
371040	5.6	HMA	non-moisture	0.0606	5.676568	0.33903
			moisture	0.344		
		Evth	non-moisture	1.06	1.924528	
			moisture	2.04		
371352	6.6	HMA	non-moisture	0.797	4.629862	0.227487
			moisture	3.69		
		Evth	non-moisture	26.3	1.053232	
			moisture	27.7		
371028	9.8	HMA	non-moisture	0.0313	3.482428	0.455411
			moisture	0.109		
		Evth	non-moisture	1.28	1.585938	
			moisture	2.03		
371006	3.8	HMA	non-moisture	0.0189	4.666667	0.260704
			moisture	0.0882		
		Evth	non-moisture	0.674	1.216617	
			moisture	0.82		

Table 5.26 Pavement ME Analysis Results for WMA Evotherm Mixtures (continued)

370802	6.9	HMA	non-moisture	0.0208	4.855769	0.23699
			moisture	0.101		
		Evth	non-moisture	0.65	1.150769	
			moisture	0.748		
370859	1.4	HMA	non-moisture	279	12.7957	0.452722
			moisture	3570		
		Evth	non-moisture	169	5.792899	
			moisture	979		
371024	4.8	HMA	non-moisture	0.43	8.069767	0.426352
			moisture	3.47		
		Evth	non-moisture	2.86	3.440559	
			moisture	9.84		
371802	4.4	HMA	non-moisture	2.5	6.72	0.32572
			moisture	16.8		
		Evth	non-moisture	23.3	2.188841	
			moisture	51		
371803	5.6	HMA	non-moisture	0.761	7.069645	0.304154
			moisture	5.38		
		Evth	non-moisture	7.72	2.150259	
			moisture	16.6		

Table 5.27 Pavement ME analysis results for WMA Foam mixtures

Section ID	Total AC Thickness (in.)	Mixture	Condition	%Damage	M_W and M_H	$\frac{M_W}{M_H}$
370801	3.8	HMA	non-moisture	40.5	7.358025	1.202246
			moisture	298		
		Foam	non-moisture	156	8.846154	
			moisture	1380		
371352	6.6	HMA	non-moisture	0.797	4.629862	1.57182
			moisture	3.69		
		Foam	non-moisture	5.95	7.277311	
			moisture	43.3		
371028	9.8	HMA	non-moisture	0.0313	3.482428	2.12005
			moisture	0.109		
		Foam	non-moisture	0.363	7.38292	
			moisture	2.68		
371006	3.8	HMA	non-moisture	0.0189	4.666667	1.69105
			moisture	0.0882		
		Foam	non-moisture	0.166	7.891566	
			moisture	1.31		

Table 5.27 Pavement ME Analysis Results for WMA Foam Mixtures (continued)

370802	6.9	HMA	non-moisture	0.0208	4.855769	1.448227
			moisture	1.01E-01		
		Foam	non-moisture	0.155	7.032258	
			moisture	1.09		
371024	4.8	HMA	non-moisture	0.43	8.069767	2.289357
			moisture	3.47		
		Foam	non-moisture	1.18	18.47458	
			moisture	21.8		
371802	4.4	HMA	non-moisture	2.5	6.72	1.539855
			moisture	16.8		
		Foam	non-moisture	11.5	10.34783	
			moisture	1.19E+02		
371803	5.6	HMA	non-moisture	0.761	7.069645	1.320459
			moisture	5.38		
		Foam	non-moisture	3.61	9.33518	
			moisture	33.7		

However, in Figure 5.27, which presents the analysis results for WMA Foam, $\frac{M_W}{M_H}$ is higher than 1.0, and in some cases even higher, which indicates that the WMA Foam mixture is more susceptible to moisture than the HMA mixture, and that the Pavement ME program cannot conservatively predict the fatigue life for WMA Foam mixtures. Thus, further modifications were needed to address this problem for WMA Foam.

5.4.3.4 Development of Modification for WMA Foam for Fatigue Life Predictions in Pavement ME

5.4.3.4.1 *Introduction and Study Method*

Based on the analysis presented above, although it is conservative to use WMA Evotherm mixtures in the Pavement ME program in terms of moisture effect, and no further modification is needed, it is still necessary to develop a modification factor for WMA Foam because it is more susceptible to moisture than the HMA mixture. It was found that, based on the Pavement ME program analysis, the moisture effect on WMA Foam is on average 1.7 times that of the HMA mixture; however, this value cannot be utilized directly because the ‘worst’ condition does not represent the actual degree of moisture damage that would occur in the field. If it is postulated that AASHTO T283 moisture conditioning is the same as the eventual status of the actual moisture damage, then a process that best reflects actual moisture damage deterioration should be determined in lieu of applying this status from Day 1 of the pavement service life in the software. In other words, eventually, a value for the moisture damage in the field that is equivalent to the status that is based on applying T283 from Day 1 should be established. In this section, a reduction factor that represents the average effect of moisture damage on the fatigue life of the WMA Foam mixtures is developed.

5.4.3.4.2 *Literature Review*

First, a literature review was undertaken to determine the evolution process of moisture damage in the field. This literature review is based mainly on research conducted at two institutions: Texas A&M University (TAMU) and Delft University in the Netherlands. These examples of studies in the literature provide good background for further study.

During the relatively early years of pavement research, TAMU concentrated on the mechanisms of moisture damage. In 2005, Hefer et al. (2005) studied the moisture effect on mixtures using chemical analysis and introduced the theory of surface energy to evaluate the mixtures’ resistance to adhesive failure. Masad and Howson (Masad et al. 2006, Howson et al. 2007) later measured the surface energy of materials and established an index using surface energy to evaluate moisture damage resistance. The index is the ratio of the adhesive bond energy under dry conditions to the adhesive bond energy under wet conditions, and is denoted as $|\Delta G^{aD} / \Delta G^{aW}|$. Moisture resistance was evaluated based on the calculation of the ratio of mechanical properties under dry conditions to wet conditions. Also, dynamic mechanical analysis was performed on FAM in those studies; the mechanical indices used were the number of cycles to

failure, the dynamic shear modulus values, and the dissipated pseudo strain energy. In addition, Masad et al. (2007) presented a method to measure the diffusion coefficients. Later, in 2008, research into the mechanisms of moisture deterioration and indices used to evaluate moisture resistance was extended further (Caro et al. 2008a, 2008b, 2008c).

In 2009 and 2010, researchers (Spinel 2009, Arambula et al. 2010, Caro et al. 2010a, Caro et al. 2010b) developed a coupled micromechanical model of moisture-induced damage in asphalt mixtures and applied it in finite element simulations. This model can simulate mechanical responses while the moisture diffusion affects the mechanical properties. In terms of the mechanical aspect, the so-called *cohesive zone mode* was adopted to simulate adhesive deterioration and fracture of the aggregate-mastic interface. In terms of moisture deterioration, the cohesive degradation of the mastic was simulated using the moisture dependency of its linear viscoelastic material properties. It could be concluded that, in the above-described modeling method, the moisture effects were reflected exclusively from the deduction of a linear viscoelastic material property, i.e., the relaxation modulus; that is, the cohesive zone model was not modified specially for moisture effects, and the failure criteria were kept the same. Because the criterion for damage initiation that defines the bond strength of the adhesive zones was taken to be the quadratic nominal strain condition, and because the mechanical responses change according to the mechanical properties, the effect of moisture on the adhesive bonding strength and fracture properties could be described.

Based on the Caro studies, Joshi (2008) and Spinel (2009) found that the reduction of the relaxation modulus of asphalt mastic has a linear relationship with moisture concentration; this relationship is adopted for this study also. Furthermore, Equation (6.34), which is the relationship between the dynamic modulus and the relaxation modulus, indicates that, if the relaxation modulus changes linearly, the dynamic modulus would also change in the same way.

$$E^* = \tilde{E} \Big|_{S \rightarrow i\omega} = E_\infty + \sum_{i=1}^N E_i \frac{\omega^2 \rho_i^2 + i\omega \rho_i}{\omega^2 \rho_i^2 + 1} \quad (6.34)$$

Research into moisture damage also was being carried out at Delft University in the Netherlands at almost the same time as the TAMU research. Kringos et al. (2005, 2008) elaborated on the mechanisms of moisture damage and simulated moisture diffusion. Kringos et al. conducted similar studies in 2007 (Kringos et al. 2007). In the 2007 study, the mechanical responses under moisture deterioration were modeled and simulated in finite element programs.

It is noteworthy that Fick's law of diffusion, as shown in Equation (6.35), has been adopted in studies of moisture diffusion in asphalt. Cranks (1975) and Kringos et al. (2008) presented methods to measure the diffusion coefficient. Unlike the experimental set-up developed at TAMU where the diffusion coefficients of FAM and HMA mixtures were measured, in the Kringos studies, the mastic film was tested specially in diffusion. In order to calculate the diffusion coefficient, one of the analytical solutions of the differential equation was utilized, as shown in Equation (6.36). This solution is based on the assumption that the sheet of mastic is placed immediately in vapor and that each surface attains a concentration value that corresponds

to the equilibrium moisture capacity M_∞ for the existing vapor pressure and remains constant afterwards. If it is assumed that the moisture concentration above and underneath the pavement are at their highest since the start of the service life of the pavement, then this solution can be used in this context, although it is somewhat conservative.

$$\frac{\partial \phi}{\partial t} = D \nabla^2 \phi \quad (6.35)$$

where

ϕ = the moisture concentration;
 t = time;
and D = the diffusion coefficient.

$$\frac{M_t}{M_\infty} = 1 - \frac{8}{\pi^2} \sum_{m=0}^{\infty} \frac{1}{(2m+1)^2} e^{(-D(2m+1)^2 \pi^2 t / h^2)} \quad (6.36)$$

where

M_t = the total amount of vapor absorbed by the sample at time t ;
 M_∞ = the equilibrium sorption attained when the sorption curves reach a constant value;
and h = the sample thickness.

5.4.3.4.3 *Development of Modification for WMA Foam Mixtures*

In Section 5.4.3.3, it was found from the Pavement ME program analysis that the average moisture susceptibility value of the WMA Foam mixture is 1.7 times that of HMA materials. However, this value could not be applied directly in the program due to the concern that this value was obtained based on the assumption that AASHTO T283 moisture conditioning was applied at the start of the pavement service life. Based on the literature reviewed, a reduction of the value can be obtained by calculating the field value that is equivalent to the AASHTO T283-derived value.

The curve obtained using Equation (6.36) is plotted in Figure 5.35. For this function, $\frac{M_t}{M_\infty}$ is noted as a normalized moisture concentration. The condition derived from AASHTO T283 is assumed to be the final moisture condition of the pavement, and thus, in this case, M_∞ is the AASHTO T283 conditioning. Likewise, AASHTO T283 conditioning is supposed to simulate the condition in the field after a certain number of years, which is denoted as '1', and in this way, the time is also normalized.

Based on the literature (Arambula et al. 2010), the diffusion coefficient of asphalt mixtures is $2.370 \text{ mm}^2/\text{h}$, and the average total asphalt concrete thickness is assumed as 200 mm. The area under the moisture concentration curve is 0.848 by integration, which is equal to the area under the red dashed line in Figure 5.35; thus, the value represented by the red dashed line could be considered as the field-equivalent value to that of AASHTO T283 moisture conditioning. Also, based on the discussion presented in the previous section, the dynamic modulus has a linear relationship with the moisture concentration; therefore, it also can be reduced by a certain value.

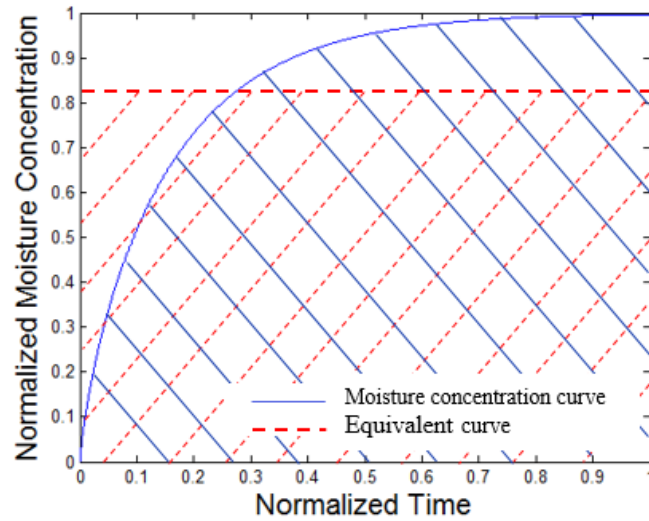


Figure 5.35 Schematic of the diffusion curve.

However, the field value that is equivalent to AASHTO T283 conditioning still cannot be used, because the method discussed above is based on the assumption that the pavement is a plane sheet with the materials having equilibrium moisture concentration on each side, and this assumption is still relatively stringent compared with the degree of moisture diffusion in the field. Therefore, another analytical solution for the Fick's law differential equation needs to be found.

Water normally exists deep down below the pavement at the beginning of the pavement's service life. Hence, the process of moisture diffusion can be simplified and modeled as diffusion in a semi-infinite medium. In addition, because water accumulates gradually below the subgrade, the moisture concentration C at the boundary of the medium can be assumed to grow linearly. Therefore, an analytical solution can be determined (Crank 1975), as follows:

$$C = kt \left[\left(1 + \frac{x^2}{2Dt} \right) \operatorname{erfc} \frac{x}{2\sqrt{Dt}} - \frac{x}{\sqrt{(\pi Dt)}} \exp \left\{ -\frac{x^2}{4Dt} \right\} \right] \quad (6.37)$$

where erfc is a standard mathematical 'error function' and can be defined as shown in Equations (6.38) and (6.39):

$$\operatorname{erf} z = \frac{2}{\pi^{1/2}} \int_0^z \exp(-\eta^2) d\eta \quad (6.38)$$

$$\operatorname{erfc} z = 1 - \operatorname{erf} z \quad (6.39)$$

and x is the perpendicular distance from a point in the diffusion area to the boundary. The corresponding boundary condition of this solution can be written as $C_0 = kt$ at $x = 0$, and the initial condition can be described as, at $t = 0$, $C = 0$ when $x > 0$.

In order to determine the field value that is equivalent to AASHTO T283 conditioning, the solution function is integrated so that the area under the concentration curve is calculated in the same way as shown for the analytical solution with the plane sheet assumption. Based on this analytical solution and the assumption, the field value equivalent to AASHTO T283 treatment is 0.15.

According to the literature, the dynamic modulus value decreases linearly as the moisture concentration grows. Therefore, in order to simulate the moisture effect according to the field value, as derived, the dynamic modulus value should be decreased by 15% from the measurement at the nonmoisture-damaged condition to the measurement after AASHTO T283 conditioning. The failure criterion was kept the same in accordance with the literature. The analysis results are presented in Table 5.28, which shows that the average value of $\frac{M_W}{M_H}$ is actually only 1.088, which means that, in the field, the moisture susceptibility of WMA Foam is 1.088 times that of HMA mixtures. Therefore, to be conservative, the fatigue life predicted for WMA Foam should be reduced by 1.088. For Pavement ME software users, the input β_{f1} should be divided by 1.088. The new local calibration factors for North Carolina are presented in Table 5.29 and the reduction factor is included.

Table 5.28 Pavement ME Output for WMA Foam under Equivalent Moisture Condition

Section ID	Total AC Thickness (in.)	Mixture	Condition	%Damage	M_W and M_H	$\frac{M_W}{M_H}$
370801	3.8	HMA	non-moisture	40.5	1.041975	1.070452
			moisture	42.2		
		Foam	non-moisture	156	1.115385	
			moisture	174		
371352	6.6	HMA	non-moisture	0.797	1.070263	1.055265
			moisture	0.853		
		Foam	non-moisture	5.95	1.129412	
			moisture	6.72		
371028	9.8	HMA	non-moisture	0.0313	1.015974	1.136121
			moisture	0.0318		
		Foam	non-moisture	0.363	1.15427	
			moisture	0.419		
371006	3.8	HMA	non-moisture	0.0189	1.677249	1.127779
			moisture	0.0317		
		Foam	non-moisture	0.166	1.891566	
			moisture	0.314		

Table 5.28 Pavement ME Output for WMA Foam under Equivalent Moisture Condition
(continued)

370802	6.9	HMA	non-moisture	0.0208	1.067308	1.063877
			moisture	2.22E-02		
		Foam	non-moisture	0.155	1.135484	
			moisture	0.176		
371024	4.8	HMA	non-moisture	0.43	2.323256	1.079724
			moisture	0.999		
		Foam	non-moisture	1.18	2.508475	
			moisture	2.96		
371802	4.4	HMA	non-moisture	2.5	1.484	1.048869
			moisture	3.71		
		Foam	non-moisture	11.5	1.556522	
			moisture	1.79E+01		
371803	5.6	HMA	non-moisture	0.761	1.681997	1.123186
			moisture	1.28		
		Foam	non-moisture	3.61	1.889197	
			moisture	6.82		

Table 5.29 Final Recommended Local Calibration Factors for Alligator Cracking Prediction Models for WMA Mixtures

Parameter	Recommended Value	
	WMA Evotherm	WMA Foam
$\beta f1$	3.5	3.21
$\beta f2$	0.72364	
$\beta f3$	0.6	
C1	0.24377	
C2	0.24377	

5.5 Summary

In this chapter, the validity of incorporating WMA Foam mixtures in the Pavement ME program was evaluated, and some modifications of the input parameters were developed based on the laboratory test results. The conclusions in this chapter are summarized as follows:

1. A correct way to apply the aging prediction model in the Pavement ME program was presented. A temperature range was determined to utilize the GAS model to predict the increase in the dynamic modulus value that is due to the effect of aging. This temperature range is 25°C to 135°C; therefore, the dynamic modulus curve is not valid for GAS model predictions.
2. When the test results for AASHTO R30 aging conditioning and the prediction results were compared for the WMA and HMA mixtures, it was found that, although the extracted and recovered binders from the short-term aged specimens could capture the trend of the increase in dynamic modulus value in the GAS model, using the RTFO-conditioned virgin binder led to relatively better accuracy in the predictions for both the WMA and HMA mixtures.
3. The WMA mixtures produced higher permanent deformation levels than the HMA mixture. However, with regard to the aging effect on the rutting predictions of the WMA mixtures, the effect of aging on the rutting depths of the WMA Evotherm and HMA mixtures was not significant based on the statistical analysis results, and was significant only under extreme conditions for the WMA Foam mixture. In terms of the strain ratio, which is the parameter on which the Pavement ME program is based, the aging effect was not significant. Therefore, it is valid and conservative to use the Pavement ME program to predict rutting depths of WMA mixtures.

4. For fatigue life predictions in the Pavement ME program, a parameter input method for small material-specific parameters was developed, which allows the Pavement ME program to utilize the material properties of North Carolina local materials.
5. The effects of moisture on fatigue life and bottom-up cracking predictions were evaluated. It was found from the structure-wise analysis in the Pavement ME program that the moisture susceptibility of the WMA Evotherm and HMA mixtures was similar, whereas the WMA Foam mixture was the most sensitive to moisture. Based on the literature and Pavement ME analysis, it was found that the predicted fatigue life of WMA Foam mixtures should be reduced by a factor of 1.088.

CHAPTER 6 SUMMARY AND CONCLUSIONS

In this study, the properties of two types of WMA mixtures commonly used in North Carolina, WMA Foam and WMA Evotherm, were evaluated and compared with a corresponding HMA control mixture. The aging effects on rutting performance as well as the moisture damage effects on the fatigue cracking properties of the WMA mixtures were investigated. Input recommendations for the implementation of the WMA mixtures into the Pavement ME program were developed based on the evaluation of the properties of the WMA mixtures. The findings of the study are summarized as follows.

6.1 Comparison between WMA and HMA Mixtures

Dynamic modulus tests for stiffness, TRLPD tests for rutting performance, and direct tension tests for fatigue properties were conducted using the WMA and HMA study mixtures. The conclusions, based on comparisons, are as follows:

1. In terms of stiffness, the dynamic modulus values of the HMA mixture were always higher than those of the two WMA mixtures. The modulus values of the two WMA mixtures were similar to each other.
2. In terms of rutting, the HMA mixture exhibited less permanent deformation than the two WMA mixtures, which indicates that the HMA mixture was more rutting-resistant than the two WMA mixtures. With regard to the strain ratio of permanent strain to resilient strain, the differences among the HMA and WMA mixtures were not significant.
3. In terms of fatigue properties, the HMA mixtures showed more fatigue resistance than both WMA mixtures and the fatigue properties of WMA Evotherm and WMA Foam were similar.

6.2 Evaluation of Aging and Moisture Effects on Mixture Properties

1. Aging had a significant effect on the dynamic modulus values of the WMA mixtures. The modulus values of the mixtures increased as the aging level increased. However, the differences in the modulus values of the HMA mixture between STA and LTA1 were not significant.
2. As for the aging effect on rutting, the effect on the permanent deformation of the WMA Foam mixtures was significant, but the rutting performance of WMA Evotherm and HMA mixtures were not sensitive to aging. Furthermore, regarding the strain ratio of the permanent deformation to the resilient strain for the two WMA mixtures and the HMA mixture, the aging effect was not significant according to statistical analysis.

3. With respect to the aging effect on the fatigue properties of the mixtures, the WMA Foam mixture was more sensitive to aging than the WMA Evotherm and HMA mixtures.
4. According to the tests results, moisture damage led to a reduction in the dynamic modulus values of the WMA and HMA mixtures. The decrease in modulus value due to moisture was greater for WMA Foam than for the WMA Evotherm and HMA mixtures.
5. With regard to the effect of moisture on the fatigue properties of the mixtures, WMA Evotherm was the least susceptible to moisture of the three tested mixtures.

6.3 Input Recommendations for the Incorporation of WMA Mixtures into the Pavement ME Program

1. Because aging occurs mainly within the top few inches of the pavement, and because bottom-up fatigue cracking is related to the properties of the bottom asphalt concrete layer, it is not necessary to make adjustments to the fatigue cracking predictions in the Pavement ME program due to the aging effect. Also, according to previous studies, the effect of moisture damage on rutting is minor; therefore, a study of the effects of moisture on rutting performance was not conducted.
2. According to the statistical analysis results, the effect of aging on the strain ratio in the rutting tests, which dominates the permanent deformation predictions in the Pavement ME program, is not significant. Therefore, it is not necessary to modify the input parameters for rutting predictions when WMA mixtures are used in the Pavement ME analysis.
3. For the fatigue predictions, a 1.088 reduction factor must be incorporated for the fatigue life prediction of WMA Foam mixtures due to the relatively high moisture susceptibility of this WMA technology. This factor can be merged into the local calibrations for WMA Foam mixtures.
4. It must be noted that different aging effects on fatigue performance of HMA and WMA mixtures cannot be accurately reflected in the local calibration factors because of the rigid way of GAS model being implemented in the Pavement ME program. Also the Pavement ME program does not account for the effect of moisture damage explicitly through a model; therefore, incorporation of different moisture susceptibility between HMA and WMA mixtures in the local calibration factors is only approximate at best. A more mechanistic pavement design methodology that expresses the effects of aging and moisture damage through performance models is warranted in order to fully capture the difference between HMA and WMA mixtures.

REFERENCES

- Ali, A., A. Abbas, M. Nazzal, A. Alhasan, A. Roy and D. Powers (2013). Effect of temperature reduction, foaming water content, and aggregate moisture content on performance of foamed warm mix asphalt. *Construction and Building Materials* 48: 1058-1066.
- Ali, A. W., A. R. Abbas, M. Nazzal, and D. Powers (2012). Laboratory evaluation of foamed warm mix asphalt. *International Journal of Pavement Research and Technology* 5(2): 93-93.
- Anderson, R. M. (2008). *Engineering Properties, Emissions, and Field Performance of Warm Mix Asphalt Technologies*.
- Arago, F. T. S., J. Lee, Y. Kim, and P. Karki (2010). Material-specific effects of hydrated lime on the properties and performance behavior of asphalt mixtures and asphaltic pavements. *Construction and Building Materials* 24: 538-544.
- Arambula, E., S. Caro, and E. Masad (2010). Experimental measurement and numerical simulation of water vapor diffusion through asphalt pavement materials. *Journal of Materials in Civil Engineering*: 588-598.
- Archilla, A., and L. Diaz (2011). Effects of asphalt mixture properties on permanent deformation response. *Journal of the Transportation Research Board* 2210: 1-8. Washington, D.C..
- Azari, H., A. Mohseni, and N. Gibson (2008). Verification of Rutting Predictions from Mechanistic Empirical Pavement Design Guide Using Accelerated Loading Facility Data. *Journal of the Transportation Research Board* 2057:157-167. Washington, D.C..
- Bennert, T., A. Maher, and R. Sauber (2011). Influence of production temperature and aggregate moisture content on the initial performance of warm-mix asphalt. *Journal of Transportation Research Record* 2208: 97-107. Washington, D. C..
- Biligiri, K. P., and G. B. Way (2014). Predicted E* dynamic moduli of the Arizona mixes using asphalt binders placed over a 25-Year Period. *Construction and Building Materials* 54:520-532.
- Bonaquist, R. (2011). *Mix Design Practices for Warm Mix Asphalt*. NCHRP Report 691.
- Bayat, A., and M. Knight (2010), Validation of Hot-Mix Asphalt Dynamic Modulus using Field Measured Pavement Response, *Journal of Transportation Research Record*, Pavement Management: 138-145. Washington D. C..
- Caliendo, C. (2012). Local calibration and implementation of the Mechanistic-Empirical Pavement Design Guide for flexible pavement design. *Journal of Transportation Engineering* 138(3): 348–360. Washington D. C..

- Caro, S., D. P. Beltran, A. E. Alvarez, and C. Estakhri (2012). Analysis of moisture damage susceptibility of warm mix asphalt (WMA) mixtures based on Dynamic Mechanical Analyzer (DMA) testing and a fracture mechanics model. *Construction and Building Materials* 35: 460-467.
- Caro, S., E. Masad, G. Airey, and A. Bhasin (2008). Probabilistic analysis of fracture in asphalt mixtures caused by moisture damage. *Journal of the Transportation Research Board* 2057:28-36. Washington D. C..
- Caro, S., E. Masad, A. Bhasin, and D. Little (2010). Coupled micromechanical model of moisture-induced damage in asphalt mixtures. *Journal of Materials in Civil Engineering*: 380-388.
- Caro, S., E. Masad, A. Bhasin, and D. Little (2010). Micromechanical modeling of the influence of material properties on moisture-induced damage in asphalt mixtures. *Construction and Building Materials*: 1184-1192.
- Caro, S., E. Masad, A. Bhasin, and D. N. Little (2008). Moisture susceptibility of asphalt mixtures, Part 1: mechanisms. *International Journal of Pavement Engineering* 9: 81-98.
- Caro, S., E. Masad, A. Bhasin, and D. N. Little (2008). Moisture susceptibility of asphalt mixtures, Part 2: characterisation and modelling. *International Journal of Pavement Engineering* 9: 99-114.
- Crank, J. (1975). *The Mathematics of Diffusion*. Oxford: Clarendon Press.
- El-Badaway, S., F. Bayomy, and A. Awed (2012). Performance of MEPDG Dynamic Modulus Predictive Models for Asphalt Concrete Mixtures: Local Calibration for Idaho. *Journal of Materials in Civil Engineering* 24(11): 1412–1421.
- Erik, O. (2011). Evaluation of the Mechanistic–Empirical Pavement Design Guide model for permanent deformations in asphalt concrete. *International Journal of Pavement Engineering* 12(1):1-12.
- Flintsch, G. W., A. Loulizi, S. D. Diefenderfer, K. A. Galal, and B. K. Diefenderfer (2007). *Asphalt Materials Characterization in Support of Implementation of the Proposed Mechanistic-Empirical Pavement Design Guide*. Final contract report, vtrc 07-cr10.
- Gandhi, T., W. Rogers, and S. Amirkhanian (2010). Laboratory evaluation of warm mix asphalt ageing characteristics. *International Journal of Pavement Engineering* 11(2): 133-142.
- Hall, K. D., D. X. Xiao, and K. C. P. Wang (2011). Calibration of the Mechanistic-Empirical Pavement Design Guide for flexible pavement design in Arkansas. *Journal of the Transportation Research Board* 2226: 135-141. Washington, D. C..

Hefer, A. W., D. N. Little, and R. L. Lytton (2005). A synthesis of theories and mechanisms of bitumen-aggregate adhesion including recent advances in quantifying the effects of water. *Journal of the Association of Asphalt Paving Technologists* 74: 139-196.

Hesami, S., H. Roshani, G. H. Hamed and A. Azarhoosh (2013). Evaluate the mechanism of the effect of hydrated lime on moisture damage of warm mix asphalt. *Construction and Building Materials* 47: 935-941.

Hou, T. (2009). *Fatigue Performance Prediction of North Carolina Mixtures Using Simplified Viscoelastic Continuum Damage Model*. M.S. dissertation, NC State University, Raleigh, NC.

Howson, J., E. A. Masad, A. Bhasin, V. C. Branco, E. Arambula, R. Lytton, and D. Little (2007). *System for the Evaluation of Moisture Damage Using Fundamental Material Properties*. College Station, Texas Transportation Institute.

Jadoun, F. M. (2011). *Calibration of the Flexible Pavement Distress Prediction Models in the Mechanistic Empirical Pavement Design Guide (MEPDG) for North Carolina*. Ph.D. dissertation, NC State University, Raleigh, NC.

Joshi, N. P. (2008). *Analyses of Deformation in Viscoelastic Sandwich Composites Subject to Moisture Diffusion*. M.S. dissertation, Texas A&M University.

Kasozi, A. M., E. Y. Hajj, P. E. Sebaaly, and J. C. Elkins (2012). Evaluation of foamed warm-mix asphalt incorporating recycled asphalt pavement for volumetric and mechanical properties. *International Journal of Pavement Research and Technology* 5(2): 75-75.

Khodaii, A., H. K. Tehrani, and H. F. Haghshenas (2012). Hydrated lime effect on moisture susceptibility of warm mix asphalt. *Construction and Building Materials* 36: 165-170.

Kim, Y. R., J. Zhang, and H. Ban (2012). Moisture damage characterization of warm-mix asphalt mixtures based on laboratory-field evaluation. *Construction and Building Materials* 31(1): 204-211.

Kringos, N. and A. Scarpas (2005). Raveling of asphalt mixes due to water damage. *Journal of the Transportation Research Board*, No. 1929: 79-87. Washington, D. C..

Kringos, N., A. Scarpas, A. Copeland, and J. Youtcheff (2008). Modelling of combined physical-mechanical moisture-induced damage in asphaltic mixes. Part 2: moisture susceptibility parameters. *International Journal of Pavement Engineering*: 129-151.

Kringos, N., A. Scarpas, and C. Kasbergen (2007). Three dimensional elasto-visco-plastic finite element model for combined physical-mechanical moisture induced damage in asphaltic mixes. *Journal of the Association of Asphalt Paving Technologists*: 495-542.

- Kringos, N., T. Scarpas, C. Kasbergen, and P. Selvadurai (2008). Modelling of combined physical–mechanical moisture-induced damage in asphaltic mixes, Part 1: governing processes and formulations. *International Journal of Pavement Engineering* 9: 115-128.
- Kutay, M. E. and H. I. Ozturk (2012). Investigation of moisture dissipation in foam-based warm mix asphalt using synchrotron-based X-ray microtomography. *Journal of Materials in Civil Engineering* 24(6): 674-683.
- Leng, Z., A. Gamez, and I. L. Al-Qadi (2014). Mechanical property characterization of warm-mix asphalt prepared with chemical additives. *Journal of Materials in Civil Engineering* 26(2): 304.
- Masad, E., E. Arambula, R. A. Ketcham, A. R. Abbas, and A. E. Martin (2007). Nondestructive measurements of moisture transport in asphalt mixtures. *Journal of the Association of Asphalt Paving Technologists* 76: 919-952.
- Masad, E. A., C. Zollinger, R. Bulut, D. N. Little, and R. L. Lytton (2006). Characterization of HMA moisture damage using surface energy and fracture properties. *Journal of the Association of Asphalt Paving Technologists* 75.
- Muthadi, N. R., and Y. R. Kim (2008). Local calibration of Mechanical-Empirical Pavement Design Guide for flexible pavement design. *Journal of the Transportation Research Board*, No. 2087:131-141. Washington, D. C..
- National Center for Asphalt Technology (NCAT) (2012). Market analysis identifies strengths, needs of WMA. *Asphalt Technology E-News* 24: 13-14.
- Porras, J. D., E. Y. Hajj, P. E. Sebaaly, S. Kass, and T. Liske (2012). Performance evaluation of field-produced warm-mix asphalt mixtures in Manitoba, Canada. *Transportation Research Record* 2294(2294): 64-73.
- Prowell, B., G. Hurley, and E. Crews (2007). Field performance of warm-mix asphalt at National Center for Asphalt Technology Test Track. *Transportation Research Record: Journal of the Transportation Research Board* 1998(-1): 96-102.
- Punith, V. S., F. P. Xiao, and S. N. Amirkhanian (2011). Effects of moist aggregates on the performance of warm mix asphalt mixtures containing non-foaming additives. *Journal of Testing and Evaluation* 39(5): 847-857.
- Rodezno, M. C., and K. Kaloush (2009). Comparison of asphalt rubber and conventional mixture properties and considerations for MEPDG implementation. *Journal of the Transportation Research Board*, 3292:132-141. Washington, D.C..
- Rushing, J. F., M. Mejias-Santiago, and J. D. Doyle (2013). Assessment of warm-mix asphalt for heavy traffic airfields. *Transportation Research Record* 2371: 41-48.

Sargand, S., M. D. Nazzal, A. Al-Rawashdeh, and D. Powers (2012). Field evaluation of warm-mix asphalt technologies. *Journal of Materials in Civil Engineering* 24(11): 1343-1349.

Spinel, S. C. (2009). *A Coupled Micromechanical Model of Moisture-Induced Damage in Asphalt Mixtures: Formulation and Applications*. Ph.D. dissertation, Texas A&M University.

Tarefder, R. and J. Rodriguez-Ruiz (2013). Local Calibration of MEPDG for Flexible Pavements in New Mexico. *Journal of Transportation Engineer* 139(10): 981–991.

Xiao, F. P., V. S. Punith, and B. J. Putman (2013). Effect of compaction temperature on rutting and moisture resistance of foamed warm-mix-asphalt mixtures. *Journal of Materials in Civil Engineering* 25(9): 1344-1352.

APPENDICES

APPENDIX A TABLES AND FIGURES ABOUT AGING EFFECT ON PERMANENT STRAIN

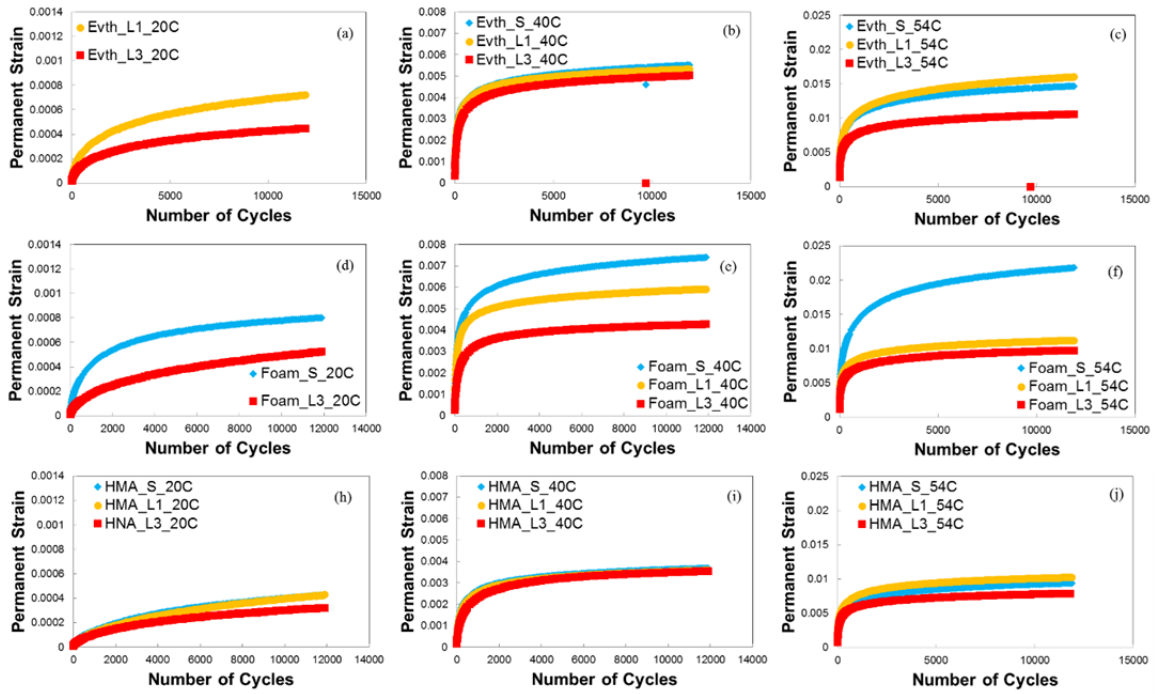


Figure A.1 Comparisons of permanent strain with different aging levels in arithmetic scale.

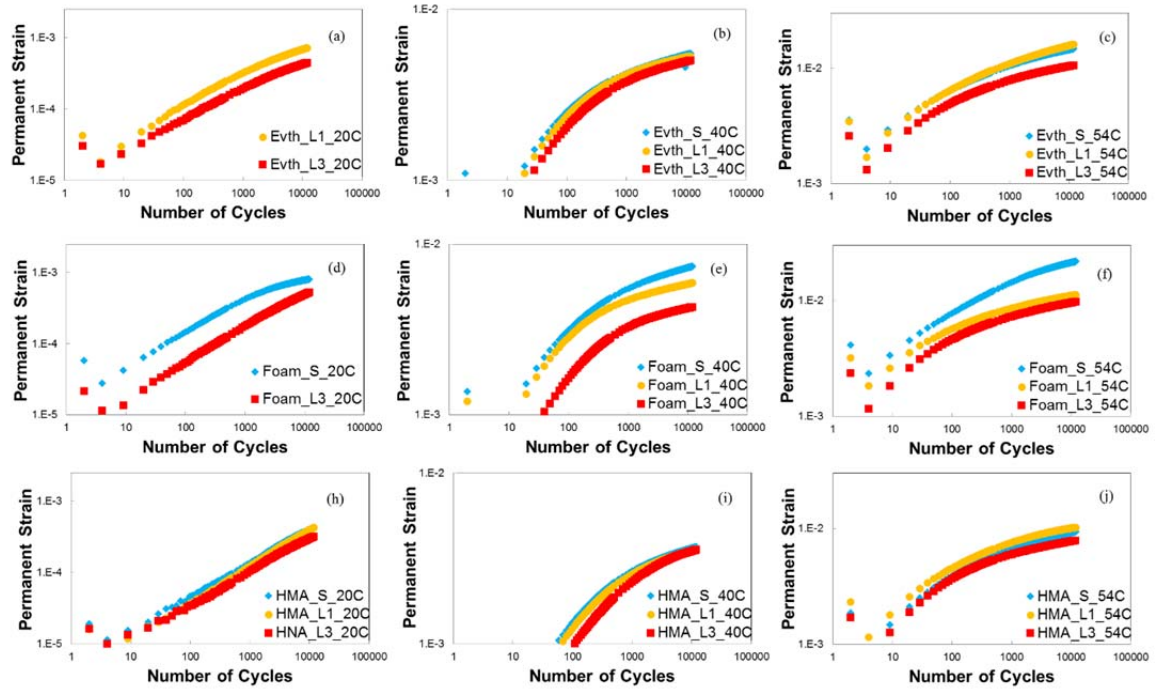


Figure A.2 Comparisons of permanent strain with different aging levels in log-log scale.

Table A-1 T-test Results of Permanent Strain of WMA Evotherm for Different Aging Levels: (a) at 20°C, (b) at 40°C, and (c) at 54°C

(a)

Permanent Strain @ 5,000 Cycles_ Evth_ 20°C					
arithmetic scale			log-log scale		
ST	L1	L3	ST	L1	L3
	0.000565	0.000279			-3.55458
		0.000421			-3.37622
P-values					
ST vs. L1	L1 vs. L3	L3 vs. ST	ST vs. L1	L1 vs. L3	L3 vs. ST
Permanent Strain @ 8,500 Cycles_ Evth_ 20°C					
arithmetic scale			log-log scale		
ST	L1	L3	ST	L1	L3
	0.000659	0.000327			-3.485
		0.000487			-3.31262
P-values					
ST vs. L1	L1 vs. L3	L3 vs. ST	ST vs. L1	L1 vs. L3	L3 vs. ST
Permanent Strain @ 12,000 Cycles_ Evth_ 20°C					
arithmetic scale			log-log scale		
ST	L1	L3	ST	L1	L3
	0.000719	0.000364		-3.14308	-3.43856
		0.000529			-3.27673
P-values					
ST vs. L1	L1 vs. L3	L3 vs. ST	ST vs. L1	L1 vs. L3	L3 vs. ST

(b)

Permanent Strain @ 5,000 Cycles_Evth_ 40°C					
arithmetic scale			log-log scale		
ST	L1	L3	ST	L1	L3
0.005859	0.004725	0.004921	-2.23215	-2.32556	-2.30798
0.004313	0.005224	0.004373	-2.36522	-2.28202	-2.35924
P-values					
ST vs. L1	L1 vs. L3	L3 vs. ST	ST vs. L1	L1 vs. L3	L3 vs. ST
0.451673	0.234636	0.322873	0.474277	0.234352	0.33637
Permanent Strain @ 8,500 Cycles_Evth_ 40°C					
arithmetic scale			log-log scale		
ST	L1	L3	ST	L1	L3
0.006158	0.004939	0.005152	-2.21055	-2.30632	-2.28806
0.004538	0.005447	0.004618	-2.34317	-2.26383	-2.33559
P-values					
ST vs. L1	L1 vs. L3	L3 vs. ST	ST vs. L1	L1 vs. L3	L3 vs. ST
0.436149	0.245117	0.320744	0.458421	0.244863	0.334406
Permanent Strain @ 12,000 Cycles_Evth_ 40°C					
arithmetic scale			log-log scale		
ST	L1	L3	ST	L1	L3
0.006346	0.005066	0.005296	-2.1975	-2.29535	-2.27605
0.004683	0.005583	0.00477	-2.32943	-2.25315	-2.32151
P-values					
ST vs. L1	L1 vs. L3	L3 vs. ST	ST vs. L1	L1 vs. L3	L3 vs. ST
0.423551	0.256143	0.31801	0.445268	0.255943	0.331522

(c)

Permanent Strain @ 5,000 Cycles_ Evth_54°C					
arithmetic scale			log-log scale		
ST	L1	L3	ST	L1	L3
0.014214	0.013652	0.009605	-1.84728	-1.86481	-2.01748
0.013315	0.014835	0.009755	-1.87567	-1.82872	-2.01076
P-values					
ST vs. L1	L1 vs. L3	L3 vs. ST	ST vs. L1	L1 vs. L3	L3 vs. ST
0.292715	0.008323	0.006116	0.293729	0.005908	0.004503
Permanent Strain @ 8,500 Cycles_ Evth_54°C					
arithmetic scale			log-log scale		
ST	L1	L3	ST	L1	L3
0.01506	0.014671	0.010127	-1.82217	-1.83353	-1.99454
0.01417	0.015965	0.010334	-1.84863	-1.79682	-1.98574
P-values					
ST vs. L1	L1 vs. L3	L3 vs. ST	ST vs. L1	L1 vs. L3	L3 vs. ST
0.232496	0.008094	0.005343	0.232848	0.00572	0.00401
Permanent Strain @ 12,000 Cycles_ Evth_54°C					
arithmetic scale			log-log scale		
ST	L1	L3	ST	L1	L3
0.015559	0.015307	0.010439	-1.80802	-1.81511	-1.98134
0.01468	0.01667	0.010686	-1.83328	-1.77807	-1.9712
P-values					
ST vs. L1	L1 vs. L3	L3 vs. ST	ST vs. L1	L1 vs. L3	L3 vs. ST
0.198026	0.007951	0.004947	0.197741	0.005615	0.003783

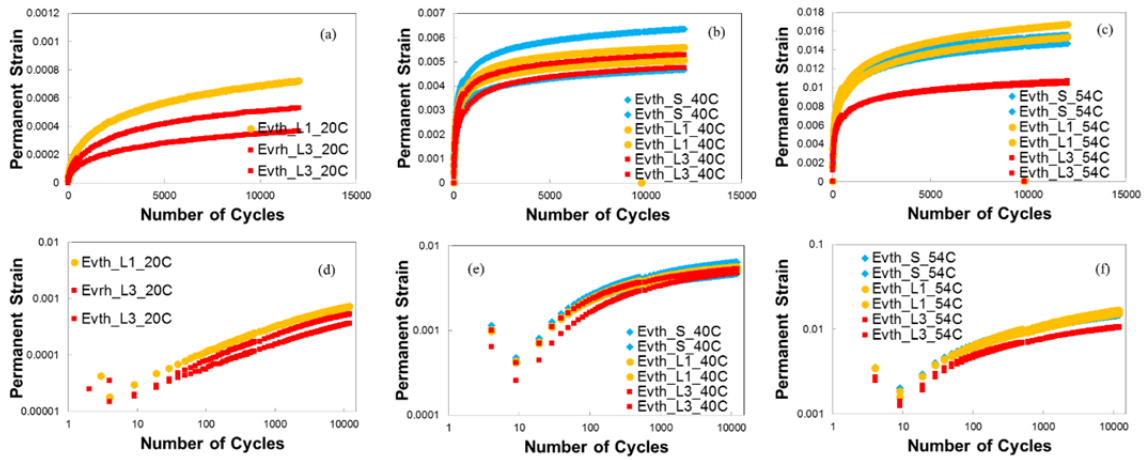


Figure A.3 Comparisons of permanent deformation levels among replicates with different aging levels for WMA Evotherm.

Table A-2 T-test Results of Permanent Strain of WMA Foam for Different Aging Levels: (a) at 20°C, (b) at 40°C, and (c) at 54°C

(a)

Permanent Strain @ 5,000 Cycles_Foam_ 20°C					
arithmetic scale			log-log scale		
ST	L1	L3	ST	L1	L3
0.000642		0.000386	-3.1928		-3.41392
0.000729		0.000357	-3.13699		-3.44793
P-values					
ST vs. L1	L1 vs. L3	L3 vs. ST	ST vs. L1	L1 vs. L3	L3 vs. ST
		0.010507			0.007378
Permanent Strain @ 8,500 Cycles_Foam_ 20°C					
arithmetic scale			log-log scale		
ST	L1	L3	ST	L1	L3
0.000701		0.000479	-3.15449		-3.3195
0.000815		0.000444	-3.08859		-3.35298
P-values					
ST vs. L1	L1 vs. L3	L3 vs. ST	ST vs. L1	L1 vs. L3	L3 vs. ST
		0.019331			0.014186
Permanent Strain @ 12,000 Cycles_Foam_ 20°C					
arithmetic scale			log-log scale		
ST	L1	L3	ST	L1	L3
0.00074		0.000543	-3.13106		-3.26481
0.000863		0.000503	-3.06396		-3.2985
P-values					
ST vs. L1	L1 vs. L3	L3 vs. ST	ST vs. L1	L1 vs. L3	L3 vs. ST
		0.025282			0.01957

(b)

Permanent Strain @ 5,000 Cycles_ Foam_40°C					
arithmetic scale			log-log scale		
ST	L1	L3	ST	L1	L3
0.006777	0.005043	0.003947	-2.16899	-2.29734	-2.40375
	0.005728	0.004389		-2.24198	-2.35762
P-values					
ST vs. L1	L1 vs. L3	L3 vs. ST	ST vs. L1	L1 vs. L3	L3 vs. ST
	0.048165			0.045576	
Permanent Strain@ 8,500 Cycles_ Foam_40°C					
arithmetic scale			log-log scale		
ST	L1	L3	ST	L1	L3
0.007157	0.005277	0.004126	-2.14526	-2.2776	-2.38444
	0.005954	0.004543		-2.22517	-2.34261
P-values					
ST vs. L1	L1 vs. L3	L3 vs. ST	ST vs. L1	L1 vs. L3	L3 vs. ST
	0.042187			0.03949	
Permanent Strain @ 12,000 Cycles_ Foam_40°C					
arithmetic scale			log-log scale		
ST	L1	L3	ST	L1	L3
0.007397	0.005452	0.004237	-2.13095	-2.26344	-2.37289
	0.00608	0.004636		-2.21607	-2.33385
P-values					
ST vs. L1	L1 vs. L3	L3 vs. ST	ST vs. L1	L1 vs. L3	L3 vs. ST
	0.035082			0.032923	

(c)

Permanent Strain @ 5,000 Cycles_ Foam_54°C					
arithmetic scale			log-log scale		
ST	L1	L3	ST	L1	L3
0.019476	0.009797	0.008843	-1.71051	-2.0089	-2.05341
0.019902	0.009954	0.008607	-1.70111	-2.00199	-2.06516
P-values					
ST vs. L1	L1 vs. L3	L3 vs. ST	ST vs. L1	L1 vs. L3	L3 vs. ST
0.000267	0.007415	0.000246	0.000189	0.007821	0.000226
Permanent Strain @ 8,500 Cycles_ Foam_54°C					
arithmetic scale			log-log scale		
ST	L1	L3	ST	L1	L3
0.020922	0.010369	0.009316	-1.67939	-1.98426	-2.03079
0.022294	0.010453	0.008921	-1.65181	-1.98075	-2.04958
P-values					
ST vs. L1	L1 vs. L3	L3 vs. ST	ST vs. L1	L1 vs. L3	L3 vs. ST
0.001873	0.011741	0.001625	0.000959	0.013189	0.000989
Permanent Strain @ 12,000 Cycles_ Foam_54°C					
arithmetic scale			log-log scale		
ST	L1	L3	ST	L1	L3
0.0218	0.010712	0.009592	-1.66154	-1.97012	-2.01809
0.023853	0.010752	0.009202	-1.62245	-1.9685	-2.0361
P-values					
ST vs. L1	L1 vs. L3	L3 vs. ST	ST vs. L1	L1 vs. L3	L3 vs. ST
0.003565	0.010422	0.003	0.001776	0.011806	0.001554

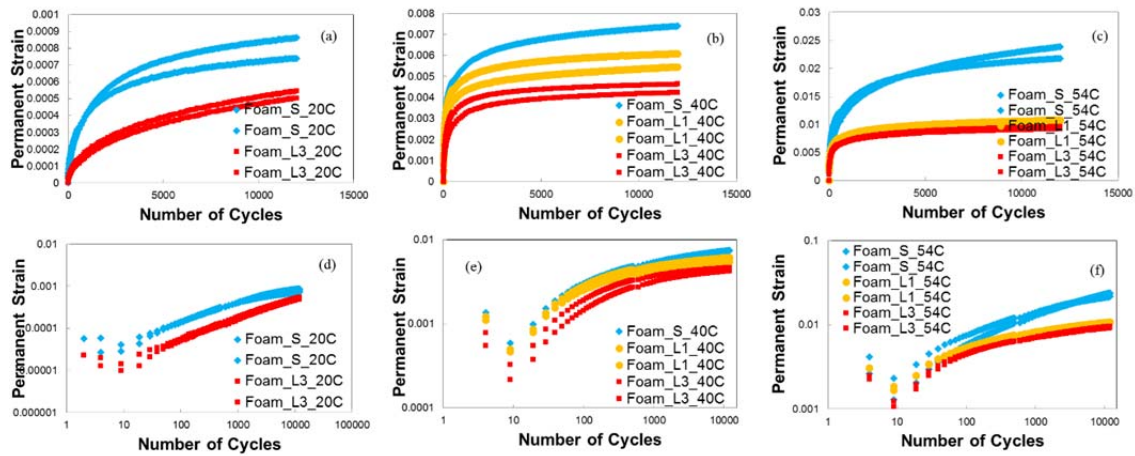


Figure A.4 Comparisons of permanent deformation levels among replicates with different aging levels for WMA Foam.

Table A-3 T-test Results of Permanent Strain of HMA Mixtures for Different Aging Levels: (a) at 20°C, (b) at 40°C, and (c) at 54°C

(a)

Permanent Strain @ 5,000 Cycles_ HMA_20°C					
arithmetic scale			log-log scale		
ST	L1	L3	ST	L1	L3
0.000262	0.000234	0.000226	-3.58188	-3.63153	-3.64576
0.00035	0.000342	0.00023	-3.45551	-3.46623	-3.63774
P-values					
ST vs. L1	L1 vs. L3	L3 vs. ST	ST vs. L1	L1 vs. L3	L3 vs. ST
0.408402	0.193116	0.110207	0.399522	0.189174	0.095699
Permanent Strain @ 8,500 Cycles_ HMA_20°C					
arithmetic scale			log-log scale		
ST	L1	L3	ST	L1	L3
0.000328	0.000294	0.000277	-3.4838	-3.53146	-3.55708
0.000425	0.000437	0.000289	-3.37119	-3.35984	-3.53957
P-values					
ST vs. L1	L1 vs. L3	L3 vs. ST	ST vs. L1	L1 vs. L3	L3 vs. ST
0.453374	0.184105	0.097525	0.437943	0.178023	0.084015
Permanent Strain @ 12,000 Cycles_ HMA_20°C					
arithmetic scale			log-log scale		
ST	L1	L3	ST	L1	L3
0.000371	0.000341	0.000313	-3.43015	-3.46702	-3.50476
0.000481	0.000515	0.00033	-3.31766	-3.28846	-3.48208
P-values					
ST vs. L1	L1 vs. L3	L3 vs. ST	ST vs. L1	L1 vs. L3	L3 vs. ST
0.494439	0.172632	0.099425	0.487144	0.163697	0.086329

(b)

Permanent Strain @ 5,000 Cycles_ HMA_40°C					
arithmetic scale			log-log scale		
ST	L1	L3	ST	L1	L3
0.003005	0.00285	0.002665	-2.52213	-2.54509	-2.57429
0.003754	0.003716	0.003441	-2.42552	-2.42992	-2.46338
P-values					
ST vs. L1	L1 vs. L3	L3 vs. ST	ST vs. L1	L1 vs. L3	L3 vs. ST
0.440949	0.364974	0.302998	0.436204	0.366461	0.301424
Permanent Strain @ 8,500 Cycles_ HMA_40°C					
arithmetic scale			log-log scale		
ST	L1	L3	ST	L1	L3
0.003206	0.00302	0.002829	-2.4941	-2.51994	-2.54837
0.003942	0.003929	0.00364	-2.4043	-2.4057	-2.43886
P-values					
ST vs. L1	L1 vs. L3	L3 vs. ST	ST vs. L1	L1 vs. L3	L3 vs. ST
0.44061	0.365753	0.299537	0.434287	0.367333	0.297272
Permanent Strain @ 12,000 Cycles_ HMA_40°C					
arithmetic scale			log-log scale		
ST	L1	L3	ST	L1	L3
0.003325	0.00312	0.002926	-2.47825	-2.50583	-2.53379
0.004058	0.004053	0.00375	-2.39167	-2.39218	-2.42593
P-values					
ST vs. L1	L1 vs. L3	L3 vs. ST	ST vs. L1	L1 vs. L3	L3 vs. ST
0.438139	0.364059	0.293718	0.431159	0.365853	0.291386

(c)

Permanent Strain @ 5,000 Cycles_ HMA_54°C					
arithmetic scale			log-log scale		
ST	L1	L3	ST	L1	L3
0.008291	0.009425	0.007045	-2.08141	-2.02573	-2.15211
0.008385		0.007499	-2.07649	#NUM!	-2.12498
P-values					
ST vs. L1	L1 vs. L3	L3 vs. ST	ST vs. L1	L1 vs. L3	L3 vs. ST
		0.022128			0.024792
Permanent Strain @ 8,500 Cycles_ HMA_54°C					
arithmetic scale			log-log scale		
ST	L1	L3	ST	L1	L3
0.008981	0.009935	0.007442	-2.04666	-2.00282	-2.12832
0.008937		0.00788	-2.0488	#NUM!	-2.10348
P-values					
ST vs. L1	L1 vs. L3	L3 vs. ST	ST vs. L1	L1 vs. L3	L3 vs. ST
		0.013788			0.015933
Permanent Strain @ 12,000 Cycles_ HMA_54°C					
arithmetic scale			log-log scale		
ST	L1	L3	ST	L1	L3
0.009408	0.010227	0.0077	-2.02652	-1.99024	-2.11349
0.009237		0.008103	-2.03448	#NUM!	-2.09136
P-values					
ST vs. L1	L1 vs. L3	L3 vs. ST	ST vs. L1	L1 vs. L3	L3 vs. ST
		0.011445			0.012856

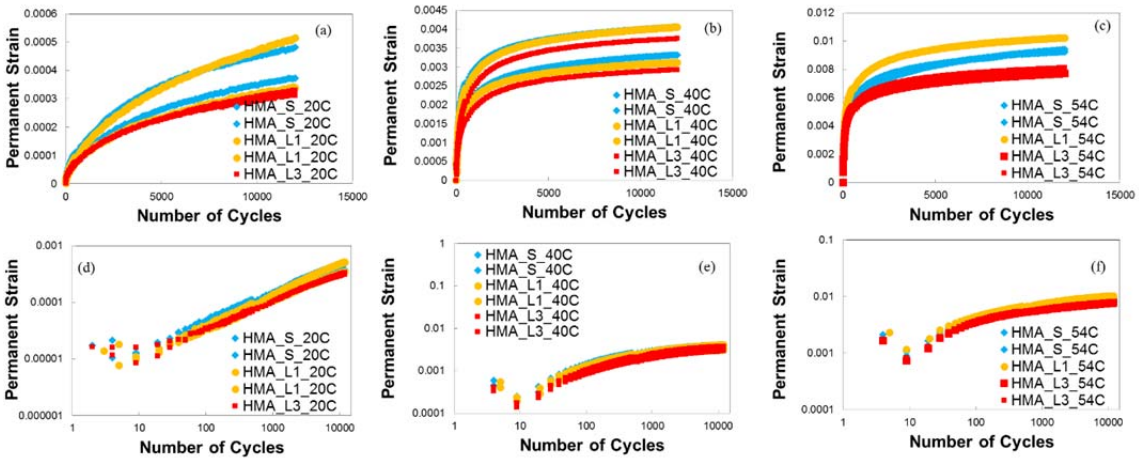


Figure A.5 Comparisons of permanent deformation levels among replicates with different aging levels for HMA mixture.

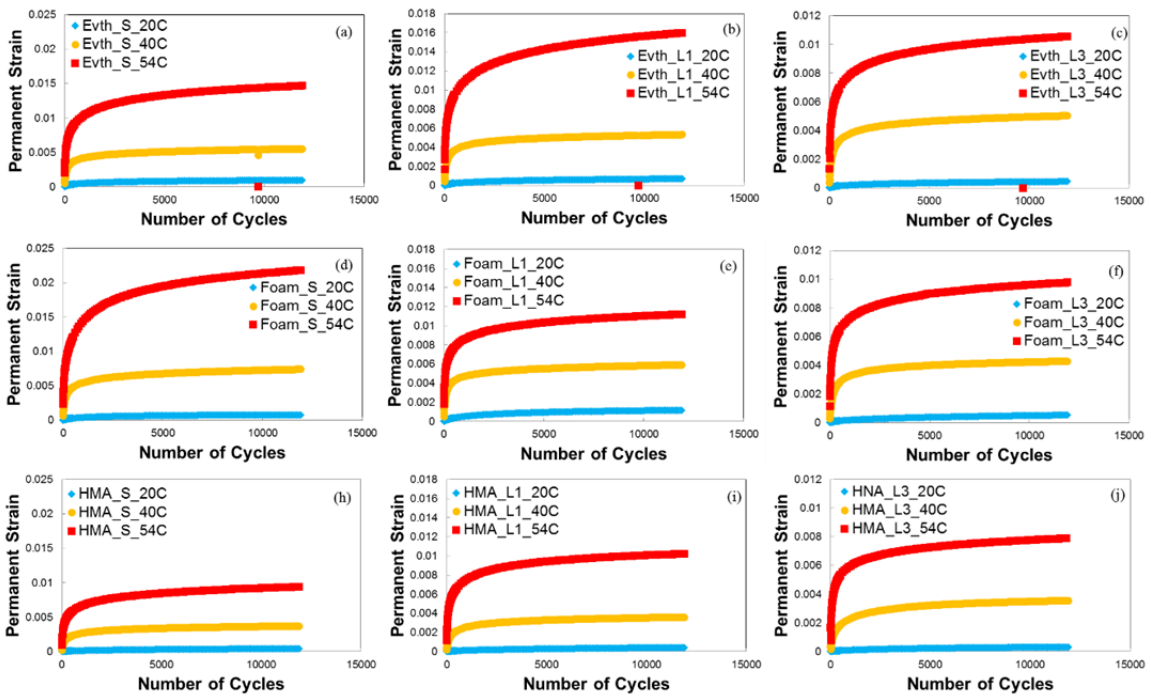


Figure A.6 Comparisons of permanent strain levels at different test temperatures in arithmetic scale.

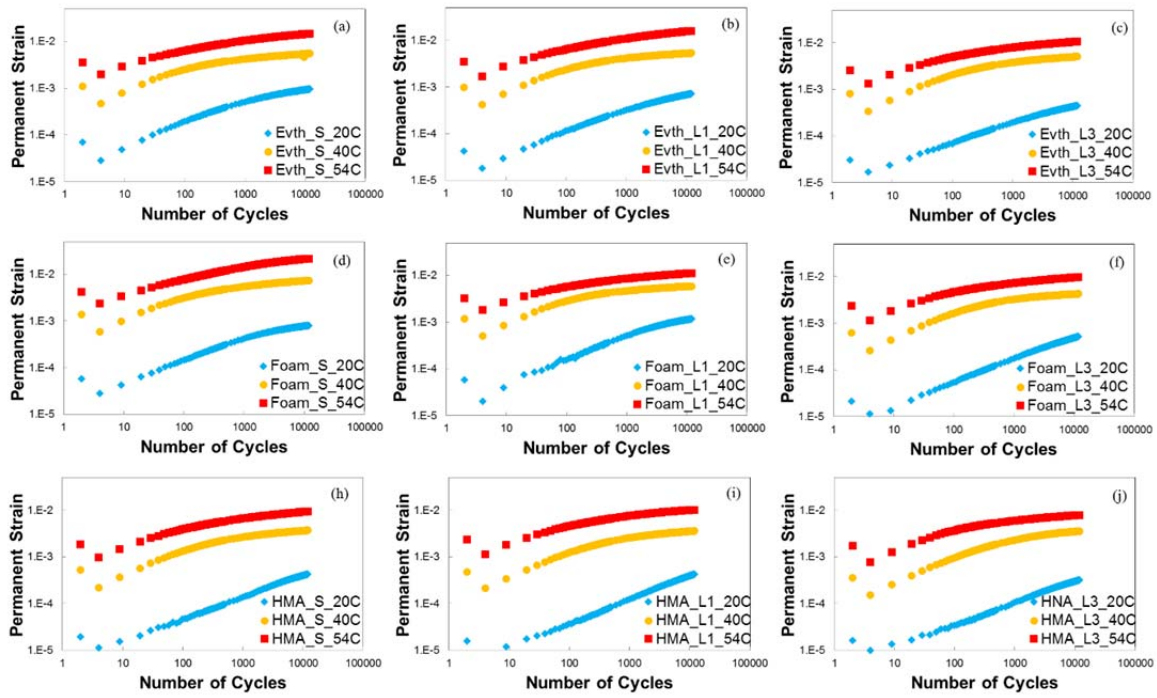


Figure A.7 Comparisons of permanent strain levels at different test temperatures in log-log scale.

Table A-4 T-test Results of Permanent Strain for Short-Term Aging of Conditioned Mixtures at Different Test Temperatures: (a) WMA Evotherm, (b) WMA Foam, and (c) HMA

(a)

Permanent Strain @ 5,000 Cycles_ Evth_STA					
arithmetic scale			log-log scale		
20°C	40°C	54°C	20°C	40°C	54°C
	0.005859	0.014214		-2.23215	-1.84728
	0.004313	0.013315		-2.36522	-1.87567
P-values					
20 vs. 40	40 vs. 54	54 vs. 20	20 vs. 40	40 vs. 54	54 vs. 20
	0.005229			0.011685	
Permanent Strain @ 8,500 Cycles_ Evth_STA					
arithmetic scale			log-log scale		
20°C	40°C	54°C	20°C	40°C	54°C
	0.006158	0.01506		-2.21055	-1.82217
	0.004538	0.01417		-2.34317	-1.84863
P-values					
20 vs. 40	40 vs. 54	54 vs. 20	20 vs. 40	40 vs. 54	54 vs. 20
	0.004902			0.011333	
Permanent Strain @ 12,000 Cycles_ Evth_STA					
arithmetic scale			log-log scale		
20°C	40°C	54°C	20°C	40°C	54°C
	0.006346	0.015559		-2.1975	-1.80802
	0.004683	0.01468		-2.32943	-1.83328
P-values					
20 vs. 40	40 vs. 54	54 vs. 20	20 vs. 40	40 vs. 54	54 vs. 20
	0.004726			0.011121	

(b)

Permanent Strain @ 5,000 Cycles_ Foam_STA					
arithmetic scale			log-log scale		
20°C	40°C	54°C	20°C	40°C	54°C
0.000642	0.006777	0.019476	-3.1928	-2.16899	-1.71051
0.000729		0.019902	-3.13699		-1.70111
P-values					
20 vs. 40	40 vs. 54	54 vs. 20	20 vs. 40	40 vs. 54	54 vs. 20
		6.54E-05			0.000188
Permanent Strain @ 8,500 Cycles_ Foam_STA					
arithmetic scale			log-log scale		
20°C	40°C	54°C	20°C	40°C	54°C
0.000701	0.007157	0.020922	-3.15449	-2.14526	-1.67939
0.000815		0.022294	-3.08859	#NUM!	-1.65181
P-values					
20 vs. 40	40 vs. 54	54 vs. 20	20 vs. 40	40 vs. 54	54 vs. 20
		0.000544			0.000301
Permanent Strain @ 12,000 Cycles_ Foam_STA					
arithmetic scale			log-log scale		
20°C	40°C	54°C	20°C	40°C	54°C
0.00074	0.007397	0.0218	-3.13106	-2.13095	-1.66154
0.000863		0.023853	-3.06396	#NUM!	-1.62245
P-values					
20 vs. 40	40 vs. 54	54 vs. 20	20 vs. 40	40 vs. 54	54 vs. 20
		0.001087			0.000355

(c)

Permanent Strain @ 5,000 Cycles_ HMA_STA					
arithmetic scale			log-log scale		
20°C	40°C	54°C	20°C	40°C	54°C
0.000262	0.003005	0.008291	-3.58188	-2.52213	-2.08141
0.00035	0.003754	0.008385	-3.45551	-2.42552	-2.07649
P-values					
20 vs. 40	40 vs. 54	54 vs. 20	20 vs. 40	40 vs. 54	54 vs. 20
0.007356	0.00287	3.24E-05	0.002872	0.007337	0.000962
Permanent Strain @ 8,500 Cycles_ HMA_STA					
arithmetic scale			log-log scale		
20°C	40°C	54°C	20°C	40°C	54°C
0.000328	0.003206	0.008981	-3.4838	-2.4941	-2.04666
0.000425	0.003942	0.008937	-3.37119	-2.4043	-2.0488
P-values					
20 vs. 40	40 vs. 54	54 vs. 20	20 vs. 40	40 vs. 54	54 vs. 20
0.006612	0.002328	1.93E-05	0.002687	0.006142	0.000831
Permanent Strain @ 12,000 Cycles_ HMA_STA					
arithmetic scale			log-log scale		
20°C	40°C	54°C	20°C	40°C	54°C
0.000371	0.003325	0.009408	-3.43015	-2.47825	-2.02652
0.000481	0.004058	0.009237	-3.31766	-2.39167	-2.03448
P-values					
20 vs. 40	40 vs. 54	54 vs. 20	20 vs. 40	40 vs. 54	54 vs. 20
0.006328	0.002222	6.51E-05	0.002833	0.005679	0.000879

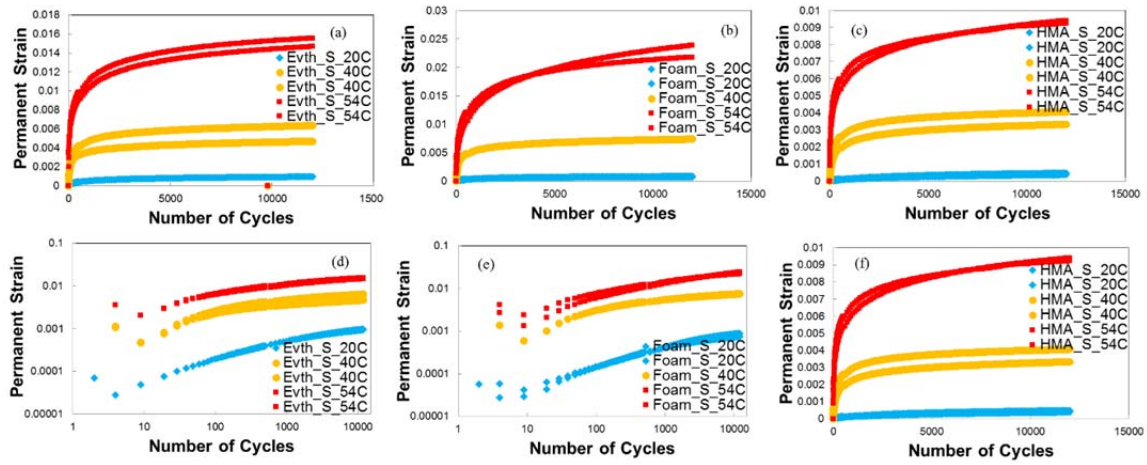


Figure A.8 Comparisons of permanent deformation levels for short-term aging replicates tested at different temperatures in arithmetic scale and log-log scale.

Table A-5 T-test Results of Permanent Strain of Long-Term Aging Level 1 Conditioned Mixtures at Different Test Temperatures: (a) WMA Evotherm, (b) WMA Foam, and (c) HMA

(a)

Permanent Strain @ 5,000 Cycles_ Evth_LTA1					
arithmetic scale			log-log scale		
20°C	40°C	54°C	20°C	40°C	54°C
0.000565	0.004725	0.013652	-3.24794	-2.32556	-1.86481
	0.005224	0.014835		-2.28202	-1.82872
P-values					
20 vs. 40	40 vs. 54	54 vs. 20	20 vs. 40	40 vs. 54	54 vs. 20
	0.00238			0.001903	
Permanent Strain @ 8,500 Cycles_ Evth_LTA1					
arithmetic scale			log-log scale		
20°C	40°C	54°C	20°C	40°C	54°C
0.000659	0.004939	0.014671	-3.18109	-2.30632	-1.83353
	0.005447	0.015965		-2.26383	-1.79682
P-values					
20 vs. 40	40 vs. 54	54 vs. 20	20 vs. 40	40 vs. 54	54 vs. 20
	0.00234			0.001775	
Permanent Strain @ 12,000 Cycles_ Evth_LTA1					
arithmetic scale			log-log scale		
20°C	40°C	54°C	20°C	40°C	54°C
0.000719	0.005066	0.015307	-3.14308	-2.29535	-1.81511
	0.005583	0.01667	#NUM!	-2.25315	-1.77807
P-values					
20 vs. 40	40 vs. 54	54 vs. 20	20 vs. 40	40 vs. 54	54 vs. 20
	0.002319			0.001718	

(b)

Permanent Strain @ 5,000 Cycles_ Foam_LTA1					
arithmetic scale			log-log scale		
20°C	40°C	54°C	20°C	40°C	54°C
	0.005043	0.009797		-2.29734	-2.0089
	0.005728	0.009954		-2.24198	-2.00199
P-values					
20 vs. 40	40 vs. 54	54 vs. 20	20 vs. 40	40 vs. 54	54 vs. 20
	0.003039			0.005483	
Permanent Strain @ 8,500 Cycles_ Foam_LTA1					
arithmetic scale			log-log scale		
20°C	40°C	54°C	20°C	40°C	54°C
	0.005277	0.010369		-2.2776	-1.98426
	0.005954	0.010453		-2.22517	-1.98075
P-values					
20 vs. 40	40 vs. 54	54 vs. 20	20 vs. 40	40 vs. 54	54 vs. 20
	0.002512			0.004707	
Permanent Strain @ 12,000 Cycles_ Foam_LTA1					
arithmetic scale			log-log scale		
20°C	40°C	54°C	20°C	40°C	54°C
	0.005452	0.010712		-2.26344	-1.97012
	0.00608	0.010752		-2.21607	-1.9685
P-values					
20 vs. 40	40 vs. 54	54 vs. 20	20 vs. 40	40 vs. 54	54 vs. 20
	0.001997			0.003795	

(c)

Permanent Strain @ 5,000 Cycles_ HMA_LTA1					
arithmetic scale			log-log scale		
20°C	40°C	54°C	20°C	40°C	54°C
0.000234	0.00285	0.009425	-3.63153	-2.54509	-2.02573
0.000342	0.003716		-3.46623	-2.42992	#NUM!
P-values					
20 vs. 40	40 vs. 54	54 vs. 20	20 vs. 40	40 vs. 54	54 vs. 20
0.010275			0.004444		
Permanent Strain @ 8,500 Cycles_ HMA_LTA1					
arithmetic scale			log-log scale		
20°C	40°C	54°C	20°C	40°C	54°C
0.000294	0.00302	0.009935	-3.53146	-2.51994	-2.00282
0.000437	0.003929		-3.35984	-2.4057	#NUM!
P-values					
20 vs. 40	40 vs. 54	54 vs. 20	20 vs. 40	40 vs. 54	54 vs. 20
0.010594			0.005411		
Permanent Strain @ 12,000 Cycles_ HMA_LTA1					
arithmetic scale			log-log scale		
20°C	40°C	54°C	20°C	40°C	54°C
0.000341	0.00312	0.010227	-3.46702	-2.50583	-1.99024
0.000515	0.004053		-3.28846	-2.39218	#NUM!
P-values					
20 vs. 40	40 vs. 54	54 vs. 20	20 vs. 40	40 vs. 54	54 vs. 20
0.010921			0.006368		

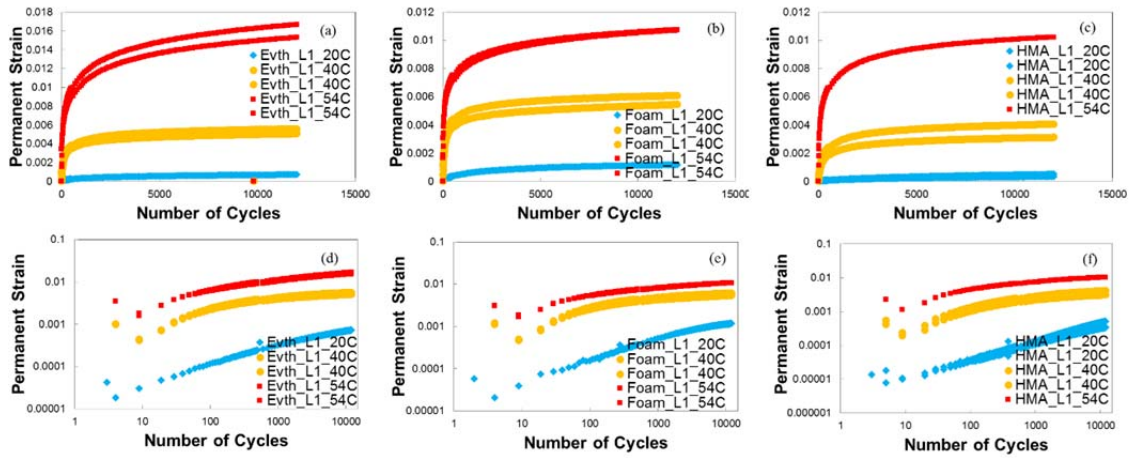


Figure A.9 Comparisons of permanent deformation levels for long-term aging Level 1 conditioned replicates tested at different temperatures in arithmetic scale and log-log scale.

Table A-6 T-test Results of Permanent Strain of Long-Term Aging Level 3 Conditioned Mixtures at Different Test Temperatures: (a) WMA Evotherm, (b) WMA Foam, and (c) HMA

(a)

Permanent Strain @ 5,000 Cycles_ Evth_LTA3					
arithmetic scale			log-log scale		
20°C	40°C	54°C	20°C	40°C	54°C
0.000279	0.004921	0.009605	-3.55458	-2.30798	-2.01748
0.000421	0.004373	0.009755	-3.37622	-2.35924	-2.01076
P-values					
20 vs. 40	40 vs. 54	54 vs. 20	20 vs. 40	40 vs. 54	54 vs. 20
0.002153	0.001583	6.1E-05	0.003327	0.00324	0.00188
Permanent Strain @ 8,500 Cycles_ Evth_LTA3					
arithmetic scale			log-log scale		
20°C	40°C	54°C	20°C	40°C	54°C
0.000327	0.005152	0.010127	-3.485	-2.28806	-1.99454
0.000487	0.004618	0.010334	-3.31262	-2.33559	-1.98574
P-values					
20 vs. 40	40 vs. 54	54 vs. 20	20 vs. 40	40 vs. 54	54 vs. 20
0.001926	0.001429	8.86E-05	0.003349	0.002799	0.001866
Permanent Strain @ 12,000 Cycles_ Evth_LTA3					
arithmetic scale			log-log scale		
20°C	40°C	54°C	20°C	40°C	54°C
0.000364	0.005296	0.010439	-3.43856	-2.27605	-1.98134
0.000529	0.00477	0.010686	-3.27673	-2.32151	-1.9712
P-values					
20 vs. 40	40 vs. 54	54 vs. 20	20 vs. 40	40 vs. 54	54 vs. 20
0.001797	0.001376	0.000107	0.003121	0.002587	0.001713

(b)

Permanent Strain @ 5,000 Cycles_ Foam_LTA3					
arithmetic scale			log-log scale		
20°C	40°C	54°C	20°C	40°C	54°C
0.000386	0.003947	0.008843	-3.41392	-2.40375	-2.05341
0.000357	0.004389	0.008607	-3.44793	-2.35762	-2.06516
P-values					
20 vs. 40	40 vs. 54	54 vs. 20	20 vs. 40	40 vs. 54	54 vs. 20
0.001695	0.001506	0.000101	0.000372	0.00272	8.6E-05
Permanent Strain @ 8,500 Cycles_ Foam_LTA3					
arithmetic scale			log-log scale		
20°C	40°C	54°C	20°C	40°C	54°C
0.000479	0.004126	0.009316	-3.3195	-2.38444	-2.03079
0.000444	0.004543	0.008921	-3.35298	-2.34261	-2.04958
P-values					
20 vs. 40	40 vs. 54	54 vs. 20	20 vs. 40	40 vs. 54	54 vs. 20
0.001454	0.001791	0.000261	0.000379	0.002495	0.00011
Permanent Strain @ 12,000 Cycles_ Foam_LTA3					
arithmetic scale			log-log scale		
20°C	40°C	54°C	20°C	40°C	54°C
0.000543	0.004237	0.009592	-3.26481	-2.37289	-2.01809
0.000503	0.004636	0.009202	-3.2985	-2.33385	-2.0361
P-values					
20 vs. 40	40 vs. 54	54 vs. 20	20 vs. 40	40 vs. 54	54 vs. 20
0.001305	0.001571	0.000243	0.000385	0.002156	0.000116

(c)

Permanent Strain @ 5,000 Cycles_ HMA_LTA3					
arithmetic scale			log-log scale		
20°C	40°C	54°C	20°C	40°C	54°C
0.000226	0.002665	0.007045	-3.64576	-2.57429	-2.15211
0.00023	0.003441	0.007499	-3.63774	-2.46338	-2.12498
P-values					
20 vs. 40	40 vs. 54	54 vs. 20	20 vs. 40	40 vs. 54	54 vs. 20
0.009163	0.005576	0.000519	0.001221	0.010902	4.43E-05
Permanent Strain @ 8,500 Cycles_ HMA_LTA3					
arithmetic scale			log-log scale		
20°C	40°C	54°C	20°C	40°C	54°C
0.000277	0.002829	0.007442	-3.55708	-2.54837	-2.12832
0.000289	0.00364	0.00788	-3.53957	-2.43886	-2.10348
P-values					
20 vs. 40	40 vs. 54	54 vs. 20	20 vs. 40	40 vs. 54	54 vs. 20
0.009187	0.005338	0.000441	0.001376	0.010695	5.63E-05
Permanent Strain @ 12,000 Cycles_ HMA_LTA3					
arithmetic scale			log-log scale		
20°C	40°C	54°C	20°C	40°C	54°C
0.000313	0.002926	0.0077	-3.50476	-2.53379	-2.11349
0.00033	0.00375	0.008103	-3.48208	-2.42593	-2.09136
P-values					
20 vs. 40	40 vs. 54	54 vs. 20	20 vs. 40	40 vs. 54	54 vs. 20
0.009092	0.00498	0.000353	0.001472	0.01031	6.49E-05

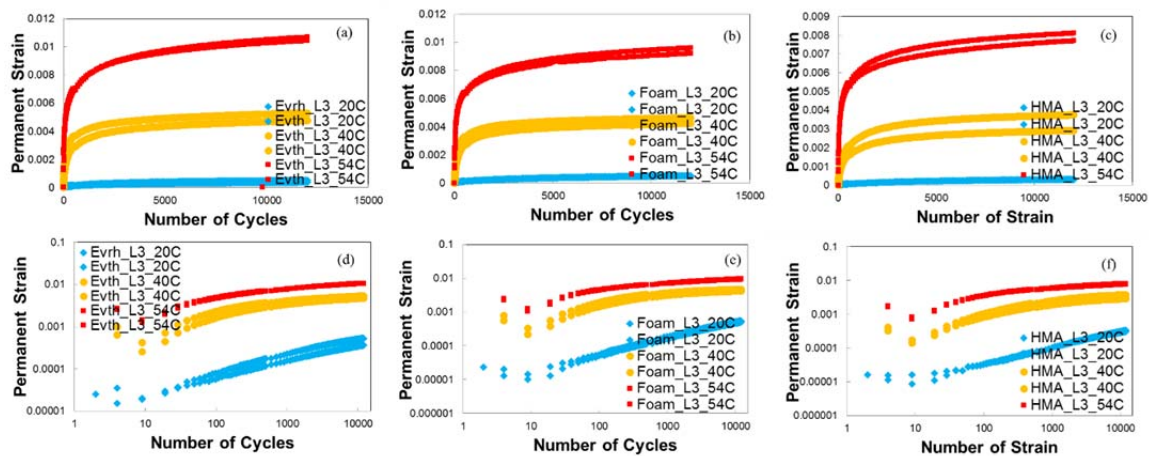


Figure A.10 Comparisons of permanent deformation levels for long-term aging Level 3 conditioned replicates tested at different temperatures in arithmetic scale and log-log scale.

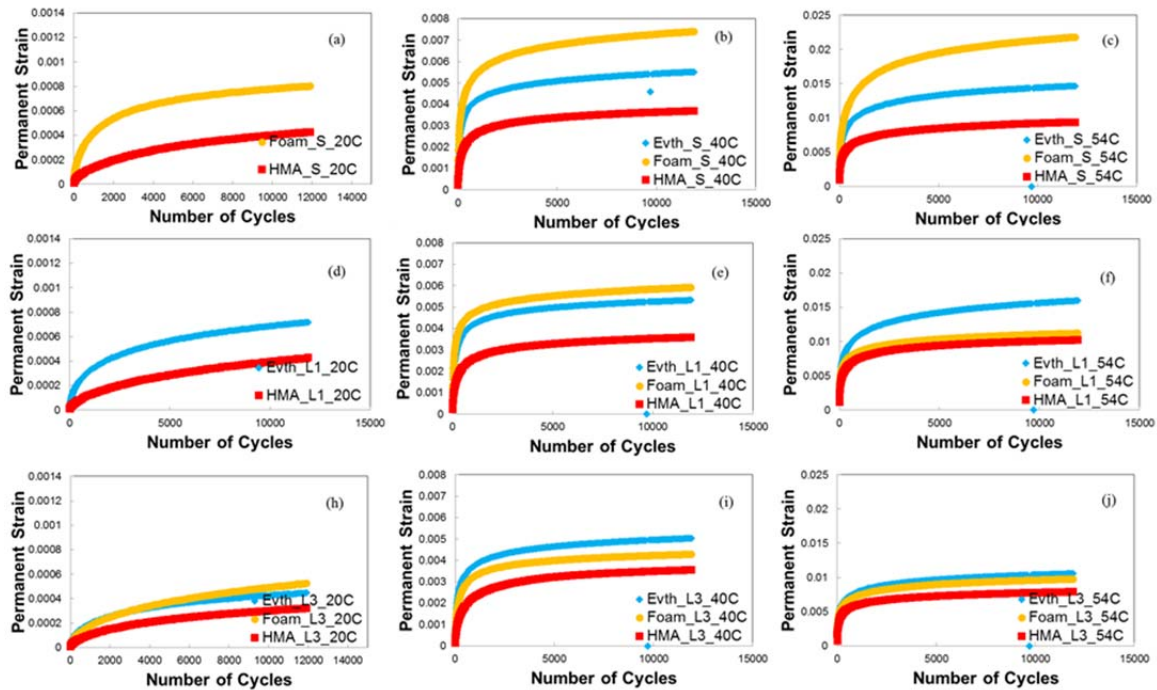


Figure A.11 Comparisons of permanent strain levels among different mixtures in arithmetic scale.

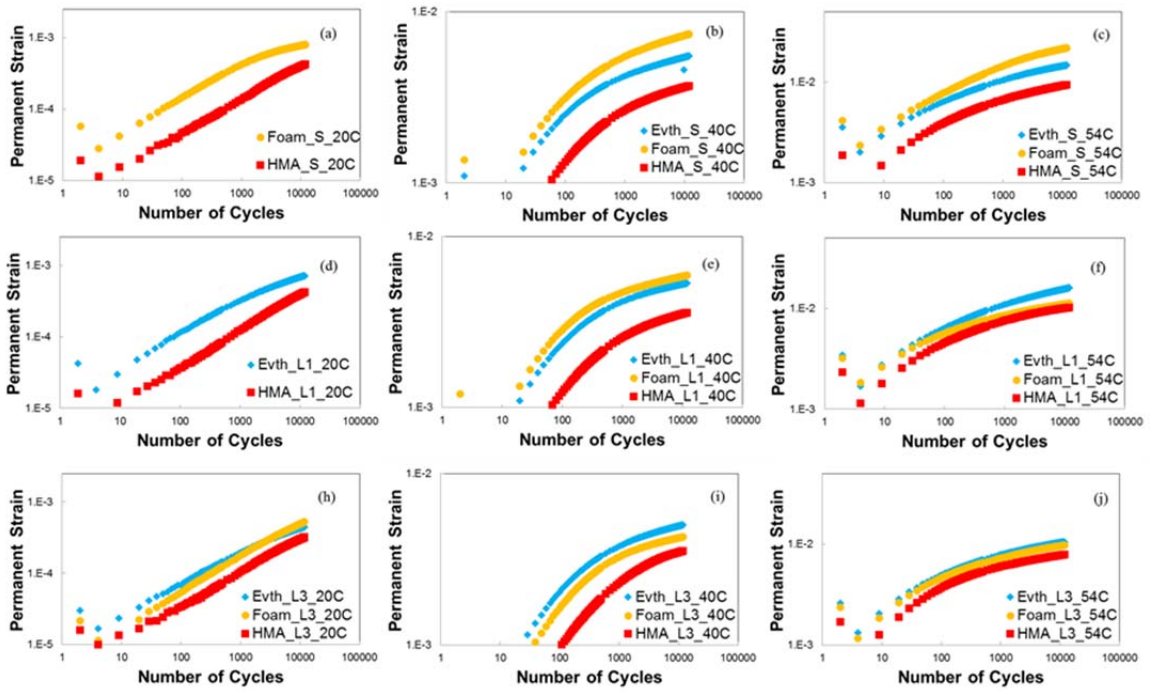


Figure A.12 Comparisons of permanent strain levels among different mixtures in log-log scale.

Table A-7 T-test Results of Permanent Strain for Different Mixtures at 20°C: (a) Short-Term Aging Conditioning, (b) Long-Term Aging Condition Level 1, and (c) Long-Term Aging Condition Level 3

(a)

Permanent Strain @ 5,000 Cycles_ STA_20°C					
arithmetic scale			log-log scale		
Evth	Foam	HMA	Evth	Foam	HMA
	0.000642	0.000262		-3.1928	-3.58188
	0.000729	0.00035		-3.13699	-3.45551
P-values					
Evth vs. Foam	Foam vs. HMA	HMA vs. Evth	Evth vs. Foam	Foam vs. HMA	HMA vs. Evth
	0.012991			0.018033	
Permanent Strain @ 8,500 Cycles_ STA_20°C					
arithmetic scale			log-log scale		
Evth	Foam	HMA	Evth	Foam	HMA
	0.000701	0.000328		-3.15449	-3.4838
	0.000815	0.000425		-3.08859	-3.37119
P-values					
Evth vs. Foam	Foam vs. HMA	HMA vs. Evth	Evth vs. Foam	Foam vs. HMA	HMA vs. Evth
	0.018387			0.021289	
Permanent Strain @ 12,000 Cycles_ STA_20°C					
arithmetic scale			log-log scale		
Evth	Foam	HMA	Evth	Foam	HMA
	0.00074	0.000371		-3.13106	-3.43015
	0.000863	0.000481		-3.06396	-3.31766
P-values					
Evth vs. Foam	Foam vs. HMA	HMA vs. Evth	Evth vs. Foam	Foam vs. HMA	HMA vs. Evth
	0.022654			0.02591	

(b)

Permanent Strain @ 5,000 Cycles_ LTA1_20°C					
arithmetic scale			log-log scale		
Evth	Foam	HMA	Evth	Foam	HMA
0.000565		0.000234	-3.24794		-3.63153
		0.000342			-3.46623
P-values					
Evth vs. Foam	Foam vs. HMA	HMA vs. Evth	Evth vs. Foam	Foam vs. HMA	HMA vs. Evth
Permanent Strain @ 8,500 Cycles_ LTA1_20°C					
arithmetic scale			log-log scale		
Evth	Foam	HMA	Evth	Foam	HMA
0.000659		0.000294	-3.18109		-3.53146
		0.000437			-3.35984
P-values					
Evth vs. Foam	Foam vs. HMA	HMA vs. Evth	Evth vs. Foam	Foam vs. HMA	HMA vs. Evth
Permanent Strain @ 12,000 Cycles_ LTA1_20°C					
arithmetic scale			log-log scale		
Evth	Foam	HMA	Evth	Foam	HMA
0.000719		0.000341	-3.14308		-3.46702
		0.000515			-3.28846
P-values					
Evth vs. Foam	Foam vs. HMA	HMA vs. Evth	Evth vs. Foam	Foam vs. HMA	HMA vs. Evth

(c)

Permanent Strain @ 5,000 Cycles_ LTA3_ 20°C					
arithmetic scale			log-log scale		
Evth	Foam	HMA	Evth	Foam	HMA
0.000279	0.000386	0.000226	-3.55458	-3.41392	-3.64576
0.000421	0.000357	0.00023	-3.37622	-3.44793	-3.63774
P-values					
Evth vs. Foam	Foam vs. HMA	HMA vs. Evth	Evth vs. Foam	Foam vs. HMA	HMA vs. Evth
0.397854	0.005192	0.114216	0.37032	0.003398	0.093443
Permanent Strain @ 8,500 Cycles_ LTA3_ 20°C					
arithmetic scale			log-log scale		
Evth	Foam	HMA	Evth	Foam	HMA
0.000327	0.000479	0.000277	-3.485	-3.3195	-3.55708
0.000487	0.000444	0.000289	-3.31262	-3.35298	-3.53957
P-values					
Evth vs. Foam	Foam vs. HMA	HMA vs. Evth	Evth vs. Foam	Foam vs. HMA	HMA vs. Evth
0.287274	0.005385	0.130396	0.274991	0.00392	0.11326
Permanent Strain @ 12,000 Cycles_ LTA3_ 20°C					
arithmetic scale			log-log scale		
Evth	Foam	HMA	Evth	Foam	HMA
0.000364	0.000543	0.000313	-3.43856	-3.26481	-3.50476
0.000529	0.000503	0.00033	-3.27673	-3.2985	-3.48208
P-values					
Evth vs. Foam	Foam vs. HMA	HMA vs. Evth	Evth vs. Foam	Foam vs. HMA	HMA vs. Evth
0.230449	0.005799	0.134345	0.22746	0.004536	0.119232

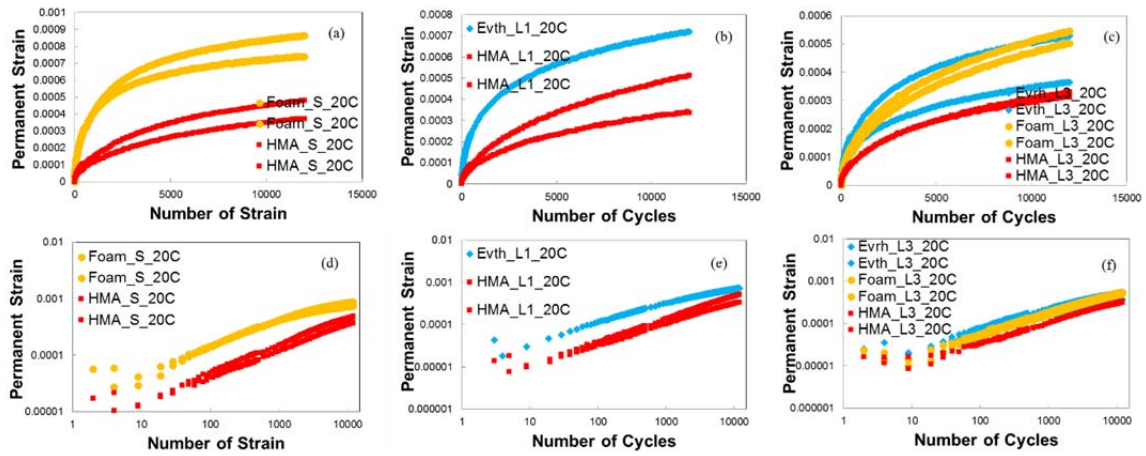


Figure A.13 Comparisons of permanent deformation levels among replicates of different mixtures at 20°C.

Table A-8 T-test Results of Permanent Strain for Different Mixtures at 40°C: (a) Short-Term Aging Conditioning, (b) Long-Term Aging Condition Level 1, and (c) Long-Term Aging Condition Level 3

(a)

Permanent Strain @ 5,000 Cycles_ STA_ 40°C					
arithmetic scale			log-log scale		
Evth	Foam	HMA	Evth	Foam	HMA
0.005859	0.006777	0.003005	-2.23215	-2.16899	-2.52213
0.004313		0.003754	-2.36522		-2.42552
P-values					
Evth vs. Foam	Foam vs. HMA	HMA vs. Evth	Evth vs. Foam	Foam vs. HMA	HMA vs. Evth
		0.092667			0.08345
Permanent Strain @ 8,500 Cycles_ STA_ 40°C					
arithmetic scale			log-log scale		
Evth	Foam	HMA	Evth	Foam	HMA
0.006158	0.007157	0.003206	-2.21055	-2.14526	-2.4941
0.004538		0.003942	-2.34317		-2.4043
P-values					
Evth vs. Foam	Foam vs. HMA	HMA vs. Evth	Evth vs. Foam	Foam vs. HMA	HMA vs. Evth
		0.092191			0.082145
Permanent Strain @ 12,000 Cycles_ STA_ 40°C					
arithmetic scale			log-log scale		
Evth	Foam	HMA	Evth	Foam	HMA
0.006346	0.007397	0.003325	-2.1975	-2.13095	-2.47825
0.004683		0.004058	-2.32943		-2.39167
P-values					
Evth vs. Foam	Foam vs. HMA	HMA vs. Evth	Evth vs. Foam	Foam vs. HMA	HMA vs. Evth
		0.091292			0.080906

(b)

Permanent Strain @ 5,000 Cycles_ LTA1_ 40°C					
arithmetic scale			log-log scale		
Evth	Foam	HMA	Evth	Foam	HMA
0.004725	0.005043	0.00285	-2.32556	-2.29734	-2.54509
0.005224	0.005728	0.003716	-2.28202	-2.24198	-2.42992
P-values					
Evth vs. Foam	Foam vs. HMA	HMA vs. Evth	Evth vs. Foam	Foam vs. HMA	HMA vs. Evth
0.217295	0.031288	0.038611	0.217376	0.038154	0.048169
Permanent Strain @ 8,500 Cycles_ LTA1_ 40°C					
arithmetic scale			log-log scale		
Evth	Foam	HMA	Evth	Foam	HMA
0.004939	0.005277	0.00302	-2.30632	-2.2776	-2.51994
0.005447	0.005954	0.003929	-2.26383	-2.22517	-2.4057
P-values					
Evth vs. Foam	Foam vs. HMA	HMA vs. Evth	Evth vs. Foam	Foam vs. HMA	HMA vs. Evth
0.211669	0.03173	0.040385	0.211629	0.03907	0.050099
Permanent Strain @ 12,000 Cycles_ LTA1_ 40°C					
arithmetic scale			log-log scale		
Evth	Foam	HMA	Evth	Foam	HMA
0.005066	0.005452	0.00312	-2.29535	-2.26344	-2.50583
0.005583	0.00608	0.004053	-2.25315	-2.21607	-2.39218
P-values					
Evth vs. Foam	Foam vs. HMA	HMA vs. Evth	Evth vs. Foam	Foam vs. HMA	HMA vs. Evth
0.195406	0.030314	0.041365	0.195192	0.038367	0.051102

(c)

Permanent Strain @ 5,000 Cycles_ LTA3_ 40°C					
arithmetic scale			log-log scale		
Evth	Foam	HMA	Evth	Foam	HMA
0.004921	0.003947	0.002665	-2.30798	-2.40375	-2.57429
0.004373	0.004389	0.003441	-2.35924	-2.35762	-2.46338
P-values					
Evth vs. Foam	Foam vs. HMA	HMA vs. Evth	Evth vs. Foam	Foam vs. HMA	HMA vs. Evth
0.153424	0.06487	0.039201	0.152706	0.074068	0.046868
Permanent Strain @ 8,500 Cycles_ LTA3_ 40°C					
arithmetic scale			log-log scale		
Evth	Foam	HMA	Evth	Foam	HMA
0.005152	0.004126	0.002829	-2.28806	-2.38444	-2.54837
0.004618	0.004543	0.00364	-2.33559	-2.34261	-2.43886
P-values					
Evth vs. Foam	Foam vs. HMA	HMA vs. Evth	Evth vs. Foam	Foam vs. HMA	HMA vs. Evth
0.123114	0.068677	0.038402	0.122024	0.07833	0.046509
Permanent Strain @ 12,000 Cycles_ LTA3_ 40°C					
arithmetic scale			log-log scale		
Evth	Foam	HMA	Evth	Foam	HMA
0.005296	0.004237	0.002926	-2.27605	-2.37289	-2.53379
0.00477	0.004636	0.00375	-2.32151	-2.33385	-2.42593
P-values					
Evth vs. Foam	Foam vs. HMA	HMA vs. Evth	Evth vs. Foam	Foam vs. HMA	HMA vs. Evth
0.10636	0.069267	0.03708	0.105017	0.079104	0.045249

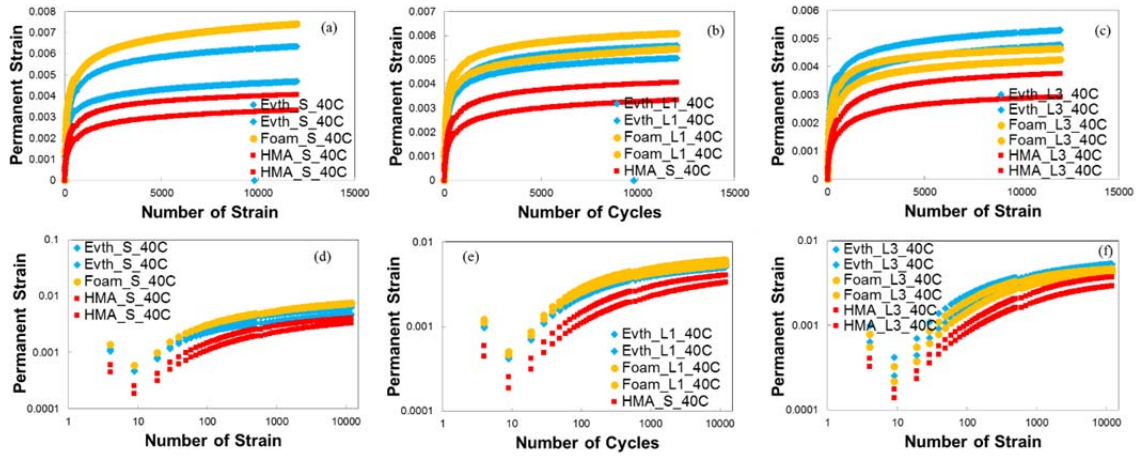


Figure A.14 Comparisons of permanent deformation levels among replicates of different mixtures at 40°C.

Table A-9 T-test Results of Permanent Strain for Different Mixtures at 54°C: (a) Short-Term Aging Conditioning, (b) Long-Term Aging Condition Level 1, and (c) Long-Term Aging Condition Level 3.

(a)

Permanent Strain @ 5,000 Cycles_ STA_54°C					
arithmetic scale			log-log scale		
Evth	Foam	HMA	Evth	Foam	HMA
0.014214	0.019476	0.008291	-1.84728	-1.71051	-2.08141
0.013315	0.019902	0.008385	-1.87567	-1.70111	-2.07649
P-values					
Evth vs. Foam	Foam vs. HMA	HMA vs. Evth	Evth vs. Foam	Foam vs. HMA	HMA vs. Evth
0.00349	0.000184	0.003436	0.004549	0.000101	0.002179
Permanent Strain @ 8,500 Cycles_ STA_54°C					
arithmetic scale			log-log scale		
Evth	Foam	HMA	Evth	Foam	HMA
0.01506	0.020922	0.008981	-1.82217	-1.67939	-2.04666
0.01417	0.022294	0.008937	-1.84863	-1.65181	-2.0488
P-values					
Evth vs. Foam	Foam vs. HMA	HMA vs. Evth	Evth vs. Foam	Foam vs. HMA	HMA vs. Evth
0.006698	0.001465	0.003075	0.006215	0.000654	0.001942
Permanent Strain @ 12,000 Cycles_ STA_54°C					
arithmetic scale			log-log scale		
Evth	Foam	HMA	Evth	Foam	HMA
0.015559	0.0218	0.009408	-1.80802	-1.66154	-2.02652
0.01468	0.023853	0.009237	-1.83328	-1.62245	-2.03448
P-values					
Evth vs. Foam	Foam vs. HMA	HMA vs. Evth	Evth vs. Foam	Foam vs. HMA	HMA vs. Evth
0.010179	0.002884	0.002959	0.008275	0.001313	0.00198

(b)

Permanent Strain @ 5,000 Cycles_ LTA1_54°C					
arithmetic scale			log-log scale		
Evth	Foam	HMA	Evth	Foam	HMA
0.013652	0.009797	0.009425	-1.86481	-2.0089	-2.02573
0.014835	0.009954		-1.82872	-2.00199	#NUM!
P-values					
Evth vs. Foam	Foam vs. HMA	HMA vs. Evth	Evth vs. Foam	Foam vs. HMA	HMA vs. Evth
0.009078			0.006571		
Permanent Strain @ 8,500 Cycles_ LTA1_54°C					
arithmetic scale			log-log scale		
Evth	Foam	HMA	Evth	Foam	HMA
0.014671	0.010369	0.009935	-1.83353	-1.98426	-2.00282
0.015965	0.010453		-1.79682	-1.98075	#NUM!
P-values					
Evth vs. Foam	Foam vs. HMA	HMA vs. Evth	Evth vs. Foam	Foam vs. HMA	HMA vs. Evth
0.008509			0.005964		
Permanent Strain @ 12,000 Cycles_ LTA1_54°C					
arithmetic scale			log-log scale		
Evth	Foam	HMA	Evth	Foam	HMA
0.015307	0.010712	0.010227	-1.81511	-1.97012	-1.99024
0.01667	0.010752		-1.77807	-1.9685	#NUM!
P-values					
Evth vs. Foam	Foam vs. HMA	HMA vs. Evth	Evth vs. Foam	Foam vs. HMA	HMA vs. Evth
0.008206			0.005663		

(c)

Permanent Strain @ 5,000 Cycles_ LTA3_ 54°C					
arithmetic scale			log-log scale		
Evth	Foam	HMA	Evth	Foam	HMA
0.009605	0.008843	0.007045	-2.01748	-2.05341	-2.15211
0.009755	0.008607	0.007499	-2.01076	-2.06516	-2.12498
P-values					
Evth vs. Foam	Foam vs. HMA	HMA vs. Evth	Evth vs. Foam	Foam vs. HMA	HMA vs. Evth
0.010363	0.014835	0.004859	0.010859	0.016539	0.006193
Permanent Strain @ 8,500 Cycles_ LTA3_ 54°C					
arithmetic scale			log-log scale		
Evth	Foam	HMA	Evth	Foam	HMA
0.010127	0.009316	0.007442	-1.99454	-2.03079	-2.12832
0.010334	0.008921	0.00788	-1.98574	-2.04958	-2.10348
P-values					
Evth vs. Foam	Foam vs. HMA	HMA vs. Evth	Evth vs. Foam	Foam vs. HMA	HMA vs. Evth
0.018944	0.01928	0.00439	0.020193	0.019906	0.005402
Permanent Strain @ 12,000 Cycles_ LTA3_ 54°C					
arithmetic scale			log-log scale		
Evth	Foam	HMA	Evth	Foam	HMA
0.010439	0.009592	0.0077	-1.98134	-2.01809	-2.11349
0.010686	0.009202	0.008103	-1.9712	-2.0361	-2.09136
P-values					
Evth vs. Foam	Foam vs. HMA	HMA vs. Evth	Evth vs. Foam	Foam vs. HMA	HMA vs. Evth
0.018498	0.016667	0.00389	0.01947	0.017022	0.004591

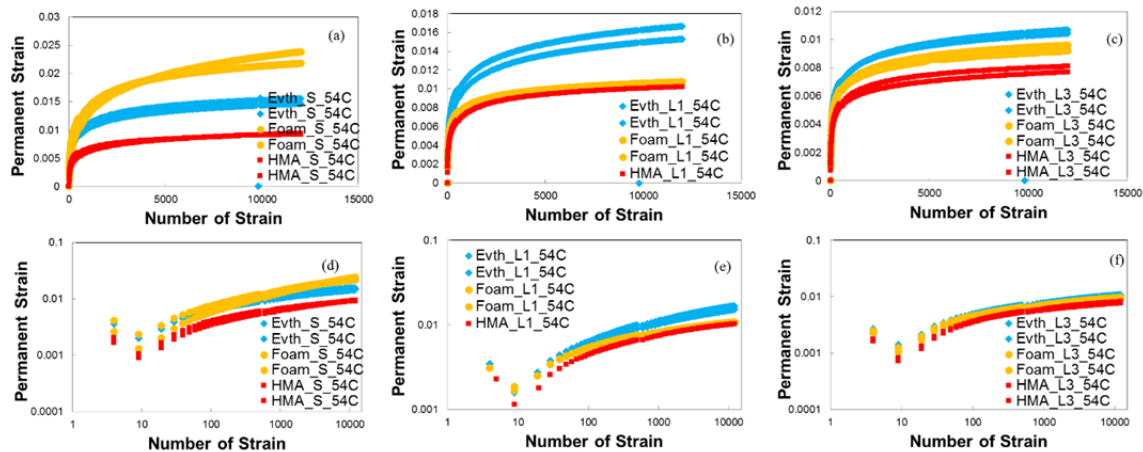


Figure A.15 Comparisons of permanent deformation levels among replicates of different mixtures at 54°C.

APPENDIX B TABLES AND FIGURES ABOUT AGING EFFECT ON STRAIN RATIO OF PERMANENT STRAIN TO RESILIENT STRAIN

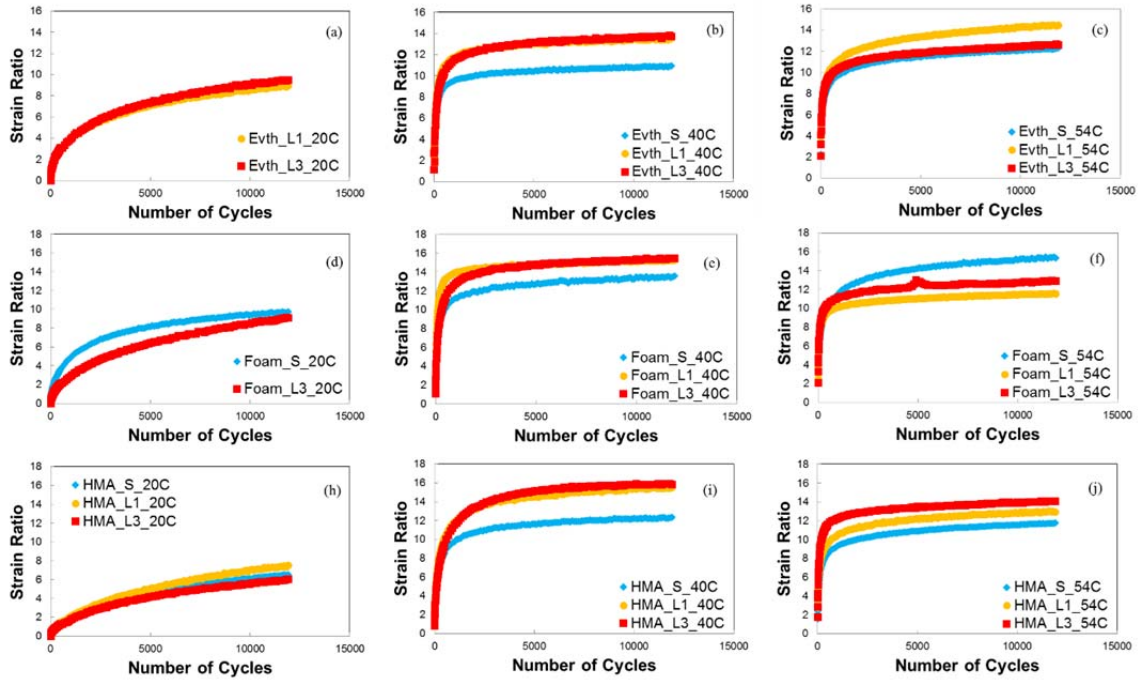


Figure B.1 Comparisons of strain ratios with different aging levels in arithmetic scale.

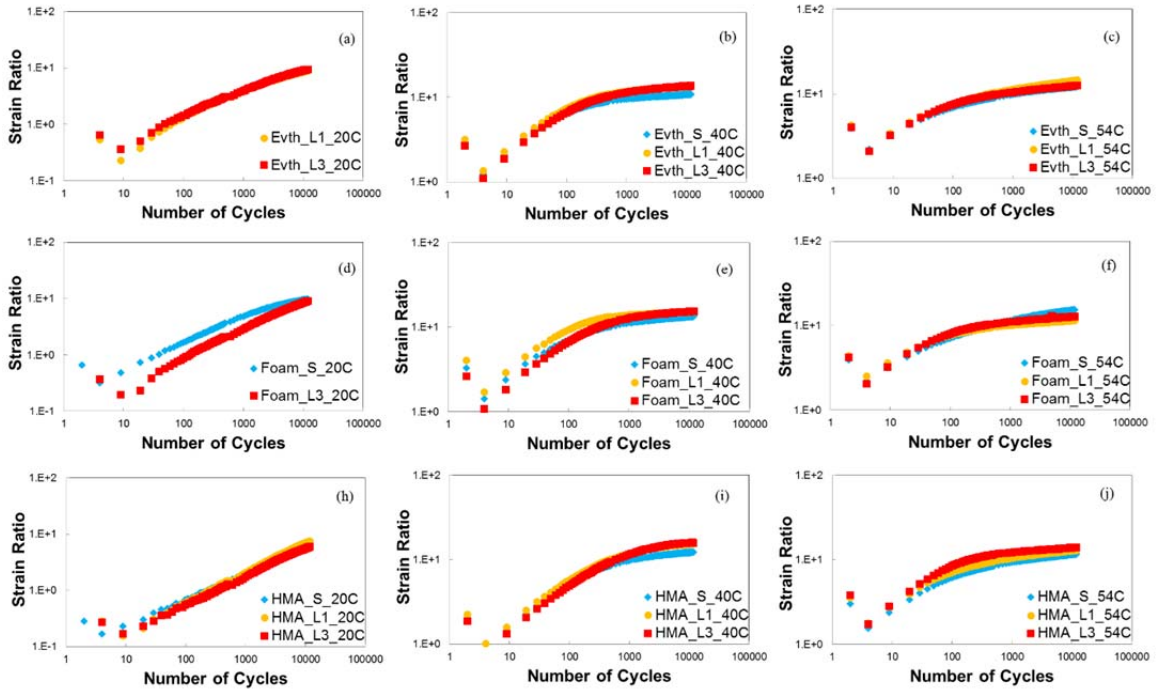


Figure B.2 Comparisons of strain ratios with different aging levels in log-log scale.

Table B-1 T-test Results of Strain Ratios for WMA Evotherm at Different Aging Levels: (a) at 20°C, (b) at 40°C, and (c) at 54°C

a)

Strain Ratio @ 5,000 Cycles_Evth_20°C					
arithmetic scale			log-log scale		
ST	L1	L3	ST	L1	L3
	7.141502	5.152874			0.71205
		9.623962			0.983354
P-values					
ST vs. L1	L1 vs. L3	L3 vs. ST	ST vs. L1	L1 vs. L3	L3 vs. ST
Strain Ratio @ 8,500 Cycles_Evth_20°C					
arithmetic scale			log-log scale		
ST	L1	L3	ST	L1	L3
	8.155994	5.932188			0.773215
		11.46401			1.059337
P-values					
ST vs. L1	L1 vs. L3	L3 vs. ST	ST vs. L1	L1 vs. L3	L3 vs. ST
Strain Ratio @ 12,000 Cycles_Evth_20°C					
arithmetic scale			log-log scale		
ST	L1	L3	ST	L1	L3
	8.979274	6.553235			0.816456
		12.36862			1.092321
P-values					
ST vs. L1	L1 vs. L3	L3 vs. ST	ST vs. L1	L1 vs. L3	L3 vs. ST

(b)

Strain Ratio @ 5,000 Cycles_Evth_ 40°C					
arithmetic scale			log-log scale		
ST	L1	L3	ST	L1	L3
10.89405	12.59632	12.26551	1.037189	1.100244	1.088686
9.922292	13.39525	14.03911	0.996612	1.126951	1.14734
P-values					
ST vs. L1	L1 vs. L3	L3 vs. ST	ST vs. L1	L1 vs. L3	L3 vs. ST
0.02716	0.443467	0.056595	0.028844	0.451782	0.052567
Strain Ratio @ 8,500 Cycles_Evth_ 40°C					
arithmetic scale			log-log scale		
ST	L1	L3	ST	L1	L3
11.29919	12.72356	13.02858	1.053047	1.104609	1.114897
10.07441	13.81084	14.08564	1.00322	1.14022	1.148776
P-values					
ST vs. L1	L1 vs. L3	L3 vs. ST	ST vs. L1	L1 vs. L3	L3 vs. ST
0.043834	0.369501	0.035532	0.045641	0.369172	0.037512
Strain Ratio @ 12,000 Cycles_Evth_ 40°C					
arithmetic scale			log-log scale		
ST	L1	L3	ST	L1	L3
11.58211	13.02858	12.6895	1.063788	1.114897	1.103444
10.27509	14.08564	14.69109	1.011786	1.148776	1.167054
P-values					
ST vs. L1	L1 vs. L3	L3 vs. ST	ST vs. L1	L1 vs. L3	L3 vs. ST
0.044416	0.458539	0.073542	0.046902	0.466595	0.070514

(c)

Strain Ratio @ 5,000 Cycles_ Evth_54°C					
arithmetic scale			log-log scale		
ST	L1	L3	ST	L1	L3
11.46044	12.59632	11.31418	1.059201	1.100244	1.053623
11.4558	13.39525	12.4257	1.059025	1.126951	1.094321
P-values					
ST vs. L1	L1 vs. L3	L3 vs. ST	ST vs. L1	L1 vs. L3	L3 vs. ST
0.030673	0.120857	0.267943	0.027575	0.122527	0.270612
Strain Ratio @ 8,500 Cycles_ Evth_54°C					
arithmetic scale			log-log scale		
ST	L1	L3	ST	L1	L3
12.3397	13.43433	11.74404	1.091305	1.128216	1.069818
11.99485	14.59956	12.91518	1.078995	1.16434	1.1111
P-values					
ST vs. L1	L1 vs. L3	L3 vs. ST	ST vs. L1	L1 vs. L3	L3 vs. ST
0.046542	0.088907	0.407599	0.042589	0.089404	0.414149
Strain Ratio @ 12,000 Cycles_ Evth_54°C					
arithmetic scale			log-log scale		
ST	L1	L3	ST	L1	L3
14.17402	13.79157	11.99134	1.151493	1.139614	1.078868
12.2867	15.04503	13.1922	1.089435	1.177393	1.120317
P-values					
ST vs. L1	L1 vs. L3	L3 vs. ST	ST vs. L1	L1 vs. L3	L3 vs. ST
0.202186	0.085001	0.31282	0.202462	0.085224	0.316099

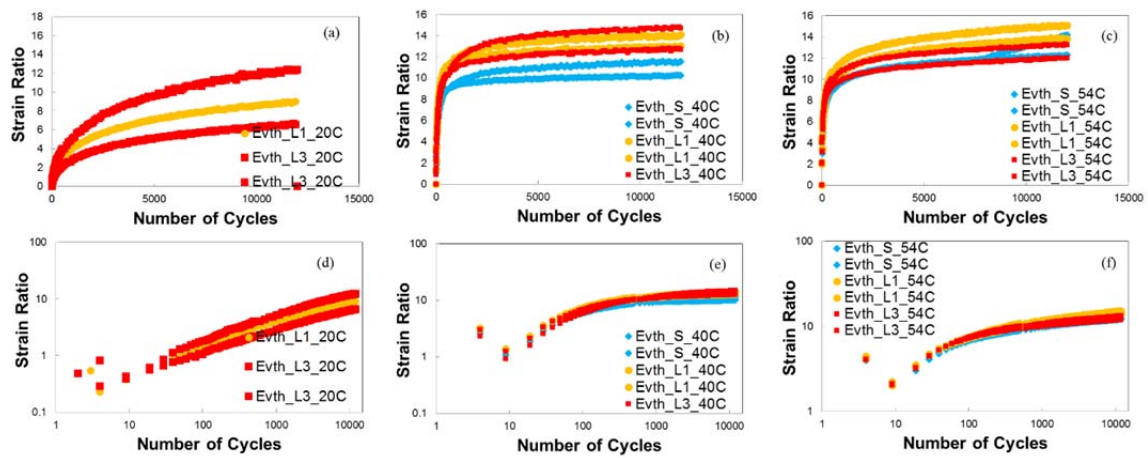


Figure B.3 Comparisons of strain ratios among replicates with different aging levels for WMA Evotherm.

Table B-2 T-test Results of Permanent Strain Ratios for WMA Foam among Different Aging Levels: (a) at 20°C, (b) at 40°C, and (c) at 54°C

(a)

Strain Ratio @ 5,000 Cycles_Foam_ 20°C					
arithmetic scale			log-log scale		
ST	L1	L3	ST	L1	L3
7.504659		6.941492	0.875331		0.841453
8.849322		5.985289	0.94691		0.777085
P-values					
ST vs. L1	L1 vs. L3	L3 vs. ST	ST vs. L1	L1 vs. L3	L3 vs. ST
		0.086701			0.084291
Strain Ratio @ 8,500 Cycles_Foam_ 20°C					
arithmetic scale			log-log scale		
ST	L1	L3	ST	L1	L3
8.252886		8.696009	0.916606		0.93932
10.01729		7.313989	1.00075		0.864154
P-values					
ST vs. L1	L1 vs. L3	L3 vs. ST	ST vs. L1	L1 vs. L3	L3 vs. ST
		0.209705			0.209536
Strain Ratio @ 12,000 Cycles_Foam_ 20°C					
arithmetic scale			log-log scale		
ST	L1	L3	ST	L1	L3
8.879583		9.868516	0.948393		0.994252
10.55557		8.284869	1.023482		0.918286
P-values					
ST vs. L1	L1 vs. L3	L3 vs. ST	ST vs. L1	L1 vs. L3	L3 vs. ST
		0.317089			0.317193

(b)

Strain Ratio @ 5,000 Cycles_ Foam_40°C					
arithmetic scale			log-log scale		
ST	L1	L3	ST	L1	L3
12.73183	13.44824	14.6257	1.104891	1.128666	1.165117
	15.42935	15.68564		1.188348	1.195502
P-values					
ST vs. L1	L1 vs. L3	L3 vs. ST	ST vs. L1	L1 vs. L3	L3 vs. ST
	0.294356			0.290897	
Strain Ratio @ 8,500 Cycles_ Foam_40°C					
arithmetic scale			log-log scale		
ST	L1	L3	ST	L1	L3
13.2394	13.66436	15.11122	1.121868	1.135589	1.1793
	15.59484	15.94732		1.192981	1.202688
P-values					
ST vs. L1	L1 vs. L3	L3 vs. ST	ST vs. L1	L1 vs. L3	L3 vs. ST
	0.241248			0.239784	
Strain Ratio @ 12,000 Cycles_ Foam_40°C					
arithmetic scale			log-log scale		
ST	L1	L3	ST	L1	L3
13.60369	13.58569	15.35089	1.133657	1.133082	1.186134
	15.87612	16.27989		1.200744	1.211651
P-values					
ST vs. L1	L1 vs. L3	L3 vs. ST	ST vs. L1	L1 vs. L3	L3 vs. ST
	0.236372			0.234877	

(c)

Strain Ratio @ 5,000 Cycles_ Foam_54°C					
arithmetic scale			log-log scale		
ST	L1	L3	ST	L1	L3
14.25064	11.30305	11.75784	1.153834	1.053196	1.070328
16.95711	10.94626	13.74333	1.229352	1.039266	1.138092
P-values					
ST vs. L1	L1 vs. L3	L3 vs. ST	ST vs. L1	L1 vs. L3	L3 vs. ST
0.040824	0.124142	0.11561	0.031612	0.11785	0.113564
Strain Ratio @ 8,500 Cycles_ Foam_54°C					
arithmetic scale			log-log scale		
ST	L1	L3	ST	L1	L3
14.96906	11.7026	12.07905	1.175195	1.068282	1.082033
18.50324	11.23492	12.02638	1.267248	1.05057	1.080135
P-values					
ST vs. L1	L1 vs. L3	L3 vs. ST	ST vs. L1	L1 vs. L3	L3 vs. ST
0.048988	0.065592	0.058882	0.037323	0.067787	0.046547
Strain Ratio @ 12,000 Cycles_ Foam_54°C					
arithmetic scale			log-log scale		
ST	L1	L3	ST	L1	L3
15.33064	11.88811	12.46742	1.18556	1.075113	1.095777
19.50535	11.37183	12.24402	1.290154	1.05583	1.087924
P-values					
ST vs. L1	L1 vs. L3	L3 vs. ST	ST vs. L1	L1 vs. L3	L3 vs. ST
0.055286	0.061539	0.068229	0.041713	0.063394	0.054216

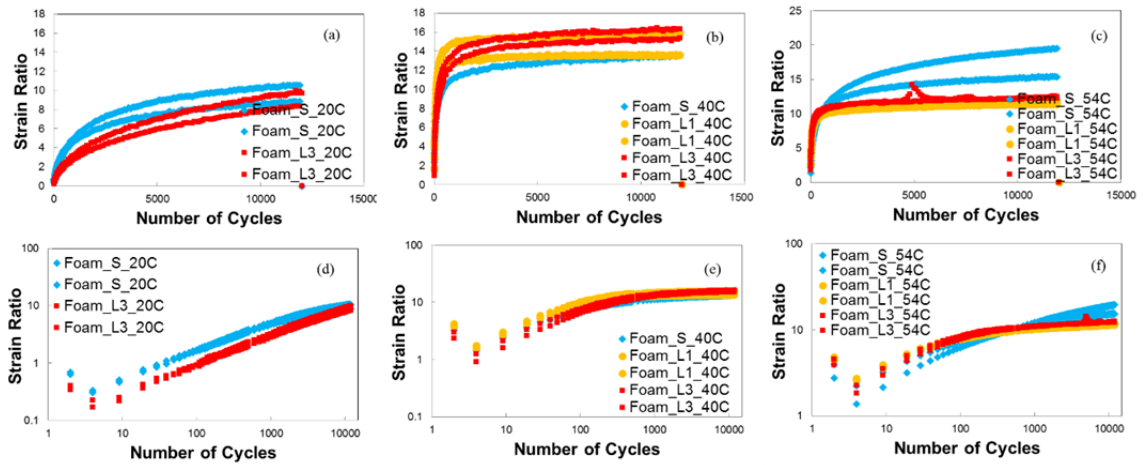


Figure B.4 Comparisons of strain ratios among replicates with different aging levels for WMA Foam.

Table B-3 T-test Results of Strain Ratios for HMA Mixtures among Different Aging Levels: (a) at 20°C, (b) at 40°C, and (c) at 54°C

(a)

Strain Ratio @ 5,000 Cycles_ HMA_20°C					
arithmetic scale			log-log scale		
ST	L1	L3	ST	L1	L3
4.031286	4.440774	4.221761	0.605444	0.647459	0.625494
5.296495	5.728652	4.143566	0.723989	0.758052	0.617374
P-values					
ST vs. L1	L1 vs. L3	L3 vs. ST	ST vs. L1	L1 vs. L3	L3 vs. ST
0.343463	0.148458	0.263491	0.342532	0.140066	0.271026
Strain Ratio @ 8,500 Cycles_ HMA_20°C					
arithmetic scale			log-log scale		
ST	L1	L3	ST	L1	L3
5.094207	5.646302	5.224059	0.707077	0.751764	0.718008
6.488092	7.271562	5.277425	0.812117	0.861628	0.722422
P-values					
ST vs. L1	L1 vs. L3	L3 vs. ST	ST vs. L1	L1 vs. L3	L3 vs. ST
0.29822	0.13781	0.259752	0.299315	0.128172	0.26594
Strain Ratio @ 12,000 Cycles_ HMA_20°C					
arithmetic scale			log-log scale		
ST	L1	L3	ST	L1	L3
5.768832	6.628273	5.922251	0.761088	0.8214	0.772487
7.302311	8.5912	6.04776	0.86346	0.934054	0.781595
P-values					
ST vs. L1	L1 vs. L3	L3 vs. ST	ST vs. L1	L1 vs. L3	L3 vs. ST
0.239665	0.120165	0.274235	0.240213	0.108371	0.281876

(b)

Strain Ratio @ 5,000 Cycles_ HMA_ 40°C					
arithmetic scale			log-log scale		
ST	L1	L3	ST	L1	L3
10.86398	12.38435	13.55399	1.035989	1.092873	1.132067
12.43678	16.61517	16.50677	1.094708	1.220505	1.217662
P-values					
ST vs. L1	L1 vs. L3	L3 vs. ST	ST vs. L1	L1 vs. L3	L3 vs. ST
0.167013	0.428034	0.090364	0.16158	0.417515	0.084653
Strain Ratio @ 8,500 Cycles_ HMA_ 40°C					
arithmetic scale			log-log scale		
ST	L1	L3	ST	L1	L3
11.32464	12.68839	13.95263	1.054024	1.103406	1.144656
12.74515	17.64943	17.35552	1.105345	1.246731	1.239438
P-values					
ST vs. L1	L1 vs. L3	L3 vs. ST	ST vs. L1	L1 vs. L3	L3 vs. ST
0.174225	0.443342	0.09432	0.168405	0.430804	0.086209
Strain Ratio @ 12,000 Cycles_ HMA_ 40°C					
arithmetic scale			log-log scale		
ST	L1	L3	ST	L1	L3
11.57699	12.82351	14.33945	1.063596	1.108007	1.156533
13.11984	18.21532	17.59216	1.117929	1.260437	1.245319
P-values					
ST vs. L1	L1 vs. L3	L3 vs. ST	ST vs. L1	L1 vs. L3	L3 vs. ST
0.187742	0.450123	0.0911	0.18371	0.433635	0.084256

(c)

Strain Ratio @ 5,000 Cycles_ HMA_54°C					
arithmetic scale			log-log scale		
ST	L1	L3	ST	L1	L3
11.40035	12.18612	14.99973	1.056918	1.085866	1.176083
10.06244		11.99022	1.002703		1.078827
P-values					
ST vs. L1	L1 vs. L3	L3 vs. ST	ST vs. L1	L1 vs. L3	L3 vs. ST
		0.117656			0.110771
Strain Ratio @ 8,500 Cycles_ HMA_54°C					
arithmetic scale			log-log scale		
ST	L1	L3	ST	L1	L3
12.0952	12.69333	15.31799	1.082613	1.103575	1.185202
10.465		12.32842	1.019739		1.090908
P-values					
ST vs. L1	L1 vs. L3	L3 vs. ST	ST vs. L1	L1 vs. L3	L3 vs. ST
		0.13692			0.132479
Strain Ratio @ 12,000 Cycles_ HMA_54°C					
arithmetic scale			log-log scale		
ST	L1	L3	ST	L1	L3
12.53475	12.88881	15.49023	1.098116	1.110213	1.190058
10.68156		12.60436	1.028635		1.100521
P-values					
ST vs. L1	L1 vs. L3	L3 vs. ST	ST vs. L1	L1 vs. L3	L3 vs. ST
		0.14543			0.142595

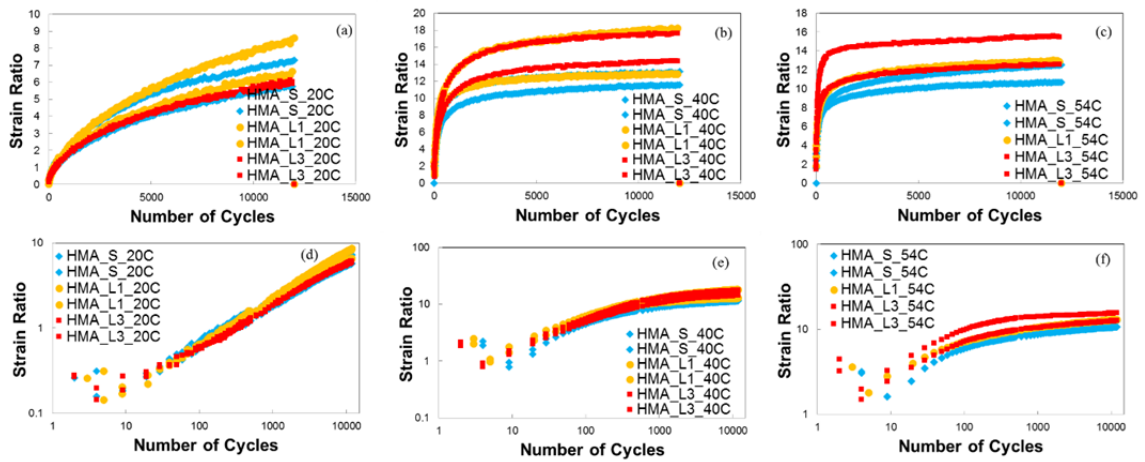


Figure B.5 Comparisons of strain ratios among replicates with different aging levels for HMA mixtures.

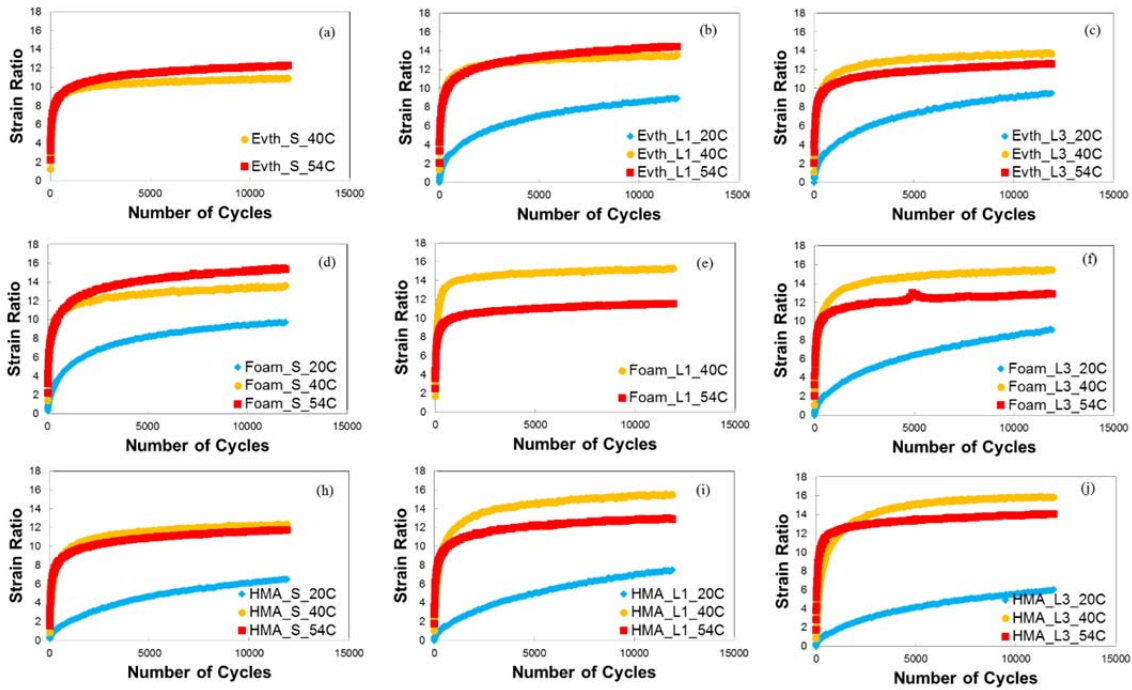


Figure B.6 Comparisons of strain ratios for different temperatures in arithmetic scale.

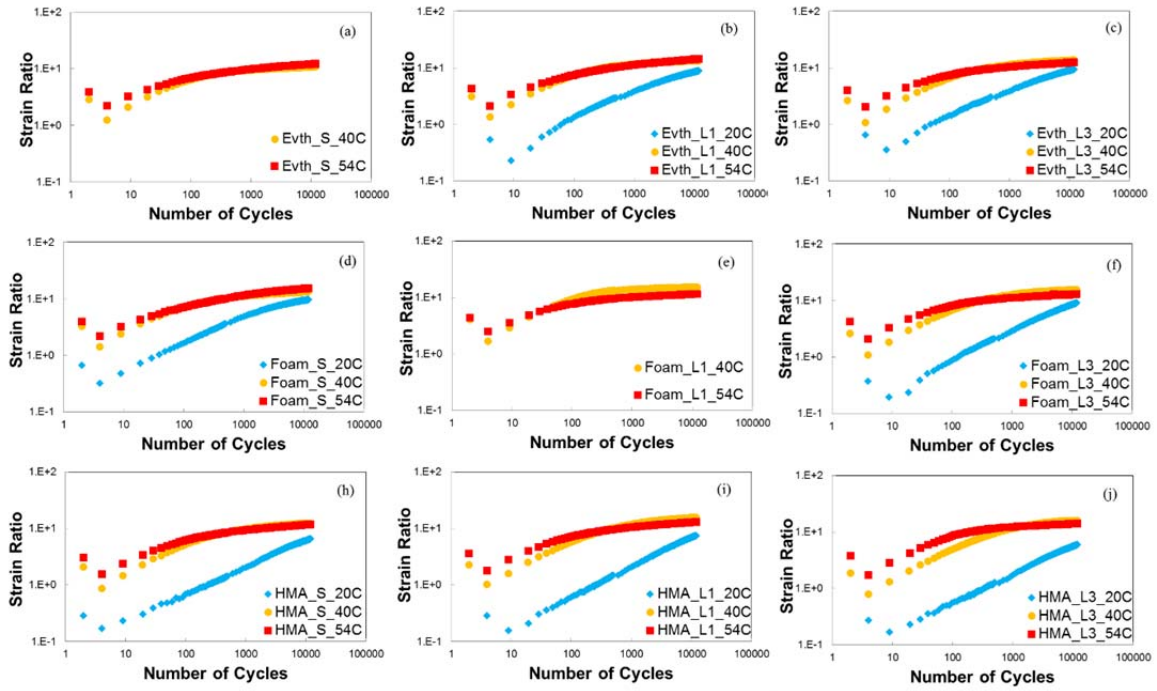


Figure B.7 Comparisons of strain ratios for different test temperatures in log-log scale.

Table B-4 T-test Results of Permanent Strain for Short-Term Aging Conditioned Mixtures at Different Test Temperatures: (a) WMA Evotherm, (b) WMA Foam, and (c) HMA

(a)

Strain Ratio @ 5,000 Cycles_ Evth_STA					
arithmetic scale			log-log scale		
20°C	40°C	54°C	20°C	40°C	54°C
	10.89405	11.46044		1.037189	1.059201
	9.922292	11.4558		0.996612	1.059025
P-values					
20 vs. 40	40 vs. 54	54 vs. 20	20 vs. 40	40 vs. 54	54 vs. 20
	0.081631			0.086482	#NUM!
Strain Ratio @ 8,500 Cycles_ Evth_STA					
arithmetic scale			log-log scale		
20°C	40°C	54°C	20°C	40°C	54°C
	11.29919	12.3397		1.053047	1.091305
	10.07441	11.99485		1.00322	1.078995
P-values					
20 vs. 40	40 vs. 54	54 vs. 20	20 vs. 40	40 vs. 54	54 vs. 20
	0.072717			0.078201	
Strain Ratio @ 12,000 Cycles_ Evth_STA					
arithmetic scale			log-log scale		
20°C	40°C	54°C	20°C	40°C	54°C
	11.58211	14.17402		1.063788	1.151493
	10.27509	12.2867		1.011786	1.089435
P-values					
20 vs. 40	40 vs. 54	54 vs. 20	20 vs. 40	40 vs. 54	54 vs. 20
	0.091394			0.088934	

(b)

Strain Ratio @ 5,000 Cycles_ Foam_STA					
arithmetic scale			log-log scale		
20°C	40°C	54°C	20°C	40°C	54°C
7.504659	12.73183	14.25064	0.875331	1.104891	1.153834
8.849322		16.95711	0.94691	#NUM!	1.229352
P-values					
20 vs. 40	40 vs. 54	54 vs. 20	20 vs. 40	40 vs. 54	54 vs. 20
		0.019495			0.016364
Strain Ratio @ 8,500 Cycles_ Foam_STA					
arithmetic scale			log-log scale		
20°C	40°C	54°C	20°C	40°C	54°C
8.252886	13.2394	14.96906	0.916606	1.121868	1.175195
10.01729		18.50324	1.00075	#NUM!	1.267248
P-values					
20 vs. 40	40 vs. 54	54 vs. 20	20 vs. 40	40 vs. 54	54 vs. 20
		0.030684			0.026024
Strain Ratio @ 12,000 Cycles_ Foam_STA					
arithmetic scale			log-log scale		
20°C	40°C	54°C	20°C	40°C	54°C
8.879583	13.60369	15.33064	0.948393	1.133657	1.18556
10.55557		19.50535	1.023482	#NUM!	1.290154
P-values					
20 vs. 40	40 vs. 54	54 vs. 20	20 vs. 40	40 vs. 54	54 vs. 20
		0.037877			0.029767

(c)

Strain Ratio @ 5,000 Cycles_ HMA_STA					
arithmetic scale			log-log scale		
20°C	40°C	54°C	20°C	40°C	54°C
4.031286	10.86398	11.40035	0.605444	1.035989	1.056918
5.296495	12.43678	10.06244	0.723989	1.094708	1.002703
P-values					
20 vs. 40	40 vs. 54	54 vs. 20	20 vs. 40	40 vs. 54	54 vs. 20
0.010119	0.233662	0.01113	0.013096	0.233829	0.015211
Strain Ratio @ 8,500 Cycles_ HMA_STA					
arithmetic scale			log-log scale		
20°C	40°C	54°C	20°C	40°C	54°C
5.094207	11.32464	12.0952	0.707077	1.054024	1.082613
6.488092	12.74515	10.465	0.812117	1.105345	1.019739
P-values					
20 vs. 40	40 vs. 54	54 vs. 20	20 vs. 40	40 vs. 54	54 vs. 20
0.012236	0.278667	0.018059	0.015884	0.277554	0.020677
Strain Ratio @ 12,000 Cycles_ HMA_STA					
arithmetic scale			log-log scale		
20°C	40°C	54°C	20°C	40°C	54°C
5.768832	11.57699	12.53475	0.761088	1.063596	1.098116
7.302311	13.11984	10.68156	0.86346	1.117929	1.028635
P-values					
20 vs. 40	40 vs. 54	54 vs. 20	20 vs. 40	40 vs. 54	54 vs. 20
0.016637	0.300883	0.02594	0.020338	0.29897	0.027837

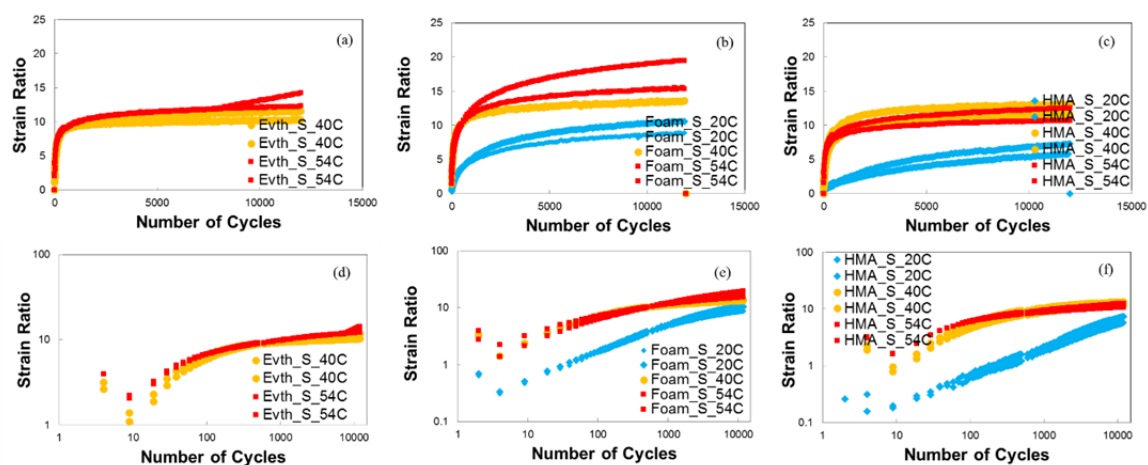


Figure B.8 Comparisons of strain ratios among short-term aging replicates tested at different temperatures in arithmetic scale and log-log scale.

Table B-5 T-test Results of Strain Ratios of Long-Term Aging Level 1 Conditioned Mixtures at Different Test Temperatures: (a) WMA Evotherm, (b) WMA Foam, and (c) HMA

(a)

Strain Ratio @ 5,000 Cycles_ Evth_LTA1					
arithmetic scale			log-log scale		
20°C	40°C	54°C	20°C	40°C	54°C
7.141502	12.59632	12.59632	0.85379	1.100244	1.100244
	13.39525	13.39525		1.126951	1.126951
P-values					
20 vs. 40	40 vs. 54	54 vs. 20	20 vs. 40	40 vs. 54	54 vs. 20
	0.5			0.5	
Strain Ratio @ 8,500 Cycles_ Evth_LTA1					
arithmetic scale			log-log scale		
20°C	40°C	54°C	20°C	40°C	54°C
8.155994	12.72356	13.43433	0.911477	1.104609	1.128216
	13.81084	14.59956	#NUM!	1.14022	1.16434
P-values					
20 vs. 40	40 vs. 54	54 vs. 20	20 vs. 40	40 vs. 54	54 vs. 20
	0.223044			0.223042	
Strain Ratio @ 12,000 Cycles_ Evth_LTA1					
arithmetic scale			log-log scale		
20°C	40°C	54°C	20°C	40°C	54°C
8.979274	13.02858	13.79157	0.953241	1.114897	1.139614
	14.08564	15.04503	#NUM!	1.148776	1.177393
P-values					
20 vs. 40	40 vs. 54	54 vs. 20	20 vs. 40	40 vs. 54	54 vs. 20
	0.201859			0.201758	

(b)

Strain Ratio @ 5,000 Cycles_ Foam_LTA1					
arithmetic scale			log-log scale		
20°C	40°C	54°C	20°C	40°C	54°C
	13.44824	11.30305		1.128666	1.053196
	15.42935	10.94626		1.188348	1.039266
P-values					
20 vs. 40	40 vs. 54	54 vs. 20	20 vs. 40	40 vs. 54	54 vs. 20
	0.04058			0.03354	
Strain Ratio @ 8,500 Cycles_ Foam_LTA1					
arithmetic scale			log-log scale		
20°C	40°C	54°C	20°C	40°C	54°C
	13.66436	11.7026		1.135589	1.068282
	15.59484	11.23492		1.192981	1.05057
P-values					
20 vs. 40	40 vs. 54	54 vs. 20	20 vs. 40	40 vs. 54	54 vs. 20
	0.043079			0.036569	
Strain Ratio @ 12,000 Cycles_ Foam_LTA1					
arithmetic scale			log-log scale		
20°C	40°C	54°C	20°C	40°C	54°C
	13.58569	11.88811		1.133082	1.075113
	15.87612	11.37183		1.200744	1.05583
P-values					
20 vs. 40	40 vs. 54	54 vs. 20	20 vs. 40	40 vs. 54	54 vs. 20
	0.059201			0.051081	

(c)

Strain Ratio @ 5,000 Cycles_ HMA_LTA1					
arithmetic scale			log-log scale		
20°C	40°C	54°C	20°C	40°C	54°C
4.440774	12.38435	12.18612	0.647459	1.092873	1.085866
5.728652	16.61517		0.758052	1.220505	#NUM!
P-values					
20 vs. 40	40 vs. 54	54 vs. 20	20 vs. 40	40 vs. 54	54 vs. 20
0.02549			0.016452		
Strain Ratio @ 8,500 Cycles_ HMA_LTA1					
arithmetic scale			log-log scale		
20°C	40°C	54°C	20°C	40°C	54°C
5.646302	12.68839	12.69333	0.751764	1.103406	1.103575
7.271562	17.64943		0.861628	1.246731	#NUM!
P-values					
20 vs. 40	40 vs. 54	54 vs. 20	20 vs. 40	40 vs. 54	54 vs. 20
0.039639			0.027579		
Strain Ratio @ 12,000 Cycles_ HMA_LTA1					
arithmetic scale			log-log scale		
20°C	40°C	54°C	20°C	40°C	54°C
6.628273	12.82351	12.88881	0.8214	1.108007	1.110213
8.5912	18.21532		0.934054	1.260437	#NUM!
P-values					
20 vs. 40	40 vs. 54	54 vs. 20	20 vs. 40	40 vs. 54	54 vs. 20
0.055117			0.041885		

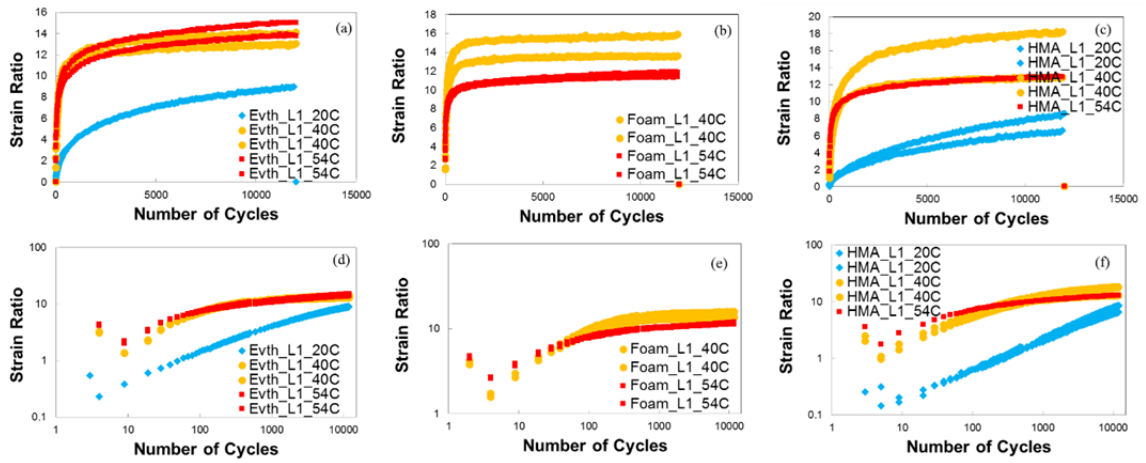


Figure B.9 Comparisons of strain ratios among long-term aging Level 1 conditioned replicates tested at different temperatures in arithmetic scale and log-log scale.

Table B-6 T-test Results of Strain Ratios of Long-Term Aging Level 3 Conditioned Mixtures at Different Test Temperatures: (a) WMA Evotherm, (b) WMA Foam, and (c) HMA

(a)

Strain Ratio @ 5,000 Cycles_ Evth_LTA3					
arithmetic scale			log-log scale		
20°C	40°C	54°C	20°C	40°C	54°C
5.152874	12.26551	11.31418	0.71205	1.088686	1.053623
9.623962	14.03911	12.4257	0.983354	1.14734	1.094321
P-values					
20 vs. 40	40 vs. 54	54 vs. 20	20 vs. 40	40 vs. 54	54 vs. 20
0.069382	0.172585	0.095567	0.095407	0.171297	0.120406
Strain Ratio @ 8,500 Cycles_ Evth_LTA3					
arithmetic scale			log-log scale		
20°C	40°C	54°C	20°C	40°C	54°C
5.932188	13.02858	11.74404	0.773215	1.114897	1.069818
11.46401	14.08564	12.91518	1.059337	1.148776	1.1111
P-values					
20 vs. 40	40 vs. 54	54 vs. 20	20 vs. 40	40 vs. 54	54 vs. 20
0.113287	0.129977	0.163831	0.136617	0.130683	0.17571
Strain Ratio @ 12,000 Cycles_ Evth_LTA3					
arithmetic scale			log-log scale		
20°C	40°C	54°C	20°C	40°C	54°C
6.553235	12.6895	11.99134	0.816456	1.103444	1.078868
12.36862	14.69109	13.1922	1.092321	1.167054	1.120317
P-values					
20 vs. 40	40 vs. 54	54 vs. 20	20 vs. 40	40 vs. 54	54 vs. 20
0.151405	0.222968	0.201119	0.164807	0.223368	0.203589

(b)

Strain Ratio @ 5,000 Cycles_ Foam_LTA3					
arithmetic scale			log-log scale		
20°C	40°C	54°C	20°C	40°C	54°C
6.941492	14.6257	11.75784	0.841453	1.165117	1.070328
5.985289	15.68564	13.74333	0.777085	1.195502	1.138092
P-values					
20 vs. 40	40 vs. 54	54 vs. 20	20 vs. 40	40 vs. 54	54 vs. 20
0.003338	0.083025	0.014684	0.004538	0.088472	0.012098
Strain Ratio @ 8,500 Cycles_ Foam_LTA3					
arithmetic scale			log-log scale		
20°C	40°C	54°C	20°C	40°C	54°C
8.696009	15.11122	12.07905	0.93932	1.1793	1.082033
7.313989	15.94732	12.02638	0.864154	1.202688	1.080135
P-values					
20 vs. 40	40 vs. 54	54 vs. 20	20 vs. 40	40 vs. 54	54 vs. 20
0.005663	0.007104	0.013984	0.009009	0.005602	0.020621
Strain Ratio @ 12,000 Cycles_ Foam_LTA3					
arithmetic scale			log-log scale		
20°C	40°C	54°C	20°C	40°C	54°C
9.868516	15.35089	12.46742	0.994252	1.186134	1.095777
8.284869	16.27989	12.24402	0.918286	1.211651	1.087924
P-values					
20 vs. 40	40 vs. 54	54 vs. 20	20 vs. 40	40 vs. 54	54 vs. 20
0.009029	0.00927	0.027322	0.013103	0.0076	0.03549

(c)

Strain Ratio @ 5,000 Cycles_ HMA_LTA3					
arithmetic scale			log-log scale		
20°C	40°C	54°C	20°C	40°C	54°C
4.221761	13.55399	14.99973	0.625494	1.132067	1.176083
4.143566	16.50677	11.99022	0.617374	1.217662	1.078827
P-values					
20 vs. 40	40 vs. 54	54 vs. 20	20 vs. 40	40 vs. 54	54 vs. 20
0.009018	0.27107	0.012573	0.00299	0.270196	0.004586
Strain Ratio @ 8,500 Cycles_ HMA_LTA3					
arithmetic scale			log-log scale		
20°C	40°C	54°C	20°C	40°C	54°C
5.224059	13.95263	15.31799	0.718008	1.144656	1.185202
5.277425	17.35552	12.32842	0.722422	1.239438	1.090908
P-values					
20 vs. 40	40 vs. 54	54 vs. 20	20 vs. 40	40 vs. 54	54 vs. 20
0.012863	0.251865	0.014547	0.00498	0.252033	0.00626
Strain Ratio @ 12,000 Cycles_ HMA_LTA3					
arithmetic scale			log-log scale		
20°C	40°C	54°C	20°C	40°C	54°C
5.922251	14.33945	15.49023	0.772487	1.156533	1.190058
6.04776	17.59216	12.60436	0.781595	1.245319	1.100521
P-values					
20 vs. 40	40 vs. 54	54 vs. 20	20 vs. 40	40 vs. 54	54 vs. 20
0.012788	0.23532	0.015313	0.005451	0.235309	0.007303

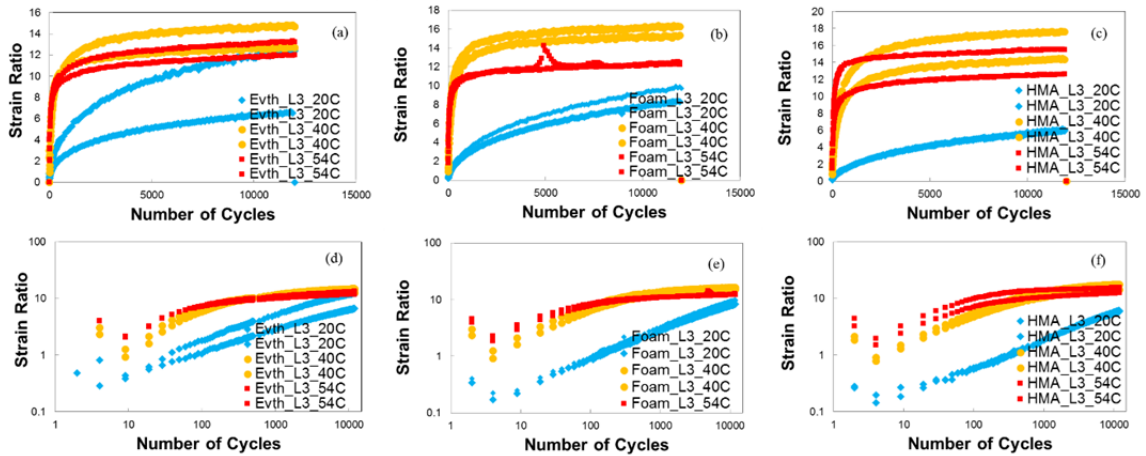


Figure B.10 Comparisons of strain ratios among long-term aging conditioned replicates tested at different temperatures in arithmetic scale and log-log scale.

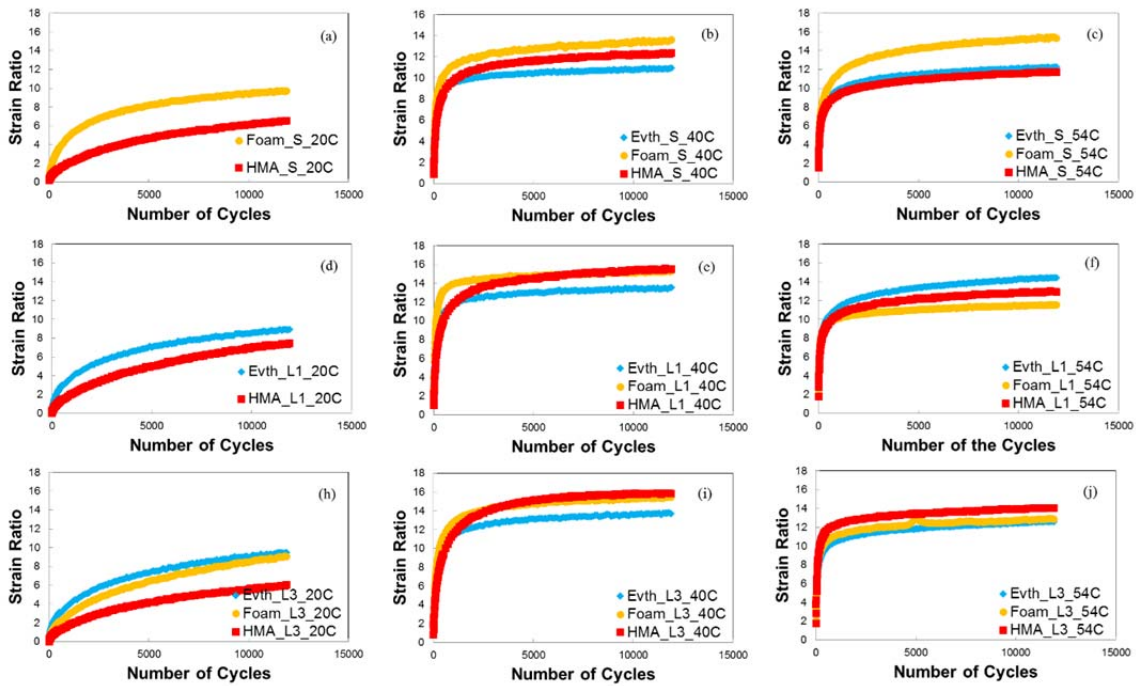


Figure B.11 Comparisons of strain ratios for different mixtures in arithmetic scale.

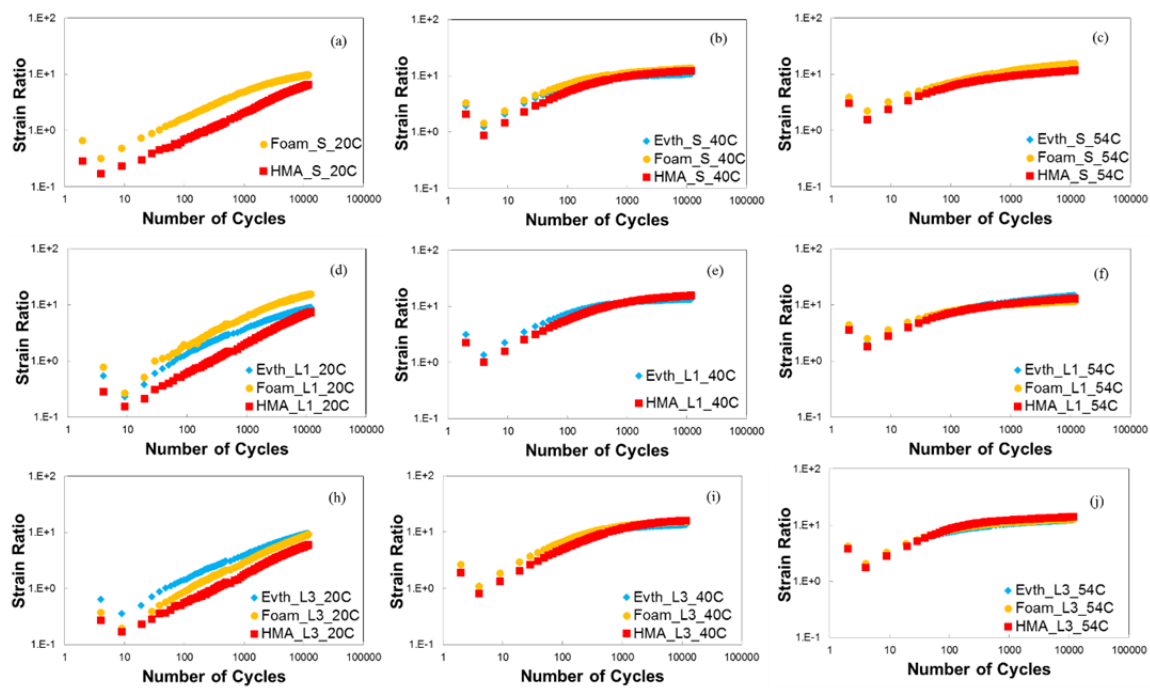


Figure B.12 Comparisons of strain ratios for different mixtures in log-log scale.

Table B-7T-test Results of Strain Ratios for Different Mixtures at 20°C: (a) Short-Term Aging Conditioning, (b) Long-Term Aging Condition Level 1, and (c) Long-Term Aging Condition Level 3

(a)

Strain Ratio @ 5,000 Cycles_ STA_20°C					
arithmetic scale			log-log scale		
Evth	Foam	HMA	Evth	Foam	HMA
	7.504659	4.031286		0.875331	0.605444
	8.849322	5.296495		0.94691	0.723989
P-values					
Evth vs. Foam	Foam vs. HMA	HMA vs. Evth	Evth vs. Foam	Foam vs. HMA	HMA vs. Evth
	0.031317			0.035345	
Strain Ratio @ 8,500 Cycles_ STA_20°C					
arithmetic scale			log-log scale		
Evth	Foam	HMA	Evth	Foam	HMA
	8.252886	5.094207		0.916606	0.707077
	10.01729	6.488092		1.00075	0.812117
P-values					
Evth vs. Foam	Foam vs. HMA	HMA vs. Evth	Evth vs. Foam	Foam vs. HMA	HMA vs. Evth
	0.048445			0.048893	
Strain Ratio @ 12,000 Cycles_ STA_20°C					
arithmetic scale			log-log scale		
Evth	Foam	HMA	Evth	Foam	HMA
	8.879583	5.768832		0.948393	0.761088
	10.55557	7.302311		1.023482	0.86346
P-values					
Evth vs. Foam	Foam vs. HMA	HMA vs. Evth	Evth vs. Foam	Foam vs. HMA	HMA vs. Evth
	0.053649			0.055837	

(b)

Strain Ratio @ 5,000 Cycles_ LTA1_ 20°C					
arithmetic scale			log-log scale		
Evth	Foam	HMA	Evth	Foam	HMA
7.141502		4.440774	0.85379		0.647459
		5.728652			0.758052
P-values					
Evth vs. Foam	Foam vs. HMA	HMA vs. Evth	Evth vs. Foam	Foam vs. HMA	HMA vs. Evth
Strain Ratio @ 8,500 Cycles_ LTA1_ 20°C					
arithmetic scale			log-log scale		
Evth	Foam	HMA	Evth	Foam	HMA
8.155994		5.646302	0.911477		0.751764
		7.271562			0.861628
P-values					
Evth vs. Foam	Foam vs. HMA	HMA vs. Evth	Evth vs. Foam	Foam vs. HMA	HMA vs. Evth
Strain Ratio @ 12,000 Cycles_ LTA1_ 20°C					
arithmetic scale			log-log scale		
Evth	Foam	HMA	Evth	Foam	HMA
8.979274		6.628273	0.953241		0.8214
		8.5912			0.934054
P-values					
Evth vs. Foam	Foam vs. HMA	HMA vs. Evth	Evth vs. Foam	Foam vs. HMA	HMA vs. Evth

(c)

Strain Ratio @ 5,000 Cycles_ LTA3_ 20°C					
arithmetic scale			log-log scale		
Evth	Foam	HMA	Evth	Foam	HMA
5.152874	6.941492	4.221761	0.71205	0.841453	0.625494
9.623962	5.985289	4.143566	0.983354	0.777085	0.617374
P-values					
Evth vs. Foam	Foam vs. HMA	HMA vs. Evth	Evth vs. Foam	Foam vs. HMA	HMA vs. Evth
0.36246	0.020751	0.144027	0.404338	0.014277	0.118697
Strain Ratio @ 8,500 Cycles_ LTA3_ 20°C					
arithmetic scale			log-log scale		
Evth	Foam	HMA	Evth	Foam	HMA
5.932188	8.696009	5.224059	0.773215	0.93932	0.718008
11.46401	7.313989	5.277425	1.059337	0.864154	0.722422
P-values					
Evth vs. Foam	Foam vs. HMA	HMA vs. Evth	Evth vs. Foam	Foam vs. HMA	HMA vs. Evth
0.415289	0.028821	0.169416	0.465333	0.020212	0.152065
Strain Ratio @ 12,000 Cycles_ LTA3_ 20°C					
arithmetic scale			log-log scale		
Evth	Foam	HMA	Evth	Foam	HMA
6.553235	9.868516	5.922251	0.816456	0.994252	0.772487
12.36862	8.284869	6.04776	1.092321	0.918286	0.781595
P-values					
Evth vs. Foam	Foam vs. HMA	HMA vs. Evth	Evth vs. Foam	Foam vs. HMA	HMA vs. Evth
0.455104	0.030058	0.177265	0.495354	0.021332	0.163749

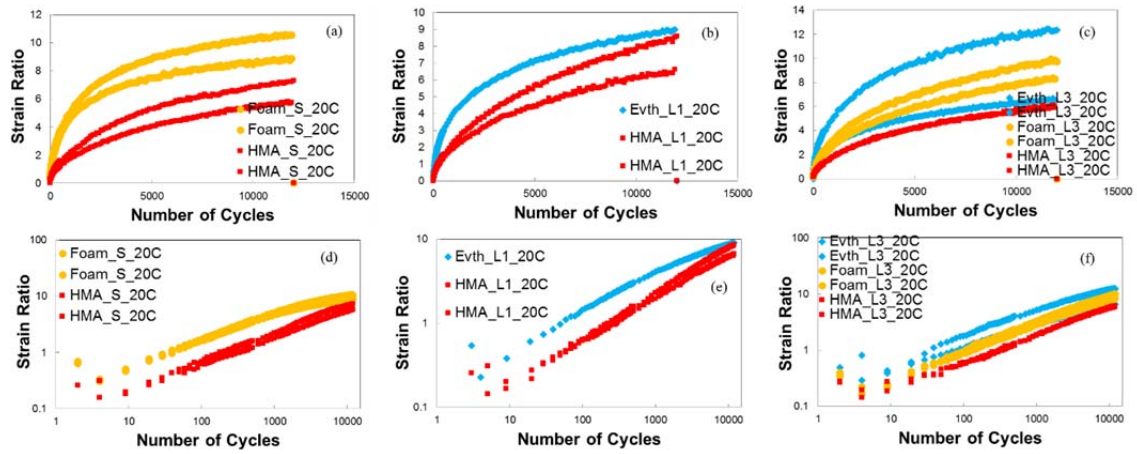


Figure B.13 Comparisons of strain ratios among replicates of different mixtures at 20°C.

Table B-8 T-test Results of Strain Ratios for Different Mixtures at 40°C: (a) Short-Term Aging Conditioning, (b) Long-Term Aging Condition Level 1, and (c) Long-Term Aging Condition Level 3

(a)

Strain Ratio @ 5,000 Cycles_ STA_40°C					
arithmetic scale			log-log scale		
Evth	Foam	HMA	Evth	Foam	HMA
10.89405	12.73183	10.86398	1.037189	1.104891	1.035989
9.922292		12.43678	0.996612		1.094708
P-values					
Evth vs. Foam	Foam vs. HMA	HMA vs. Evth	Evth vs. Foam	Foam vs. HMA	HMA vs. Evth
		0.155584			0.153747
Strain Ratio @ 8,500 Cycles_ STA_40°C					
arithmetic scale			log-log scale		
Evth	Foam	HMA	Evth	Foam	HMA
11.29919	13.2394	11.32464	1.053047	1.121868	1.054024
10.07441		12.74515	1.00322		1.105345
P-values					
Evth vs. Foam	Foam vs. HMA	HMA vs. Evth	Evth vs. Foam	Foam vs. HMA	HMA vs. Evth
		0.143572			0.143099
Strain Ratio @ 12,000 Cycles_ STA_40°C					
arithmetic scale			log-log scale		
Evth	Foam	HMA	Evth	Foam	HMA
11.58211	13.60369	11.57699	1.063788	1.133657	1.063596
10.27509		13.11984	1.011786		1.117929
P-values					
Evth vs. Foam	Foam vs. HMA	HMA vs. Evth	Evth vs. Foam	Foam vs. HMA	HMA vs. Evth
		0.147688			0.147129

(b)

Strain Ratio @ 5,000 Cycles_ LTA1_ 40°C					
arithmetic scale			log-log scale		
Evth	Foam	HMA	Evth	Foam	HMA
12.59632	13.44824	12.38435	1.100244	1.128666	1.092873
13.39525	15.42935	16.61517	1.126951	1.188348	1.220505
P-values					
Evth vs. Foam	Foam vs. HMA	HMA vs. Evth	Evth vs. Foam	Foam vs. HMA	HMA vs. Evth
0.154613	0.490774	0.278549	0.151623	0.49088	0.288302
Strain Ratio @ 8,500 Cycles_ LTA1_ 40°C					
arithmetic scale			log-log scale		
Evth	Foam	HMA	Evth	Foam	HMA
12.72356	13.66436	12.68839	1.104609	1.135589	1.103406
13.81084	15.59484	17.64943	1.14022	1.192981	1.246731
P-values					
Evth vs. Foam	Foam vs. HMA	HMA vs. Evth	Evth vs. Foam	Foam vs. HMA	HMA vs. Evth
0.1719	0.429087	0.266012	0.170387	0.45085	0.274887
Strain Ratio @ 12,000 Cycles_ LTA1_ 40°C					
arithmetic scale			log-log scale		
Evth	Foam	HMA	Evth	Foam	HMA
13.02858	13.58569	12.82351	1.114897	1.133082	1.108007
14.08564	15.87612	18.21532	1.148776	1.200744	1.260437
P-values					
Evth vs. Foam	Foam vs. HMA	HMA vs. Evth	Evth vs. Foam	Foam vs. HMA	HMA vs. Evth
0.225145	0.406501	0.274582	0.225879	0.427389	0.285678

(c)

Strain Ratio @ 5,000 Cycles_ LTA3_ 40°C					
arithmetic scale			log-log scale		
Evth	Foam	HMA	Evth	Foam	HMA
12.26551	14.6257	13.55399	1.088686	1.165117	1.132067
14.03911	15.68564	16.50677	1.14734	1.195502	1.217662
P-values					
Evth vs. Foam	Foam vs. HMA	HMA vs. Evth	Evth vs. Foam	Foam vs. HMA	HMA vs. Evth
0.096019	0.471806	0.194685	0.09996	0.457763	0.193751
Strain Ratio @ 8,500 Cycles_ LTA3_ 40°C					
arithmetic scale			log-log scale		
Evth	Foam	HMA	Evth	Foam	HMA
13.02858	15.11122	13.95263	1.114897	1.1793	1.144656
14.08564	15.94732	17.35552	1.148776	1.202688	1.239438
P-values					
Evth vs. Foam	Foam vs. HMA	HMA vs. Evth	Evth vs. Foam	Foam vs. HMA	HMA vs. Evth
0.049807	0.474847	0.180153	0.051375	0.492372	0.177072
Strain Ratio @ 12,000 Cycles_ LTA3_ 40°C					
arithmetic scale			log-log scale		
Evth	Foam	HMA	Evth	Foam	HMA
12.6895	15.35089	14.33945	1.103444	1.186134	1.156533
14.69109	16.27989	17.59216	1.167054	1.211651	1.245319
P-values					
Evth vs. Foam	Foam vs. HMA	HMA vs. Evth	Evth vs. Foam	Foam vs. HMA	HMA vs. Evth
0.096974	0.468621	0.177822	0.102202	0.484444	0.176089

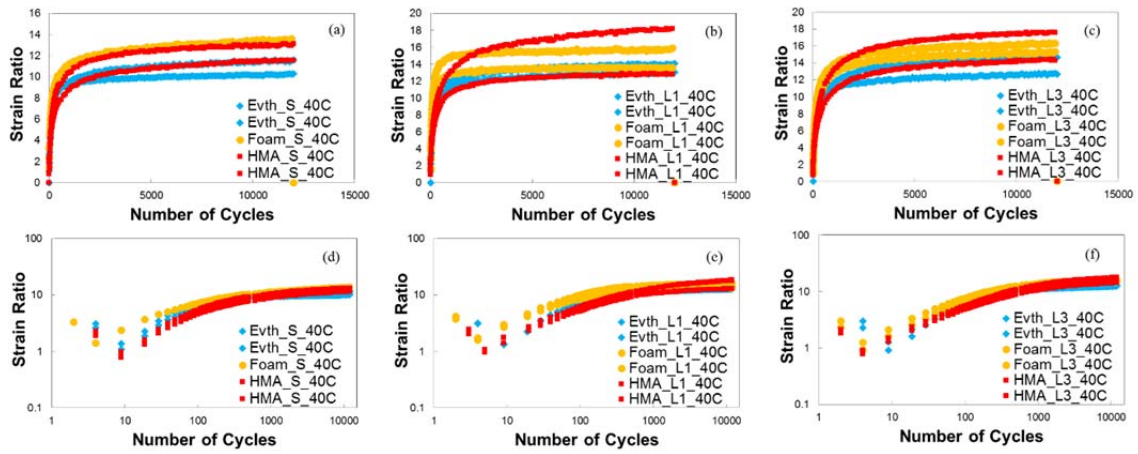


Figure B.14 Comparisons of strain ratios among replicates of different mixtures at 40°C.

Table B-9 T-test Results of Strain Ratios for Different Mixtures at 54°C: (a) Short-Term Aging Conditioning, (b) Long-Term Aging Condition Level 1, and (c) Long-Term Aging Condition Level 3

(a)

Strain Ratio @ 5,000 Cycles_ STA_ 54°C					
arithmetic scale			log-log scale		
Evth	Foam	HMA	Evth	Foam	HMA
11.46044	14.25064	11.40035	1.059201	1.153834	1.056918
11.4558	16.95711	10.06244	1.059025	1.229352	1.002703
P-values					
Evth vs. Foam	Foam vs. HMA	HMA vs. Evth	Evth vs. Foam	Foam vs. HMA	HMA vs. Evth
0.046035	0.042029	0.19541	0.036255	0.036778	0.196361
Strain Ratio @ 8,500 Cycles_ STA_ 54°C					
arithmetic scale			log-log scale		
Evth	Foam	HMA	Evth	Foam	HMA
12.3397	14.96906	12.0952	1.091305	1.175195	1.082613
11.99485	18.50324	10.465	1.078995	1.267248	1.019739
P-values					
Evth vs. Foam	Foam vs. HMA	HMA vs. Evth	Evth vs. Foam	Foam vs. HMA	HMA vs. Evth
0.061812	0.053577	0.199241	0.0497	0.046369	0.200018
Strain Ratio @ 12,000 Cycles_ STA_ 54°C					
arithmetic scale			log-log scale		
Evth	Foam	HMA	Evth	Foam	HMA
12.53475	15.33064	11.57699	1.098116	1.18556	1.063596
10.68156	19.50535	13.11984	1.028635	1.290154	1.117929
P-values					
Evth vs. Foam	Foam vs. HMA	HMA vs. Evth	Evth vs. Foam	Foam vs. HMA	HMA vs. Evth
0.062987	0.075198	0.300883	0.05438	0.064974	0.29897

(b)

Strain Ratio @ 5,000 Cycles_ LTA1_ 54°C					
arithmetic scale			log-log scale		
Evth	Foam	HMA	Evth	Foam	HMA
12.59632	11.30305	12.18612	1.100244	1.053196	1.085866
13.39525	10.94626		1.126951	1.039266	#NUM!
P-values					
Evth vs. Foam	Foam vs. HMA	HMA vs. Evth	Evth vs. Foam	Foam vs. HMA	HMA vs. Evth
0.025279			0.023261		
Strain Ratio @ 8,500 Cycles_ LTA1_ 54°C					
arithmetic scale			log-log scale		
Evth	Foam	HMA	Evth	Foam	HMA
13.43433	11.7026	12.69333	1.128216	1.068282	1.103575
14.59956	11.23492		1.16434	1.05057	#NUM!
P-values					
Evth vs. Foam	Foam vs. HMA	HMA vs. Evth	Evth vs. Foam	Foam vs. HMA	HMA vs. Evth
0.027838			0.024841		
Strain Ratio @ 12,000 Cycles_ LTA1_ 54°C					
arithmetic scale			log-log scale		
Evth	Foam	HMA	Evth	Foam	HMA
13.79157	11.88811	12.88881	1.139614	1.075113	1.110213
15.04503	11.37183		1.177393	1.05583	#NUM!
P-values					
Evth vs. Foam	Foam vs. HMA	HMA vs. Evth	Evth vs. Foam	Foam vs. HMA	HMA vs. Evth
0.027161			0.024119		

(c)

Strain Ratio @ 5,000 Cycles_ LTA3_ 54°C					
arithmetic scale			log-log scale		
Evth	Foam	HMA	Evth	Foam	HMA
11.31418	11.75784	14.99973	1.053623	1.070328	1.176083
12.4257	13.74333	11.99022	1.094321	1.138092	1.078827
P-values					
Evth vs. Foam	Foam vs. HMA	HMA vs. Evth	Evth vs. Foam	Foam vs. HMA	HMA vs. Evth
0.25994	0.359861	0.208831	0.262091	0.366377	0.208537
Strain Ratio @ 8,500 Cycles_ LTA3_ 54°C					
arithmetic scale			log-log scale		
Evth	Foam	HMA	Evth	Foam	HMA
11.74404	12.07905	15.31799	1.069818	1.082033	1.185202
12.91518	12.02638	12.32842	1.1111	1.080135	1.090908
P-values					
Evth vs. Foam	Foam vs. HMA	HMA vs. Evth	Evth vs. Foam	Foam vs. HMA	HMA vs. Evth
0.341587	0.178988	0.225199	0.347255	0.175234	0.226356
Strain Ratio @ 12,000 Cycles_ LTA3_ 54°C					
arithmetic scale			log-log scale		
Evth	Foam	HMA	Evth	Foam	HMA
11.99134	12.46742	15.49023	1.078868	1.095777	1.190058
13.1922	12.24402	12.60436	1.120317	1.087924	1.100521
P-values					
Evth vs. Foam	Foam vs. HMA	HMA vs. Evth	Evth vs. Foam	Foam vs. HMA	HMA vs. Evth
0.368184	0.181469	0.225004	0.374392	0.178218	0.22604

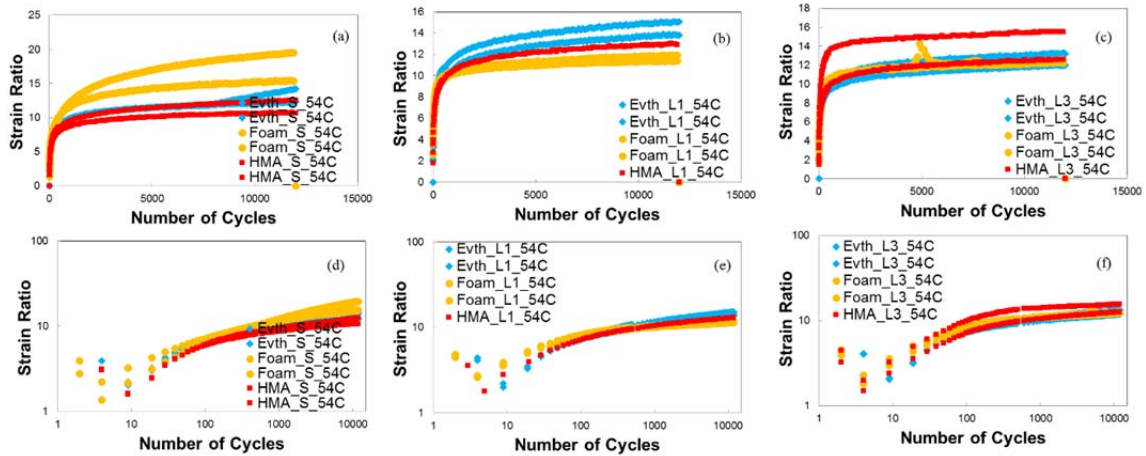


Figure B.15 Comparisons of strain ratios among replicates of different mixtures at 54°C.

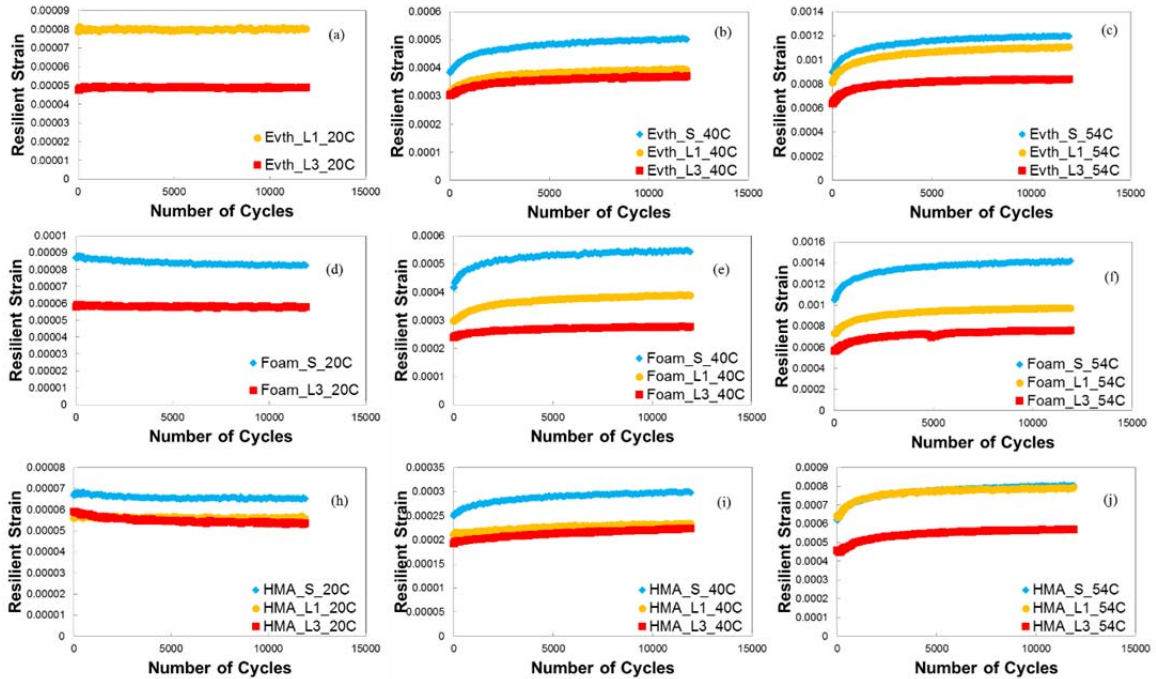


Figure B.16 Comparisons of resilient strain levels with different aging levels in arithmetic scale.

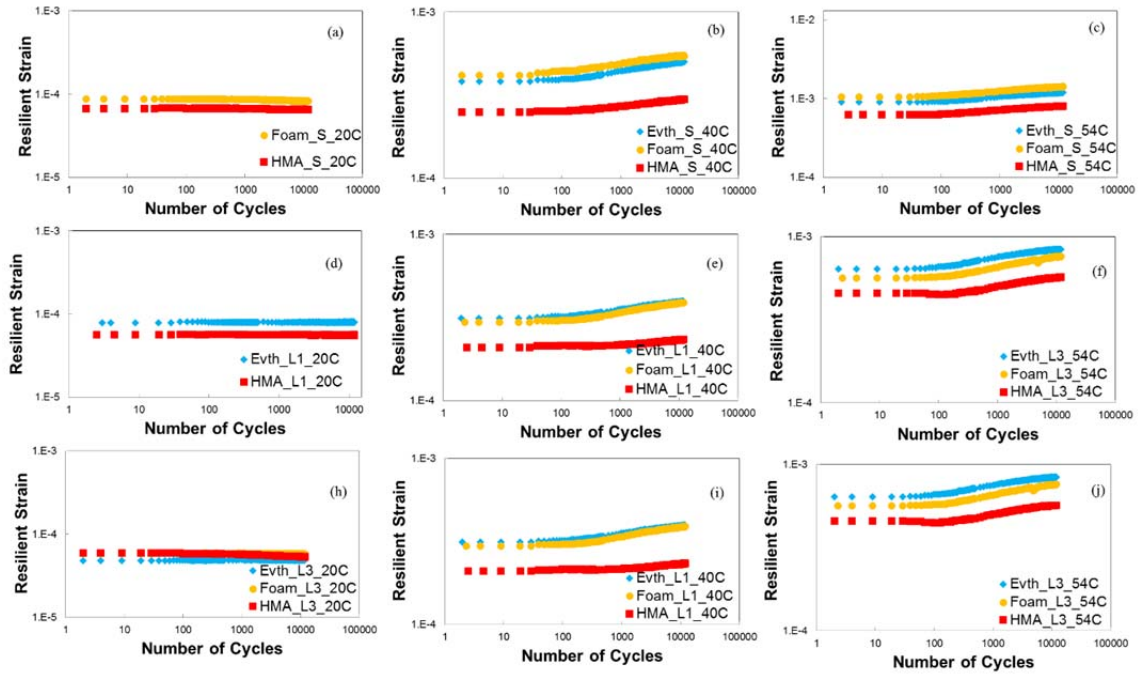


Figure B.17 Comparisons of strain ratios with different aging levels in log-log scale.

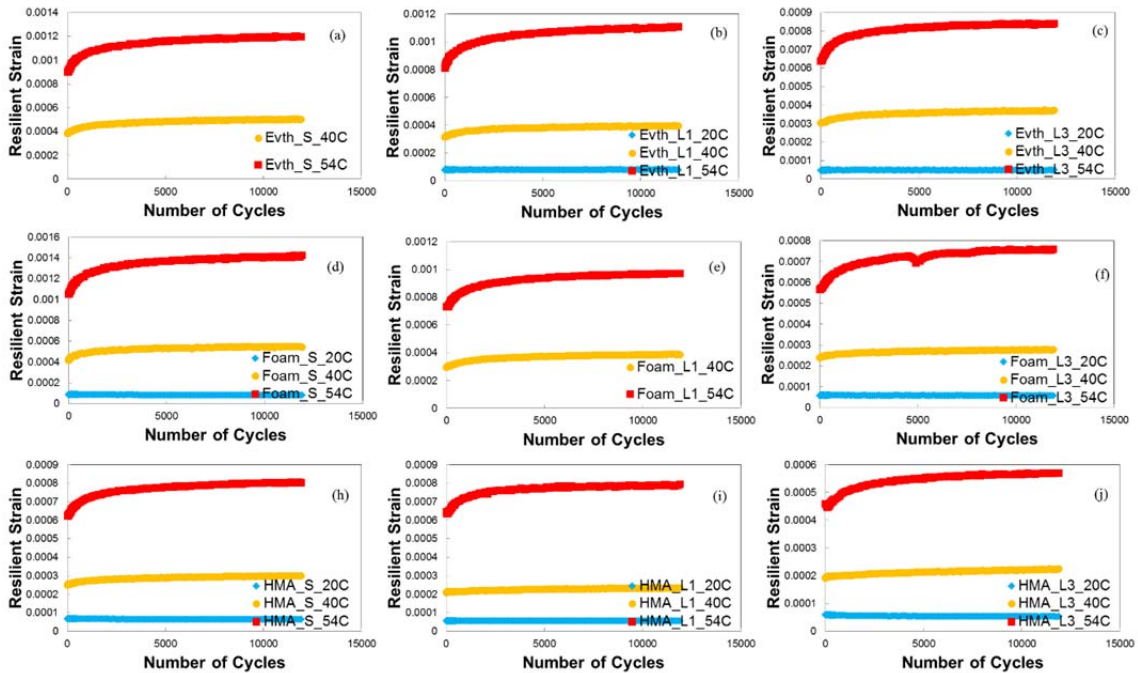


Figure B.18 Comparisons of resilient strain levels at different temperatures in arithmetic scale.

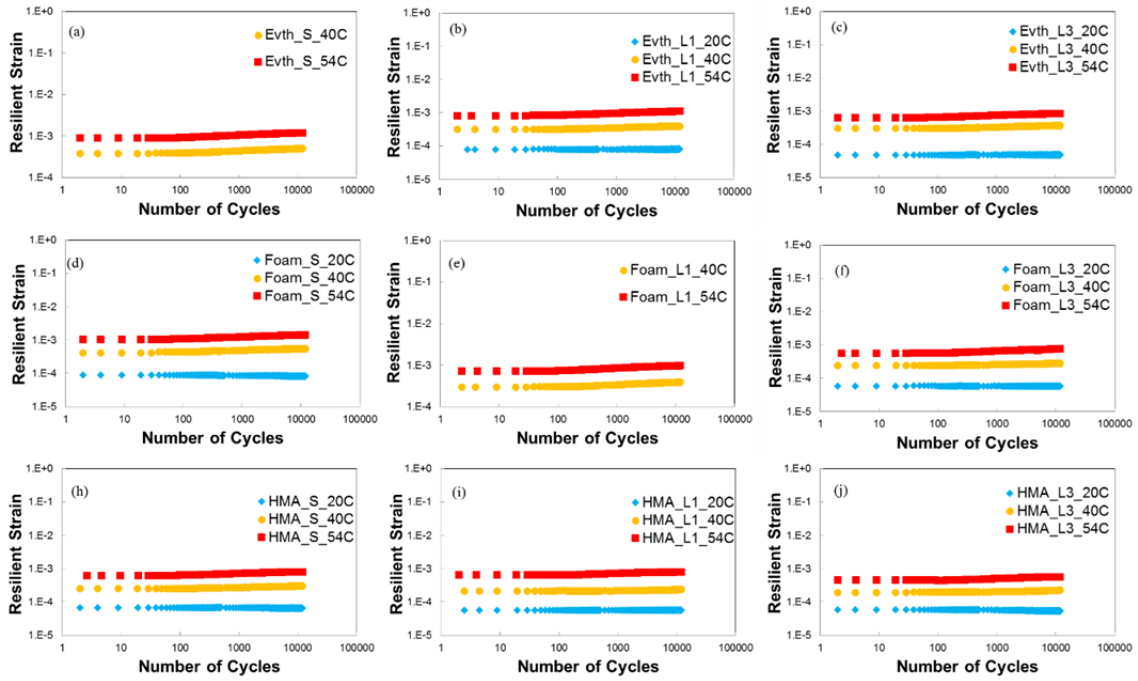


Figure B.19 Comparisons of resilient strain levels at different test temperatures in log-log scale.

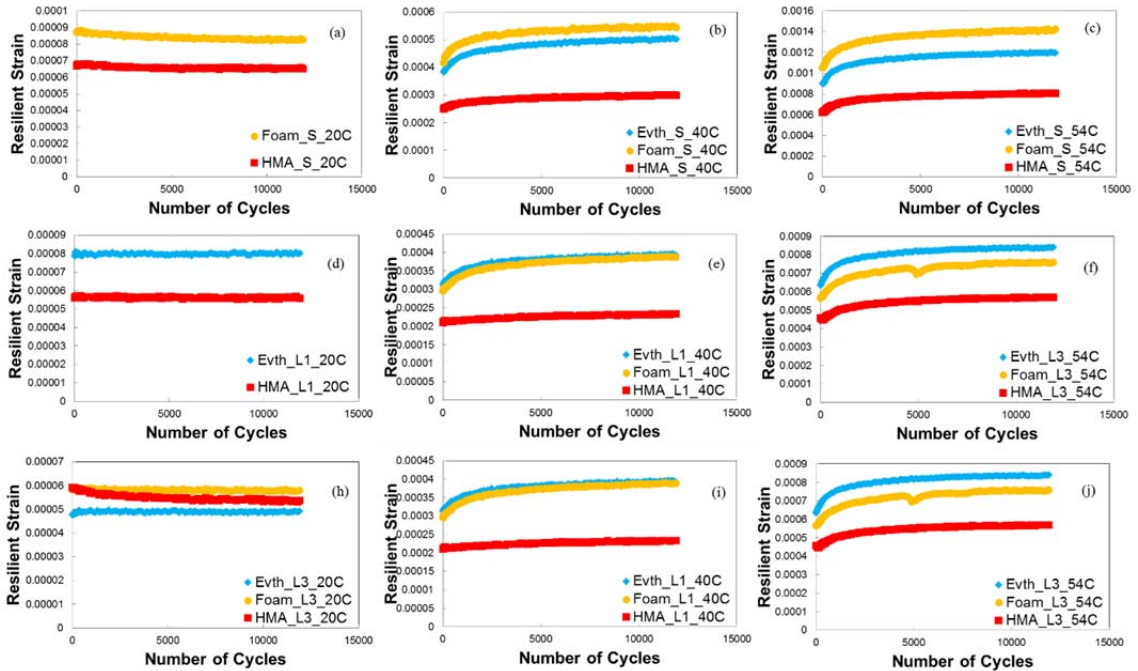


Figure B.20 Comparisons of resilient strain levels for different mixtures in arithmetic scale.

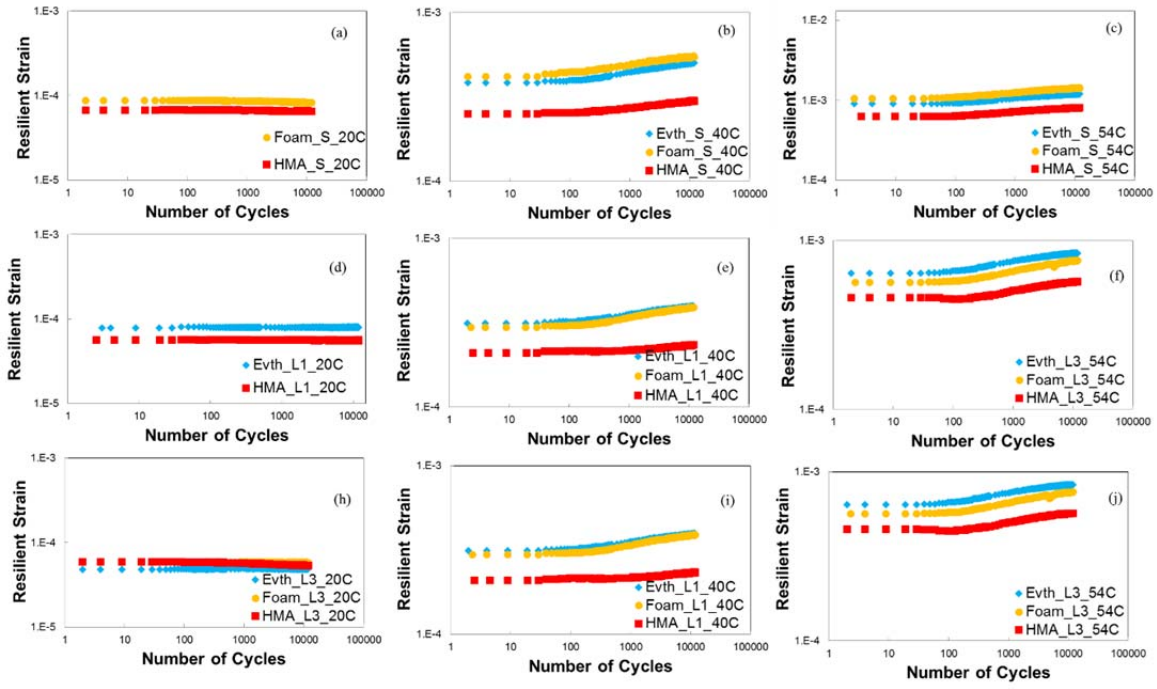


Figure B.21 Comparisons of resilient strain levels for different mixtures in log-log scale.

APPENDIX C THE USE OF CYCLIC DIRECT TENSION TESTS AND DIGITAL IMAGING ANALYSIS TO EVALUATE MOISTURE SUSCEPTIBILITY OF WARM MIX ASPHALT CONCRETE

C.1 Abstract

This Appendix C presents the simplified *viscoelastic* continuum damage (S-VECD) material model, which is based on cyclic direct tension testing and layered viscoelastic analysis (LVEA), for the evaluation of moisture susceptibility of asphalt concrete. The visual stripping inspection afforded by digital imaging analysis is also proposed as an intuitive and straightforward method for moisture susceptibility evaluation. These methods were applied to a Superpave 19-mm hot mix asphalt (HMA) mixture and corresponding warm mix asphalt (WMA) mixtures modified by a polyethylene wax-type additive with and without an anti-stripping agent. It was found that the fatigue life predicted by the S-VECD and LVEA models has a strong correlation with the percentage of stripping determined from specimen surfaces that were fractured during the cyclic direct tension testing of the HMA and WMA mixtures with various asphalt contents. Finally, the WMA mixture with a polyethylene wax-type additive combined with an anti-stripping agent was found to lead to a longer fatigue life and less stripping than the WMA mixture with only a pure polyethylene wax-type additive. The findings from this work should provide guidance to agencies and material engineers in developing asphalt binder modifiers that lengthen the fatigue life of pavements and reduce moisture susceptibility.

C.2 Introduction

Moisture susceptibility is a phenomenon that accelerates the occurrence of distresses such as fatigue cracking in asphalt concrete pavements. The acceleration of fatigue cracking is based on complicated mechanisms that need to be considered in terms of material properties and structural factors. The most commonly used moisture susceptibility test is the indirect tension (IDT) test that uses the indirect tensile strength ratio (TSR) from unconditioned and moisture-conditioned specimens as an indicator of the moisture susceptibility of a particular mixture. Although the test method uses the tensile strength of the material, it is important to recognize that compressive loading is applied indirectly to cause the tensile stress. Another type of mechanical test that is commonly used by agencies for moisture susceptibility evaluation is the Hamburg wheel tracking (HWT) test. Again, this test uses compressive loading at an elevated temperature to induce moisture damage in asphalt concrete specimens. However, due to their lack of sensitivity to moisture, these tests tend to be used only as screening types of testing.

Table C.1 presents the currently available moisture conditioning procedures and mechanical tests that are typically used to evaluate moisture susceptibility. As summarized in Table C.1, the currently available mechanical tests for the evaluation of moisture susceptibility utilize either

compressive stress or tensile stress indirectly as induced by compressive loading. These test methods are not sensitive to capturing the effects of moisture damage because the state of stress they cause is not the optimal state to measure the sensitive changes in the material properties that are due to moisture damage.

Table C.1 Currently Available Moisture Susceptibility Tests

Moisture Susceptibility Test	Standard Method	Mechanical Test	Moisture Conditioning Procedure	Moisture Susceptibility Indicator
Boiling Test	ASTM D 3625	None	Boiling Water	Visual Observation of Stripping
Static Immersion Test	AASHTO T 182	None	Immersing in Water at 25°C for 16-18 hours	Visual Observation of Stripping
Lottman Test	NCHRP 246	Monotonic Indirect Tension Test	Vacuum Saturation with Water: 4-year Performance Additional Freeze (15 hr, -18°C)-thaw (24 hr, 60°C) cycles: 4-12 years	Indirect Tensile Strength Ratio
Tunncliffe and Root Test	ASTM D 4867	Monotonic Indirect Tension Test	Vacuum Saturation with Water	Indirect Tensile Strength Ratio
Modified Lottman Test	AASHTO T 283	Monotonic Indirect Tension Test	Vacuum Saturation with Water/Additional Boiling Water (24 hr, 60°C)	Indirect Tensile Strength Ratio
Immersion-Compression Test	AASHTO T 165	Monotonic Compressive Strength Test	Freeze (15 hr, -18°C)-thaw (24 hr, 60°C) cycles	Indirect Tensile Strength Ratio
Hamburg Wheel-Tracking Test	AASHTO T 324	Wheel Tracking Test in Water		Stripping Inflection Point

Moisture damage is caused mainly by adhesive failure between the aggregate and asphalt binder. The state of stress that is most suitable for testing the adhesive properties at the interface of two materials is tensile stress, and the simplest form of test method that measures the tensile properties of a material is the direct tension test. The NCHRP 9-26A project suggests that the use of cyclic direct tension tests that employ cored and cut specimens should be investigated for moisture susceptibility evaluation, because such tests may be able to overcome the high variability of air void distribution in the specimens and in the strength test results for compressive mode testing (1).

In this study, the simplified viscoelastic continuum damage (S-VECD) model combined with layered linear viscoelastic analysis (LVEA) is suggested to determine the moisture susceptibility of a hot mix asphalt (HMA) mixture and warm mix asphalt (WMA) mixtures with various

asphalt contents. Digital imaging analysis of the fractured surfaces of the asphalt specimens is developed as a reference for moisture susceptibility. The mechanical properties and fatigue life data of unconditioned and moisture-conditioned asphalt mixtures are compared against the stripping percentages determined from digital imaging analysis to determine the best indicator for moisture susceptibility of the asphalt mixtures.

C.3 Objectives

The objectives of the study discussed in this Appendix C are: (1) to investigate the S-VECD model combined with LVEA as a means of evaluating the moisture susceptibility of HMA and WMA mixtures; (2) to develop a digital imaging analysis method as a reference method to determine moisture susceptibility; and (3) to identify moisture susceptibility indicators based on the material properties and fatigue life data that are predicted from the coupled S-VECD and LVEA models.

C.4 Experimental Program and Analysis Methods

C.4.1. Materials and Mix Design

LEADCAP KW-A and KW-B are polyethylene wax-type additives that play an important role in reducing mixing and compaction temperatures while increasing the workability of the production procedure. The KW-B additive is modified by an additional anti-stripping agent. For this study, three granite aggregate stockpiles (19~13.2 mm, 13.2~4.75 mm, and sub 4.75 mm) and PG 64-16 binder were used. The aggregate structure for all the study mixtures is coarse 19 mm nominal maximum aggregate size (NMAS) comprised of 25% 12.5 mm, 20% 9.5 mm, 17% #4, 12% #8, 6% #16, 7% #30, 4% #50, 4% #100, 3% #200, and 2% hydrated lime. The dosage rate used for the KW-A and KW-B additives is 1.5% of the total asphalt binder weight based on viscosity and economic considerations. The HMA mixture was mixed at 160°C and compacted at 140°C in accordance with the requirement for PG 64-16 binder. The HMA mixture was aged at the compaction temperature for 1 hour (referred to as short-term oven aging). The LEADCAP WMA mixtures were mixed at 130°C (aggregate: 130°C, binder: 160°C) and compacted at 115°C. The aging temperature and conditioning time used in this study were 115°C and 1 hour, respectively.

All of the Superpave mix designs were performed to meet the 4% air void requirement using a gyratory compactor with 100 gyrations. The optimal asphalt contents of each HMA, KW-A, and KW-B mixture were determined as 4.9%, 4.3%, and 4.3%, respectively. In order to evaluate the effects of asphalt binder content and the LEADCAP additive on moisture susceptibility, the KW-A mixture with 4.5% asphalt content and the KW-B mixture with 4.9% asphalt content were selected for testing. All specimens were compacted to a height of 178 mm and a diameter of 150 mm. To obtain specimens of uniform air void distribution, these samples were cored and cut to a height of 150 mm with a 75-mm diameter for the dynamic modulus and controlled crosshead (CX) cyclic direct tension tests.

C.4.2. Test Set-up

A closed-loop servo-hydraulic machine manufactured by MTS was used for the load-controlled tension-compression dynamic modulus and CX cyclic direct tension tests that employ the S-VECD model. An asphalt concrete dummy specimen was placed inside the temperature chamber to monitor the actual temperature of the specimens during testing. Data acquisition programs were prepared using LabVIEW software for data collection and analysis. Vertical deformations were measured in the middle of the specimen using four linear variable differential transducers (LVDTs) with a gauge length of 100 mm. DEVCON® steel putty was used to glue the steel end plates and targets for the LVDTs that were used for testing the specimens.

C.4.3. Mechanical Testing

Two main tests were carried out in this study: (1) the dynamic modulus test was performed to determine the linear viscoelastic characteristics, and (2) the CX cyclic direct tension test was implemented to describe the viscoelastic damage characteristics. After the CX cyclic direct tension tests were completed, the tested specimens were split into two pieces and the stripped areas on the fractured surfaces were visually analyzed. All tests were conducted using both moisture-conditioned and unconditioned specimens. In the following subsections, the moisture conditioning procedure and other mechanical test methods used in this study are described briefly.

Moisture Conditioning Procedure

The moisture conditioning procedure found in AASHTO T 283 (4) was applied to cored and cut specimens. After applying vacuum pressure of 13~67 kPa to specimens submerged in a vacuum container at 25°C in order to match a saturation level of 65%~80%, the saturated specimens were placed in a water bath at 60°C for 24 hours. After completely conditioning the specimens for moisture damage, the hot specimens were transferred to a water bath at room temperature to cool. The wet specimens were dried using an electric fan at room temperature and then core-dried one after the other to minimize thermal stress. The completely dried moisture-conditioned specimens thus could be used to avoid the effects of changing saturation levels during testing.

Dynamic Modulus Tests

Dynamic modulus testing was performed in load-controlled mode in axial tension-compression following the protocol given in AASHTO TP 62-03 (5). Tests were completed for all mixtures at -10°C, 5°C, 20°C, 40°C, and 54.4°C and at frequencies of 25, 10, 5, 1, 0.5, and 0.1 Hz. Load levels were determined by a trial and error process so that the resulting strain amplitudes were between 50 and 70 microstrains to prevent damage to the specimens. The dynamic modulus values were fitted for the coefficients of the sigmoidal function and time-temperature shift factors by optimizing the dynamic modulus mastercurve. After determining the shift factors, the dynamic modulus was converted to the relaxation modulus, $E(t)$, of the Prony series form to obtain a constitutive relationship between the strain and stress in the time domain. Finally, a

power term, alpha (α), used in VECD theory, was calculated from the maximum log-log slope, m , of the relaxation modulus versus time relationship.

Controlled Crosshead (CX) Cyclic Direct Tension Tests

The viscoelastic damage characteristics were determined by conducting CX cyclic direct tension tests at 19°C and 10 Hz. All tests were performed at two different strain amplitudes (relatively high strain and low strain). The high strain amplitude targets the fatigue failure at around 1,000 cycles, and the low strain amplitude targets the failure at about 10,000 cycles. The resulting two sets of cycle test data were used to develop the S-VECD model. Fingerprint dynamic modulus tests were conducted to check the variability of the test specimens before running the CX cyclic direct tension tests. Checking for specimen variability is important so that the linear viscoelastic properties obtained from the dynamic modulus tests can be used properly in the VECD analysis.

In this study, the fatigue life of the specimens was determined by observing the change in phase angle in the CX cyclic tests. Figure C.1 shows a typical pattern of change in phase angle during an entire CX cyclic test. The phase angle increases until strain localization occurs, and then decreases. The opposite occurs around the failure point, which makes the determination of the number of cycles to failure accurate and consistent.

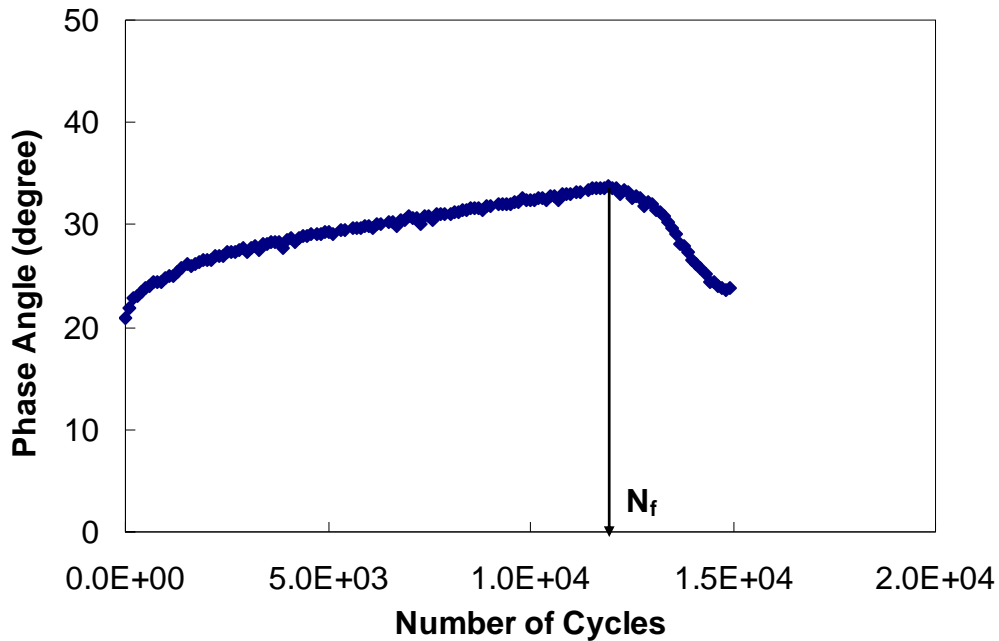


Figure C.1 Fatigue life definition of a typical controlled crosshead cyclic test indicating number of cycles to failure (N_f).

Once the number of cycles to failure was determined from each test, the C value at the failure cycle (C_f) was extracted and used as the failure criterion to determine the number of cycles to failure from the predicted results using the VECD model. This prediction methodology is described in the next section.

C.4.4. Fatigue Performance Analysis

In this study, the fatigue performance of different mixtures with and without moisture conditioning was analyzed by combining the VECD model and the pavement responses determined from the structural analysis of the pavements. Specifically, the strain kernel at the bottom of the asphalt layer under a moving load first was determined from the LVEA pavement model. This strain kernel was then input to the VECD model, and the fatigue life was determined by applying the C_f failure criterion. The reason for this combined analysis is explained later using actual test data in subsection C.5.1.

The LVEA model developed at North Carolina State University was used to calculate the pavement responses. This model performs three-dimensional calculations of stresses and strains in a layered system under moving loads. The pavement selected for this study had a 10-cm thick asphalt layer over the subgrade with an elastic modulus of 70 MPa. The temperature gradient of the asphalt layer was determined by first dividing the asphalt layer into three sublayers. The average temperature of each of the three sublayers was determined from the data obtained from the Enhanced Integrated Climatic Model (EICM) for April 2004 in Raleigh, North Carolina. This temperature gradient resulted in the dynamic modulus gradient along the depth of the asphalt layer in the calculation of the strain kernel.

A single moving wheel load was simulated using contact pressure of 758 kPa, contact area of 0.3 m x 0.18 m, and velocity of 26.8 m/sec for a rectangular wheel load. The single wheel moving load was applied repeatedly to the pavement until the strain response of a steady-state condition was obtained. The pavement response in the steady-state condition then was used as a repeated constant input loading history for the S-VECD model.

C.4.5. Digital Imaging Analysis of Fractured Surface

After running the CX cyclic tests, the stripped area of the fractured surface could be measured by making visual observations based on the selection of fine mesh and a numerical pixel counting method. Visual observation using the mesh selection method is an accurate but time-consuming approach to determine the stripping percentage. Figure C.2 (a) presents an original image taken from a digital image scanner, and Figure C.2 (b) presents a stripping quantification result of 36.6% from the fine mesh selection method using Count Tool in the Adobe Photoshop program. The numerical pixel counting method is a simple and fast approach to counting pixels that are related to stripping, but a threshold value for the grayscales should be determined to distinguish the stripping and non-stripping areas on the fractured surfaces.

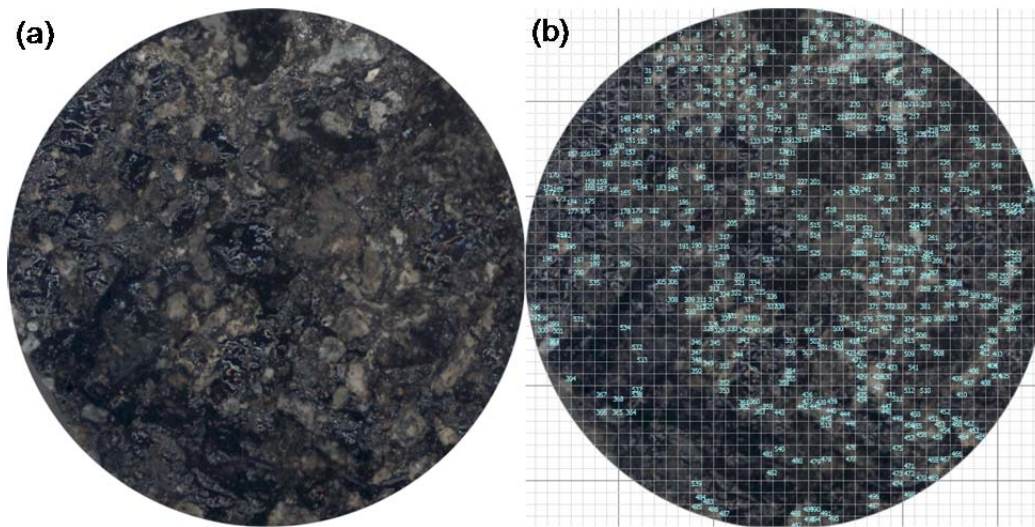


Figure C.2 Percentage of stripping determined by fine mesh selection: (a) original image and (b) 44 x 44 fine mesh on original image.

JPEGs, BMPs ('bitmaps'), GIFs (graphics interchange formats), and TIFFs (tag image file formats) are commonly used digital image formats. Among these formats, JPEG images are the most commonly used because they can present millions of colors and compress data to create small images. The downfall of JPEG files, however, is that they lose quality when they are saved. BMP images provide high image quality; as the name suggests, they present a map containing many 'bits' of an image. Because BMP files do not compress the image, no image loss occurs through any sort of modification process. GIF files are useful only for basic color usage, such as internet icons. TIFF files are used for a perfectly detailed image of a massive image size. For this study, in order to satisfy the need for high image quality and minimize the possibility of image loss, the BMP format was selected to quantify the stripping area.

One BMP image file consists of pixels that describe actual objects or landscapes. With an increase in the number of pixels, the quality of the picture increases. Each pixel in a BMP file contains color or gray information. The grayscale with 8 bits has only one layer that consists of 256 different states of grays (0: perfect black and 255: perfect white). By determining a threshold value within the grayscale, white and black pixels can be distinguished. Thus, the stripping area of a fractured surface can be quantified by counting the number of white pixels, and asphalt binder can be quantified by counting the number of black pixels. Because of the simplicity of the associated numerical analysis and image quality, the 8-bit grayscale mode was selected for counting the white and black pixels in this study. The BMP RGB color file was converted to 8-bit grayscale mode using the RGB2Gray function in MATLAB. The gray states (0~255) of a scanned surface can be seen for each pixel also using MATLAB.

Percentage of Stripping Quantification Protocol

The protocol used in this study to quantify the percentage of stripping in the fractured specimens is as follows. A digital image scanner was utilized instead of a camera to maintain a constant image size of the fractured surfaces and to maintain the quality of the BMP RGB color files.

1. The glued steel end plates are cut from the specimens that have fractured during the CX cyclic tension testing.
2. A thin transparent glass plate is placed on the area to be scanned so that it protects the scanned area from damage caused by the sharp surface of the fractured specimen.
3. A box is placed over the fractured specimen on the scanner to block any outside light.
4. The surface of the fractured specimen is scanned into a BMP RGB color file.
5. The scanned image of the fractured surface is inspected to calculate the actual stripping percentage using the mesh selection method.
6. The BMP RGB color file is converted to 8-bit grayscale mode using the RGB2Gray function in the MATLAB program.
7. Threshold values are determined that distinguish the black (asphalt binder) and white (stripped area) pixels on the fractured surface by matching the stripping percentage results obtained from the visual mesh selection method.
8. After determining the threshold values for all the mixtures, regenerated images with gray states of 0 (black) and 240 (white) are compared with the original images.
9. The stripping percentages can be calculated rapidly using a pixel counting method.

Mesh Selection Method by Visual Observation

First, the original scanned RGB color images of the fractured surfaces were imported into the Adobe Photoshop program. Second, after drawing fine grids (44 cells in the horizontal direction and 44 cells in the vertical direction) on the image file, the cells, which included stripping, were selected manually and counted using Count Tool in the program. Finally, the stripping percentages were calculated using the ratio of the number of total mesh components on a fractured surface to the number of mesh components that included stripping. Because the fractured surface was a circular area 75 mm in diameter and the image file was a 75-mm x 75-mm square area, the total number of mesh components of a fractured surface could be estimated to be 1520.53 by using the ratio of square area to circle area.

Pixel Counting Method by Numerical Analysis

First, the gray states between 0 and 255 on the scanned surface were given for each pixel using MATLAB. Second, the pixels in a fractured specimen surface were counted by extracting the background of a grayscale of 255 (perfect white) from an image file in MATLAB. The grayscales of the fractured surface were observed as between 20 and 240. Third, the pixels in the stripping area of the surface were counted by using the gray states that fell between the threshold value and 240. Finally, the stripping percentages were calculated using the ratio of the total number of pixels on the fractured surface to the number of pixels that included stripping. The method used to determine the threshold grayscale value is described in the next section.

C.5 Discussion of Results

Figure C.3 presents the overall flow of testing and analysis used in this study. The schematic illustration describes the material level testing, pavement response calculations, and digital imaging analysis to evaluate the fatigue performance and moisture susceptibility of the mixes selected for this study.

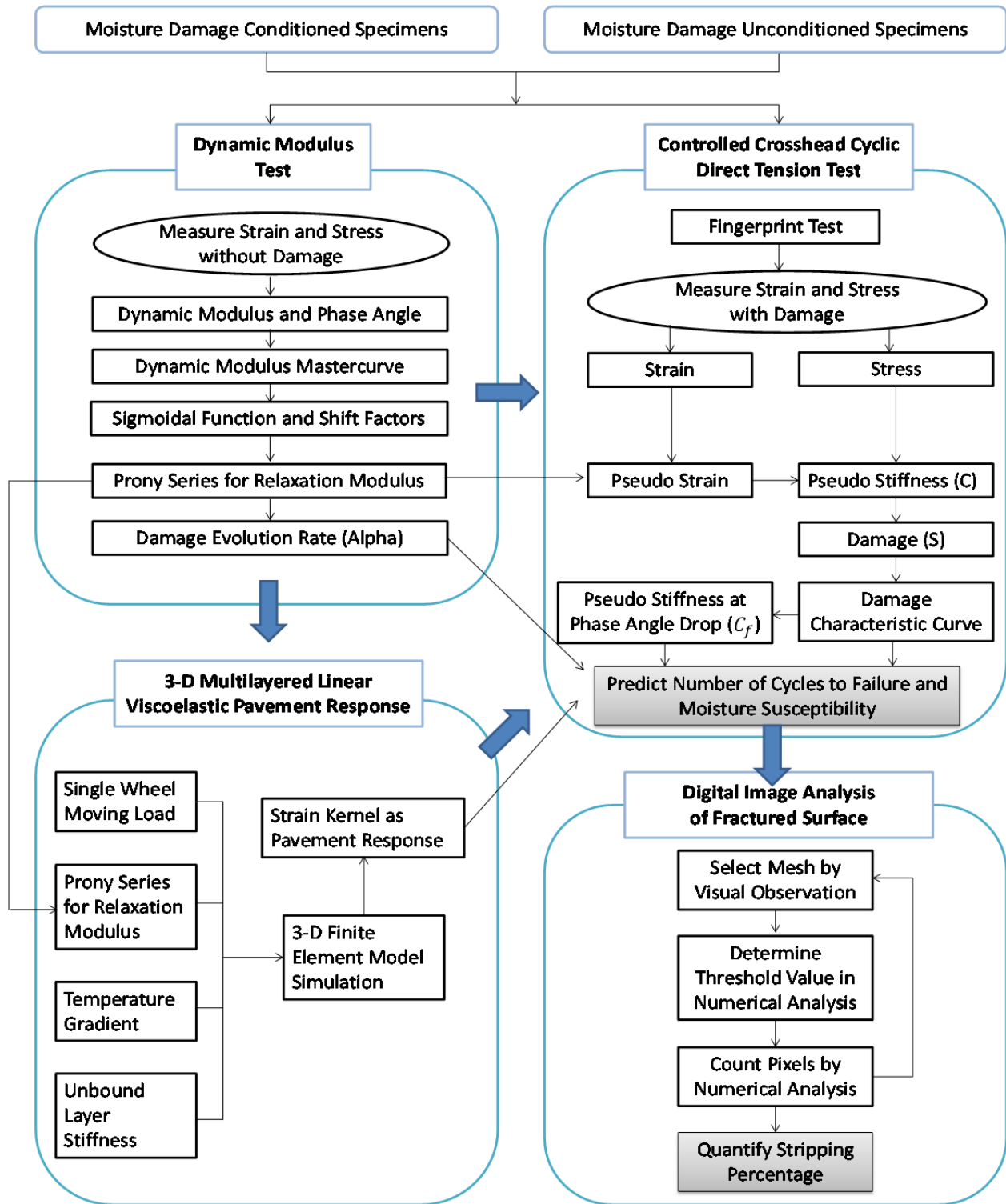


Figure C.3 Overall flow chart for testing and analysis.

C.5.1. Fatigue Life Comparison at the Material Level

The most common way to present fatigue data is to use the initial tensile strain and the number of cycles to failure (N_f) from a series of fatigue tests. Figure C.4 presents such results from the controlled CX cyclic direct tension tests of two different mixtures with and without moisture conditioning. This plot clearly demonstrates the incorrect way of estimating the fatigue cracking resistance of different mixtures using the tensile strain versus N_f relationship. If the fatigue life (i.e., N_f) of each of the two mixtures with and without moisture conditioning is compared at a constant strain level (as shown by the dashed horizontal line in Figure C.4), it is expected that the mixture that has been subjected to moisture conditioning would have a higher N_f value and therefore greater fatigue cracking resistance than the unconditioned specimen. This conclusion is, of course, incorrect based on observations from actual pavements in service.

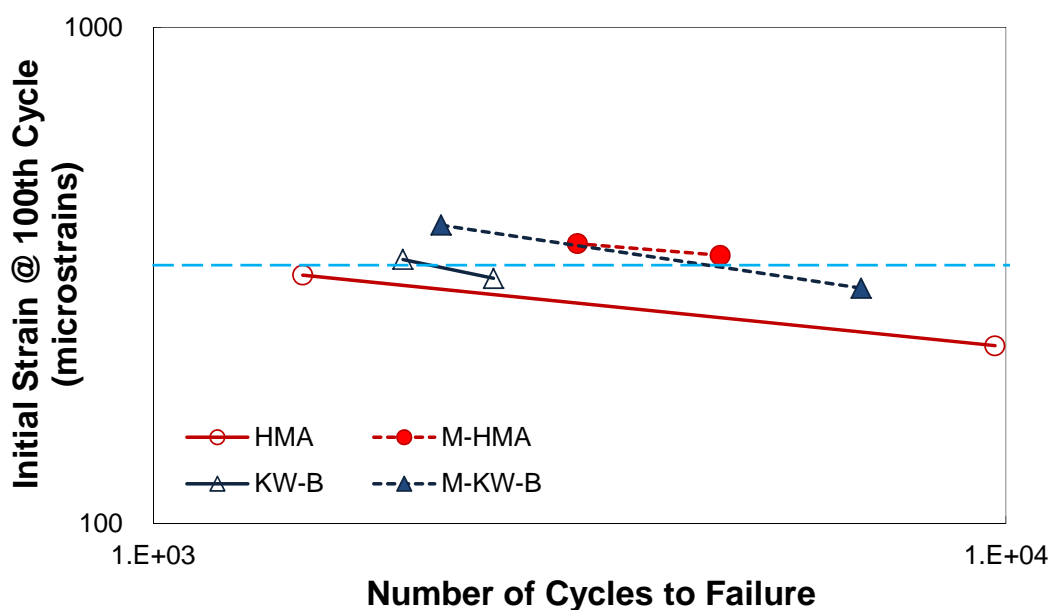


Figure C.4 Traditional tensile strain-based fatigue relationships for unconditioned and moisture-conditioned specimens.

Clearly then, both a material model (such as the relationship shown in Figure C.4) and a structural model of a pavement are needed to properly evaluate the fatigue performance of a mixture. That is, different mixtures with different stiffness values would result in different tensile strain values at the bottom of the asphalt layer in a pavement structure; therefore, the constant tensile strain assumption represented by the horizontal dashed line in Figure C.4 is not valid. When mixtures with and without moisture conditioning are placed in the pavement, the tensile strain at the bottom of the moisture-conditioned asphalt layer would be greater than that of the unconditioned asphalt mixture. Therefore, the fatigue life of the moisture-conditioned mixture would be shorter than that of the unconditioned mixture in this pavement system.

For this study, the S-VECD material model is combined with the LVEA pavement structural model to evaluate the fatigue cracking resistance of unconditioned and moisture-conditioned HMA and WMA mixtures with varying asphalt contents. The use of LVEA-predicted pavement responses coupled with the S-VECD model was verified using field performance data obtained from the Federal Highway Administration Accelerated Load Facility (FHWA ALF) (6). The ranking of the fatigue performance of pavement sections tested under the FHWA ALF project was predicted accurately using the results from the S-VECD model coupled with LVEA (6).

C.5.2. Fatigue Life Comparison Using the Combined Material and Structural Models

Figure C.5 presents a summary of the testing and analysis results for all the study mixtures. Figure C.5 (a) presents the dynamic modulus mastercurves of all the mixtures, and Figure C.5 (b) shows the strain kernel response results of the LVEA simulations at the bottom of the selected pavement. Both results indicate that a low stiffness value for the KW-A mixture caused high levels of transverse strain in the pavement simulations, whereas a high stiffness value for the KW-B mixture led to a low pavement strain response. These figures also show that the mixtures became less stiff as the asphalt content increased.

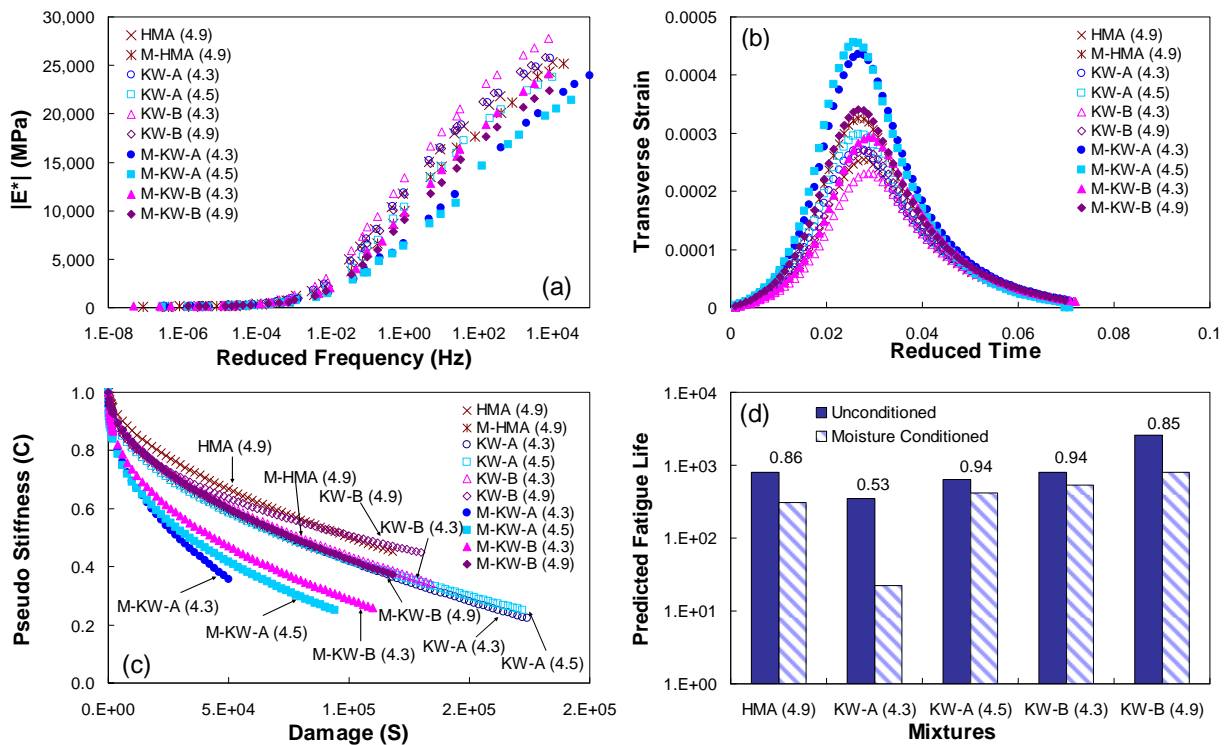


Figure C.5 Mechanical properties and predicted strain and fatigue life data of study mixtures.

Figure C.5 (c) demonstrates how fast the material integrity represented by pseudo stiffness (C) decreased as the damage (S) increased. The moisture-conditioned KW-A mixtures with 4.3% and 4.5% asphalt contents and the KW-B mixture with 4.3% asphalt content show a rapid decrease in material integrity with an increase in damage compared to the other HMA and KW-B mixtures

with 4.9% asphalt content. It should be mentioned that the amount of damage at failure is also an important factor in characterizing fatigue resistance. In Figure C.5 (c), the last point on each curve indicates the fatigue failure. The figure shows that the moisture-conditioned KW-A mixture with 4.3% asphalt content had an extremely small amount of accumulated damage at failure, whereas the unconditioned KW-A mixture had a large amount of accumulated damage at failure. However, a comparison of only the damage characteristic curves cannot yield reliable information about the different mixtures' fatigue resistance, because the energy that is input by mechanical force is consumed not only in creating and propagating cracks in the material, but also in deforming the material. Therefore, it is important to include both stiffness and damage characteristics of a material when determining fatigue cracking resistance.

Figure C.5 (d) presents the prediction results from the coupled S-VECD and LVEA models. The strain kernel for each of the mixtures shown in Figure C.5 (b) was input to the damage characteristic curve of the mixture shown in Figure C.5 (c) to determine the fatigue life of the mixture. This coupled method ensures that both the stiffness and damage characteristics are taken into account in determining the fatigue resistance of a mixture. Figure C.5 (d) indicates that the KW-A mixture with 4.3% asphalt content shows a likelihood of an unfavorable (short) fatigue life and unfavorable moisture susceptibility, whereas the KW-B mixture with 4.9% asphalt content indicates a favorable (long) fatigue life and favorable moisture resistance. Also, the KW-B mixture with 4.3% asphalt content exhibited better fatigue resistance and moisture resistance than the HMA mixture with 4.9% asphalt content. The moisture susceptibility of the KW-A mixture was found to be very sensitive to the asphalt content. The KW-B mixture with 4.9% asphalt content exhibited the most favorable fatigue resistance and moisture resistance. This improvement over the KW-A mixture without an anti-stripping agent demonstrates the benefits of adding an anti-stripping agent.

The approach taken to determine the grayscale threshold value for the percentage of stripping calculations is shown in Figure C.6 (a) and (b). The threshold value was changed systematically in the digital images obtained from the fracture surfaces of all the mixtures to develop a series of curves, shown in Figure C.6 (b). Then, the percentages of stripping determined from the manual visual mesh selection method for the different mixtures were used to find the corresponding grayscale values using the curves shown in Figure C.6 (b). The average of the corresponding grayscale values obtained from the different mixtures is 63. This threshold value was used in the numerical pixel counting method to determine the percentage of stripping values for the different mixtures. These values are plotted in Figure C.6 (a) along with the percentage of stripping values determined from the visual mesh selection method. The values obtained from the two methods compare reasonably well, indicating the validity of using the grayscale value of 63 as the threshold value. Additional analysis using threshold values between 50 and 70 provided a consistent stripping percentage ranking order.

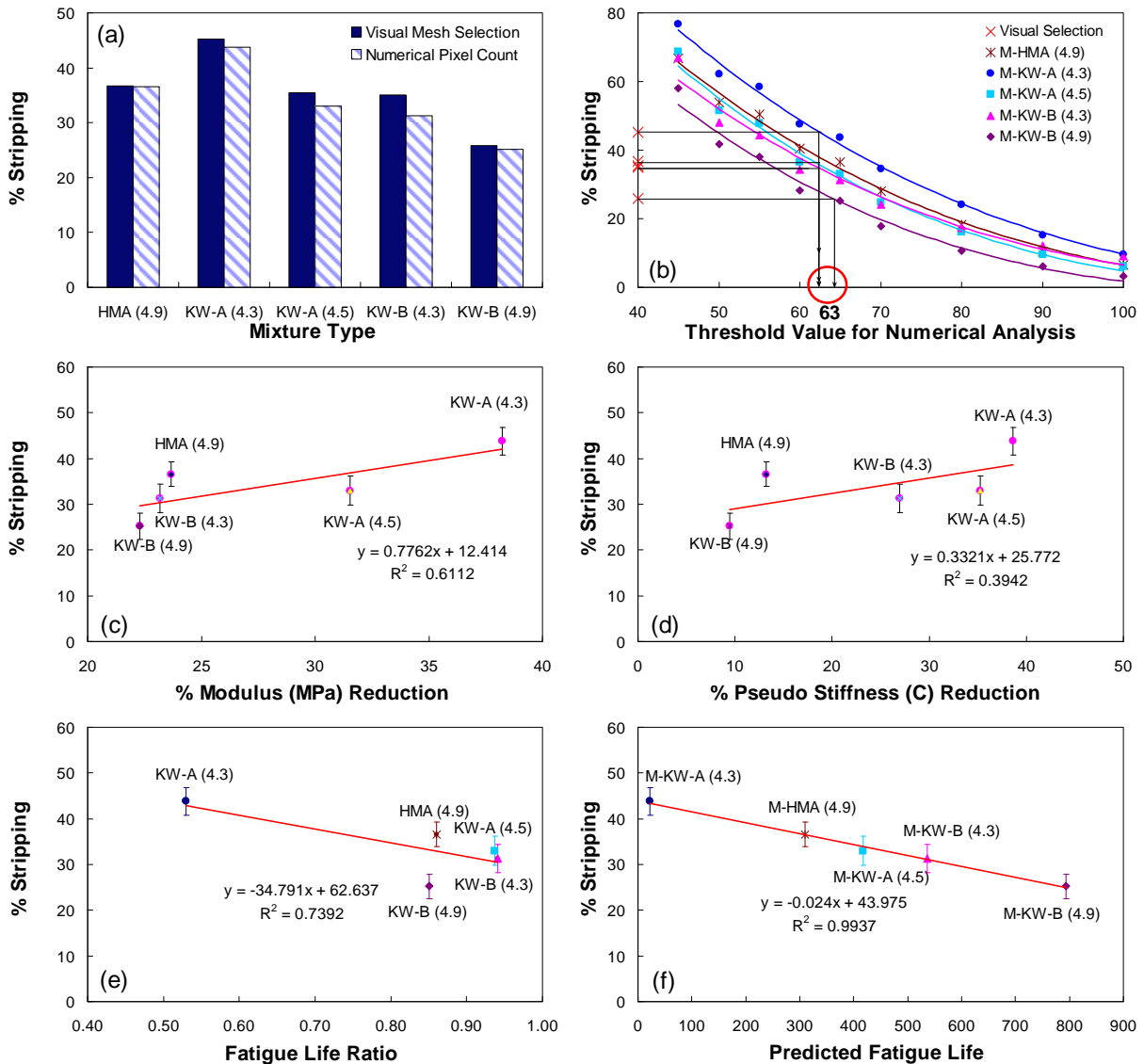


Figure C.6 (a) Percentage of stripping using visual mesh selection and numerical pixel count, (b) determination of threshold value, and (c)-(f) percentage of stripping versus various moisture susceptibility indicators.

Figure C.6 (c) to (f) present the percentages of stripping determined from the digital images of the fractured surfaces of the study mixtures plotted against the material properties determined from mechanical testing and the fatigue life predicted from the coupled mechanistic models. The reduction in dynamic modulus value was calculated using the modulus values at 20°C and 10 Hz. The reduction in pseudo stiffness was determined using the C values at the S value of 70,000. It can be seen that the reductions in dynamic modulus and pseudo stiffness values due to moisture conditioning do not have a strong relationship with the percentage of stripping values. Meanwhile, Figure C.6 (e) to (f) show relatively strong relationships between the percentage of

stripping values and indicators using the predicted fatigue life. Note that in Figure C.6 (e), the fatigue life ratio was determined by dividing the difference in fatigue life between the unconditioned and moisture-conditioned specimens by the fatigue life of the unconditioned specimens. A very strong correlation is shown in Figure C.6 (f) between the percentage of stripping and the predicted fatigue life of the moisture-conditioned specimens. This strong correlation may be due to the fact that the same aggregate and base binders were used in all the mixtures.

Finally, Figure C.7 illustrates the analyzed stripping percentages using the pixel counting method and the determined threshold value of 63. The comparison between the original image and the regenerated image consists of only two gray states of 0 (asphalt binder) and 240 (stripped area). It can be seen that the stripped areas were captured reasonably well using the threshold value of 63. However, this value would change depending on the type of aggregate and binder used in a particular mixture. Therefore, the digital imaging analysis method presented in this study needs to be applied to a wide range of mixtures to develop a database for threshold values.

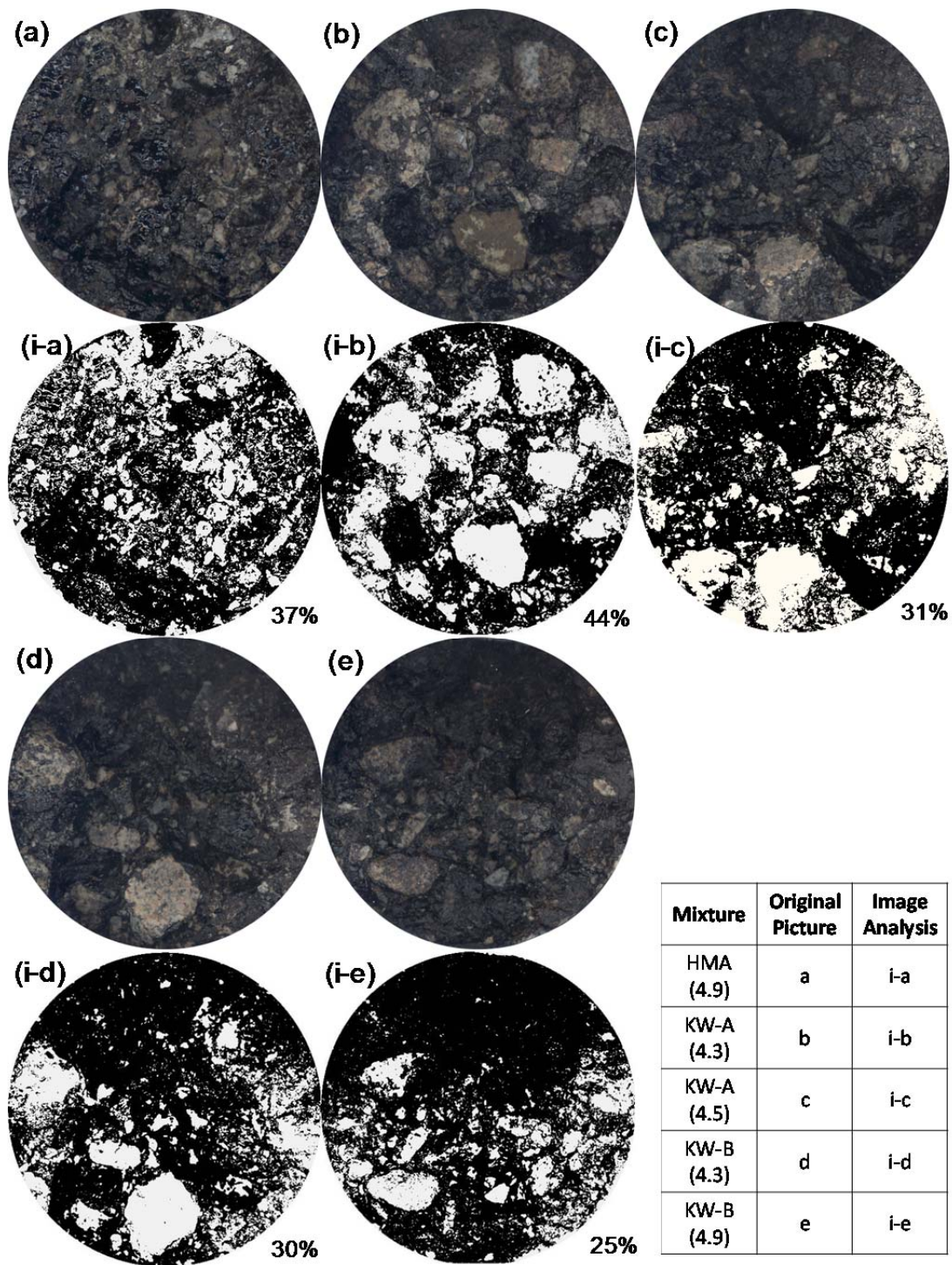


Figure C.7 Comparisons between original images and digital images analyzed with threshold value 63.

C.6 Conclusions

The following key findings were obtained from the results of the cyclic direct tension tests with and without moisture conditioning and the digital imaging analysis method:

- The digital imaging analysis method developed in this study captures the degree of stripping fairly well.
- Stripping percentages of fractured specimens can be quantified consistently using a pixel counting method after determining threshold values via the mesh selection method.
- The fatigue life predicted from the coupled S-VECD and LVEA models has a strong correlation with the percentage of stripping area determined from the fractured specimen surfaces.
- The asphalt content of a mixture has a significant effect on the fatigue performance as well as the moisture susceptibility of the mixture. In this study, this effect was found to be greater for the KW-A WMA mixture without an anti-stripping agent than for the KW-B mixture with an anti-stripping agent.
- A polyethylene wax-type additive combined with an anti-stripping agent (KW-B) leads to a more favorable fatigue life and less stripping than the pure polyethylene wax-type additive (KW-A).

References

1. Azari, H. *Documentation of Precision Estimates of AASHTO T283: Resistance of Compacted Hot Mix Asphalt (HMA) to Moisture-Induced Damage*. Publication NCHRP Project 9-26A, Transportation Research Board. Sept. 2010.
2. Park, S., Y. R. Kim, and R. Schapery. A Viscoelastic Continuum Damage Model and Its Application to Uniaxial Behavior of Asphalt Concrete. *Mechanics of Materials*, Vol. 24, No. 4, 1996, pp. 241-255.
3. Kim, Y. R. and D. N. Little. One-Dimensional Constitutive Modeling of Asphalt Concrete. *ASCE Journal of Engineering Mechanics*, Vol. 116, No. 4, 1990, pp. 751-772.
4. Association of American State Highway and Transportation Officials. *AASHTO T 283 (Mod.) Resistance of Compacted Bituminous Mixture to Moisture Induced Damage*. N.C Department of Transportation.
http://www.ncdot.org/doh/operations/dp_chief_eng/constructionunit/paveconst/Asphalt_Mgmt/TSR/tsr2.htm. Accessed July 15, 2011.
5. AASHTO. *AASHTO TP-62 Standard Method of Test for Determining Dynamic Modulus of Hot-Mix Asphalt Concrete Mixtures*. Washington, D.C. 2003.

6. Underwood, B. S., M. Eslaminia, S. Thirunavukkarasu, M. N. Guddati, and Y. R. Kim. Asphalt Concrete Pavement Response and Fatigue Performance Modeling using Advanced Techniques, *Proceedings of the 11th International Conference on Asphalt Pavements*, ISAP, Nagoya, Japan. August, 2010.

APPENDIX D PERFORMANCE-BASED MOISTURE SUSCEPTIBILITY EVALUATION OF WARM MIX ASPHALT CONCRETE THROUGH LABORATORY TESTS AND DIGITAL IMAGING ANALYSES

D.1 Abstract

The study reported in this Appendix D employed the cyclic direct tension test, indirect tensile (IDT) strength test, and Hamburg wheel tracking (HWT) test to evaluate the moisture susceptibility of warm mix asphalt (WMA) mixtures. The stripped areas that were quantified via digital imaging analysis were derived from the cyclic direct tension, IDT, and HWT test results and compared with the mechanical properties of the mixtures to identify sensitive moisture susceptibility indicators. These methodologies were applied to a Superpave 9.5-mm hot mix asphalt (HMA) mixture and five corresponding WMA mixtures that use the following technologies: (1) Evotherm 3G that contains a chemical additive, (2) foaming, (3) WMA-A that contains a chemical additive and is currently under development, (4) WMA-B that contains an organic additive and is currently under development, and (5) WMA-C that also contains an organic additive (different from that used in WMA-B) and is also currently under development. Fatigue life ratios obtained from the simplified viscoelastic continuum damage model combined with layered viscoelastic analysis were determined to be the most sensitive indicators for moisture susceptibility. The stripping inflection points (SIPs) derived from the HWT tests also indicated good sensitivity to moisture conditioning; however, each SIP was affected by the permanent deformation characteristics of a given mixture as well as its moisture susceptibility, thereby making the observations inconclusive.

D.2 Introduction

Moisture damage has been observed as a stripping phenomenon. Stripping is defined as “the breaking of the adhesive bond between the aggregate surface and the asphalt cement (adhesion failure)” in an asphalt mixture (1). Stripping is a complicated phenomenon that needs to be considered in terms of the type and use of a particular mix, binder characteristics, aggregate characteristics, environment, traffic, construction practice, and the use/non-use of anti-stripping additives (2). A literature review indicates that there are six different mechanisms of stripping: (1) detachment, (2) displacement (film rupture), (3) spontaneous emulsification, (4) pore pressure, (5) hydraulic scour, and (6) pH instability. Detachment is related to the weak adhesive bond that causes a separation of the asphalt film from the surface of the aggregate. Displacement is explained by a break or disruption of the asphalt film on the aggregate surface. Spontaneous emulsification is an inverted emulsion of water droplets that cause the adhesive bond to break; that is, once the emulsion formulation penetrates the aggregate surface, the adhesive bond is broken. Pore pressure causes progressive adhesion and cohesion failure and is accelerated by the stress imparted to the entrapped water in the asphalt mixture that is caused by repeated traffic

loading. Hydraulic scour occurs on the saturated surface of an asphalt pavement due to tire pressure. Finally, pH instability is a chemical reaction that affects the adhesion between the asphalt and the aggregate due to the pH of the contact water. pH values below 4 dissolve amine and lime from the aggregate surface (3). In most cases, stripping starts at the bottom of the asphalt layer and then propagates upwards due to the tensile behavior of the structure and the presence of water above the subgrade (4). Other types of stripping, such as potholes and raveling, can be observed on the surface of an asphalt pavement and also can be caused by pore pressure and hydraulic scour that are due to traffic loading.

Various moisture susceptibility evaluation methods that can be applied to asphalt mixtures are currently available. Indirect tensile (IDT) strength tests and Hamburg wheel tracking (HWT) tests have been widely used in accordance with AASHTO T 283 and AASHTO T 324, respectively. The IDT test can measure the cohesion resistance of the binder as well as the frictional resistance of the aggregate. If the adhesive bond is poor, failure may occur at the aggregate-binder interface (5). However, it has been reported that the IDT test has some shortcomings because it can cause: (1) permanent deformation under the loading strip, (2) non-uniform strain distribution, (3) an unrealistic representation of the stress state, and (4) local failure at the support due to high stress (6). The HWT test can measure the stripping inflection point (SIP), i.e., the number of wheel passes at the intersection of the creep slope and the stripping slope, as a moisture susceptibility indicator. Here, the stripping slope is the accumulation of permanent deformation due to moisture damage. The main shortcoming of the HWT test is that it is difficult to distinguish the permanent deformation due to viscous flow from the permanent deformation due to moisture damage at high temperatures, because dry specimens are not tested in the current specifications (7). Additional disadvantages of both tests include that the indices produced from these tests can be used only for pass-fail criteria and cannot be used with mechanistic pavement analysis to predict the performance of asphalt pavements.

Cyclic direct tension tests have been used to determine the material stiffness, damage, and a failure criterion, which together constitute the essential components of the viscoelastic continuum damage (VECD) model. The simplified viscoelastic continuum damage (S-VECD) model was designed to reduce the computational time required by the VECD model and to overcome the limitations associated with the Asphalt Mixture Performance Tester (AMPT), such as the low capacity of the load cell. Details of the simplification procedures are explained in the literature (8).

Cyclic direct tension tests also allow users to predict the fatigue performance of asphalt mixtures under varying loading and environmental conditions from only a few test runs. In addition, the fatigue life of asphalt pavements can be predicted when the cyclic direct tension test results are input to a structural finite element analysis. Two levels of pavement analysis have been developed by the research team at North Carolina State University: (1) layered viscoelastic analysis (LVEA) and (2) layered viscoelastic continuum damage (LVECD) analysis. Both of these analysis techniques perform three-dimensional moving load simulations. The LVEA calculates stresses and strains at specified evaluation points in the pavement and utilizes the material-level S-VECD model to determine the fatigue life of the asphalt mixture at each of

those evaluation points. The LVECD analysis performs a more comprehensive cracking evaluation by applying the S-VECD model for each element in the pavement structure and produces damage contours for the entire pavement structure. Recently, the cyclic direct tension test along with the AASHTO T283 moisture conditioning procedure and these pavement level analysis methods have been used together to evaluate the effects of moisture damage on the cracking performance of asphalt pavements (9).

In order to evaluate these laboratory tests' abilities to determine the amount of moisture damage, the fractured and scoured surfaces used for the mechanical tests were quantified using digital imaging analyses and compared against the predicted fatigue performance and mechanical properties determined from these tests. These results are discussed in this study.

D.3 Objectives

The objectives of this study are: (1) to investigate performance-related moisture susceptibility analysis methods by using the S-VECD material model coupled with LVEA and LVECD structural analysis at two levels; (2) to develop stripping quantification procedures for the IDT and HWT tests using digital imaging analyses; and (3) to identify moisture susceptibility indicators from the cyclic direct tension, IDT, and HWT tests that best relate to the stripped areas determined from the digital imaging analysis.

D.4 Experimental Program and Analysis Methods

D.4.1. WMA Technology, Binder Modification, and Specimen Fabrication

This study employed a control HMA mixture and five different WMA mixtures. The WMA technologies include Evotherm 3G that has a chemical additive, foaming, WMA-A that contains a chemical additive and is currently under development, WMA-B that contains an organic additive and is currently under development, and WMA-C that also contains an organic additive (different from that used in WMA-B) and is also currently under development. These WMA technologies can be grouped into three main categories. The first category includes the Evotherm 3G and WMA-A with chemical additives that induce a low internal friction of the asphalt binder using a surface-active agent, resulting in improved mixing and compaction at low temperatures. The second WMA technology category is foaming technology that uses a nozzle to spread water throughout the asphalt binder and turns the water into steam and small bubbles. The steam and small bubbles serve to reduce the binder viscosity by expanding the volume of the binder. The Foamer machine produced by Pavement Technology, Inc. (PTI) was used in this study. The third WMA technology category is represented by the WMA-B and WMA-C mixes that contain organic wax additives that reduce asphalt viscosity by the lubricant effect of an oily wax when they are heated above the point of crystallization.

The control HMA mixture was composed of 9.5-mm nominal maximum aggregate size (NMAS) granite aggregate, 19% reclaimed asphalt pavement (RAP), and 6.7% (5.2% from virgin binder and 1.5% from RAP) PG 70-22 binder, as derived from the Superpave volumetric mix design. The same mix design was used for each of the five WMA mixtures. For the binder modification, the Evotherm and WMA-A chemical additives were added to the asphalt binder at 130°C at 0.5% by weight of total asphalt. No anti-stripping agents were used for these two WMA mixtures. For the foamed mix, an anti-stripping agent of 0.7% by weight of total asphalt was added at 130°C in the same manner as used for modifying the binder of the HMA mix. Then, 2% water by weight of total asphalt was injected into the asphalt binder at 157°C using the PTI Foamer. In contrast to the above modifications, the organic powder type of WMA-B and the chip type of WMA-C were spread on top of the asphalt binder when mixing the aggregate at 135°C with the binder at 157°C at 0.5% and 1.5% by weight of total asphalt, respectively. The temperatures of the aggregate, RAP, and binder for all of the WMA mixtures at the time of mixing were 135°C, 110°C, and 157°C, respectively. For the HMA mixture, all the mixing temperatures were the same as those of the WMA mixtures except the aggregate temperature of 157°C.

Short-term oven aging was applied to all the WMA mixtures at 117°C for two hours according to NCHRP 9-43 and applied to the HMA mix at 135°C for four hours according to AASHTO R 30. The compaction temperatures of the WMA and HMA mixtures were 117°C and 152°C, respectively. Based on the curing time study of the Double Barrel foamed mixture, the compacted foamed WMA mixture specimens were stored for at least 12 days of curing in the laboratory before testing (10).

D.4.2. Laboratory Moisture Susceptibility Testing

In order to apply the S-VECD model to the pavement structural analysis program, the linear viscoelastic material properties obtained from the dynamic modulus tests and the viscoelastic damage properties obtained from the cyclic direct tension tests were needed to evaluate performance-based moisture susceptibility. The dynamic modulus tests were conducted in compressive cyclic stress-controlled mode to produce 50~75 microstrain in the linear viscoelastic range in accordance with AASHTO TP 79 and PP 61. The cyclic direct tension tests were conducted in tensile cyclic actuator displacement control mode to reach failure at approximately 1,000, 10,000, and 100,000 cycles at 19°C and 10 Hz loading frequency. The test samples that were fractured inside the linear variable differential transducer (LVDT) were used to characterize the viscoelastic damage.

Two common specification tests, the IDT strength test and the HWT test, were carried out to develop the stripping quantification procedures and to determine the moisture susceptibility indicators that relate to the stripped areas. The IDT strength tests were performed in compressive mode with a constant actuator displacement rate at 25°C. Based on NCHRP 9-26A recommendations, cored and cut specimens were used for the IDT tests in order to overcome the high variability of air void distribution found in the strength test results. The number of aggregate breakage instances on the fractured surface was counted by visual inspection, except the areas under the loading strip (which could not be seen). The HWT test was carried out in

compressive mode by rolling a steel wheel on the surface of two gyratory specimens underwater at 50°C. The testing was stopped at either 20,000 passes or at a rut depth of 20 mm. The procedures for all of the laboratory moisture susceptibility tests and corresponding stripping mechanisms are summarized in Table D.1.

Table D.1 Laboratory Moisture Susceptibility Tests and Their Stripping Mechanisms

Moisture Susceptibility Tests		Cyclic Direct Tension	IDT	HWT
Specification		AASHTO TP107	AASHTO T283	AASHTO T324
Measurement		Fatigue life deteriorated due to tensile behavior	Cohesion and fractional resistance by strength	Rut depth deteriorated due to hydraulic scour and pore pressure
Test Temperature		19°C	25°C	50°C
Mode of Testing		Cyclic tensile mode of actuator displacement control	Compressive mode of actuator displacement rate of 50 mm/min.	Cyclic compressive mode by rolling a steel wheel
Moisture Conditioning Procedure		Saturated specimens at a level of 65%~80% in a water bath at 60°C for 24 hours	Saturated specimens at a level of 65%~80% in a water bath at 60°C for 24 hours	Underwater at 50°C while running test
Stripping Mechanisms	Detachment	Primary	Primary	-
	Displacement (Film Rupture)	Secondary	Secondary	-
	Emulsification	-	-	-
	Hydraulic Scour	-	-	Primary
	Pore Pressure	-	-	Secondary
	pH Instability	-	-	-

D.4.3. Performance-Based Moisture Susceptibility Evaluation

Fatigue performance predictions of asphalt pavements require consideration of the material characterizations using structural pavement response analysis. In this study, the S-VECD model was used to characterize the viscoelastic material properties with growing damage, and two different pavement response analysis programs, the LVEA and LVECD programs, were utilized to model the pavement structure. The first proposed method measures the moisture susceptibility by predicting the ratio of the remaining fatigue life of bottom-up cracking with and without

moisture conditioning in a simple and fast manner. The second proposed method investigates moisture susceptibility by comparing the damage contours (cracking potential) with and without moisture conditioning at the end of the long-term analysis period, which can simulate both bottom-up and top-down cracking in an accurate and sophisticated manner.

S-VECD Model Combined with Layered Viscoelastic Analysis

One simple and fast evaluation method can derive the single steady-state strain kernel that is caused by the bending moment in the LVEA program at an isothermal condition at the bottom-central nodal point of the asphalt pavement. The strain kernel is then applied to the S-VECD model as a loading history input. The fatigue life is determined by determining the number of cycles to failure (N_f) until the constant repeated kernel reaches the internal state variable (S) of the damage at failure. Detailed analysis procedures can be found in the literature (9).

In this study, the elastic modulus values of 227 MPa and 196 MPa were used to represent the base and subgrade layers in sound condition, respectively. These values were measured at US 76 in Wilmington, North Carolina using a dynamic cone penetrometer (12). The asphalt layer thicknesses of 100 mm and 300 mm were used to simulate a thin and thick pavement, respectively. The single temperature of 19°C was used to represent the spring season for this analysis. The single moving load was a rectangular contact area that was 17.78 cm wide and 27.994 cm long, with an axle load of 40 kN, tire pressure of 758 kPa, and design velocity of 2.682 m/s.

S-VECD Model Combined with Layered Viscoelastic Continuum Damage Analysis

The LVECD program is a three-dimensional pavement structure program that can capture the effects of viscoelasticity, thermal stress, hourly temperature variations, hourly truck distribution, and moving traffic load (tire pressure, contact area shape, shear traction, and tire configuration). The LVECD analysis calculates all the stresses and strains at all the nodal points in the pavement structure and simulates the material integrity as crack potential. Another main feature of the LVECD program is that it can efficiently reduce computational time using Fourier transform-based layered analysis. Finally, the program has been verified to simulate fatigue cracking that is due to a bending moment at the bottom of the asphalt layer and the shear force at the edge of the tire on top of the asphalt layer by comparing the results to field observations (12). Additional information about the LVECD program can be found in the literature (13).

In order to account for the effect of temperature variation on fatigue performance, temperature data were obtained from the Enhanced Integrated Climatic Model (EICM) for the Wilmington, North Carolina area. In order to make the computational time for this study more efficient, one day was divided into three time segments so that constant average temperatures and traffic passes could be used instead of data for every hour. All other inputs, such as the base and subgrade modulus values and pavement thicknesses and design loads, were identical to those used for the LVEA. It has been reported that the Lottman test found in AASHTO T 283 is designed to reflect the field performance at 4 to 12 years (14), and several long-term pavement performance (LTPP)

test sections showed a stripping problem after 12 years (15). In this study, it is assumed that the moisture conditioning procedure simulates 12 years of pavement performance in the field. Therefore, the equivalent of 1 million and 100 million load applications over 12 years were applied to the thin and thick pavements, respectively. Figure D.1 presents an analysis flow chart to compare the two evaluation methods.

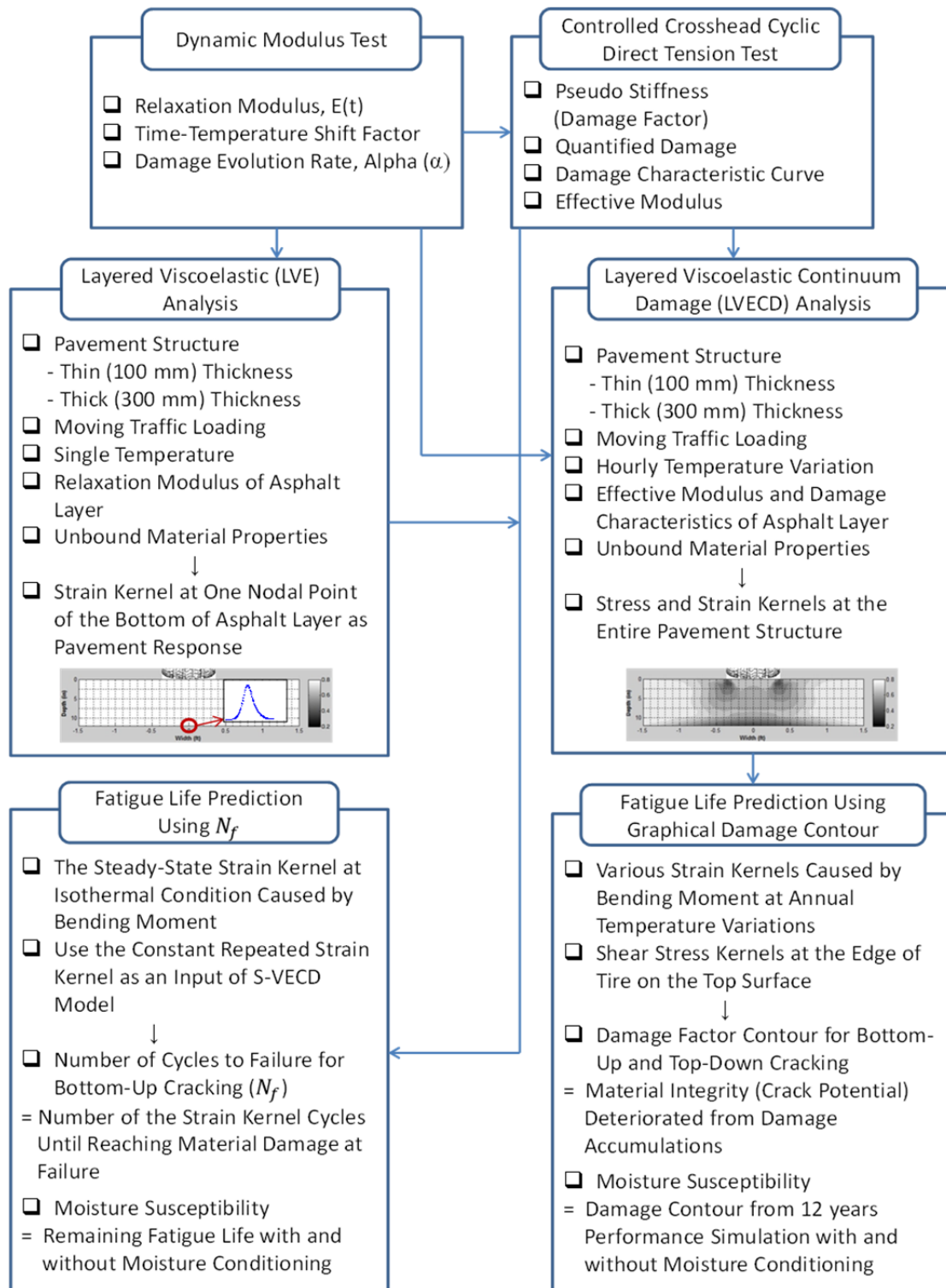


Figure D.1 Analysis flow chart of performance-based moisture susceptibility evaluations.

D.4.4. Development of Stripping Quantification Procedures for the IDT and HWT Tests

It is well known that the visual observation of stripping can serve as significant evidence in evaluating the moisture susceptibility of asphalt concrete. Recently, the authors successfully quantified the fractured surfaces used in cyclic direct tension tests by employing two different methods: pixel counting and visual mesh selection. The pixel counting method identifies the pixels in 256 different gray states in a scanned image file of the fractured surface and then classifies those states into two states by determining a threshold value among the gray states using MATLAB. The visual mesh selection method counts the number of fine mesh elements that are contained in a stripped area by clicking on each mesh element in the scanned image file using Count Tool in the Adobe Photoshop program. Detailed information can be found in the literature (9).

In this study, IDT and HWT tests were used to develop the stripping quantification procedure. The difficulty of the IDT tests is determining the threshold value from three different failure modes, and the difficulty of the HWT tests is scanning the scoured surface of the tested specimens that have a hump of lateral movement at the edge of the wheel path.

Instead of using one threshold value, the IDT test requires two threshold values to quantify stripping by differentiating the aggregate breakage areas and asphalt mastic failure surface areas from the stripped areas. First, the fractured surface used in the IDT test must be scanned to obtain a BMP (bitmap) pixel-based format for the digital imaging file. The BMP format was selected for this study because it does not allow any image loss throughout the analysis process. Second, the first threshold value (threshold value 1) needs to be determined such that the aggregate breakage (white) areas can be distinguished from the stripped (gray) areas as well as the asphalt mastic (black) failure by matching the aggregate breakage areas from the threshold method with the aggregate breakage percentage results obtained from the visual mesh selection method. Third, the pixels related to the aggregate breakage area in the image file need to be excluded for the next step. Fourth, the second threshold value (threshold value 2) needs to be determined such that the stripped areas (gray) and the asphalt mastic failure (black) areas are distinguishable by matching the stripped areas determined from the threshold method with the stripping percentage results obtained from the visual mesh selection method. Fifth, the final stripping percentages can be calculated using the two threshold values by differentiating the aggregate breakage areas and asphalt mastic failure surface areas from the stripped areas.

The digital imaging analysis of the HWT test results is almost the same as for the cyclic direct tension test results, but the HWT test needs a new threshold value to quantify the stripping due to the nature of permanent deformation testing. Because the stripped areas are on rutted surfaces, all of the scanned images for the HWT tests are lighter than those for the cyclic direct tension tests due to the gap between the stripped area and the platen of the scanner. The main difficulty of scanning the tested samples is the humps that are caused by the lateral movement of the permanent deformation. In order to scan the scoured surface as closely as possible to the platen,

the hump needs to be cut vertically using a saw, and then the humps can easily be removed by hand. The stripping quantification procedures for all of the tests are described in Figure D.2.

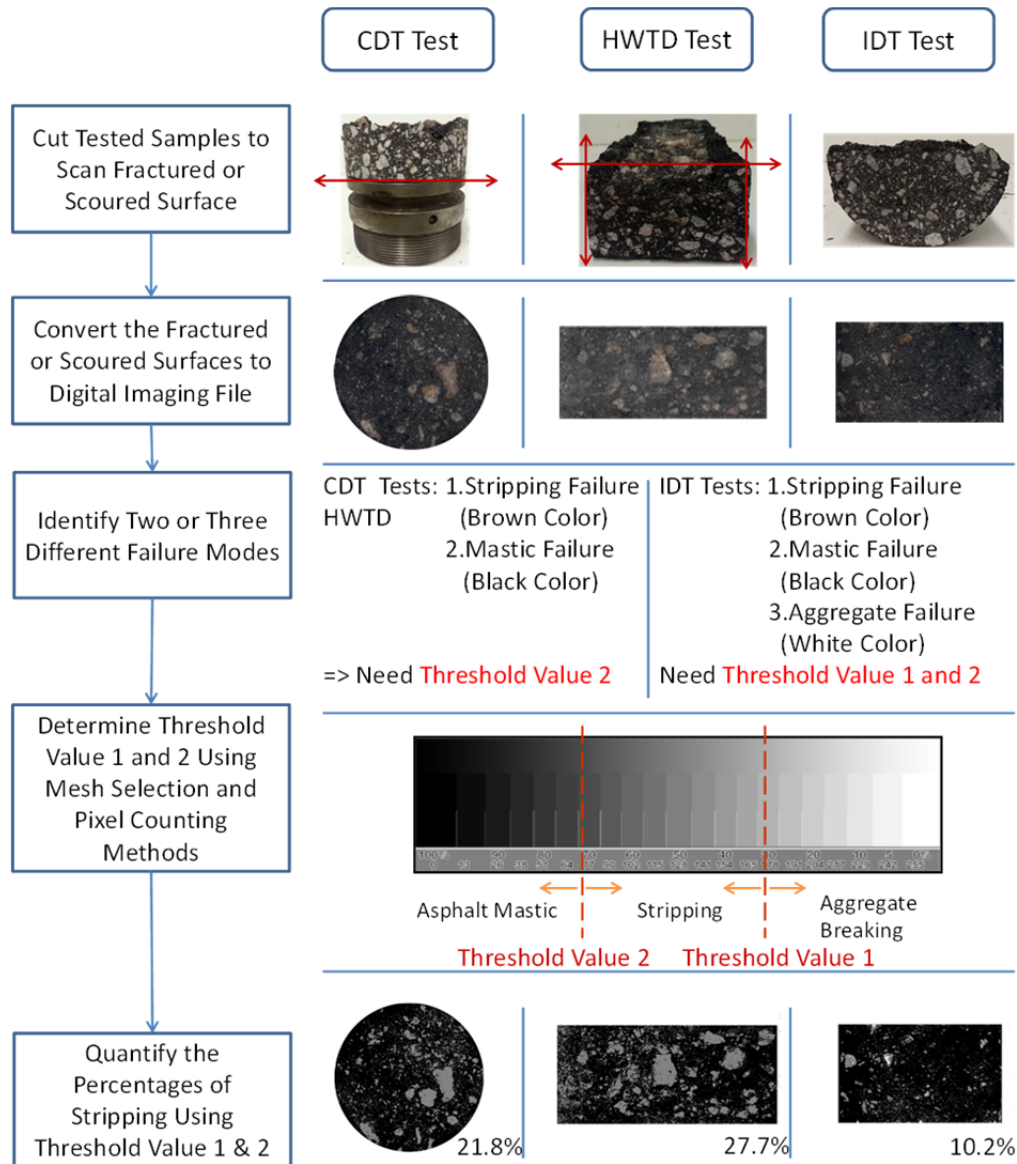


Figure D.2 Stripping quantification procedures for cyclic direct tension, IDT, and HWT tests.

D.5 Discussion of Results

This section discusses the moisture susceptibility test results for all the tests employed in this study. After running all of the moisture susceptibility tests, the fractured and scoured surfaces were examined to quantify the stripping percentages. Then, sensitive moisture susceptibility indicators were identified by comparing the indicators with their stripping percentages.

D.5.1. Performance-Based Moisture Susceptibility Evaluation Results

Figure D.3 (a) shows the linear viscoelastic properties obtained from the dynamic modulus tests. The results show that any reduction in the dynamic modulus value due to moisture conditioning is minor in the Evotherm mixture compared to the other mixtures. The damage characteristic curves shown in Figure D.3 (b) indicate that the moisture susceptibility of the Evotherm mixture is also low compared to the other mixtures by showing a small difference between the curves with and without moisture conditioning. This figure also shows that the pseudo stiffness values of the HMA mixture are higher than those of the other mixtures. Specifically, the results show that the WMA-A, WMA-B, and WMA-C mixtures have an unfavorable material integrity with growing damage when using moisture-conditioned specimens. Another significant indicator that is seen from the damage characteristic curves is the brittleness or ductility that is shown in the pseudo stiffness at the last failure point of the curves. A higher pseudo stiffness value at failure indicates that the pavement is prone to fail with a lower amount of damage. The pseudo stiffness values at failure of all the WMA mixtures with moisture conditioning are lower than that of the HMA mixture, which may be indicative of a longer fatigue life for the WMA mixtures with moisture conditioning compared to the HMA mix. The strain kernels shown in Figure D.3 (c) and (d) were derived for the pavement responses of the 100-mm and 300-mm pavements used in the LVEA using the linear viscoelastic modulus. Therefore, the amplitude of the strain kernel is strongly related to the dynamic modulus values. The higher the dynamic modulus value, the lower the strain kernel value.

By combining the linear viscoelastic properties, material integrity, damage, and brittleness, the final fatigue life can be predicted. Figure D.4 (a) and (b) show that the fatigue life ratio of the Evotherm mixture is almost identical to that of the HMA mixture, whereas the WMA-A, WMA-B, and WMA-C mixtures show more moisture susceptibility than the other mixtures. Figure D.4 (c) and (d) present the IDT test results that indicate that all of the WMA mixtures could not meet the failure criterion of 0.8 (16), and the HWT test results show that only the Evotherm and HMA mixtures could meet the failure criterion based on the SIP criterion of 10,000 passes (7). These results conflict with the fatigue life predictions derived from the cyclic direct tension tests. The failure criteria of the IDT and HWT tests were designed for conventional HMA mixtures, not WMA mixtures. Therefore, for future study, these criteria and/or the moisture conditioning procedure may need to be modified for WMA mixtures based on their field performance.

Figure D.5 presents the final damage contour comparisons with and without moisture conditioning using the S-VECD model combined with LVECD analysis for 12-year-old pavements of 100 mm and 300 mm thicknesses. The bars beside the pavement simulation results

indicate the degree to which the damage factor is related to the cracking potential. For both pavement thicknesses, the HMA and Evotherm mixtures show less moisture susceptibility than the WMA-A, WMA-B, and WMA-C mixtures, which are the same results as the fatigue life results. The results for the 100-mm pavement simulations show that both initial cracking and complete cracking propagation potentials were observed for the WMA-A, WMA-B, and WMA-C mixtures, whereas the results for the 300-mm pavement simulations show only the initial cracking potential for bottom-up cracking and top-down cracking due to moisture damage for the WMA-A, WMA-B, and WMA-C mixtures. The problem with the LVECD approach to moisture susceptibility evaluation is that moisture damage does not occur throughout the entire layer in the field as it is modeled in the LVECD program. In future, the moisture damage gradients for pavement depth, time, and climate need to be studied in order to try to match the field observations.

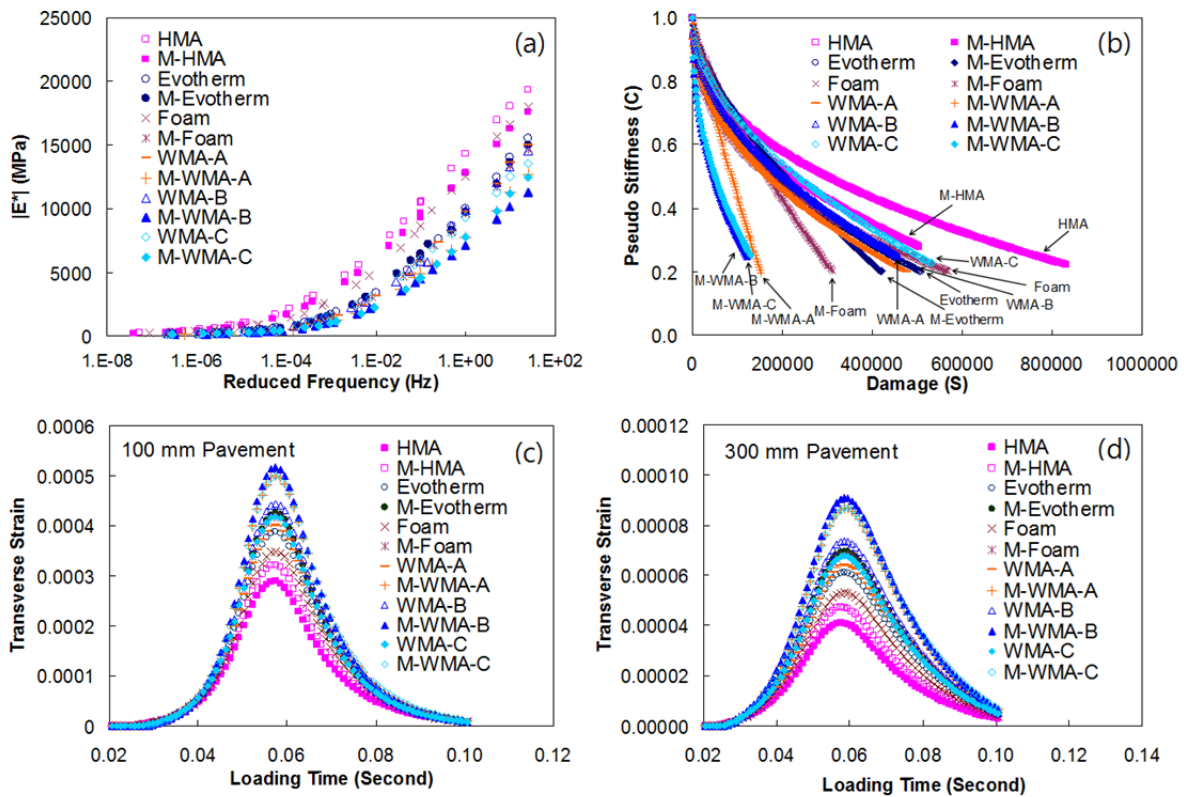


Figure D.3 Mechanical test results: (a) dynamic modulus, (b) damage characteristic curve, and (c) strain kernel at the bottom of 100-mm pavement and (d) 300-mm pavement.

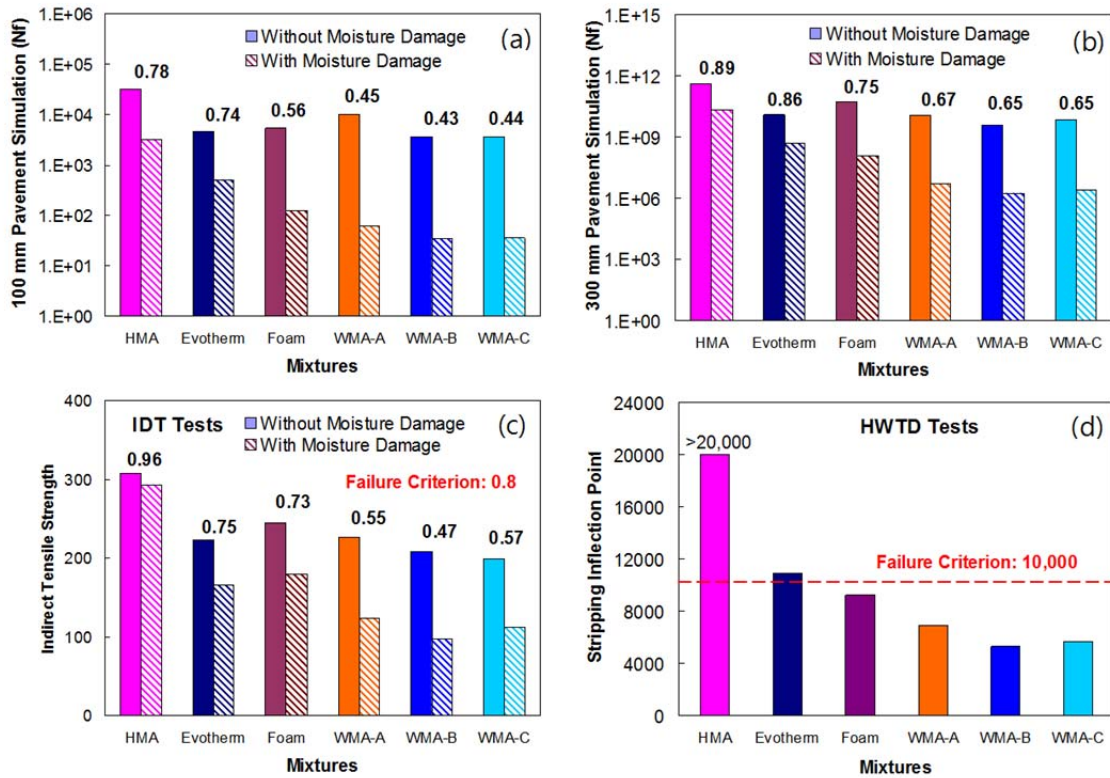


Figure D.4 Mechanical test results: (a) final fatigue life ratio of 100-mm pavement and (b) 300-mm pavement, (c) tensile strength ratio of IDT test, and (d) stripping inflection point of HWT test.

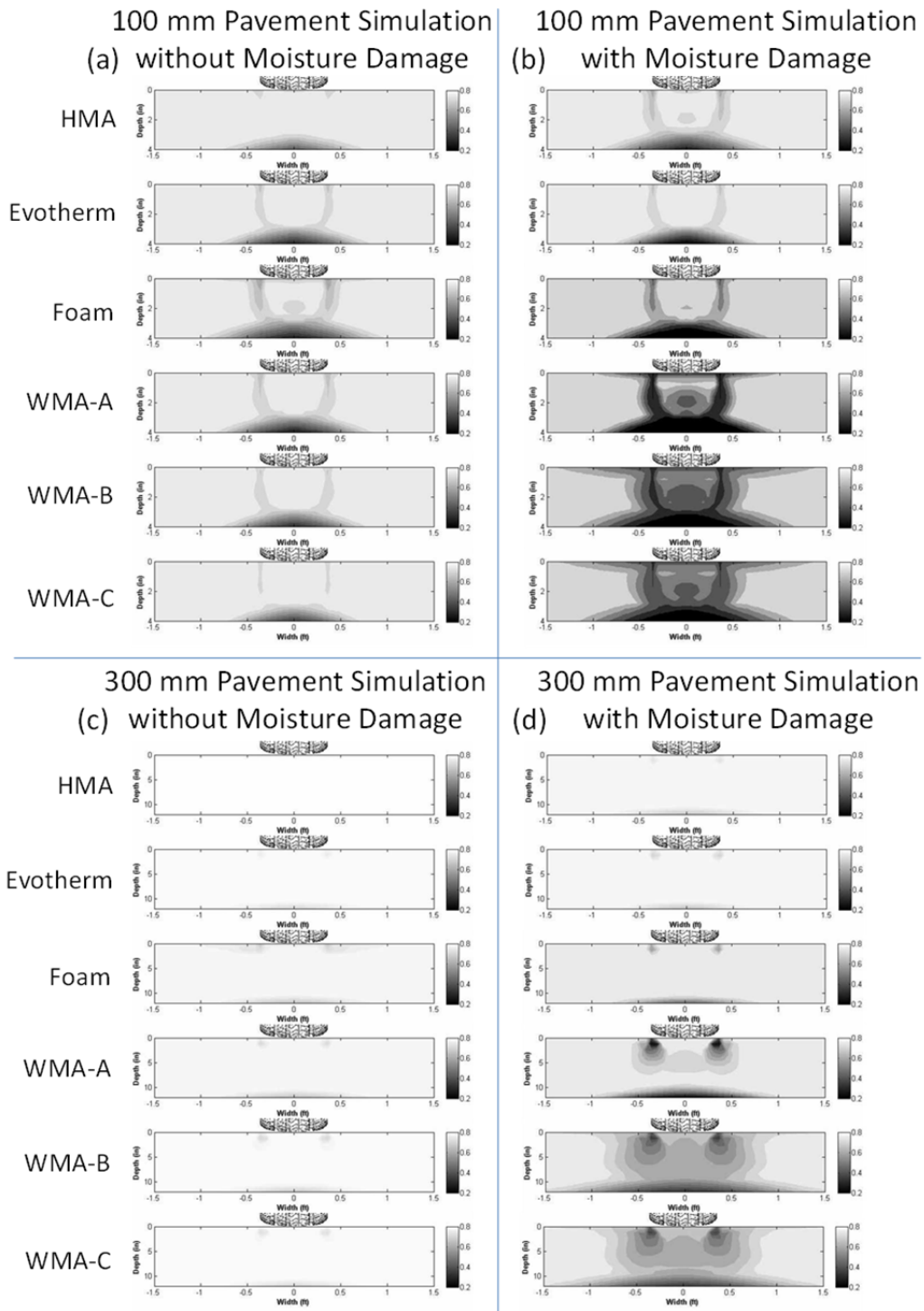


Figure D.5 Damage contour (cracking potential) comparison of 100-mm and 300-mm pavements without and with moisture conditioning.

D.5.2. Stripping Quantification Results

By adjusting the threshold value that differentiates the stripped areas and non-stripped areas, the stripping percentage changes. As shown in Figure D.6, the threshold value can be determined by matching the stripping percentage results measured from the visual mesh selection method.

Figure D.6 (a) and (b) show a way to determine the threshold value that distinguishes the black (asphalt mastic) and white (stripping) pixels for the cyclic direct tension and HWT tests. Figure D.6 (c) and (d) present a method to determine two threshold values to quantify the stripped areas of the IDT tests. Threshold value 1 in Figure D.6 (c) distinguishes the aggregate breakage (white) areas and the non-aggregate breakage (black) areas. After excluding the aggregate breakage area in the image file, threshold value 2 in Figure D.6 (d) can be determined to differentiate the asphalt mastic (black) and the stripped (white) areas by following the same procedure shown in Figure D.6 (a) and (b). As a result, the average threshold values for the cyclic direct tension, IDT, and HWT tests were derived as 63, 68 (111 for aggregate breakage threshold), and 85, respectively.

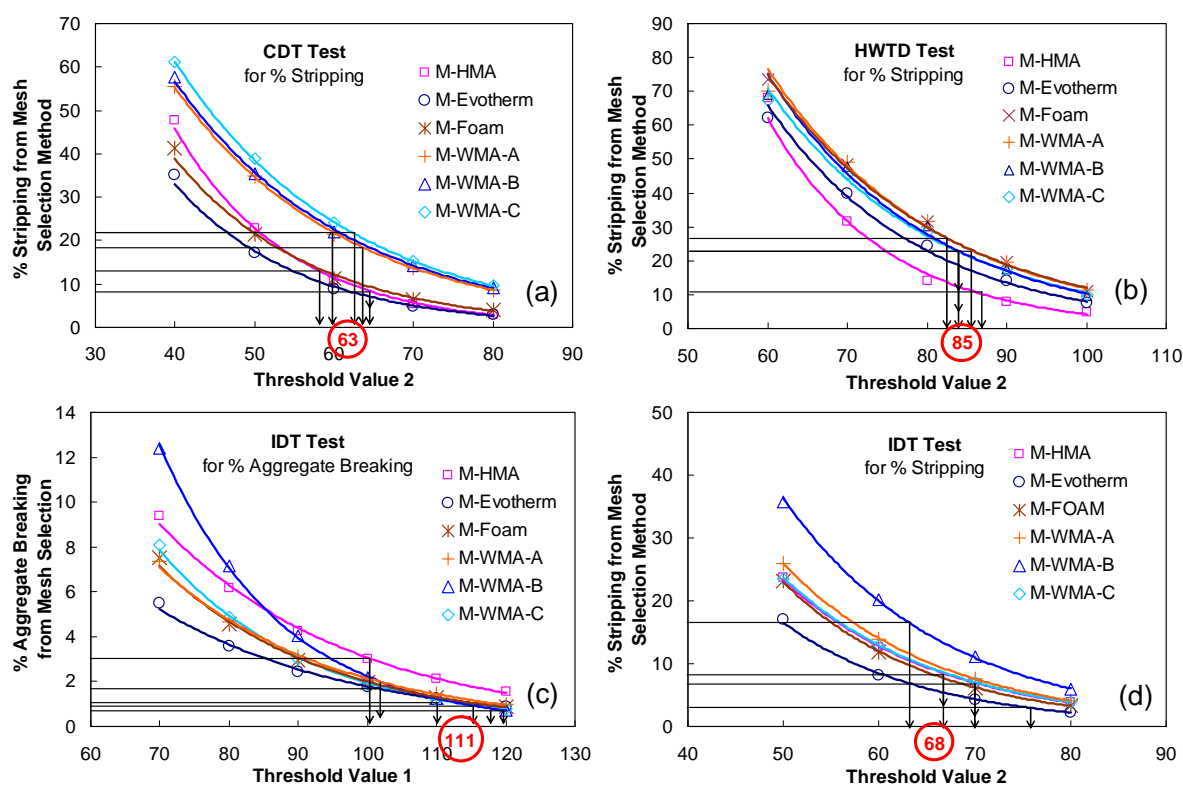


Figure D.6 Determination of threshold values for numerical analysis.

Figure D.7 (a) shows the final quantified stripping results for the cyclic direct tension, IDT, and HWT tests. The figure shows that the stripping percentages from the IDT tests are lower than those of the other tests because a different failure mechanism causes the aggregate to break.

Figure D.7 (b) through (d) present the relationships among the stripping percentage results for each test that can help improve the understanding of the stripping mechanisms of the tests. It can be seen in Figure D.7 (b) that a fairly strong correlation exists between the percentages of stripping obtained from the cyclic direct tension tests and those obtained from the IDT tests. The stripping results of the HWT tests have a weak relationship with the other test results because the stripping mechanism is different and permanent deformation is included in the stripped areas of the HWT tests.

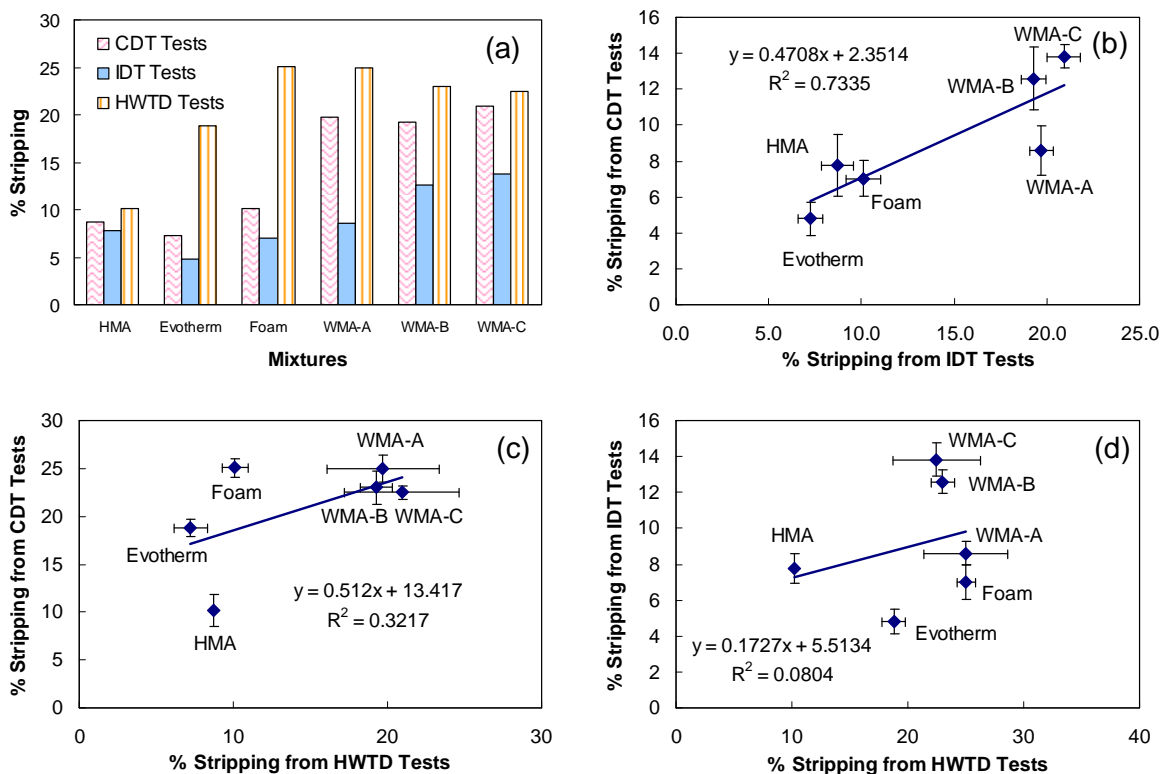


Figure D.7 Final quantified stripping results for the cyclic direct tension, IDT, and HWT tests and their relationships.

D.5.3. Identification of Sensitive Moisture Susceptibility Indicators Derived from the Cyclic Direct Tension, IDT, and HWT Tests

In order to evaluate the sensitivity of the moisture susceptibility indicators, the quantified stripping percentages were compared with the mechanical properties measured from the test methods. Figure D.8 (a) and (b) show that the quantified stripping results of the cyclic direct tension tests are strongly related to the fatigue life ratio by $R^2 = 0.88$, whereas they are less related to the dynamic modulus ratio by $R^2 = 0.56$. Figure D.8 (b) indicates that the S-VECD model combined with LVEA predicts the degree of stripping measured from the digital imaging analysis. Figure D.8 (c) and (d) indicate that the number of aggregate breakage ratios can be a slightly better moisture susceptibility indicator than the tensile strength ratio (TSR) used in IDT

tests. This finding also follows the fact that aggregate failure may occur if the adhesive bond between the aggregate and asphalt mastic is strong (5). Figure D.8 (e) and (f) indicate that the stripping percentage has a linear correlation with the SIP and a power law relationship with the rut depth. Both the stripped areas and the SIPs of the HWT tests are related to the permanent deformation that is caused by moisture damage. By conducting additional HWT tests without water at 50°C, the combined effects of moisture damage and permanent deformation can be distinguished.

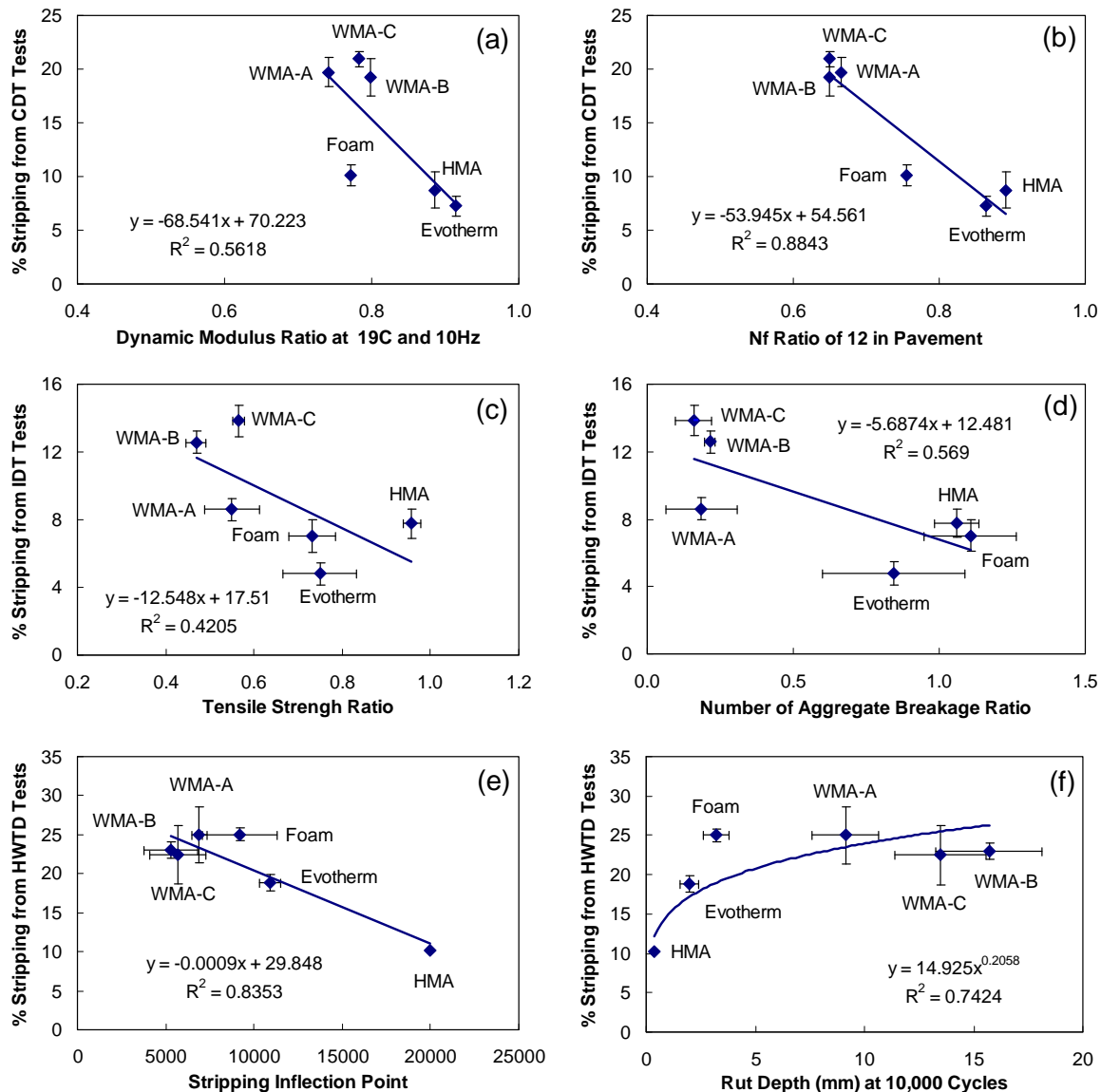


Figure D.8 Identification of sensitive moisture susceptibility indicators for cyclic direct tension, IDT, and HWT tests.

D.6 Conclusions

The following key findings were drawn from this study:

- The fatigue life ratio of pavements with and without moisture conditioning, based on results obtained using the S-VECD model combined with the LVEA program, ranks as the best indicator of moisture damage in WMA pavements. The fatigue life ratio shows a strong relationship with the corresponding stripping percentage ($R^2 = 0.88$) for the moisture susceptibility evaluation of the WMA mixtures investigated in this study.
- The SIP determined from the HWT test was found to be the second best indicator of moisture damage in WMA pavements. The SIP shows a strong relationship with the corresponding stripping percentage ($R^2 = 0.84$) for moisture susceptibility evaluation. However, this observation needs to be refined because of the difficulty encountered in differentiating the effects of permanent deformation and moisture damage on the SIP. Additional HWT tests under dry conditions may help to distinguish those combined effects.
- The stripping quantifications of IDT and HWT test results can be performed successfully by determining two threshold values that can differentiate stripping, asphalt mastic failure, and aggregate breakage on the fractured surfaces, and by modifying the tested sample of the HWT test to scan the scoured surface.
- The IDT test results indicate that the stripping percentages and number of aggregate breakage ratios may be used as improved moisture susceptibility indicators when compared to the TSR results.
- The damage contours developed from the S-VECD model combined with the LVECD program provide a sensitive means of evaluating the effects of moisture conditioning on the fatigue performance of asphalt pavements visually.
- The percentage of stripping and fatigue life ratio parameters obtained from cyclic direct tension tests and the percentage of stripping obtained from IDT tests are the recommended indicators for practitioners to use to evaluate the moisture susceptibility of WMA mixtures.

REFERENCES

1. Asphalt Institute (1981). *Cause and Prevention of Stripping in Asphalt Pavements Educational Series*. No. 10, Asphalt Institute, College Park, MD.

2. Highway Research Board (1967). *Results for the Questionnaire on Effects of Water and Moisture on Bituminous Mixes*. HRIS Selection 3P31 203837 and Highway Research Circular No. 67 (September).
3. Taylor, M. A. and N. P. Khosla (1983). Stripping of asphalt pavement: State of the art. *Journal of Transportation Research Record* 911, Transportation Research Board.
4. Kandhal, P. S. (1992) *Moisture Susceptibility of HMA Mixes: Identification of Problem and Recommended Solutions*. NCST Report 92-1, National Center for Asphalt Technology (May).
5. Majidzadra, K. and F. N. Brovold (1968). *State of the Art: Effect of Water on Bitumen-Aggregate Mixtures*. HRB, Special Report 98.
6. Huang, B., X. Shu, and Y. Tang (2005). Comparison of semi-circular bending and indirect tensile strength tests for HMA mixtures. *Advances in Pavement Engineering*: 1-12.
7. Federal Highway Administration (FHWA) *Asphalt Pavement Technology Bituminous Mixture Laboratory Equipment Hamburg Wheel Tracking Device*. U.S. Department of Transportation, FHWA.
<http://www.fhwa.dot.gov/pavement/asphalt/labs/mixtures/hamburg.cfm>. Accessed June 15, 2013.
8. Daniel J. S. and Y. R. Kim (2002). Development of a simplified fatigue test and analysis procedure using a viscoelastic continuum damage model. *Journal of Association of Asphalt Paving Technologists* 71: 619-650.
9. Lee, J., J. Lee, S. Kwon, and Y. R. Kim (2013). The use of cyclic direct tension tests and digital imaging analysis to evaluate moisture susceptibility of warm mix asphalt concrete. *Transportation Research Record: Journal of the Transportation Research Board*. In press.
10. Luis, A. H. and Y. R. Kim (2012). Effects of storage and curing times on the performance of foaming-based WMA. *Proceedings of the International Society of Asphalt Pavements (ISAP) Conference*.
11. Park, H. (2013). *Investigation of Primary Causes of Load related Cracking in Asphalt Concrete Pavement in North Carolina*. Ph.D. dissertation, North Carolina State University, Raleigh, NC.
12. Mehran, E., T. Senganal, M. N. Guddati, and Y. R. Kim (2012). Accelerated pavement performance modeling using layered viscoelastic analysis. *Proceedings of the 7th RILEM International Conference on Cracking in Pavements*: 497-506.
13. Lottman, R. P. (1982). *Predicting Moisture-Induced Damage to Asphaltic Concrete*. NCHRP Report No. 246. Transportation Research Board, National Research Council, Washington D.C.
14. Alexander, K. (2012). *Laboratory and Field Evaluation of Two Warm-Mix Additives in Connecticut and Validation of an Alternative Moisture Susceptibility Test*. Master's Thesis, University of Connecticut Graduate School, Connecticut.
15. North Carolina Department of Transportation (NCDOT) (2012). *Hot Mix Asphalt Quality Management System Superpave*.
<https://connect.ncdot.gov/resources/materials/materials/2012%20qms%20asphalt%20manual.pdf>. Accessed October 15, 2013.

APPENDIX E DEVELOPMENT OF MOISTURE CONDITIONING PROCEDURE FOR MOISTURE-INDUCED STRESS TESTER

The accelerated moisture conditioning procedure found in AASHTO T 283 can simulate long-term field moisture damage and has been used in Superpave asphalt mix design for highway agencies and departments of transportation in the United States to screen for moisture susceptibility of asphalt materials. Another moisture conditioning procedure, the Moisture-Induced Stress Tester (MIST) was developed by Instrotek to induce pore pressure from cyclic stress within a compacted asphalt mixture. MIST can control temperatures from 30°C to 60°C, pore pressure levels from 0 kPa to 517 kPa, and from 1 to 50,000 scour cycles. In addition to hot water, cyclic pore pressure helps to accelerate the moisture damage of asphalt mixtures within a reduced time.

Based on a literature review, MIST has been applied to compacted gyratory specimens to run indirect tensile (IDT) strength tests to evaluate the moisture susceptibility of four different hot mix asphalt (HMA) mixtures. It was found that the MIST conditions of 60°C, 207 kPa pore pressure, and 4000 cycles produced the same reduced strength (76%) as obtained using the AASHTO T 283 conditioning process with 60°C, 24 hours, and no pore pressure (74%). Some researchers utilized MIST moisture conditioning and IDT strength ratio tests to evaluate the moisture susceptibility of foamed warm mix asphalt (WMA) mixtures. The MIST conditions of 40°C water temperature, 276 kPa air pressure, and 1000 scouring cycles were used. The results showed that the tensile strength ratios used in AASHTO T 283 moisture conditioning caused more moisture damage than those used by MIST.

The literature review also showed that MIST can significantly reduce the moisture conditioning time by increasing either the pore pressure or water temperature. If the MIST conditions can produce the same amount of moisture damage as the AASHTO T 283 conditions using an accelerated method for pore pressure, then agencies and contractors can continue to use the current database of moisture susceptibility test results and significantly reduce moisture conditioning time using pore pressure, without the need for an additional vacuum process in order to match the saturation levels of 65%~80% found in AASHTO T 283.

Therefore, the main purpose of this study is to find universal conditions to use with MIST that can cause the same damage characteristics and stripping as those of the AASHTO T 283 procedure for mechanical test specimens. Currently, most specimens are cored and cut from gyratory specimens to ensure uniformly distributed air voids throughout the height and diameter for use with the Asphalt Mixture Performance Tester (AMPT). Because the moisture susceptibility of asphalt pavement is strongly related to bottom-up cracking due to moisture from the subgrade, the cyclic direct tension fatigue test, which was adopted as a fatigue performance test for the AMPT, was used in this study to develop the moisture conditioning procedure for MIST.

The framework needed to develop a moisture conditioning procedure for MIST is presented as the flow chart in Figure E.1. First, the asphalt mixtures that are known to be susceptible to moisture and not susceptible to moisture need to be selected to evaluate whether the MIST test conditions can sensitively distinguish moisture susceptibility in the mixtures. Second, the mechanical test specimens are cored and cut from gyratory specimens to use in MIST. Third, no vacuum is needed for the cored and cut specimens to match the target saturation level. Fourth, visual inspection for permanent deformation is made after applying various MIST conditions so that the moisture-conditioned specimens can be used for fatigue performance testing. Fifth, cyclic direct tension tests and digital imaging analyses are carried out to find the MIST conditions that produce the same fatigue characteristics and stripping percentages as are found in the current moisture damage procedure in AASHTO T 283. Various kinds of asphalt mixtures need to be tested to determine the standard testing protocol for MIST.

In this study, two different asphalt mixtures were used: (1) WMA mixture with PG 58-28 binder used in Manitoba, Canada and (2) HMA mixture with PG 64-22 binder used in North Carolina.

The WMA mixture is a Superpave 16-mm NMAAS asphalt mixture with PG 58-28 binder and Advera organic wax additive that makes the WMA sensitive to viscous flow due to its high water temperature. In order to determine the water temperature for MIST, a very soft asphalt mixture was selected. The water temperatures of 60°C, 40°C, and 30°C were selected to evaluate the effect of high water temperatures on the permanent deformation via visual observation.

The HMA mixture is a Superpave 9.5-mm NMAAS asphalt mixture with PG 64-22 binder, 19% reclaimed asphalt pavement (RAP), 5.1% Superpave optimal asphalt binder content of total asphalt mixture weight, and 0.7% anti-stripping agent of total asphalt content weight. This mixture was selected as a less moisture-susceptible material (i.e., a stiff asphalt mixture) used in North Carolina. A 9.5-mm NMAAS mixture with PG 64-22 binder, 19% RAP, 4.5% asphalt binder, and no anti-stripping agent was selected as the moisture-susceptible material. By comparing the less moisture-susceptible asphalt mixture and the moisture-susceptible asphalt mixture, a moisture conditioning procedure for MIST could be investigated.

In order to accelerate moisture damage conditioning using MIST, the stabilized maximum pore pressure of 276 kPa was used. Applying pressure higher than 276 kPa could result in puncturing the MIST bladder.

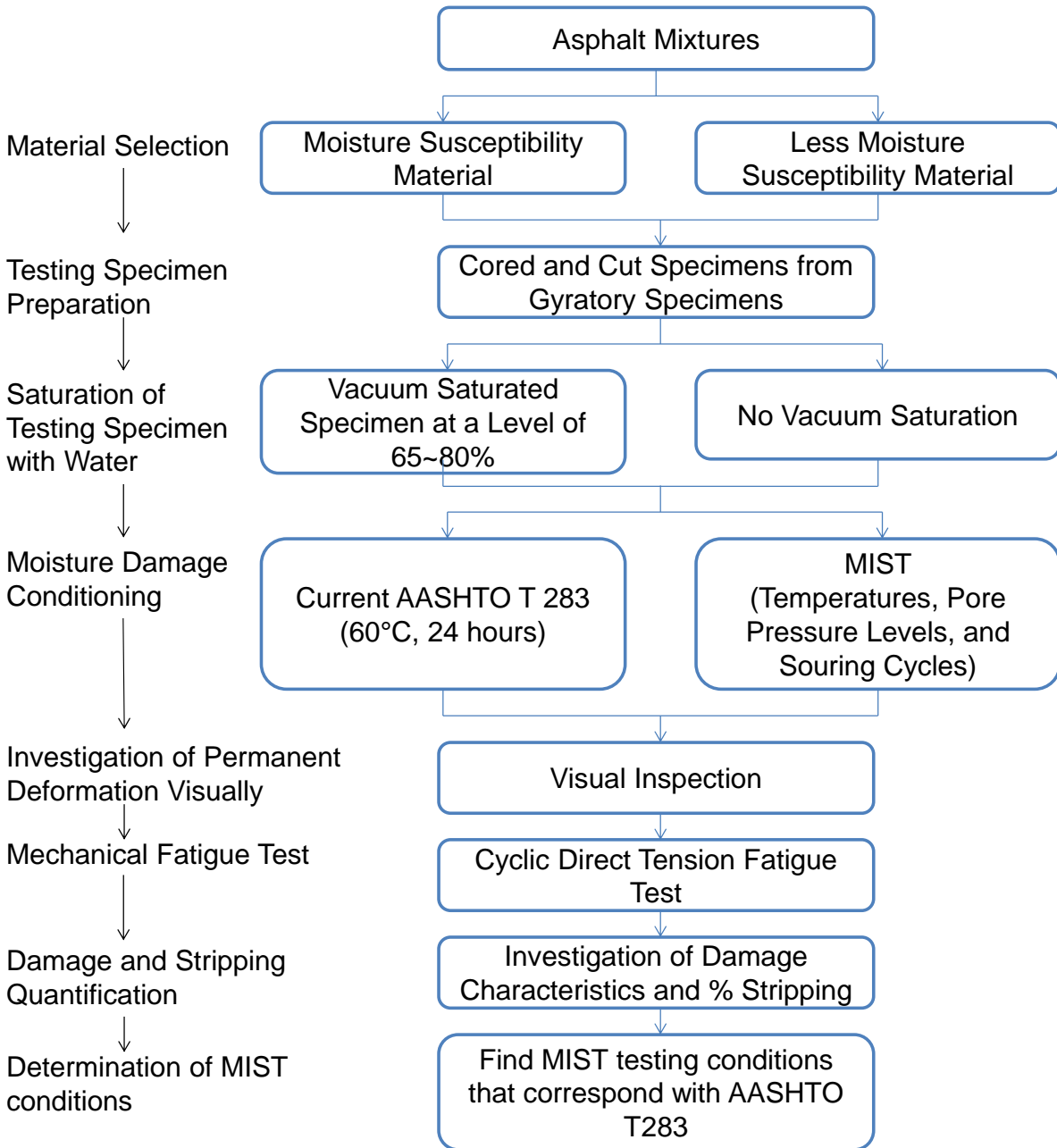


Figure E.1 Flow chart of moisture conditioning protocol development of MIST for mechanical test specimens.

E.1 Determination of Water Temperature for MIST by Visual Observation of Permanent Deformation

Figure E.2 (a), (b), and (c) show that the soft asphalt mixtures were completely disintegrated due to the high water temperature of 60°C with 1000, 3000, and 9000 hydraulic cycles at 276 kPa

pore pressure. It seems that the water temperature of 60°C was too hot to apply the hydraulic stress of 276 kPa when using the soft asphalt mixture with the wax additive and low PG grade binder. Also, Figure E.2 (d) indicates that a small deformation occurred at the water temperature of 40°C and 9000 cycles of 276 kPa pore pressure. However, no permanent deformation was visually observed at the MIST conditions of 40°C, 276 kPa, and 6000 hydraulic cycles, indicating that moisture damage only affects the viscoelastic material properties related to fatigue cracking. In addition, no permanent deformation occurred using the maximum 48000 cycles at 276 kPa at the water temperature of 30°C, as shown in Figure E.2 (e) and (f).

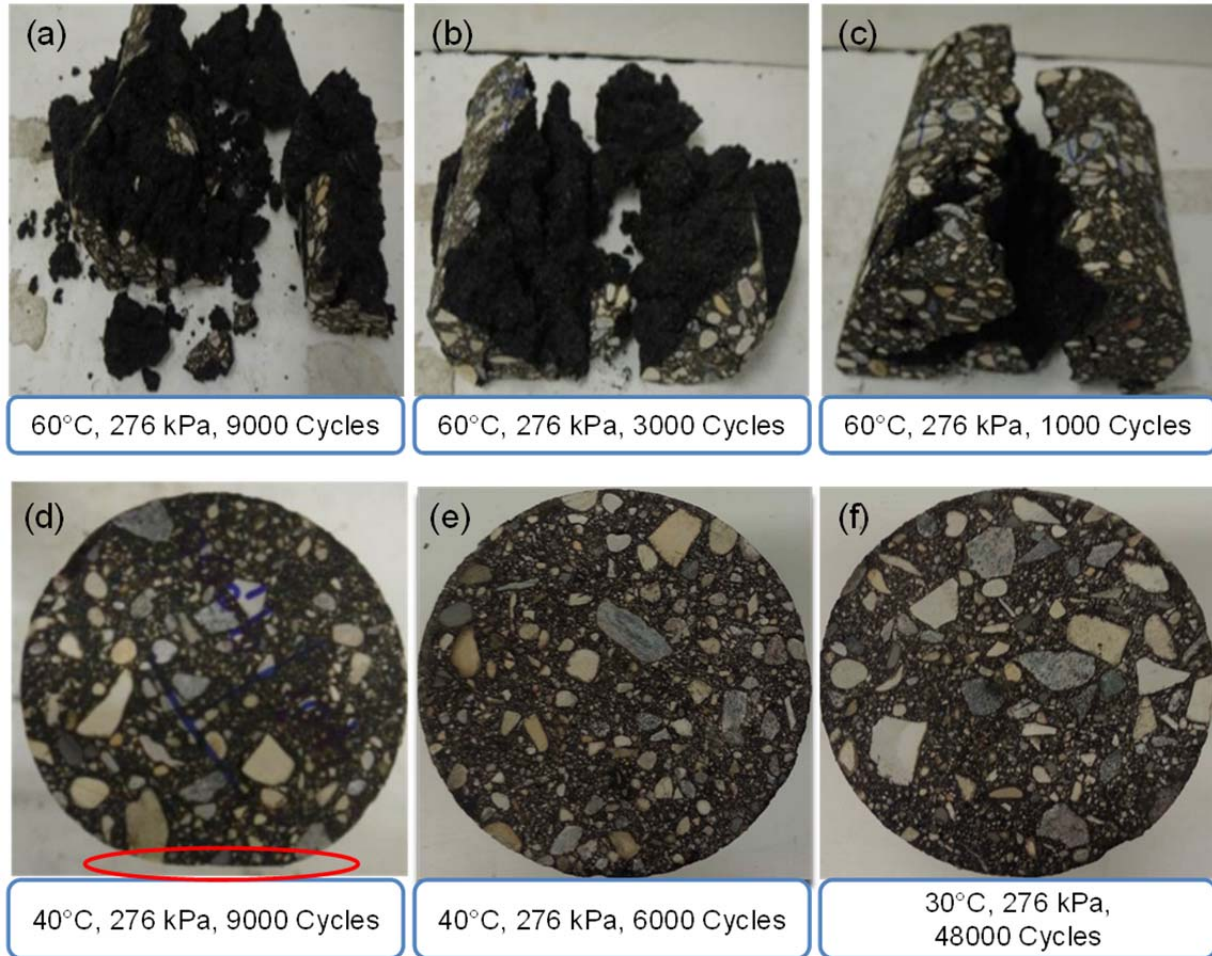


Figure E.2 Investigation of permanent deformation under various MIST test conditions.

E.2 Determination of Number of Hydraulic Cycles for MIST by Damage and Stripping Quantification

In addition to the visual observations of permanent deformation, moisture damage and stripping were quantified using the S-VECD model and digital imaging analyses to find the MIST conditions that best correspond to the current moisture conditioning procedure found in

AASHTO T 283. In order to determine the number of hydraulic cycles, the Superpave 9.5-mm NMAS asphalt mixture with 0.7% anti-stripping agent was used as the less moisture-susceptible mixture. By modifying the optimum binder content and binder properties of the Superpave mix design to 0.6% less binder content and no anti-stripping agent, a moisture-susceptible asphalt mixture was produced. Table E.1 outlines the experimental plan of mechanical fatigue testing that was undertaken to help determine the MIST conditions that can sensitively distinguish moisture susceptibility.

Table E.1 Experimental Plan to Determine MIST Conditions for Mechanical Testing

Moisture Conditioning			Moisture- Susceptible Material	Less Moisture- Susceptible Material
AASHTO T 283	60°C, 24 hr	Vacuum Saturation at 65%-80%	√	√
MIST	40°C	3000 Cycles (2.5 hours)	√	√
		6000 Cycles (5 hours)	√	√
	30°C	48000 Cycles (40 hours, maximum)	√	√

Figure E.3 (a) shows the damage characteristic results derived using the moisture damage conditions found in AASHTO T 283 and the three different MIST conditions using the moisture-susceptible asphalt mixture. The damage characteristic curves for the AASHTO conditions are similar to those for the MIST conditions at 40°C and 6000 hydraulic cycles (warm water temperature with short cycles of hydraulic pressure) and 30°C and 48000 hydraulic cycles (intermediate water temperature with long cycles of hydraulic pressure), but the AASHTO procedure indicate significantly different damage deterioration compared with the MIST condition of 40°C and 3000 hydraulic cycles. For the less moisture-susceptible asphalt mixture, no significant differences are evident among the damage characteristic curves derived from all the moisture damage conditioning procedures, as shown in Figure E.3 (b).

Finally, digital imaging analysis was conducted to quantify the percentage of stripping on the fractured surface of the cyclic direct tension test specimens. The results indicate that the MIST condition of 40°C water temperature, 6000 hydraulic cycles, and 276 kPa pore pressure led to stripping on the fractured surface that was identical to that derived using the AASHTO T 283 conditions.

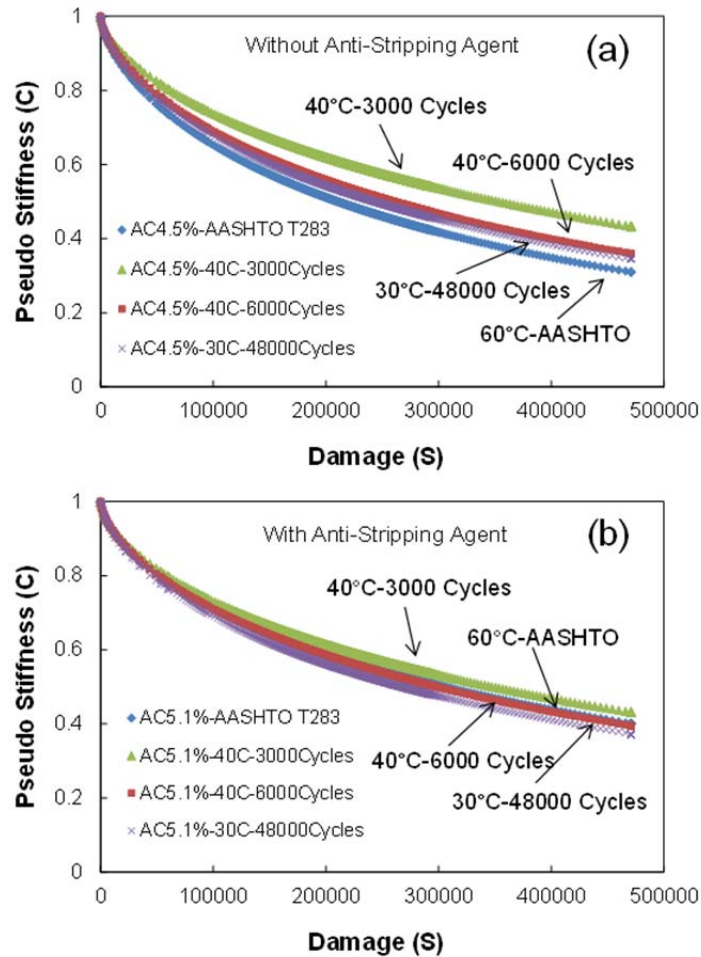


Figure E.3 Change in damage characteristic curves derived from different moisture conditioning procedures.

E.3 Proposed Moisture Conditioning Procedure for MIST

Table E.2 shows the stripping percentages obtained through digital imaging analysis. The threshold value of 63 was used to quantify the stripping percentages for the fractured specimens after cyclic direct tension testing using the moisture conditions presented in Table E.2.

Table E.2 Stripping Quantification Results for Moisture Damage Derived Using AASHTO T 283 and Various MIST Conditions for Moisture-Susceptible and Less Moisture-Susceptible Mixtures

% Stripping	Asphalt Content 4.5%, No Anti-Stripping Agent	Asphalt Content 5.1%, 0.7% Anti-Stripping Agent
60°C, 24 hours, AASHTO T 283	8.56 %	4.43 %
40°C, 276 kPa, 3,000 Cycles	6.76 %	3.75 %
40°C, 276 kPa, 6,000 Cycles	8.55 %	4.36 %
30°C, 276 kPa, 48,000 Cycles	7.94 %	5.55 %

Based on the outcomes of the damage characteristics of the S-VECD model and stripping quantifications of digital imaging analysis shown in Figure E.3 and Table E.2, the authors recommend setting MIST conditions at 40°C, 276 kPa, and 6000 cycles, which correspond to the AASHTO T 283 conditions. These conditions are based only on the results of one mixture. In future study, a wide range of asphalt mixtures should be investigated to build up the database to determine standard MIST conditions that can sensitively evaluate moisture susceptibility for mechanical performance tests and digital imaging analyses.

In the overall study presented in this report, the moisture susceptibility of various warm mix asphalt (WMA) mixtures was investigated using laboratory mechanical tests and digital imaging analysis. The laboratory tests included: 1) the cyclic direct tension test, 2) the indirect tensile (IDT) strength test, and 3) the Hamburg wheel tracking (HWT) test. The mechanical test results were compared against the results obtained from digital imaging analysis to identify sensitive moisture susceptibility indicators. Finally, a MIST conditioning procedure was proposed that uses moisture-conditioned specimens that are similar to those used for AASHTO T 283 conditioning.

The following conclusions have been drawn based on the analytical, numerical, and experimental research conducted in this study:

Stripping Quantification through Digital Imaging Analyses

- The digital imaging analysis method developed in this study captures the degree of stripping fairly well.
- The stripping percentages of the fractured specimens can be quantified consistently using a pixel counting method after determining threshold values via the mesh selection method.

- The stripping quantifications of the IDT and HWT test results were derived successfully by determining two threshold values that can differentiate stripping, asphalt mastic failure, and aggregate breakage on the fractured surfaces, and by modifying the tested sample of the HWT test to scan the scoured surface.

Performance-Based Moisture Susceptibility Evaluation

- The fatigue life predicted from the coupled S-VECD and LVEA models has a strong correlation with the percentage of stripping area determined from the fractured specimen surfaces.
- The asphalt content of a mixture has a significant effect on the fatigue performance as well as the moisture susceptibility of the mixture. This effect is found to be greater for the KW-A WMA mixture without an anti-stripping agent than for the KW-B mixture with an anti-stripping agent.
- A polyethylene wax-type additive combined with an anti-stripping agent (KW-B) leads to a longer fatigue life and less stripping than the pure polyethylene wax-type additive (KW-A).
- The fatigue life ratios of pavements with and without moisture conditioning, based on results obtained using the S-VECD model combined with the LVEA program, rank as the best indicators of moisture damage in WMA pavements. The fatigue life ratio showed a strong relationship with the corresponding stripping percentage ($R^2 = 0.88$) for the moisture susceptibility evaluation of the WMA mixtures investigated in this study.
- The SIP determined from the HWT tests was found to be the second best indicator of moisture damage in WMA pavements. The SIP showed a strong relationship with the corresponding stripping percentage ($R^2 = 0.84$) for moisture susceptibility evaluation. However, this observation needs to be refined because of the difficulty encountered in differentiating the effects of permanent deformation and moisture damage on the SIP. Additional HWT tests under dry conditions may help to distinguish those combined effects.
- The IDT test results indicate that the stripping percentages and number of aggregate breakage ratios may be used as improved moisture susceptibility indicators when compared to tensile strength ratio (TSR) results.
- The damage contours developed from the S-VECD model combined with the LVECD program provide a sensitive means of visually evaluating the effects of moisture conditioning on the fatigue performance of asphalt pavements.
- The percentage of stripping and fatigue life ratio parameters obtained from cyclic direct tension tests and the percentages of stripping obtained from IDT tests are the

recommended indicators for practitioners to use to evaluate the moisture susceptibility of WMA mixtures.

New Moisture Conditioning Procedure

- Through the damage and stripping quantification analyses, it was found that Moisture-Induced Stress Tester (MIST) conditions of 40°C, 276 kPa, and 6000 cycles can produce the same damage accumulation and stripped areas that correspond to those conditions used in the current AASHTO T 283 procedure.
- MIST can successfully reduce the current moisture conditioning time by adding hydraulic cyclic pore pressure to specimens in a high temperature water bath.